



HAL
open science

Modeling and optimization of tubular polymerization reactors

Ionut Banu

► **To cite this version:**

Ionut Banu. Modeling and optimization of tubular polymerization reactors. Other. Université Claude Bernard - Lyon I; Universitatea politehnica (Bucarest), 2009. English. NNT : 2009LYO10121 . tel-00719401

HAL Id: tel-00719401

<https://theses.hal.science/tel-00719401>

Submitted on 19 Jul 2012

HAL is a multi-disciplinary open access archive for the deposit and dissemination of scientific research documents, whether they are published or not. The documents may come from teaching and research institutions in France or abroad, or from public or private research centers.

L'archive ouverte pluridisciplinaire **HAL**, est destinée au dépôt et à la diffusion de documents scientifiques de niveau recherche, publiés ou non, émanant des établissements d'enseignement et de recherche français ou étrangers, des laboratoires publics ou privés.

THÈSE
Présentée devant
L'UNIVERSITÉ CLAUDE BERNARD-LYON, FRANCE et
L'UNIVERSITÉ « POLITEHNICA » DE BUCAREST, ROUMANIE
pour l'obtention en cotutelle du
DIPLÔME DE DOCTORAT

ECOLE DOCTORALE MATERIAUX DE LYON

Présentée et soutenu publiquement le 17/07/2009 par
IONUȚ BANU

SPECIALITÉ: GÉNIE CHIMIQUE

Modeling and optimization of tubular polymerization reactors

Directeurs de thèse:

M. Jean-Pierre PUAUX Professeur, UCBLyon1

M. Grigore BOZGA Professeur, UPB

JURY:

M. Fernand PLA	Professeur Emerite, ENSIC	Rapporteur
M. Șerban AGACHI	Professeur, Université BABES-BOLYAI	Rapporteur
M. Phillipe CASSAGNAU	Professeur, UCBLyon1	Examineur
M. Iosif NAGY	Maître de Conférences, UPB	Examineur
M. Jean-Pierre PUAUX	Professeur, UCBLyon1	
M. Grigore BOZGA	Professeur, UPB	
M. Horia IOVU	Professeur, UPB	President

TABLE OF CONTENTS

<i>Index of figures</i>	6
<i>Index of tables</i>	9
Acknowledgements	13
1. Introduction	15
2. Optimization of polymerization processes in tubular reactors. Case study: the polymerization of methyl methacrylate	19
2.1. Literature survey	20
2.1.1. Introduction	20
2.1.2. Polymerization techniques	22
2.1.3. Mechanism and kinetics of the free radical polymerization	23
Kinetic mechanism of free radical polymerization [4, 5]	24
Hypotheses used for the kinetic modeling of polymerization reactions	26
Relations for polymer characteristics	27
2.1.4. Methyl methacrylate polymerization	28
Gel effect models for MMA free radical polymerization	29
Published kinetic models for MMA polymerization in solution	33
2.1.5. Mathematical models for tubular MMA polymerization reactor	33
Plug flow reactor model	33
Laminar flow reactor model	39
2.1.6. Optimization of tubular polymerization reactors	41
Pontryagin's Minimum Principle (MP)	43
The Genetic Algorithms	45
2.2. Simulation of a tubular reactor for MMA polymerization in solution	48
2.2.1. Selection of the kinetic model	48
2.2.2. Simulation of the laminar flow polymerization reactor	50
Influence of tube diameter	54
Influence of initiator concentration	56
Influence of monomer concentration	57
2.2.3. Comparison of laminar flow and plug flow reactor simulation results	58
2.3. Optimization of MMA tubular polymerization reactor	59
2.3.1. A comparison of variational and genetic algorithms performances in the optimization of plug flow MMA polymerization reactor [55]	59
Optimization by Minimum Principle method	60
Genetic Algorithm	64
Results and discussions	65
2.3.2. Laminar flow and plug-flow tubular reactors optimization by a Genetic Algorithm	68

Optimization problem 1 _____	68
Optimization results for a laminar flow tubular reactor _____	69
Optimization results for a jacketed plug-flow reactor _____	73
<i>Optimization Problem 2: Maximization of the polymer production</i> _____	77
Optimization of a laminar flow tubular reactor _____	78
Optimization of the plug-flow polymerization reactor _____	80
2.4. Conclusions _____	82
3. Modeling and optimization of the PLA synthesis process by reactive extrusion _____	85
3.1. Literature survey _____	86
Historical survey and PLA practical applications _____	86
Monomers and polymerization processes _____	87
L-lactide ring-opening polymerization. Polymerization initiators and mechanisms _____	88
PLA thermal and rheological properties _____	96
PLA reactive extrusion _____	97
3.2. Experimental study of the L-lactide polymerization kinetics _____	97
3.2.1. Experimental set-up, materials and polymerization method _____	97
Experimental apparatus _____	97
Materials _____	99
Method _____	99
3.2.2. Polymer characterization _____	100
Nuclear magnetic resonance _____	100
Size-exclusion chromatography (SEC) _____	101
Infrared spectroscopy (FT-IR) _____	104
3.2.3. Experimental results _____	105
A. L-lactide polymerization initiated by stannous octoate _____	105
Temperature influence _____	107
Initiator concentration influence _____	109
B. L-lactide polymerization initiated by stannous octoate and co-initiated by triphenyl phosphine _____	109
Temperature influence _____	111
M/I influence _____	114
3.2.4. Polymerization kinetics modeling _____	115
A. Estimation results for L-lactide polymerization initiated by stannous octoate _____	118
B. Estimation results for L-lactide polymerization initiated by stannous octoate and co-initiated by triphenylphosphine _____	121
3.3. Experimental study of reactive extrusion process _____	123
3.3.1. Extruder characteristics _____	123
3.3.2. Polymerization procedure _____	124
L-lactide initiated with stannous octoate _____	124

L-lactide initiated with stannous octoate/triphenyl phosphine _____	124
3.3.3. Experimental results of reactive extrusion _____	124
3.4. Modeling of the flow and mixing of the melting material in the extruder.	
Evaluation of the residence time distribution in the extruder by the simulator Ludovic® _____	128
3.4.1. Experimental study of polymer flow in the twin-screw extruder _____	129
3.4.2. RTD evaluation for melted polypropylene flow by Ludovic® simulator _____	131
3.5. Mathematical modeling of the PLA reactive extrusion _____	133
3.5.1. Modeling of polymer flow by axial dispersion model. Evaluation of the Pe values _____	134
3.5.2. Flow simulation by Ludovic® software for PLA reactive extrusion _____	135
3.5.3. <i>Mathematical modeling of reactive extrusion process</i> _____	138
Polymerization modeling by axial dispersion model approach (Ludovic simulation) _____	138
TSE extruder as a compartment model _____	139
Comparison of simulation results predicted by the two modeling approaches _____	141
3.6. Reactive extrusion optimization study _____	144
3.7. Conclusions _____	146
4. General Conclusions _____	149
Original results _____	150
Suggestions for future work _____	152
5. Appendix 1: PLA reactive extrusion simulation by Ludovic. RTD curves and compartment model data _____	155
Flow rate: 0.75 kg/h, Screw speed: 50 rpm _____	156
Flow rate: 0.75 kg/h, Screw speed: 200 rpm _____	157
Flow rate: 0.75 kg/h, Screw speed: 300 rpm _____	158
Flow rate: 1.25 kg/h, Screw speed: 50 rpm _____	159
Flow rate: 1.25 kg/h, Screw speed: 200 rpm _____	160
Flow rate: 1.25 kg/h, Screw speed: 300 rpm _____	161
Flow rate: 1.5 kg/h, Screw speed: 50 rpm _____	162
Flow rate: 1.5 kg/h, Screw speed: 200 rpm _____	163
6. List of publications _____	165
A. Journal papers _____	165
B. Papers published in the proceedings of national and international conferences _____	165
C. National and international conferences communications _____	165
7. References _____	166

Index of figures

<i>Figure 2.1. Calculated monomer conversion and number-average molecular weights profiles</i>	49
<i>Figure 2.2. Profiles for monomer conversion (left) and axial velocity (right), at different positions (z) along the reactor</i>	54
<i>Figure 2.3. Number-average molecular weights (left) and temperature (right) profiles, at different positions (z) along the reactor</i>	54
<i>Figure 2.4. Radial profiles of monomer conversion, at different positions along the reactor. Left: Reactor 2; Right: Reactor 3</i>	55
<i>Figure 2.5. Radial profiles for number-average molecular weights, at different positions (z) along the reactor. Left: Reactor 2; Right: Reactor 3</i>	56
<i>Figure 2.6. Radial profiles for temperature, at different positions (z) along the reactor. Left: Reactor 2; Right: Reactor 3</i>	56
<i>Figure 2.7. Monomer conversion profiles for feed initiator concentration of 0.025 mole/L (left) and 0.1 mole/L (right)</i>	56
<i>Figure 2.8. Number average molecular weight profiles for feed initiator concentration of 0.025 mole/L (left) and 0.1 mole/L (right)</i>	57
<i>Figure 2.9. Monomer conversion profiles for smallest ($w_s = 0.3$, left) and highest ($w_s = 0.7$, right) feed weight solvent fractions</i>	57
<i>Figure 2.10. Number-average molecular weight for smallest ($w_s = 0.3$, left) and highest ($w_s = 0.7$, right) feed solvent fraction</i>	58
<i>Figure 2.11. Plug flow and laminar flow reactor simulated monomer conversion and number-average molecular weights axial profiles (Reactor 1)</i>	59
<i>Figure 2.12. Starting temperature profiles (A) and the corresponding minimum profiles (B)</i>	63
<i>Figure 2.13. Performance index vs. iteration number</i>	64
<i>Figure 2.14. Temperature profiles calculated by Minimum Principle and Genetic Algorithm</i>	66
<i>Figure 2.15. Optimal state variables profiles</i>	67
<i>Figure 2.16 Optimal jacket temperature values (NJ=8); left: $X_d = 0.5$, right: $X_d = 0.8$</i>	71
<i>Figure 2.17. Reaction temperature profiles on radial direction calculated with the optimal control policy (NJ=8, A: $X_d = 0.5$, B: $X_d = 0.8$)</i>	72
<i>Figure 2.18. Monomer conversion profiles on radial direction calculated with the optimal control policy (NJ=8);left: $X_d = 0.5$; right: $X_d = 0.8$</i>	72
<i>Figure 2.19. Number-average molecular weight profiles on radial direction calculated with the optimal control policy (NJ=8);left: $X_d = 0.5$, right: $X_d = 0.8$</i>	72
<i>Figure 2.20. Polydispersion index profiles on radial direction calculated with the optimal control policy (NJ=8, A: $X_d = 0.5$, B: $X_d = 0.8$)</i>	73
<i>Figure 2.21. Initiator concentration profiles on radial direction calculated with the optimal control policy (NJ=8);left: $X_d = 0.5$, right: $X_d = 0.8$</i>	73

Figure 2.22 Velocity profiles on radial direction calculated with the optimal control policy (NJ=8);left: $X_d = 0.5$, right: $X_d = 0.8$	73
Figure 2.23. Optimal thermal agent profile for the plug-flow reactor (A: $X_d = 0.5$, B: $X_d = 0.8$)	75
Figure 2.24. Monomer conversion profiles (optimization problem1, plug-flow reactor, A: $X_d = 0.5$, B: $X_d = 0.8$)	75
Figure 2.25. Polymer molecular weights profiles (optimization problem1, plug-flow reactor, A: $X_d = 0.5$, B: $X_d = 0.8$)	76
Figure 2.26. Reaction temperature profiles (optimization problem1, plug-flow reactor, A: $X_d = 0.5$, B: $X_d = 0.8$)	76
Figure 2.27. Initiator concentration profiles (optimization problem1, plug-flow reactor, A: $X_d = 0.5$, B: $X_d = 0.8$)	77
Figure 2.28. Polydispersion index profile (optimization problem 1, plug-flow reactor)	77
Figure 2.29. Optimal jacket temperature profile (laminar flow reactor, optimization problem 2)	79
Figure 2.30. Monomer conversion (left) and number-average weight (right) profiles (laminar flow reactor, optimization problem 2)	79
Figure 2.31. Reaction temperature (left) and initiator concentration (right) profiles (laminar flow reactor, optimization problem 2)	80
Figure 2.32. Polydispersion index (left) and flow velocity (right) profiles (laminar flow reactor, optimization problem 2)	80
Figure 2.33. Optimal jacket temperature profile (plug-flow reactor, optimization problem 2)	81
Figure 2.34. Monomer conversion (left) and number-average weight (right) profiles (plug-flow reactor, optimization problem 2)	81
Figure 2.35. Reaction temperature (left) and initiator concentration (right) profiles (plug-flow reactor, optimization problem 2)	82
Figure 2.36. Polydispersion index profile (plug-flow reactor, optimization problem 2)	82
Figure 3.1. Cationic mechanism of lactide polymerization [101]	91
Figure 3.2. HAAKE Rheocord Mixer simplified schema	98
Figure 3.3. DSM Micro 15 TS Compounder	98
Figure 3.4. Detailed view of the reaction chamber	99
Figure 3.5. Characteristic proton positions for L-LA and PLA	101
Figure 3.6. Example of $^1\text{H-NMR}$ spectra of PLA	101
Figure 3.7. SEC chromatogram for a PLA/L-LA mixture	103
Figure 3.8. FT-IR spectra for $M/I = 4500$ series	104
Figure 3.9. FT-IR spectra for $M/I = 2250$ series	105
Figure 3.10. Monomer conversion and number-average molecular weight profiles (M/I of 2250, initiator SnOct_2)	108
Figure 3.11. Monomer conversion and number-average molecular weight profiles (M/I of 4500, initiator SnOct_2)	108
Figure 3.12. Monomer conversion and number-average molecular weight profiles for a temperature of 195°C (initiator SnOct_2)	109
Figure 3.13. Monomer conversion and number-average molecular weights profiles for a M/I of 4500 (Initiator $\text{SnOct}_2/\text{TPP}$)	112
Figure 3.14. Polydispersion index for a M/I of 4500 (Initiator $\text{SnOct}_2/\text{TPP}$)	112
Figure 3.15. Monomer conversion and number-average molecular weights profiles for a M/I of 2250 (Initiator $\text{SnOct}_2/\text{TPP}$)	113

Figure 3.16. Polydispersity index for a M/I of 2250 (Initiator SnOct ₂ /TPP)	113
Figure 3.17. Comparison of monomer conversion and number-average molecular weights profiles for the kinetics and reproducibility tests (Initiator SnOct ₂ /TPP)	114
Figure 3.18. Monomer conversions and number-average molecular weights profiles at a temperature of 195 °C (Initiator SnOct ₂ /TPP).....	114
Figure 3.19. Number-average molecular weights at a temperature of 195 °C (Initiator SnOct ₂ /TPP)	115
Figure 3.20. Mechanism of polymerization of dilactide in the presence of stannous octoate	116
Figure 3.21. Time dependence of L-lactide conversion, M/I=2250 (initiator SnOct ₂).....	119
Figure 3.22. Time dependence of the number average molecular weight, M/I=2250 (initiator SnOct ₂).....	120
Figure 3.23. Time dependence of L-lactide conversion, M/I=4500 (initiator SnOct ₂).....	120
Figure 3.24. Time dependence of number average molecular weight, M/I=4500 (initiator SnOct ₂)	120
Figure 3.25. Experimental vs. calculated monomer conversion for kinetic experiments (initiator SnOct ₂ /TPP).....	122
Figure 3.26. Experimental vs. calculated number average molecular weight for kinetic experiments (initiator SnOct ₂ /TPP).....	122
Figure 3.27. Screw profile for L-lactide polymerization initiated by SnOct ₂ /TPP (Screw 1)	123
Figure 3.28. Screw profile for L-lactide polymerization initiated by SnOct ₂ (Screw 2).....	124
Figure 3.29. RTD curves at constant flow rate and variable screw speed (left: 0.75 kg/h, right: 1.25 kg/h).....	130
Figure 3.30. RTD curves at 1.5 kg/h and variable screw speed	130
Figure 3.31. RTD curves at constant screw speed and variable flow rate (left: 50 rpm, right: 300 rpm).....	130
Figure 3.32. Experimental (points) and calculated (line) values of polypropylene viscosity	131
Figure 3.33. Simulated RTD curve: 0.75 kg/h, 50 rpm.....	132
Figure 3.34. Simulated RTD curve: 0.75 kg/h, 200 rpm.....	132
Figure 3.35. Simulated RTD curve: 0.75 kg/h, 300 rpm.....	132
Figure 3.36. Comparison of RTD curves for a flow rate of 1.25 kg/h and screw speed of 200 rpm	135
Figure 3.37. Comparison of RTD curves for a flow rate of 1.25 kg/h and screw speed of 300 rpm	135
Figure 3.38. Published [121] and calculated viscosity values at 200 °C	136
Figure 3.39. Residence time for the viscosity model 1	136
Figure 3.40. Residence time for the viscosity model 2	137
Figure 3.41. Filling ratio for the viscosity model 1	137
Figure 3.42. Filling ratio for the viscosity model 2	138
Figure 3.43. Simulated chemical transformation for a M/I of 2250 (initiator SnOct ₂ /TFF, flow rate 1.25 kg/h, screw speed 50 rpm)	141
Figure 3.44. Twin screw extruder simulation by the two modeling approaches (DA Model – axial dispersion model, Compartment Model – Compartment model).....	142
Figure 3.45. Monomer conversion profiles for both M/I ratios at a flow rate 0.75 kg/h;.....	143
Figure 3.46. Number-average molecular weights profiles for both M/I ratios at a flow rate 0.75 kg/h; left: 200 rpm, right: 300 rpm	143
Figure 3.47. Optimal temperature profile for the reactive extrusion optimization problem	146
Figure 3.48. Monomer conversion and number-average molecular weights	146

<i>Figure_Apx 1. Ludovic simulated RTD curve (0.75 kg/h, 50 rpm)</i>	156
<i>Figure_Apx 2. Local and global residence time profiles (0.75 kg/h, 50 rpm)</i>	156
<i>Figure_Apx 3. Ludovic simulated RTD curve (0.75 kg/h, 200 rpm)</i>	157
<i>Figure_Apx 4. Local and global residence time profiles (0.75 kg/h, 200 rpm)</i>	157
<i>Figure_Apx 5. Ludovic simulated RTD curve (0.75 kg/h, 300 rpm)</i>	158
<i>Figure_Apx 6. Local and global residence time profiles (0.75 kg/h, 300 rpm)</i>	158
<i>Figure_Apx 7. Ludovic simulated RTD curve (1.25 kg/h, 50 rpm)</i>	159
<i>Figure_Apx 8. Local and global residence time profiles (1.25 kg/h, 50 rpm)</i>	159
<i>Figure_Apx 9. Ludovic simulated RTD curve (1.25 kg/h, 200 rpm)</i>	160
<i>Figure_Apx 10. Local and global residence time profiles (1.25 kg/h, 200 rpm)</i>	160
<i>Figure_Apx 11. Ludovic simulated RTD curve (1.25 kg/h, 300 rpm)</i>	161
<i>Figure_Apx 12. Local and global residence time profiles (1.25 kg/h, 300 rpm)</i>	161
<i>Figure_Apx 13. Ludovic simulated RTD curve (1.5 kg/h, 50 rpm)</i>	162
<i>Figure_Apx 14. Local and global residence time profiles (1.5 kg/h, 50 rpm)</i>	162
<i>Figure_Apx 15. Ludovic simulated RTD curve (1.5 kg/h, 200 rpm)</i>	163
<i>Figure_Apx 16. Local and global residence time profiles (1.5 kg/h, 200 rpm)</i>	163

Index of tables

<i>Table 2.1. Kinetic mechanism for free-radical solution polymerization process</i>	25
<i>Table 2.2. Gel effect constitutive equations proposed by Chiu, Carrat and Soong [13, 16]</i>	32
<i>Table 2.3. Working conditions for MMA solution polymerization studies</i>	34
<i>Table 2.4. The Arrhenius expressions for the kinetic constants proposed by different authors</i>	36
<i>Table 2.5. Operating conditions for reactor simulation</i>	49
<i>Table 2.6. Tubular reactor characteristics</i>	50
<i>Table 2.7. Thermal conductivity constitutive equations [31]</i>	53
<i>Table 2.8. Reactor configurations</i>	55
<i>Table 2.9. Working conditions for reactor optimization</i>	62
<i>Table 2.10. Specified values in the performance index expression</i>	62
<i>Table 2.11. Minimization results by the MP algorithm for different initialization profiles</i>	63
<i>Table 2.12. Performance index values after 200 iterations</i>	65
<i>Table 2.13. Performance index values after 500 iterations</i>	65
<i>Table 2.14. Optimization results for polymerization reactor in laminar flow</i>	70
<i>Table 2.15. Weighting coefficients in performance index (2.126)</i>	71
<i>Table 2.16. Optimization results for a plug-flow polymerization reactor</i>	74
<i>Table 2.17. Weighting coefficients in performance index (2.126)</i>	78

Table 2.18. Results of the laminar flow tubular reactor optimization problem	78
Table 2.19. Results of the plug-flow reactor optimization problem 2.....	81
Table 3.1. Conversion values estimated by ¹ H-NMR and GPC for two kinetic experiments (initiator SnOct ₂)	103
Table 3.2. Polymer characteristics for 170 °C and M/I = 2250 (initiator SnOct ₂).....	105
Table 3.3. Polymer characteristics for 185 °C and M/I = 2250(initiator SnOct ₂).....	105
Table 3.4. Polymer characteristics for 195 °C and M/I = 2250(initiator SnOct ₂).....	106
Table 3.5. Polymer characteristics for 185 °C and M/I = 4450(initiator SnOct ₂).....	106
Table 3.6. Polymer characteristics for 195 °C and M/I = 4500(initiator SnOct ₂).....	106
Table 3.7. Polymer characteristics for 200 °C and M/I = 225. First experiment (initiator SnOct ₂).....	106
Table 3.8. Polymer characteristics for 200 °C and M/I = 225. Second experiment (initiator SnOct ₂).....	107
Table 3.9. Time evolution of polymer characteristics for 185 °C and M/I = 4500 (initiator SnOct ₂ /TPP).....	110
Table 3.10. Time evolution of polymer characteristics for 195 °C and M/I = 4500 (initiator SnOct ₂ /TPP).....	110
Table 3.11. Time evolution of polymer characteristics for 205 °C and M/I = 4500 (initiator SnOct ₂ /TPP).....	110
Table 3.12. Time evolution of polymer characteristics for 185 °C and M/I = 2250 (initiator SnOct ₂ /TPP).....	111
Table 3.13. Time evolution of polymer characteristics for 195 °C and M/I = 2250 (initiator SnOct ₂ /TPP).....	111
Table 3.14. Calculated kinetic parameters values [124]	119
Table 3.15. The calculated kinetic parameters for the L-lactide – SnOct ₂ polymerization system	121
Table 3.16. Estimated values for the kinetic parameters (initiator SnOct ₂ /TPP)	121
Table 3.17. The calculated kinetic parameters for the L-lactide – (initiator SnOct ₂ /TPP).....	122
Table 3.18. Reactive extrusion results at 200 °C and M/I = 2250 on Screw 1 (initiator SnOct ₂ /TPP).....	126
Table 3.19. Reactive extrusion results at 200 °C and M/I = 4500 on Screw 1(initiator SnOct ₂ /TPP).....	126
Table 3.20. Reactive extrusion of L-lactide initiated by stannous octoate (Screw 2, initiator SnOct ₂).....	127
Table 3.21. Reactive extrusion results at 200 °C and M/I = 225 on Screw 1 (initiator SnOct ₂)	127
Table 3.22. Carreau-Yasuda parameters for PP model	131
Table 3.23. Experimental and simulated residence times at 200 °C.....	133
Table 3.24. Estimated parameters of the axial dispersion model	134
Table 3.25. Estimated values for the parameters of the Carreau-Yasuda viscosity model	136
Table 3.26. AD model parameters for Ludovic simulated RTD.....	138
Table 3.27. The parameters for 1.25 kg/h, 50 rpm, screw 1 (Figure 3.27) and viscosity model 1 (Table 3.25).....	140
Table 3.28. Experimental and predicted polymer characteristics for M/I = 2250 (initiator SnOct ₂ /TPP).....	144
Table 3.29. Experimental and predicted polymer characteristics for M/I = 4500(initiator SnOct ₂ /TPP).....	144
Table 3.30. Reactive extrusion optimization results.....	145
Table_Apx 1. Compartment model parameters (0.75 kg/h, 50 rpm).....	157
Table_Apx 2. Compartment model parameters (0.75 kg/h, 200 rpm).....	158
Table_Apx 3. Compartment model parameters (0.75 kg/h, 300 rpm).....	159
Table_Apx 4. Compartment model parameters (1.25 kg/h, 50 rpm).....	160

<i>Table_Apx 5. Compartment model parameters (1.25 kg/h, 200 rpm).....</i>	<i>161</i>
<i>Table_Apx 6. Compartment model parameters (1.25 kg/h, 300 rpm).....</i>	<i>162</i>
<i>Table_Apx 7. Compartment model parameters (1.5 kg/h, 50 rpm).....</i>	<i>163</i>
<i>Table_Apx 8. Compartment model parameters (1.5 kg/h, 200 rpm).....</i>	<i>164</i>

Acknowledgements

First I have to mention that this work was realized by a scientific collaboration with “Laboratoire des Materiaux Polymeres and Biomateriaux”, University Claude Bernard, Lyon, and I wish to thank my supervisors, prof. dr. ing. Grigore BOZGA from University “Politehnica” of Bucharest and prof. Jean-Pierre PUAUX from University Claude Bernard, Lyon I, who guided me all these years through the Ph. D. studies. Their constant support, patience, transfer of knowledge and trust made this thesis possible.

I wish also to express my gratitude to conf. dr. ing. Gheorghe SOARE that guided my first steps in the research field of chemical engineering and offered me the possibility to begin this Ph. D. thesis. I want to thank also to conf. dr. ing. Iosif NAGY and conf. dr. ing. Sorin BÎLDEA for their valuable suggestions.

Prof. dr. ing. Șerban AGACHI (University Babes-Bolyai, Cluj-Napoca, Romania) and Prof. Fernand PLA (Ecole Nationale Superieure des Industries Chimiques, Nancy, France) that accepted to examine this work as reporters and members of the jury. I thank them strongly for their helpful advices and observations.

I am eager to express my gratitude to members of the jury that they accepted to judge this work: Prof. Phillipe CASSAGNAU (Universite Claude Bernard, Lyon) and conf. dr. ing. Iosif NAGY (University Politehnica of Bucharest).

I would like to thank all the staff of the Department of Chemical Engineering, University Politehnica and of the Laboratoire des Materiaux Polymeres and Biomateriaux, University Claude Bernard, Lyon, for the inspiring and cordial atmosphere. My special thanks for Flavien MELIS that help me a lot, not only with the experimental part realized in the French Laboratory but also from the human point of view. He was able to imbue me with a better understanding of

the nature of french people, life and culture and also made me tasting some of the natural landscapes of this country by the interesting trips organized along my research stages. Many thanks to my friends, ing. Doriana Stanciu for helping me with the interpretation of the different polymer analysis presented in this work, ing. Iulian BANU and his wife, Laura, for their incommensurable support in difficult moments and the continuous friendship.

For their financial support I would like to thank the French Government of Foreign and European Affairs and the Rhone-Alpes region for the provided scholarships and the The National University Research Council of Romania, for the Research Grant.

Last but not least, I am very grateful to my family and all other friends not mentioned here, who were always there for me.

1. Introduction

The tubular reactors have the advantage of higher transformation rates and consequently higher reagent conversions, compared with stirred tank reactors, respectively a more uniform product quality and a more simple operation. In the field of polymerization processes, the utilization of the tubular reactors is feasible for the reaction mixtures presenting limited variations of viscosity, such as the solution or emulsion polymerization processes, and pre-polymerization steps for bulk polymerization respectively. Due to these limitations, there are a relatively small number of publications dealing with the optimization of tubular polymerization reactors.

A particular category of tubular reactors are the extruders, often used to perform the polymerization processes (reactive extrusion). The high pumping capacity of the extruder screw allows the processing of viscous polymer mixtures, avoiding the limitations generated by the important viscosity increases during polymerization.

The goal of this thesis is the investigation of the modeling and optimization particularities of tubular polymerization reactors, highlighting the performances of two important optimization algorithms appropriate for these applications.

The thesis is structured in 4 chapters, among which the first has an introductory role and the last one presents the main conclusions of the work. The theoretical and experimental research and their results are presented in the chapters 2 and 3.

In Chapter 2 of the work a modeling and optimization case study that reveals the particularities of these applications to polymerization tubular reactors will be described. Among the optimization algorithms currently used in the field of chemical engineering, the most popular appear to be the Minimum Principle of Pontryagin and Genetic Algorithms respectively. In order to compare the performances of these two algorithms, we will select as case study the methyl methacrylate solution polymerization, a reaction system well described by an important number of kinetic studies published in the literature. The most representative, among the published kinetic models for this system, will be selected by reactor simulations in identical working conditions. Based on the selected kinetic model, mathematical models of the polymerization tubular reactor in ideal (plug-flow) and non-ideal (bi-dimensional laminar model) flow hypotheses will be then developed.

In order to compare the performances of the mentioned optimization algorithms, an optimization problem based on the ideal flow model, having as objective to produce a polymer with imposed characteristics (number-average molecular weight and polydispersion index) at a given monomer conversion will be formulated. By the formulation of the performance index, number of variables and mathematical model structure used to describe the process behavior, this problem can be considered as one of average complexity. In order to solve this optimization

problem, computer programs based both on Minimum Principle of Pontryagin and Genetic Algorithms respectively will be developed. A comparison of the two optimization algorithms will be further developed in terms of efforts associated for preparation of solving procedure, convergence to the optimum and computing time. In the second part of Chapter 2 a more complex optimization study of tubular MMA polymerization reactor by a Genetic Algorithm will be presented. Several optimization problems with an increased number of control variables will be formulated and solved, describing the tubular polymerization reactor by plug-flow and laminar flow models respectively.

Chapter 3 will present a modeling and optimization study of L-lactide polymerization in co-rotating twin-screw extruders. In spite of the commercial importance of this polymer, there are only few published works treating the polymerization process kinetics. The experimental and theoretical researches presented in this chapter will involve three steps:

i) The experimental study of L-lactide polymerization kinetics with different initiation systems and elaboration of the kinetic model of the process. The stannous octoate alone and stannous octoate/triphenyl phosphine initiation systems will be tested for representative operating conditions. A kinetic model for the L-lactide polymerization process will be then developed and the parameters will be estimated by a nonlinear parameters estimation procedure.

ii) The study of flow and mixing of the L-lactide/poly(lactide) melt along the extruder and elaboration of two flow models (axial dispersion model and a compartment type model). The flow of reaction mixture along the extruder screw will be simulated by the commercial software Ludovic®. To check the validity of this approach, an evaluation of Ludovic® simulator ability in predicting the flow and mixing characteristics in TSE will be performed by using RTD experiments with polypropylene melt in the same apparatus. The characteristics of a L-lactide/poly(lactide) mixture flow in the extruder, will be determined by Ludovic® simulations, for the operating conditions of practical interest. These simulations will provide the necessary data for evaluation of the parameters of the flow models used in polymerization process calculation.

iii) The experimental study of the L-lactide polymerization in a co-rotating twin screw extruder and the mathematical modeling and simulation of this reactive extrusion process. Based on the previously proposed kinetic model and the calculated polymer mixture flow characteristics, the simulation of the reactive extrusion by different mathematical models will be performed. The model results will be then compared with experimental results. Finally, a problem concerning the optimization of the thermal regime for the L-lactide reactive extrusion process will be developed and solved.

The thesis will end with a chapter presenting the general conclusions and the proposal for

future developments of the subject.

The experimental studies presented in this work were performed at Laboratoire des Matériaux Polymères and Biomatériaux of University Claude Bernard, Lyon, France.

The researches were partially financed by the research grant TD GR 18/09.05.2007 financed by The National University Research Council of Romania, two studentships MIRA financed by Rhône-Alpes region and an Eiffel Doctorate Scholarship financed by French Ministry of Foreign and European Affairs.

2. Optimization of polymerization processes in tubular reactors. Case study: the polymerization of methyl methacrylate

2.1. Literature survey

2.1.1. Introduction

The kinetic of the polymerization processes is usually complex, due to the high number of the consecutive-parallel reactions that define the process. Due to polymerization processes behavior, small variations in the operating conditions or physical properties of the reaction mixture could conduct to a product with no practical utility.

All the polymerization processes are highly exothermal, with thermal effects in the range 60 – 90 kJ/mole. This important amount of heat generated inside the reaction mixture must be efficiently evacuated, otherwise the temperature can reach values of few hundreds °C.

The length of the polymer chain is often in the range $10^2 - 10^4$, the molecular weights of the polymer having values of tens and hundreds of thousands kg/kmol. In the polymerization processes, due to continuous increase of the macromolecular chains, the reaction mixture viscosity rise rapidly, frequently with more than 6 orders of magnitude. The increase of reaction mixture viscosity has as main consequences the hindrance of mixing (and consequently of heat transport toward the heat transfer surfaces) and a significant change on process kinetics. The kinetic of the elementary steps is strongly influenced by the physical characteristics of the system. The rise of viscosity is favoring the diffusion control of the polymerization process (due to the limitation of diffusion transport of live polymer radicals inside the reaction medium). This phenomenon can be determinant for the overall evolution of polymerization process and is strongly interrelated to the molecular weight and physical properties of the polymer product.

These factors are inducing serious difficulties in the control of the polymerization process, particularly when applying the bulk polymerization technique or solution technique at high concentrations of monomer.

Comparing with autoclave reactors, the tubular reactors have larger heat transfer capacity (higher surface/volume ratios) and a very low degree of mixing in axial direction, these favoring a good control of thermal regime and higher values of monomer conversion. Due to their simplicity, this configuration has small fixed and operational costs. The disadvantages of these reactors are related to a significant pressure drop associated with high viscosities of the reaction mixture that are inducing also broaden residence time distributions and consequently difficulties in the control of the product quality [1].

Polymerization reactors produce materials whose characteristics are assessed in terms of strength, processability, thermal properties and so on. These qualities could be reduced to quantifiable measures (mean molecular weights, polydispersion index), but different operating parame-

ters have opposite effects on their values and usually these measures are distributions due to the complexity of the kinetics.

The mathematical models of polymerization reactors are generally constituted of highly coupled multivariable, nonlinear ordinary or partial differential equations, which require advanced numerical algorithms for obtaining proper solutions in a reasonable amount of time.

The modeling of the tubular polymerization reactors is facing difficulties regarding description of the flow and mixing, correlation of end-use and molecular properties of the polymer product and to account the role of impurities that often exert a strong influence on the process (most of them difficult or impossible to be measured) [2].

An important difficulty in polymerization process operation is that the molecular properties of polymer materials cannot be measured on-line, which means that control procedures have to rely on values provided by process models and on measured values provided with long delays by laboratories (off-line measurements) [3]. Runaway effects are usually encountered in the polymerization processes, occurring when the heat removal is much lower than the rate of generation and proper heat transfer systems have to be provided to avoid these effects.

The complexity of the polymerization reactors makes them outstanding challenges in applying nonlinear optimization and control techniques. In the industrial practice, often the main objectives are to maximize the monomer conversion and obtain a polymer with imposed characteristics (average polymerization degree, molecular weights distribution). Usually, the control of the polymer properties is achieved by using as control variables the flow rate, the cooling fluid temperature, the feed monomer and initiator concentrations. The values of these variables are subjected to practical restrictions (temperatures lower than boiling temperature of raw materials or thermal agents, flow rates lower than maximum pumping capacity, temperature variations within the limits of the thermal transfer system). An appropriate reaction temperature profile could be achieved by using a thermal agent with a specified temperature and flow rate.

At our knowledge, the literature referring the optimization of tubular polymerization reactors is rather scarce. The goal of this chapter is to investigate the modeling and optimization particularities of the tubular polymerization reactors in order to select the most appropriate algorithms. As case study we considered the process of methyl methacrylate (MMA) polymerization in solution. In order to select a kinetic model, we have reviewed the main published studies of MMA polymerization in solution and performed reactor simulations in similar operating conditions, by each kinetic model. From the simulations results, the kinetic model that proved the most representative, from the monomer conversion and polymer molecular weight points of view, was chosen to be used further in the modeling and optimization studies. Based on this ki-

netic model, the behavior of tubular reactors described by the plug-flow and laminar-flow models are studied by numerical simulations and a comparison between the polymerization process performances provided by the two flow models is performed. Several optimization problems of different complexities for the plug-flow reactor are formulated and solved by two already classical optimization methods: Pontryagin's Minimum Principle and a Genetic Algorithm. The comparison of the optimization results obtained by two numerical methods in terms of programming effort and convergence rate allowed to draw several conclusions regarding their performances in the optimization of complex chemical processes.

A simulation and optimization study of a jacketed tubular polymerization reactor is further performed. As optimization (control) variables were considered the jacket temperature, the feed temperature, the mass flow rate, the feed initiator concentration and the feed monomer concentration.

2.1.2. Polymerization techniques

In the published literature, the polymerization processes are classified in different categories, considering:

- the stoichiometry of the polymerization reactions;
- the composition of the polymeric chain;
- polymerization mechanism.

Following the polymerization mechanism, these reactions are classified in two categories: stepwise polymerizations and chain-growth polymerizations [4].

The free-radical polymerization process is a chain-growth polymerization, where the polymer chains grow in dimension in a short time, the life time of a live molecule being of the order of magnitude of seconds. This type of polymerization needs an active center. The deactivation of the polymeric chain proceeds by a termination reaction. The mean polymerization degree is strictly related to the ratio between the frequencies of addition steps and termination steps.

In chain-growth polymerization, monomers can only join active chains. Monomers contain carbon-carbon double bonds (e.g., ethylene, propylene, styrene, vinyl chloride, butadiene, esters of (meth)acrylic acid). The activity of the chain is generated by either a catalyst or an initiator. Several classes of chain-growth polymerizations can be distinguished according to the type of active center [3]:

- Coordination polymerization (active center is an active site of a catalyst);
- Free-radical polymerization (active center is a radical);

- Anionic polymerization (active center is an anion);
- Cationic polymerization (active center is a cation);

The different polymerization classes discussed above can be implemented in several ways: bulk polymerization, solution polymerization, gas-phase polymerization, slurry polymerization, suspension polymerization and emulsion polymerization. In bulk polymerization, the only components of the formulation are monomers and the catalyst or initiator. The main advantages of bulk polymerization are that a very pure polymer is produced at a high production rate per unit volume of the reactor. The drawback is that the removal of the polymerization heat is difficult because of the high viscosity of the reaction mixture associated with the high concentration of polymer. The thermal control of the reactor is more difficult in free-radical polymerization than in step-growth polymerization. The reason is that higher molecular weights are achieved in free-radical polymerization, and hence the viscosity is higher and the heat removal rate lower [3].

The thermal control of the reactor is much easier if the monomer is polymerized in solution. The solvent lowers the monomer concentration, and consequently the heat generation rate per unit volume of the reactor. In addition, the lower viscosity allows a higher heat removal rate and the solvent allows for the use of reflux condensers [3].

A way of achieving good thermal control and avoiding the use of solvents is to use suspension polymerization. In this process, drops of monomer containing the initiator are suspended in water. Each of the droplets acts as a small bulk polymerization reactor. Although the internal viscosity of the droplet increases with monomer conversion, the viscosity of the suspension remains low allowing a good heat transfer. Suspension stability and particle size are controlled by the agitation intensity as well as by the type and concentration of the suspension agents used.

Emulsion polymerization is a polymerization technique leading to polymer finely dispersed (particle diameters usually ranging from 80 to 500 nm) in a continuous medium (most often water). This product is frequently called latex. Only free-radical polymerization has been commercially implemented in emulsion polymerization [3].

The thermal control of this process is easier than for bulk polymerization. However, it is not trivial as the modest viscosity of the reaction medium and the presence of a high heat capacity continuous medium (water) are counteracted by the fast polymerization rate.

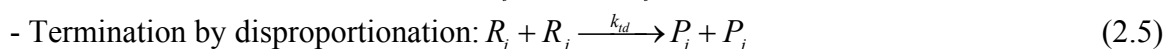
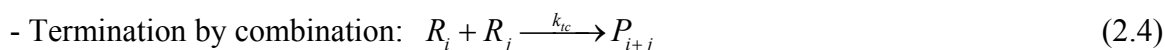
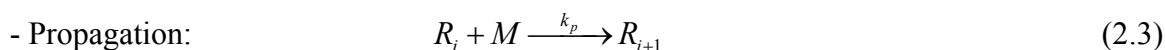
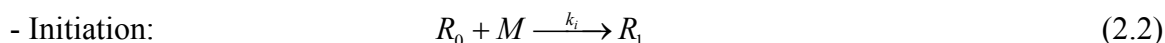
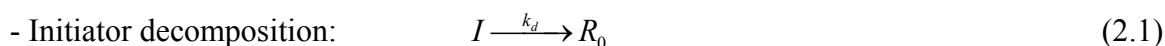
2.1.3. Mechanism and kinetics of the free radical polymerization

Due to the high complexity of the polymerization process, their kinetic models are based on simplification hypothesis, necessary in order to reduce the calculation volume and also to have results that can be practically verified.

The main objective of a polymerization process is to achieve higher monomer conversion possible and to produce a polymer with desired molecular weight and molecular weights distribution. In order to formulate a kinetic model for a certain process, firstly it is necessary to know the variables that could be practically measured. When one deals with polymerizations, one has to take into account as measurable variables the monomer conversion and also the polymer properties (degree of polymerization and the distributions of polymerization degrees).

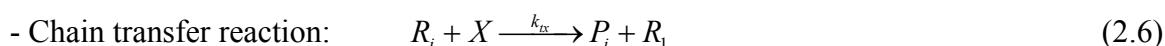
Kinetic mechanism of free radical polymerization [4, 5]

The kinetics of free radical polymerization is the best known among all the polymerization mechanisms. The basic steps for all free-radical polymerizations are: initiation, propagation and termination. The initiation is composed of two successive distinct elementary steps, initiator decomposition and polymeric chain initiation. The general scheme describing this mechanism consists of the following steps:



Where I – initiator molecule; R_i ($i = 1..∞$) – free radicals (live polymer) molecules of length “i”; P_i ($i = 1..∞$) – dead polymer molecules of length “i”; M – monomer molecules;

A more complex mechanism takes into account the side reactions of chain transfer to monomer, to chain transfer agents or to solvent (solution polymerization). There are cases where the chain transfer side reactions are not desired because they are source of small molecular weights polymers, but there could be also desired when we intend to obtain a polymer with desired molecular weights (it is necessary a well chosen chain transfer agent to control the process). The chain transfer reaction could be written as:



In relation (2.6) X could be a molecule of monomer, solvent or a chemical compound used as a chain transfer agent. When X is a polymeric chain, there are obtained macromolecules with ramifications and high molecular weights.

The total concentration of the free-radicals, in the reaction sequence (2.1) - (2.6), is in the range of $10^{-9} - 10^{-5}$ mole/L for commercial implemented polymerization processes. The free radicals are generated by different methods. The most used is the chemical way, using azoic or

peroxide compounds in small concentrations (< 1 % wt). For example, the organic peroxides are thermally decomposed by cleavage of the O – O chemical liaison. The efficiency of the initiator is usually in the range 0.2 – 1 [6]. The principal cause of losing initiator efficiency is the so called cage effect. At the initiator decomposition, the primary radicals are one in the vicinity of the others a time of $10^{-10} - 10^{-9}$ s. In this interval, the radicals are walled by solvent molecules among which they have to diffuse to initiate the polymerization reaction. The other ways to initiate a polymerization reaction are thermally, UV radiations, high energy electron beam or gamma radiations.

The propagation reaction (2.3) controls the rate of growth of the polymeric chain and its structure. In free radical polymerization the microstructure of the polymeric chain is not influenced by the initiation reaction mechanism and the initiator type. The termination reactions (combination and disproportionation) take place simultaneously and their importance depends on the monomer type and polymerization temperature. In the styrene polymerization, for instance, the termination by combination is predominant on a certain temperature range. For the methyl methacrylate polymerization, both terminations are important at small temperature, whereas at high temperatures the termination by disproportionation is predominant.

At high monomer conversions, when the circulation of the radicals is hindered due to the high reaction mixture viscosity, the active centers can continue to move and to produce bimolecular termination reactions. So, the termination rate is independent of the length of the polymeric chain. Recently it was demonstrated that the bimolecular termination can be diffusion controlled also at small monomer conversions [4].

Table 2.1. Kinetic mechanism for free-radical solution polymerization process

Polymerization step	Elementary chemical reaction	Rate expression
Initiation	$I + M \xrightarrow{k_i} R_1$	$v_i = k_i c_I c_M$
Propagation	$R_i + M \xrightarrow{k_p} R_{i+1}$	$v_p = k_p c_M c_{R_i}$
Chain termination by combination	$R_i + R_j \xrightarrow{k_{tc}} P_{i+j}$	$v_{tc} = k_{tc} c_{R_i} c_{R_j}$
Chain termination by disproportionation	$R_i + R_j \xrightarrow{k_{td}} P_i + P_j$	$v_{td} = k_{td} c_{R_i} c_{R_j}$
Chain transfer to monomer	$R_i + M \xrightarrow{k_{tm}} P_i + R_1$	$v_{tm} = k_{tm} c_M c_{R_i}$
Chain transfer to solvent	$R_i + S \xrightarrow{k_{ts}} P_i + R_1$	$v_{ts} = k_{ts} c_S c_{R_i}$

The chain transfer reactions affect only the degree of polymerization without affecting the polymerization rate. The kinetic constants for chain transfer reactions with monomer are $10^4 - 10^5$ times smaller than propagation constants. High values for these constants are achieved when the propagation radicals have very high energies (high reactivity) as is the case for ethyl-

ene, vinyl acetate and vinyl chloride polymerizations.

Based on the elementary steps (2.1) - (2.6), and considering only monomer and solvent as involved chain transfer species, the rate expressions for a free-radical solution polymerization are presented in Table 2.1. The overall chain termination constant is defined as the summation of the termination by combination and disproportionation rate constants, $k_t = k_{tc} + k_{td}$.

Hypotheses used for the kinetic modeling of polymerization reactions

Regarding the reactants depletion, the limitative reactant could be the monomer (as in majority of the cases) or the initiator (so called “dead – end”). A complex polymerization reaction concerns elementary steps and there are involved chemical species with high and low molecular weights. The reactivity of the macromolecules is given by the end groups or the active intermediates (free-radicals, ions, catalytic complexes). In the most cases it is applied the principle of equal reactivity which is stating that the reactivity of a polymeric chain is given only by its end groups and it is independent of the chain length. In that case we can use a single kinetic constant for all the propagation elementary steps. The other simplifications that could be used are the QSSA (quasi steady state assumption) and long chains approximation. The long chains approximation is based on the hypothesis that the monomer is consumed predominantly to produce polymers in the propagation step. The validity of this approximation could be confirmed studying the degree of polymerization, that in the case of the invalidation is relatively small [6].

Most of the polymerization reactions sequence involve active intermediary (free-radicals, ionic radicals, catalyst radicals). A characteristic of the chain reactions is a small concentration of active species all long the process (a typical value for the free-radical polymerization is 10^{-8} mole/L) [6]. A problem that is raised is the validity of the QSSA in situations of practical interest (high variations in kinetic constants, high rates of initiator consumption, hindered termination reactions, non-uniformities in temperature profiles).

It is also accepted that the rates expressions valid for QSSA applied to close systems are also valid for continuous reactors. It is proven that QSSA can be applied without significant errors when the life time of the active species is much shorter than the residence time of the reaction mixture in the reactor (i.e. free-radical polymerization).

Another approximation frequently used in the polymerization modeling is the constant density and viscosity of the reaction mixture [5-8]. This represents simplified approaches and, when more accurate results are desired, it is necessary to develop realistic viscosity models for the studied polymerization processes.

Relations for polymer characteristics

The distribution of chain lengths within a polymeric material may well be the most important factor in determining its end-use properties. Therefore, it will be necessary to develop a method of describing the distribution of chain lengths in a polymeric material [7]. This distribution is generally characterized by the density of distribution (differential distribution). There are several forms of differential distribution, depending on whether distributed variable is the degree of polymerization or the molar mass, and depending on whether distribution is considered in number or as a whole. The majority of the authors use distribution in number of the degrees of polymerization defined by P_i , concentration of the polymer to the degree of polymerization i (i-mer). As differential complete distribution is rather difficult to measure, polymers are characterized by the mean molecular weights. Most often used are number average molecular weights, \overline{M}_n , and weight-average molecular weight, \overline{M}_w [8]. Denoting by M_i the molecular weight of an i -mer and P_i its concentration, the definition of \overline{M}_n is:

$$\overline{M}_n = \frac{\sum_{i=1}^{\infty} M_i P_i}{\sum_{i=1}^{\infty} P_i} = \sum_{i=1}^{\infty} M_i \frac{P_i}{\sum_{i=1}^{\infty} P_i} \quad (2.7)$$

Knowing that $M_i = M_m i$ (M_m the molecular weight of the monomer) we can write:

$$\overline{M}_n = \frac{\sum_{i=1}^{\infty} M_m i P_i}{\sum_{i=1}^{\infty} P_i} = M_m \frac{\sum_{i=1}^{\infty} i P_i}{\sum_{i=1}^{\infty} P_i} = M_m \overline{r}_n \quad (2.8)$$

With \overline{r}_n - the number average degree of polymerization.

Similarly, the weight average molecular weight is defined:

$$\overline{M}_w = \sum_{i=1}^{\infty} (\text{molecular weight of } i\text{-mer})(\text{weight fraction of } i\text{-mer}) \quad (2.9)$$

$$\overline{M}_w = \sum_{i=1}^{\infty} M_i \frac{M_i P_i}{\sum_{i=1}^{\infty} M_i P_i} = \frac{\sum_{i=1}^{\infty} M_i^2 P_i}{\sum_{i=1}^{\infty} M_i P_i} = \frac{\sum_{i=1}^{\infty} M_m^2 i^2 P_i}{\sum_{i=1}^{\infty} M_m i P_i} = M_m \frac{\sum_{i=1}^{\infty} i^2 P_i}{\sum_{i=1}^{\infty} i P_i} = M_m \overline{r}_w \quad (2.10)$$

Where \overline{r}_w is the weight average degree of polymerization.

The most used moments in the polymerization modeling are the 0th, 1st and 2nd order moments for concentrations of live and dead polymers calculated by:

$$\begin{aligned}\mu_0 &= \sum_{i=1}^{\infty} P_i; & \mu_1 &= \sum_{i=1}^{\infty} iP_i; & \mu_2 &= \sum_{i=1}^{\infty} i^2 P_i \\ \lambda_0 &= \sum_{i=1}^{\infty} R_i; & \lambda_1 &= \sum_{i=1}^{\infty} iR_i; & \lambda_2 &= \sum_{i=1}^{\infty} i^2 R_i\end{aligned}\tag{2.11}$$

If we consider that in the reaction mixture we have a dead and live polymers, the number and weight average degree of polymerization could be also defined:

$$\bar{r}_n = \frac{\mu_1 + \lambda_1}{\mu_0 + \lambda_0}; \quad \bar{r}_w = \frac{\mu_2 + \lambda_2}{\mu_1 + \lambda_1}\tag{2.12}$$

The structural homogeneity of the polymer mixture is usually characterized by the polydispersion index, defined as the ratio of the two degrees of polymerization:

$$IP = \frac{\bar{r}_w}{\bar{r}_n}\tag{2.13}$$

2.1.4. Methyl methacrylate polymerization

The acrylic acid and acrylate esters are known since the middle of the 19th century. A review of acrylate esters was published in 1901 by H. Von Pechmann and O. Rohm [4, 9]. An industrial production process of acrylates was developed in 1928 by W. Bauer [10]. Solution polymers were produced from methyl methacrylate since 1927 by Rohm and Haas (Germany). Emulsion polymers were first developed on an industrial scale in 1929 - 1930 by H. Fikentscher, and were introduced on the market by BASF as a polymer dispersion named "Corialgrund" for the surface finishing of leather [4].

Acrylates can be polymerized extremely easily because their carboxyl groups are adjacent to a vinyl group. Polyacrylates are produced almost exclusively by radical polymerization; conventional radical formers (e.g., peroxides and other per compounds) or azo starters are used as initiators. Polymerization can also be initiated photochemically, by γ -rays, or by electron beams. Although ionic (particularly anionic) polymerization is possible, this process is not used industrially. The heat of reaction in the exothermic polymerization of acrylates is cca. 60 – 80 kJ/mol, and must be removed if the process is to be controlled effectively [4].

Several general disadvantages of bulk polymerization (removal of the reaction heat, insolubility of the resulting polymer in the monomer, side reactions in highly viscous systems such as the Trommsdorff effect or chain transfer with polymer) are responsible for the fact that many polymerization processes are carried out in the presence of a solvent [9].

Acrylates are polymerized as solutions in organic solvents [12-18] if the user wishes to exploit specific properties of polymers in dissolved form (e.g., low molecular mass, good flow

behavior, and homogeneous film formation after drying in paints or adhesives). Aromatic hydrocarbons such as benzene and toluene [12-18] can be used as solvents for the polymerization of acrylates of long-chain alcohols; esters (i. e. ethyl acetate [11, 12]) and ketones can be used for acrylates of short-chain alcohols [4].

Gel effect models for MMA free radical polymerization

At low monomer conversions, the viscosity of the reaction mixture is low, and the rate of reaction is controlled by the segmental diffusion (internal reorientation of the polymer chains required to bring the chains together for the polymerization take place) [3, 13]. In this stage of the process, the termination rate have relatively high values (order of magnitude $10^8 \text{ L mol}^{-1} \text{ s}^{-1}$ or higher). However, the viscosity of the reaction mixture increases rapidly with the monomer conversion (polymer concentration) and the rate at which two polymer chains encounter each other is slower than in the segmental reorientation. Consequently, the polymerization kinetics is controlled by the low frequency of reciprocal collisions of live chains through the mixtures of dead polymers. As known, the translational diffusion is affected both by chain length of the reacting polymers and the system viscosity [3].

At high monomer conversions, the system becomes so viscous that the polymers size increases more quickly due to propagation than by reciprocal combinations (due to the resistance opposed by reaction mixture to polymer diffusion). The diffusional limitations of the live and polymer dynamics, with strong effects on the propagation as well as termination rates (lowering its values) are called gel effect (or Trommsdorff effect).

Modeling the gel effect presents significant difficulties, due to the particularities of the phenomenon. As specified, its influence becomes important at high monomer conversions, particularly for bulk polymerization. However it can be significant also for solution polymerization, at high monomer to solvent ratios.

Free radical solution polymerization of MMA follows the mechanism presented in the previous paragraph. The considerable increase in the polymerization rate and in the average chain length at intermediate conversions is a phenomenon common to many monomers undergoing free radical polymerization [14]. The termination rate depends on the polymerization temperature, the mobility of the polymeric chains (diffusion), the molecular weights of the involved species and the composition of the reaction mixture.

During the last decades, several studies have been devoted to develop an isothermal diffusion-controlled model for the free radical polymerization of methyl-methacrylate (MMA).

The existing models can be separated into three groups: mechanistic, semi-empirical, and

fully empirical. Mechanistic models, developed during the middle to late seventies period, focused mainly on reptation theory (developed to explain the dynamics of entangled molecules in a network of fixed obstacles) and scaling concepts [15] while the semi-empirical models made use of many different variations on free volume theory [13].

Chiu, Carratt, and Soong developed a model (the CCS approach) based on the Fujita-Doolittle free volume theory [13]. This model was adopted by many researchers. It has been accepted by the International Union of Pure and Applied Chemistry [14]. The model allows the calculation of propagation and termination rate constants for free radical polymerization. Both diffusion and classical kinetics are considered from the start of the reaction. The effect of diffusion on overall termination rate constant (k_t) gradually increases with conversion and becomes dominant as auto-acceleration becomes more pronounced. This eliminates the need for the use of critical breakpoints and sudden introduction of diffusion effects [14]. Following the analysis of Chiu et al [13], the apparent termination rate constant can be expressed:

$$\frac{1}{k_t} = \frac{1}{k_{t,0}} + \frac{r_t^2 \lambda_0}{3D_{ef}} \quad (2.14)$$

D_{ef} is evaluated by the Fujita-Doolittle free volume theory as follows:

$$D_{ef} = D_0 \exp\left(\frac{2.3\phi_m}{A+B\phi_m}\right) \quad (2.15)$$

Where: $k_{t,0}$ is the termination rate constant at zero monomer conversion; λ_0 - the total polymer radical concentration; ϕ_m - the monomer volume fraction; A, B - adjustable parameters; D_0 - the diffusion coefficient at the limit of vanishing ϕ_m .

The relations for overall termination constant are:

$$\frac{1}{k_t} = \frac{1}{k_{t,0}} + \theta_t(T, c_{t,0}) \frac{\lambda_0}{\exp\left(\frac{2.3\phi_m}{A+B\phi_m}\right)} \quad (2.16)$$

The overall propagation reaction is given by:

$$\frac{1}{k_p} = \frac{1}{k_{p,0}} + \theta_p(T) \frac{\lambda_0}{\exp\left(\frac{2.3\phi_m}{A+B\phi_m}\right)} \quad (2.17)$$

$\theta_t = \frac{r_t^3}{3D_{ef}}$ has dimensions of time, and can be viewed as a characteristic migration time of the growing radicals, while θ_t is the characteristic monomer diffusion time, and is only a function of temperature.

The global rate constants for termination and propagation defined by these equations are calculated as the contributions of a purely chemical kinetic constant (the first term on the right hand side of both equations) and a purely diffusional one respectively (the second term on the right hand side of both equations). A and B are also treated as adjustable parameters and can be derived from experimental data. In addition, in the cited study of Chiu [20], θ_t was found by fitting experimental data which only considered AIBN as the initiator.

With other initiators, the kinetics will affect how the chain length varies with initiator loading. Therefore the correlation is not valid for other polymer/initiator systems [14].

Expressions for overall termination and propagation reactions were derived by Baillagou and Soong [16, 17] based on the kinetic data of Chiu et al [13]. The expressions (2.16) - (2.17) are rewritten as:

$$k_t = \frac{k_{t_0}}{1 + \frac{k_{t_0} \theta_t \lambda_0}{D_{ef}}}; \quad k_p = \frac{k_{p_0}}{1 + \frac{k_{p_0} \theta_p \lambda_0}{D_{ef}}} \quad (2.18)$$

Chiu et al [13] proposed a constant value of 0.03 for parameter B (expression (2.17)), because it was found to be relatively insensitive to the working conditions.

Also, the parameter A was determined from experimental data and is given by the expression:

$$A = 0.168 - 8.21 \cdot 10^{-6} (T - T_{gp})^2, \quad (2.19)$$

where $T_g = 114$ °C is the glass transition temperature for the polymer.

The gel-effect model of Chiu, Carrat and Soong are presented in a condensed mode in Table 2.2. The gel-effect model published by Fleury and reviewed by Nising [18] is an approach based on the model published by Chiu, Carrat and Soong. The aim of Fleury was to linearize the expression (2.16) of the apparent termination rate constant. The model is a good example of a semi-empirical approach adapted to the experimental conditions. The equation (2.16) was modified as:

$$\frac{1}{k_t} = \frac{1}{k_{t_0}} + \frac{1}{\exp(\alpha - \beta \times X)} \quad (2.20)$$

Table 2.2. Gel effect constitutive equations proposed by Chiu, Carrat and Soong [13, 16]

$$k_t = \frac{k_{t,0}}{1 + \frac{k_{t,0}\theta_t\lambda_0}{D_{ef}}} \quad k_p = \frac{k_{p,0}}{1 + \frac{k_{p,0}\theta_p\lambda_0}{D_{ef}}} \quad ; D_{ef} = D_0 \exp\left(\frac{2.3\phi_m}{A + B\phi_m}\right)$$

$$\theta_t = \frac{1}{4.4533 \times 10^{18} c_{I,0} \exp\left(-\frac{17413}{T}\right)}$$

$$\theta_p = \frac{1}{2.5292 \times 10^{15} \exp\left(-\frac{14092}{T}\right)}$$

$$A = 0.168 - 8.21 \times 10^{-6} (T - T_{gp})^2 ; B = 0.03$$

In equation (2.20) X is the monomer conversion and α, β adjustable parameters based on the experimental data. Fleury fitted these parameters to high-temperature (135°-165°C) batch experiments and found the following dependences on temperature, solvent fraction (w_s) and initiator concentration ($C_{I,0}$):

$$\alpha = \alpha_0 - 10.9 \times w_s + \ln\left(\frac{c_{I,0}}{c_{I,0\min}}\right)^{0.56} \quad (2.21)$$

$$\beta = \beta_0 - \frac{T - T_0}{T_{ref} - T_g} - 38.3 \times w_s + 2.32 \times \left[1 - \exp\left(-\frac{c_{I,0} / c_{I,0\min}}{3.34}\right)\right] \quad (2.22)$$

with .

The gel-effect model presented above is valid in the following range: 135°C < T < 165°C, $0 < w_s < 0.2$ and $2 \text{ mol} \times \text{m}^{-3} < c_{I,0} < 200 \text{ mol} \times \text{m}^{-3}$.

The main weakness of the Fleury model was that the author didn't take into account the influence of a chain transfer agent. This weakness was corrected by Fenouillot et al [19]. They eliminated the solvent concentration and introduced the CTA concentration in the description of gel effect. This model needs an initial concentration of CTA (instead of initiator concentration) as fixed parameter. The equations that describe the gel-effect model are:

$$\frac{1}{k_t} = \frac{1}{k_{t,0}} + \frac{1}{k_{t,0} \times \exp[\beta \times (X_c - X)]}, \text{ with } X_c = \frac{\alpha - \ln k_{t,0}}{\beta} \quad (2.23)$$

The Fenouillot parameters used in relation (2.23) are:

$$\beta = -17.85 + 0.5756 \times T - 0.002519 \times T^2$$

$$X_c = 4.289 - 0.5799 \times T + 2.0422 \times 10^{-4} \times T^2 + 0.11 \times \ln(1000 \cdot C_{CTA,0} + 3) \quad (2.24)$$

The gel effect model of Tefera et al [21, 22] considered that the apparent termination rate

constant is governed by three mechanisms: the segmental diffusion, at the early polymerization stages, the translational diffusion at intermediate conversions and the reaction diffusion taking place through the whole reaction. The model is based on the free volume theory and one of its advantages is inclusion of the molecular weight dependence. The model was reported to work in polymerization systems with CTA agents.

Published kinetic models for MMA polymerization in solution

The kinetics of the MMA polymerization process in solution was investigated in an important number of experimental and theoretical studies, proposing their own kinetic models. The temperature dependences of reaction rate constants involved in the rate expressions presented in Table 2.1 were also investigated in a significant number of published works.

The expressions for the rate constants proposed by different authors are presented in Table 2.4 and the working conditions corresponding to these kinetic studies are presented in Table 2.3.

2.1.5. Mathematical models for tubular MMA polymerization reactor

Plug flow reactor model

The plug flow reactor becomes a viable alternative in polymer processing when it is desired to exploit the kinetic advantages of the batch reactors (high conversions) and the operational advantages of continuous processing (easy operation, lack of batch-to-batch variability). Tubular reactors (approximating plug flow characteristics) are applicable in high-volume polymerizations and exhibit excellent heat transfer capabilities [7].

The mass balance equation for a species X in a plug-flow polymerization reactor could be written as:

$$\frac{d(u_z c_x)}{dz} = r_x \quad (2.25)$$

Where u_z is the velocity of the reactor mixture. In expression (2.25) the index x can denote initiator (I), monomer (M), radical concentrations distribution moments ($\lambda_i, i = 0..2$) or polymers concentrations distribution moments ($\mu_i, i = 0..2$).

The consumption rates, r_x , for MMA solution polymerization can be determined based on the kinetic scheme in Table 2.1. In this case the density variation of the reaction mixture was taken into account. Such a model was implemented by Ahn et al [20], Chang et al [21, 22].

When no density variations are taken into account, the equations (2.25) are simplified to:

$$\frac{dc_x}{dt} = r_x, \quad t = \frac{z}{u_z} \quad (2.26)$$

This type of ideal model was implemented by Baillagou et Soong [16, 17], Ponnuswamy et al [23] and Crowley et Choi [24, 25].

In paragraph 2.1.3 it is shown that balance equations for all species appearing in the reaction mixture, for free-radical polymerization, gives an infinite number of differential equations highly nonlinear, difficult to solve. The usual characterization of the free radical concentrations in the mixture is based on the method of moments, a method based on algebraic combinations between the balance equations for radicals [17]. In what follows, will be presented the deduction of the balance equations for chemical species and the equations giving moments evolutions along the reactor in the hypothesis of plug flow of reaction mixture.

Table 2.3. Working conditions for MMA solution polymerization studies

N ^o	Publication	Solvent	Initiator type/initiator efficiency	Gel effect	T, °C	Initiator and monomer conc	Reaction time, min
1	Baillagou & Soong [16, 17]	Toluene	AIBN f = 0.58	Yes	70-100	18 % wt solvent 5 m reactor with 1 cm radius	30 – tubular reactor
2	Ponnuswamy et al [23]	Toluene	AIBN f = 0.58	No	70	m _M =3.492 kg m _S =5.239 kg m _I =0.082 kg (0.05 mol/L)	~135
3	Chang & Lai [21]	Toluene	AIBN f = 0.58	Yes	70	m _M =1.71 kg m _S =2.565 kg m _I = 3.78E-4 kg (0.05 mol/L)	300 – 500
4	Scali et al [11]	Ethyl acetate	AIBN f = 0.58	Yes	70	c _{M0} /c _{I0} =400	70
5	Crowley & Choi, [24]	Ethyl acetate	AIBN f=0.1996 ; 0.2055	Yes	50-70	w _M =0.5% vol w _S =0.5% vol I = 0.046 mole/L V = 4 L	350
6	Ahn et al [20]	Ethyl acetate	BPO f=1	Yes	70	v _M =8 L v _S = 8 L v _I = 8 g	~135
7	Chang & Liao [22]	Toluene	AIBN f=0.58	No	70	m _M =3.492 kg m _S =5.239 kg m _I =0.082 kg (0.05 mole/L)	150
8	Kiparissides et al. [26]	-	AIBN f = 0.58	Yes	-	m _M = 1.1 kg m _I = 4E-3 kg V = 1.2E-3 m ³	120-200

The initiator dissociation is expressed by the reaction



and the balance equation for the initiator is:

$$u_z \frac{dC_I}{dz} = -k_d C_I \quad (2.28)$$

The monomer consumption takes place in initiation, propagation and chain transfer to monomer elementary steps. Generally, the published studies are stating that the monomer is mostly consumed in the propagation step, although some authors consider also the chain transfer to monomer responsible for this process [16]. In the last approach, the monomer balance equation is of the form:

$$u_z \frac{dC_M}{dz} = -(k_p + k_{tm}) C_M \sum_{i=1}^{\infty} R_i \quad (2.29)$$

In order to develop the equations describing the distribution moments of live and dead polymer a polymerization mechanism involving chain transfer to monomer and solvent, as well as terminations by combination and disproportionation will be considered.

As it was shown above, the sum of radical concentrations represents the 0th order moment for radical concentrations distribution (relations(2.11)), so that equation (2.29) becomes:

$$u_z \frac{dC_M}{dz} = -(k_p + k_{tm}) C_M \lambda_0 \quad (2.30)$$

The balance equation for first order live polymer has the form:

$$u_z \frac{dR_1}{dz} = 2fk_d C_I + k_{tm} c_M \sum_{j=2}^{\infty} R_j + k_{ts} c_S \sum_{j=2}^{\infty} R_j - k_p c_M R_1 - k_t R_1 \sum_{j=1}^{\infty} R_j \quad (2.31)$$

and that for every radical, R_i , is:

$$u_z \frac{dR_i}{dz} = k_p c_M R_{i-1} - k_p c_M R_i - k_{tp} c_P R_i - k_{ts} c_S R_i - k_t R_i \left(\sum_{j=1}^{\infty} R_j \right) \quad (2.32)$$

The axial variation of 0th moment can be obtained by the summation of the equations (2.32) for all R_i . The equation becomes:

$$\begin{aligned} u_z \sum_i \left(\frac{dR_i}{dz} \right) &= 2fk_d C_I - k_t \left(\sum_i R_i \right) \left(\sum_1 R_j \right) \\ u_z \frac{d\lambda_0}{dz} &= 2fk_d C_I - k_t \lambda_0^2 \end{aligned} \quad (2.33)$$

Table 2.4. The Arrhenius expressions for the kinetic constants proposed by different authors

N ^o	Publication	Kinetic constants expressions					
		Initiation ^{a)}	Propagation ^{a)}	Transfer to monomer ^{a)}	Transfer to solvent ^{a)}	Termination ratio	Termination ^{a)}
1	Baillagou & Soong [16, 17]	$k_d = 6.32 \cdot 10^{16} \exp\left(-\frac{30660}{R \cdot T}\right)$	$k_p = 2.95 \cdot 10^7 \exp\left(-\frac{4350}{R \cdot T}\right)$	$\frac{k_{tm}}{k_p} = 9.48 \cdot 10^3 \exp\left(-\frac{13380}{R \cdot T}\right)$	$\frac{k_{ts}}{k_p} = 1.01 \cdot 10^3 \exp\left(-\frac{11400}{R \cdot T}\right)$	$\frac{k_{tc}}{k_{td}} = 3.956 \cdot 10^{-4} \exp\left(\frac{4090}{R \cdot T}\right)$	$k_t = 5.88 \cdot 10^9 \exp\left(-\frac{701}{R \cdot T}\right)$
2	Ponnuwamy et al. [23]	$k_d = 60 \cdot 3.75 \cdot 10^{16} \exp\left(-\frac{33740}{R \cdot T}\right)$	$k_p = 60 \cdot 1.20 \cdot 10^9 \exp\left(-\frac{9630}{R \cdot T}\right)$	$k_{tm} = 60 \cdot 3.88 \cdot 10^{14} \exp\left(-\frac{27603}{R \cdot T}\right)$	$k_{ts} = 60 \cdot 4.41 \cdot 10^{20} \exp\left(-\frac{34443}{R \cdot T}\right)$	$\frac{k_{tc}}{k_{td}} = 1$	$k_t = 60 \cdot 2.113 \cdot 10^8 \exp\left(-\frac{1014}{R \cdot T}\right)$
3	Chang & Lai [21]	$k_d = 60 \cdot 1.053 \cdot 10^{15} \exp\left(-\frac{26640}{R \cdot T}\right)$	$k_p = 60 \cdot 4.917 \cdot 10^5 \exp\left(-\frac{3781}{R \cdot T}\right)$	$\frac{k_{tm}}{k_p} = 9.48 \cdot 10^3 \exp\left(-\frac{11630}{R \cdot T}\right)$	$\frac{k_{ts}}{k_p} = 1.01 \cdot 10^3 \exp\left(-\frac{9908}{R \cdot T}\right)$	$\frac{k_{tc}}{k_{td}} = 3.956 \cdot 10^{-3} \exp\left(\frac{3554.8}{R \cdot T}\right)$	$k_t = 60 \cdot 9.8 \cdot 10^7 \exp\left(-\frac{609.2}{R \cdot T}\right)$
4	Scali et al [27]	$k_d = 60 \cdot 1.33 \cdot 10^{15} \exp\left(-\frac{30700}{R \cdot T}\right)$	$k_p = 60 \cdot 4.41 \cdot 10^5 \exp\left(-\frac{4350}{R \cdot T}\right)$	$k_{tm} = 60 \cdot 4.62 \cdot 10^{-2} \exp\left(-\frac{888}{R \cdot T}\right)$	$k_{ts} = 60 \cdot 4.41 \cdot 10^{20} \exp\left(-\frac{34443}{R \cdot T}\right)$	$\frac{k_{tc}}{k_{td}} = 3.956 \cdot 10^{-4} \exp\left(\frac{4090}{R \cdot T}\right)$	$k_t = 60 \cdot 6.50 \cdot 10^7 \exp\left(-\frac{700}{R \cdot T}\right)$
5	Crowley & Choi, [24]	$k_d = 1.14 \cdot 10^{19} \exp\left(-\frac{34277}{R \cdot T}\right)$	$k_p = 4.2 \cdot 10^8 \exp\left(-\frac{6300}{R \cdot T}\right)$	$k_{tm} = 1.74 \cdot 10^{13} \exp\left(-\frac{17957}{R \cdot T}\right)$	$k_{ts} = 6.12 \cdot 10^{10} \exp\left(-\frac{15702}{R \cdot T}\right)$	$k_{td} = 1.06 \cdot 10^{11} \exp\left(-\frac{2800}{R \cdot T}\right)$	$k_t = k_{td}$
6	Ahn et al [20]	$k_d = 60 \cdot 1.25 \cdot 10^{18} \exp\left(-\frac{35473}{R \cdot T}\right)$	$k_p = 60 \cdot 2.94 \cdot 10^6 \exp\left(-\frac{5656}{R \cdot T}\right)$	$\frac{k_{tm}}{k_p} = 9.32 \cdot 10^4 \exp\left(-\frac{13971}{R \cdot T}\right)$	$\frac{k_{ts}}{k_p} = 8.79 \cdot 10^{-5} \exp\left(-\frac{42.6}{R \cdot T}\right)$	$\frac{k_{td}}{k_t} = 1.83 \cdot 10^{27} \exp\left(-\frac{44467}{R \cdot T}\right)$	$k_t = 60 \cdot 5.20 \cdot 10^8 \exp\left(-\frac{1394}{R \cdot T}\right)$
7	Chang & Liao [22]	$k_d = 60 \cdot 9.592 \cdot 10^{15} \exp\left(-\frac{27886.2}{R \cdot T}\right)$	$k_p = 60 \cdot 1.310 \cdot 10^{14} \exp\left(-\frac{14669.8}{R \cdot T}\right)$	$k_{tm} = 60 \cdot 2.886 \cdot 10^1 \exp\left(-\frac{8862.1}{R \cdot T}\right)$	$k_{ts} = 60 \cdot 4.487 \cdot 10^6 \exp\left(-\frac{14152.8}{R \cdot T}\right)$	$\frac{k_{tc}}{k_{td}} = 7.976 \cdot 10^{-12} \exp\left(\frac{12718}{R \cdot T}\right)$	$k_t = 60 \cdot 8.498 \cdot 10^{21} \exp\left(-\frac{18378.3}{R \cdot T}\right)$
8	Kiparissides et al. [26]	$k_d = 6.32 \cdot 10^{16} \exp\left(-\frac{30660}{R \cdot T}\right)$	$k_p = 2.95 \cdot 10^7 \exp\left(-\frac{4350}{R \cdot T}\right)$	$\frac{k_{tm}}{k_p} = 9.48 \cdot 10^3 \exp\left(-\frac{13380}{R \cdot T}\right)$	-	$\frac{k_{tc}}{k_{td}} = 3.956 \cdot 10^{-4} \exp\left(\frac{4090}{R \cdot T}\right)$	$k_t = 5.88 \cdot 10^9 \exp\left(-\frac{701}{R \cdot T}\right)$

a) k_d [min⁻¹], k_p, k_{tm}, k_{ts} [L · min⁻¹ · mole⁻¹]

By multiplying equations (2.31) and (2.32) by the corresponding “i” value for each radical and the summation of the equations so obtained, the equation for 1st distribution moment for live polymer concentrations is obtained:

$$u_z \frac{d\lambda_1}{dz} = 2fk_d C_I + k_p C_M (\lambda_0 - \lambda_1) + (k_{tm} C_M + k_{ts} C_S) (\lambda_0 - \lambda_1) - k_t \lambda_0 \lambda_1 \quad (2.34)$$

Similarly, the equation for 2nd distribution moment for live polymer concentrations can be obtained by multiplying by “i²” the equations (2.32), and summing up the results:

$$u_z \frac{d\lambda_2}{dz} = 2fk_d C_I + k_p C_M (2\lambda_1 + \lambda_0) + (k_{tm} C_M + k_{ts} C_S) (\lambda_0 - \lambda_2) - k_t \lambda_0 \lambda_2 \quad (2.35)$$

The mass balance of the dead polymer can be described by the equation:

$$u_z \frac{dP_i}{dz} = k_{tm} M R_i + k_{ts} S R_i + k_{td} R_i R_j + \frac{k_{tc}}{2} R_i R_{i-j} \quad (2.36)$$

By applying the same procedure the following equation, for the 0th order moment for dead polymers concentrations distribution is obtained:

$$u_z \frac{d\mu_0}{dz} = u_z \sum_{i=1}^{\infty} \frac{dP_i}{dz} = \frac{k_{tc}}{2} \sum_{i=1}^{\infty} \left\{ \sum_{j=1}^{i-1} R_j R_{i-j} \right\} + k_{tm} c_M \sum_{i=1}^{\infty} R_i + k_{td} \left(\sum_{j=1}^{\infty} R_j \right)^2 + k_{ts} c_S \sum_{i=1}^{\infty} R_i \quad (2.37)$$

It can be mathematically proved that:

$$\sum_{i=1}^{\infty} \sum_{j=1}^{i-1} R_j R_{i-j} = \left(\sum_{i=1}^{\infty} R_j \right)^2 \quad (2.38)$$

and equation (2.37) becomes:

$$u_z \frac{d\mu_0}{dz} = k_{tm} c_M \lambda_0 + k_{ts} c_S \lambda_0 + \left(\frac{k_{tc}}{2} + k_{td} \right) \lambda_0^2 \quad (2.39)$$

The equation of 1st order moment for the dead polymer concentrations is:

$$u_z \frac{d \sum_{i=1}^{\infty} (iP_i)}{dz} = u_z \frac{d\mu_1}{dz} = \frac{k_{tc}}{2} \sum_{i=1}^{\infty} i \sum_{j=1}^{i-1} R_j R_{i-j} + k_{tm} c_M \sum_{j=1}^{\infty} i R_j + k_{td} \left(\sum_{j=1}^{\infty} R_j \right) \left(\sum_{j=1}^{\infty} i R_j \right) + k_{ts} c_S \sum_{j=1}^{\infty} i R_j \quad (2.40)$$

$$u_z \frac{d\mu_1}{dz} = k_t \lambda_0 \lambda_1 + k_{tm} c_M \lambda_1 + k_{ts} c_S \lambda_1$$

Equation for the dead polymer concentrations second order moment is:

$$u_z \frac{d \sum_{i=1}^{\infty} (i^2 P_i)}{dz} = u_z \frac{d\mu_2}{dz} = \frac{k_{tc}}{2} \sum_{i=1}^{\infty} i^2 \sum_{j=1}^{i-1} R_j R_{i-j} + k_{tm} c_M \sum_{j=1}^{\infty} i^2 R_j + k_{td} \left(\sum_{j=1}^{\infty} R_j \right) \left(\sum_{j=1}^{\infty} i^2 R_j \right) + k_{ts} c_S \sum_{j=1}^{\infty} i^2 R_j \quad (2.41)$$

Based on the definitions of live polymer distribution moments, it can be mathematically proved that [28]:

$$\sum_{i=1}^{\infty} i^2 \sum_{j=1}^{i-1} R_j R_{i-j} = 2(\lambda_0 \lambda_2 + \lambda_1^2) \quad (2.42)$$

and the equation (2.41) becomes:

$$u_z \frac{d\mu_2}{dz} = \frac{k_{tc}}{2} (2\lambda_0 \lambda_2 + \lambda_1^2) + k_{tm} c_M \lambda_2 + k_{ts} c_S \lambda_2 + k_{td} \lambda_0 \lambda_2 \quad (2.43)$$

The first two moments, μ_0 and μ_1 , denote the concentration of the dead polymer and the total amount of monomer consumed by the dead polymer, respectively. The moments λ_0 and λ_1 have a similar meaning for the growing radical distribution [29]. Taking into account the signification of the distribution's moments, the total monomer consumption will be equal to the sum of dead and live polymer amounts:

$$\mu_1 + \lambda_1 = c_{M_0} - c_M = c_{M_0} X \quad (2.44)$$

Neglecting the contribution of the term λ_1 compared with μ_1 , the 1st order moment for dead polymer distribution could be written in a simplified way:

$$\mu_1 = c_{M_0} X \quad (2.45)$$

Where c_M , c_{M_0} denote the current and initial monomer concentration and X the monomer conversion. To minimize the calculation effort, the equation (2.40) can be replaced in the mass balance with (2.45).

By introducing the QSSA approximation $\left(\frac{d\lambda_i}{dz} = 0 \right)$, the equations (2.33) - (2.35) can be transformed into the algebraic relations:

$$\begin{aligned} \lambda_0 &= \left(\frac{2fk_d c_I}{k_t} \right)^{1/2} \\ \lambda_1 &= \frac{2fk_d c_I + (k_p c_M + k_s c_S + k_m c_M)}{k_m c_M + k_s c_S + k_t \lambda_0} \\ \lambda_2 &= \lambda_1 + \frac{2k_p c_M \lambda_1}{k_m c_M + k_s c_S + k_t \lambda_0} \end{aligned} \quad (2.46)$$

Finally, the simplified mathematical model for the polymerization plug-flow tubular reactor can be written as follows:

$$\frac{dc_I}{dz} = -\frac{k_d c_I}{u_z} \quad (2.47)$$

$$\frac{dc_M}{dz} = -\frac{k_1 c_M c_I^{1/2}}{u_z} \quad (2.48)$$

$$\frac{d\mu_0}{dz} = \frac{k_4 k_d c_I + k_2 c_M c_I^{1/2} + k_3 c_S c_I^{1/2}}{u_z} \quad (2.49)$$

$$\frac{d\mu_2}{dz} = \frac{(k_{ts} c_S + k_{tm} c_M) \lambda_2 + k_t \lambda_0 \lambda_2 + k_{tc} \lambda_1^2}{u_z} \quad (2.50)$$

$$z = 0, c_I = c_{I_0}, c_M = c_{M_0}, \mu_0 = 0, \mu_2 = 0 \quad (2.51)$$

$$\mu_1 = c_{M_0} X_M \quad (2.52)$$

Where:

$$k_1 = k_p \left(\frac{2fk_d}{k_t} \right)^{1/2}; \quad k_2 = k_{tm} \left(\frac{2fk_d}{k_t} \right)^{1/2} \quad (2.53)$$

$$k_3 = k_{ts} \left(\frac{2fk_d}{k_t} \right)^{1/2}; \quad k_4 = 2f \left(1 - \frac{\nu}{2} \right); \quad \nu = \frac{k_{tc}}{k_t} \quad (2.54)$$

Laminar flow reactor model

The description of the flow of reaction mixture in the tubular polymerization reactor by the ideal plug flow model is introducing important simplifications, particularly referring the radial velocity profile. This shortcoming becomes important even for the polymerization in solution, due to the significant increase of viscosity with the polymer concentration and molecular weight. To circumvent this inconvenient, bi-dimensional flow models including radial transport of momentum, mass and heat have to be considered. A flow model in this category is the laminar flow model. One of the challenges in the use of this model is the proper description the velocity profiles. It was underlined the existence of some difficulties in the development of flow models and determination of velocity profiles in the tubular polymerization reactors. In the most simple case, the authors considered constant axial flow velocities with small corrections due to the density changing (Husain et Hamielec [30], Baillagou et Soong [31]) and the radial flow velocities were neglected. Lynn et al [32] showed that the hypothesis of constant radial velocity profile will generate some errors due to the high variations in viscosity of the reaction mixture. Lynn et al also proposed a method to calculate the radial velocity profile. The same method was implemented by other authors (Wyman et Carter [33], Ghosh et al [34], Baillagou et Soong [31]). The study of Baillagou et Soong [17, 18, 32] discussed the situation in which the radial velocity field could be neglected when the ratio length to diameter of the tubular reactor is relatively high.

In what follows, a more realistic mathematical model of the MMA polymerization tubular reactor will be developed based on the laminar flow hypothesis. This is involving the following equations [31, 32, 35]:

a) mass balance of the monomer:

$$u_z \frac{\partial c_M}{\partial z} - D \left(\frac{\partial^2 c_M}{\partial r^2} + \frac{1}{r} \frac{\partial c_M}{\partial r} \right) + r_M = 0 \quad (2.55)$$

With boundary conditions $\frac{\partial c_M}{\partial r} = 0$ at $r = 0, R_0$

b) heat balance:

$$\rho c_p u_z \frac{\partial T}{\partial z} - k \left(\frac{\partial^2 T}{\partial r^2} + \frac{1}{r} \frac{\partial T}{\partial r} \right) - r_T = 0 \quad (2.56)$$

with boundary conditions $\frac{\partial T}{\partial r} = 0$ at $r = 0$ and $\frac{\partial T}{\partial r} = \frac{U(T - T_b)}{k}$ at $r = R_0$

u_z – axial velocity, m/s;

D – monomer diffusion coefficient, m²/s;

k – thermal diffusion coefficient, m²/s;

U – total heat transfer coefficient, W m⁻² K⁻¹;

T_b – thermal agent temperature in the jacket, °C;

In the development of these balance equations, the radial velocities, the axial diffusion coefficient and axial heat conductivity were neglected. By neglecting also the radial pressure gradient, the following expressions can be obtained for fluid velocity and pressure gradient on axial direction [35]:

$$u_z(r) = -\frac{1}{2} \frac{dP}{dz} \int_r^R \frac{r}{\eta} dr \quad (2.57)$$

$$\frac{dP}{dz} = \frac{-Q_m}{\pi \int_0^R \rho r \left(\int_r^R \frac{r}{\eta} dr \right) dr} \quad (2.58)$$

where Q_m is the total mass flow rate.

As seen, these equations are assuming that physical properties (density, viscosity) of the reaction mixture and radial transport parameters D and k are known or calculable in each point of reaction space. The fluid inside the reactor was considered to have Newtonian behavior.

In addition to monomer and heat balance equations (2.55) and (2.56) the model includes the initiator balance equation, and distribution moments for live radicals and dead polymers concentrations:

$$\frac{\partial c_I}{\partial z} = -\frac{c_I}{u_z} \frac{\partial u_z}{\partial z} + \frac{1}{u_z} \left(\frac{D}{r} \frac{\partial c_I}{\partial r} + D \frac{\partial^2 c_I}{\partial r^2} \right) + \frac{r_I}{u_z} \quad (2.59)$$

$$\frac{\partial \lambda_m}{\partial z} = -\frac{\lambda_m}{u_z} \frac{\partial u_z}{\partial z} + \frac{1}{u_z} \left(\frac{D}{r} \frac{\partial \lambda_m}{\partial r} + D \frac{\partial^2 \lambda_m}{\partial r^2} \right) + \frac{r_{\lambda_m}}{u_z}, \quad m=0..2 \quad (2.60)$$

$$\frac{\partial \mu_m}{\partial z} = -\frac{\mu_m}{u_z} \frac{\partial u_z}{\partial z} + \frac{1}{u_z} \left(\frac{D}{r} \frac{\partial \mu_m}{\partial r} + D \frac{\partial^2 \mu_m}{\partial r^2} \right) + \frac{r_{\mu_m}}{u_z}, \quad m=0..2 \quad (2.61)$$

Where r_x (x denoting initiator (I), monomer (M), and 0th 1st and 2nd order moments for radicals and polymer concentrations distribution) are the consumption rates for all species presents in the reaction mixture, calculated by:

$$r_i = -k_d c_I \quad (2.62)$$

$$r_M = -k_t c_I c_M - (k_p + k_{tm}) \lambda_0 c_M \quad (2.63)$$

$$r_{\lambda_0} = 2fk_d c_I - k_t \lambda_0^2 \quad (2.64)$$

$$r_{\lambda_1} = 2fk_d c_I + k_p c_M \lambda_0 + (k_{tm} c_M + k_{ts} c_S)(\lambda_0 - \lambda_1) - k_t \lambda_0 \lambda_1 \quad (2.65)$$

$$r_{\lambda_2} = 2fk_d c_I + 2k_p c_M \lambda_1 + k_p c_M \lambda_0 + (k_{tm} c_M + k_{ts} c_S)(\lambda_0 - \lambda_2) - k_t \lambda_0 \lambda_2 \quad (2.66)$$

$$r_{\mu_0} = (k_{tm} c_M + k_{ts} c_S) \lambda_0 + k_{td} \lambda_0^2 + \frac{k_{tc}}{2} \lambda_0^2 \quad (2.67)$$

$$r_{\mu_1} = (k_{tm} c_M + k_{ts} c_S) \lambda_1 + k_t \lambda_0 \lambda_1 \quad (2.68)$$

$$r_{\mu_2} = (k_{tm} c_M + k_{ts} c_S) \lambda_1 + k_t \lambda_0 \lambda_2 + k_{tc} \lambda_1^2 \quad (2.69)$$

2.1.6. Optimization of tubular polymerization reactors

The control of polymerization processes has as objective to provide a final product with maximum productivity and specified characteristics. In order to obtain a polymer product with given properties, the polymerization process parameters have to be kept under a tight control, allowing them to vary only in close limits.

One of the first optimization studies of polymerization processes was performed by Hicks and Ray [36]. They calculated the optimal temperature policy necessary to control the number-average chain length. Sacks et al [37] employed the Minimum Principle to calculate the optimal initiator addition policy to achieve a predetermined conversion and number-average molecular weight for a free-radical batch polymerization reactor. The policy was limited to the case of constant initiator concentration in the reactor volume.

An important literature review of MMA polymerization process optimization was published by Louie & Soong [38]. The same authors published also an optimization study concerning the minimum polydispersion index problem for the MMA photo polymerization in a semi-batch reactor. Takamatsu et al [39] published a simple method to calculate the optimal reactor temperature and initiator concentration in order to obtain a final product polymer with a prescribed molecular

weight distribution for a styrene free-radical batch polymerization reactor. Chang & Lai [21] modified the two step method presented by Takamatsu et al. [39] to find an algorithm that could be better suited for optimization of polymerization systems. More recently Chang & Liao [22] solved an optimal trajectory tracking problem, via conventional PI controller for the MMA polymerization system. Scali et al [11, 27] determined an optimal temperature profile guaranteeing products having a specified molecular weight distribution. Another optimization study for MMA batch polymerization in ethyl acetate solvent, was published by Ahn et al [20], based on a kinetic model proposed by Schmidt et al [40]. A recent study on the same subject was published by Kiparissides et al [26], aiming to determine the temperature profile leading to a polymer product with specified properties. One of few complete studies including experimental tests of the optimal control policies for MMA polymerization in a batch reactor, was published by Ponnuswamy et al [23]. This study provides detailed analysis of open-loop and closed-loop control of MMA batch polymerization reactors. Minimum-time optimal initiator policy, minimum-time optimal temperature policy and minimum polydispersity temperature policy problems were treated by using an approach based on the Pontryagin Minimum Principle.

The high number of chemical species and the multitude of elementary steps constituting the kinetic mechanism of the polymerization processes induce a more complex mathematical description comparatively with the other chemical processes and hence more complex simulation and optimization calculation. Due to the strong nonlinearities and high number of variables, the optimization of the polymerization processes implies the utilization of iterative numerical methods, generally in conditions of poor convergence. In the last decades there were proposed and tested several optimization methods in function spaces with different performances in localizing the optimum solution. Among these, large utilizations have the calculus of variations, particularly the Pontryagin's Minimum Principle (MP) and so-called Genetic Algorithms (GA).

Assuming a proper mathematical representation of the polymerization process and a suitable performance index (objective function), several existing optimization algorithms can be used to solve time and/or distributed control problems. Usually, the goal is to determine time and/or space trajectories of the control variables that correspond to an extreme (maximum or minimum) of a performance index fulfilling in the same time some physical constraints [41].

The optimization problems of chemical reactors could be classified into several categories, including selection of the best steady-state control settings (steady-state optimization), selection of the best control strategy that leads the system from an initial state to a final specified state (optimal servo control) and selection of the best control strategy that is reducing the effect of inlet variables disturbances on process performances (optimal regulatory control) [2].

The mathematical model of a polymerization tubular reactor could be written in a general formulation as [42, 43]:

$$\frac{dx}{dz} = f(x(z), u(z), z), \quad x(z_0) = x_0, \quad z_0 \leq z \leq z_f \quad (2.70)$$

Where x and u are vectors of state and control variables respectively, and z the reactor axial coordinate.

The optimization problem consists in finding a control u^* that leads the system from an initial state x_0 at $z=z_0$ to a final state x_f at $z=z_f$, so that to minimize the performance index:

$$J = h(x(z_f), z_f) + \int_{z_0}^{z_f} g(x(\tau), u(\tau), \tau) d\tau \quad (2.71)$$

In the case of terminal control problems the performance index is written:

$$J = \sum_{i=1}^N [x_i(z_f) - x_{i,d}(z_f)]^2, \text{ or } \quad J = h(x(z_f), z_f) \quad (2.72)$$

When the states x_i have different orders of magnitude, each term in the performance index (2.72) is multiplied by a weighting coefficient, in order to bring the values of all terms at the same order of magnitude. Considering a polymerization process where the objective is to realize imposed final values for monomer conversion, number-average molecular weight and polydispersion index, the performance index has the expression:

$$J = w_1 (X_M(z_f) - X_{M,d})^2 + w_2 (M_n(z_f) - M_{n,d})^2 + w_3 (IP(z_f) - IP_d)^2 \quad (2.73)$$

With X_M – monomer conversion, M_n – number-average molecular weight, IP – polydispersion index and index d denoting the imposed values of the process variables. The values of weighting coefficients, w_i , will be discussed separately for each optimization problem.

Pontryagin's Minimum Principle (MP)

One of the classical methods in solving the optimal control problems is the Pontryagin's Minimum Principle. The Minimum Principle states that a optimal control policy, $u^*(z)$, that is minimizing the performance index (2.71), is minimizing in the same time the 'Hamiltonian functional' of the problem, defined by the expression [41]:

$$H(x(z), u(z), p(z), z) = g(x(z), u(z), z) + p^T [f(x(z), u(z), z)] \quad (2.74)$$

Mathematically, the principle is written:

$$\min_{u(t)} J = \min_{u(t)} H(x^*(z), u(z), p^*(z), z) \quad (2.75)$$

In the defining expression of Hamiltonian (2.74) is introduced the vector p , usually named co-state or adjoint vector, having the same dimension as the state vector x .

In accord with this method, the following equations represent the optimality conditions [41, 44]:

$$\dot{x}^*(z) = \frac{\partial H}{\partial p}(x^*(z), u^*(z), p^*(z), z) \quad (2.76)$$

$$\dot{p}^*(z) = -\frac{\partial H}{\partial x}(x^*(z), u^*(z), p^*(z), z) \quad (2.77)$$

$$\frac{\partial H(x_{(z)}^*, u_{(z)}^*, p_{(z)}^*, z)}{\partial u} = 0 \quad (2.78)$$

or more generally:

$$H(x^*(z), u^*(z), p^*(z), z) \leq H(x^*(z), u(z), p^*(z), z) \quad (2.79)$$

for all $u(z)$ admissible on the reactor length $z \in [z_0, z_f]$. The equations (2.76) - (2.78) represents the necessary conditions for u^* to be an optimal control and x^* the corresponding optimal state trajectory [41].

The particularization of the optimality conditions for the system (2.70) and the performance index (2.71) is:

$$\dot{x}^*(z) = f(x^*(z), u^*(z), z) \quad (2.80)$$

$$\dot{p}^*(z) = -\left[\frac{\partial f}{\partial x}(x^*(z), u^*(z), z)\right]^T p^*(z) - \frac{\partial g}{\partial x}(x^*(z), u^*(z), z) \quad (2.81)$$

The boundary conditions for the $2n$ state and co-state equations (2.76) and (2.77) are defined in two different points:

$$x^*(z_0) = x_0 \quad (2.82)$$

$$p^*(z_f) = \frac{\partial h}{\partial x}(x^*(z_f), z_f) \quad (2.83)$$

The optimal solution $u^*(z)$ of equations (2.76) - (2.78) can be obtained analytically only in the case of simple state equations, generally less important from practical point of view. The polymerization process mathematical models consist of multivariable strongly nonlinear equations, so that the solution of optimization problems associated with these processes can be obtained only numerically. One of the numerical algorithms that can be used to calculate the optimal control trajectory $u^*(t)$ from the equations (2.76) - (2.78) is based on a gradient numerical technique described by Kirk [41].

The numerical algorithm is an iterative one, consisting in the following steps:

- Initialize an iteration index, $k = 0$. Guess a starting control function $u^{(k)}(z)$, integrate equations (2.70) from 0 to z_f and store the calculated state variables values;
- Using the final values for the monomer state variables stored at step (a) calculate final boundary conditions for the variables p_i , by (2.83), integrate differential equations (2.70) and calculate the gradient of the Hamiltonian:

$$\frac{\partial H^{(k)}}{\partial u} = p^T \frac{\partial f^{(k)}}{\partial u} \quad (2.84)$$

- Adjust the optimal control variable profile on the Hamiltonian gradient direction:

$$u(z)^{(k+1)} = u(z)^{(k)} - \lambda \frac{\partial H(z)^{(k)}}{\partial u} \quad (2.85)$$

(λ – a small real number used as iteration step);

- Integrate the state equations (2.70) for the new control variable profile, $u(z)^{(k+1)}$ and the new value of the performance index, $J^{(k+1)}$; calculate the improvement of the performance index:

$$\Delta = \frac{J^{(k+1)} - J^{(k)}}{J^{(k)}} \quad (2.86)$$

- Increment the iteration index k and continue with step a, until $\Delta \leq \epsilon$.

Usually, the value of the iteration step, λ , is selected at each iteration, k , by an unidirectional search procedure, so as to minimize the performance index value $J^{(k)}$ on the corresponding Hamiltonian gradient profile, $\frac{\partial H(z)^{(k)}}{\partial u}$. A drawback of this algorithm, especially for highly nonlinear and multivariable processes is its poor convergence to the global optimum and the strong dependence of this convergence on the guess of starting control function $u^{(0)}(z)$.

Consequently, the success in application of the Pontryagin's Minimum Principle is strongly dependent on the process model complexity. It is very convenient for the processes described by a reasonable number of equations in the process model.

The Genetic Algorithms

When the number of state and control variables is important and the process features a high nonlinearity, the optimization methods from the class of evolutionary algorithms are more efficient in the localization of global minimum of the performance index. In the last several years, the so-

called Genetic Algorithms (GA) has gained wide acceptance as a robust optimization algorithm in almost all areas of science and engineering. Polymer science and engineering is no exception. Furthermore, multiple-objective functions have been optimized simultaneously by this method. Chakravarthy et al [45] and Lee et al [46] were among the first to adapt simple GA and use it to optimize polymer production using decision variables that are continuous functions of time. Chakravarthy et al [47] studied the optimization of the bulk polymerization of MMA. This is an interesting and complex system because it exhibits the gel effect, which is associated with an extremely sharp increase in the monomer conversion with time at some stage of polymerization. They used the temperature history to minimize the reaction time in a batch reactor while simultaneously requiring the attainment of the design values (monomer conversion and degree of polymerization).

Lee et al [46] carried out a similar time-optimal control of a continuous-flow stirred in which random copolymerization of MMA and vinyl alcohol was taking place, during startup or grade-change. The system does not show the Trommsdorff effect but is quite complex because of the simultaneous polymerization of the two monomers. They calculated the optimal jacket temperature history and the history of the flow rate of VA to minimize the transition time. At the same time, they used two end-point constraints: the polymer product was forced to be of a desired molecular weight and the average mole fraction of VA in the polymer product was to have a desired value.

Some of the advantages of a GA include the following: optimizes with continuous or discrete variables, doesn't require derivative information, simultaneously searches from a wide sampling of the cost surface, can deal with a large number of variables, is well suited for parallel computers, optimizes variables with extremely complex cost surfaces (they can jump out of a local minimum), provides a list of optimum variables, not just a single solution, may encode the variables so that the optimization is done with the encoded variables, works with numerically generated data, experimental data, or analytical functions.

A standard genetic algorithm consists in the following steps [43, 48]:

- Generate an initial set of control policies (profiles) $P^{(0)}$ at random and set iteration index, $i = 0$;
- Evaluate the performances of all control profiles in the set $P^{(0)}$ and sort them in respect with performance index values, J ;

REPEAT

- Select the best PK profiles in the initial set $P^{(0)}$;
- Make reciprocal changes of N_c elements between pairs of selected profiles (N_c randomly calculated);

$M = S \cdot N \cdot P_{mut}$, where P_{mut} is the “probability of mutation” chosen in this study 10^{-3} , similar value with those published by Kennedy et al [49] and Marco et al [50]. The random “mutation” of a certain temperature value in the profile i at iteration k follows the relation:

$$T_j^{(i,k)} = a \cdot T_j^{(i,k-1)}, \quad i \in (1, S), \quad j \in (1, N) \quad (2.90)$$

where a are randomly generated numbers in the range $(0, 1)$.

The procedure of evaluation of the temperature profiles qualities continues with the new set so obtained and a new ‘family’ of parents and children profiles is generated in the same manner. By iterating, the set $P^{(i)}$ of temperature profiles is evaluating toward better and better performances. Finally, the temperature profile fulfilling the demanded minimization of performance index is identified. The same principle is used in the case of other control variables.

As expected, the algorithm performances (accuracy of global optimum localization and the associated computation time) are depending on the size of explored temperature interval, the number of the points defining a temperature profile, N , the number of profiles S and K involved in improvement iterations, as well as the constants P_{select} , P_{mut} and a . The identification of the best values of these algorithm parameters is a matter of exploratory calculation trials that is burdening the optimization calculus.

2.2. Simulation of a tubular reactor for MMA polymerization in solution

In order to underline the main features of the polymerization process taking place in tubular reactors, several simulation studies will be presented, before to approach the optimization problems, based on plug flow and laminar flow models. A comparison of the results provided by the two flow models will be then discussed.

2.2.1. Selection of the kinetic model

To select an appropriate kinetic model for the MMA solution polymerization process, simulation of a plug-flow reactor were performed in identical operating conditions, using the rate constants proposed by different authors, presented in Table 2.4. The simulations were performed considering the working conditions specified in Table 2.5 and the assumptions of constant density, negligible gel effect on the propagation and termination steps and isothermal operating regime.

Table 2.5. Operating conditions for reactor simulation

Process parameter	Numerical value
Feed monomer concentration, c_{M0} , mole/L	3.61
Feed initiator concentration, c_{I0} , mole/L	0.05
Solvent concentration, c_{S0} , mole/L	5.42
Reaction temperature value, T , °C	70
Reactor diameter, Dt , cm	15
L/Dt	~ 55

The plug-flow model used to simulate the polymerization reactor is expressed by relations (2.46) - (2.54). The simulation results, in terms of monomer conversion and number-average molecular weights predicted by different kinetic models, corresponding to the data in Table 2.5, are presented in Figure 2.1.

The monomer conversion curves are relatively close for six of the eight kinetic models considered, whereas two of them, respectively those published by Ponnuswamy et al [23] and Crowley and Choi [24], give significantly different conversions. Also, a rather large dispersion of average molecular weight values of polymer product is obtained onward the reaction time. However, the final values predicted by six of the models are enclosed in the range $1.4 \cdot 10^4 \div 2.1 \cdot 10^4$ kg/kmole. Values rather different are predicted by models of Ahn et al [20] and Ponnuswamy et al [23] respectively.

Taking into account the monomer conversion and molecular weight values predicted by the tested kinetic models, the most representative model appears to be that of Baillagou and Soong [17]. This model is predicting both monomer conversion and M_n values in the best agreement with the majority of the other kinetic models tested and consequently is used in all the calculations described in the following section of this work.

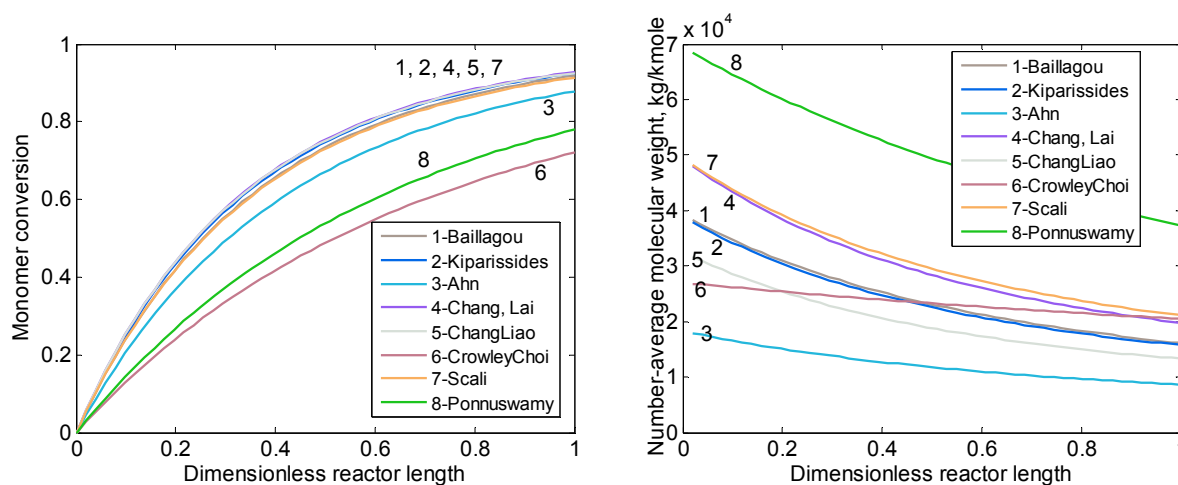


Figure 2.1. Calculated monomer conversion and number-average molecular weights profiles

2.2.2. Simulation of the laminar flow polymerization reactor

In this paragraph will be analyzed the behavior of a laminar-flow reactor in different operating conditions. In this aim, a simulation calculus is performed based on the kinetic model selected above (Baillagou and Soong [16, 17]). The gel effect is described by the model proposed by Chiu et al [13], the constitutive equations being presented in Table 2.2. The characteristics of the reactor are displayed in Table 2.6. Because of the strong exothermicity of the polymerization process, a high value of length to diameter ratio is chosen, insuring a high specific heat transfer area.

Table 2.6. Tubular reactor characteristics

Process parameter	Numerical value
Total mass flow rate / [kg/s]	10^{-3}
Feed initiator concentration (c_{i0}) / [mole/L]	0.05
Toluene mass fraction in the feed	0.5
Reactor length / [m]	8
Reactor diameter (dt) / [m]	2×10^{-2}
Feed temperature / [$^{\circ}$ C]	80
Thermal agent temperature / [$^{\circ}$ C]	80

The reactor model was presented in paragraph 2.1.5. The radial convection terms are ignored in the model, this being explained by the high length to diameter ratio of the reactor. In the axial direction, mass diffusion and heat conduction are assumed to be negligible as compared to the convective terms.

Variations of monomer conversion and consequently of mixture viscosity and density produce strong radial variations in the axial velocities. The flow is considered fully developed at the reactor entrance and the velocity profiles along the reactor axis are calculated using the method proposed by Lynn and Huff [32]. The physical properties (density, viscosity, thermal conductivity) of the reaction mixture are estimated using relations published in literature [2, 7, 17, 18].

It is considered that the main resistance to the heat transfer in radial direction occurs inside the reactor. Therefore, the overall heat transfer coefficient, U, is approximated by the internal partial heat transfer coefficient calculated by the equation (2.91), where the variation of the viscosity at the wall proximity is neglected (the ratio η / η_p approaches unity) [51]:

$$Nu = \frac{\alpha d_t}{k} = 3.66 + \frac{0.19Gz^{0.8}}{1 + 0.177Gz^{0.467}} \left(\frac{\eta}{\eta_p} \right)^{0.14} \quad (2.91)$$

Where Gz is the Graetz number, defined by $Gz = \frac{d_t}{L} \text{Re Pr}$, with Re – Reynolds number and Pr – Prandtl number. In the energy balance, as generally accepted, only the heat generated in propagation reactions and chain transfer to monomer is considered [16, 17], so that the heat genera-

tion rate is given by the expression:

$$r_T = -\Delta H_p (k_p + k_{tm}) c_M \lambda_0 \quad (2.92)$$

The polymerization reaction enthalpy, $\Delta H_p = -5.48 \times 10^4 \text{ J/mol}$, is taken from the reference [52]. The same diffusivity coefficient having a value of $D = 10^{-10} \text{ m}^2/\text{s}$ is used in equations (2.55) for all the species [31].

The partial differential equations defining the reactor model, (2.55) to (2.61) are integrated by a discretization method, the derivatives with respect to the radial direction being approximated by a second order finite difference scheme [53]. Following this discretization, the partial differential equations in respect with z and r are transformed in ordinary differential equations in respect with axial coordinate, z . By applying this method, equation (2.55) becomes:

$$\frac{dc_{M,i}}{dz} = c_{M,i+1} \frac{1}{u_{z,i}} A_i + c_{M,i} \frac{1}{u_{z,i}} \left(-\frac{\partial u_{z,i}}{\partial z} - B_i \right) + c_{M,i-1} \frac{1}{u_{z,i}} C_i + \frac{r_{M,i}}{u_{z,i}} \quad (2.93)$$

Where the coefficients A_i , B_i , C_i are given by:

$$A_i = \frac{D}{2r_i \Delta r} + \frac{D}{(\Delta r)^2}; \quad B_i = -\frac{2D}{(\Delta r)^2}; \quad C_i = -\frac{D}{2r_i \Delta r} + \frac{D}{(\Delta r)^2}, \quad i = 2, 3, \dots, N \quad (2.94)$$

At $i=1$ the equation (2.55) becomes indeterminate since both r and $\frac{\partial c_M}{\partial r}$ become zero.

Applying the l'Hospital rule and assuming symmetry about the centerline [35]:

$$A_1 = \frac{4D}{(\Delta r)^2}; \quad B_1 = -\frac{4D}{(\Delta r)^2}; \quad C_1 = 0 \quad (2.95)$$

To minimize the calculation effort, the derivative $\frac{\partial u_z}{\partial z}$ was approximated by first-order finite difference ratios:

$$\frac{\partial u_{z,k}}{\partial z} = \frac{u_{z,k} - u_{z,k-1}}{z_k - z_{k-1}} \quad (2.96)$$

where k refers to integration steps in the axial direction.

The same discretization method is applied for the heat balance equation (2.56) resulting:

$$\frac{dT_i}{dz} = T_{i+1} \frac{1}{\rho_i c_{p,i} u_{z,i}} A_{t,i} + T_i \frac{1}{\rho_i c_{p,i} u_{z,i}} (-B_{t,i}) + T_{i-1} \frac{1}{\rho_i c_{p,i} u_{z,i}} C_{t,i} + \frac{r_{T,i}}{\rho_i c_{p,i} u_{z,i}} \quad (2.97)$$

Where the coefficients $A_{t,i}$, $B_{t,i}$, $C_{t,i}$ are:

$$A_{t,i} = \frac{k}{2r_i \Delta r} + \frac{k}{(\Delta r)^2}; \quad B_{t,i} = -\frac{2k}{(\Delta r)^2}; \quad C_{t,i} = -\frac{k}{2r_i \Delta r} + \frac{k}{(\Delta r)^2}, \quad i = 2, 3, \dots, N \quad (2.98)$$

The coefficients at the centerline become:

$$A_{t,1} = \frac{4k}{(\Delta r)^2}; B_{t,1} = -\frac{4k}{(\Delta r)^2}; C_{t,1} = 0 \quad (2.99)$$

As a result, the original PDE's were transformed into a system of ODE's along the axial coordinate, including a number of equations N times larger than original one (N- number of discretization intervals in radial direction). The ODE's were solved by a Runge-Kutta procedure method implemented in MATLAB[®] [54].

In order to avoid the difficulties of a multicomponent diffusion problem, the reaction mixture was treated as a pseudo-binary system. The polymer molecules and radicals were lumped as one component (high molecular species) and monomer, initiator and solvent as second constituent (low molecular species). The same diffusivity was therefore used in the balance equations (2.55), (2.59) - (2.61).

The expression used to calculate the viscosity is a complex function of reaction mixture composition and temperature [31]:

$$\begin{aligned} \eta(cP) &= \eta_m + 0.6c_p^{1.4} \exp\left(\frac{0.8}{f}\right), \text{ for } c_p < 0.13 \text{ g/cm}^3 \\ \eta(cP) &= \eta_m + 200c_p^{4.2} \exp\left(\frac{0.8}{f}\right), \text{ for } c_p > 0.13 \text{ g/cm}^3 \\ \eta_m(cP) &= \exp\left[2.303\left(\frac{0.115}{0.025 + 10^{-3}(T(^{\circ}C) + 106)} - 1\right)\right] \\ f &= \left[0.025 + 10^{-3}(T(^{\circ}C) + 106)\phi_m\right] + \left[0.025 + 10^{-3}(T(^{\circ}C) + 180)\phi_s\right] + \\ &+ \left[0.025 + 0.48 \cdot 10^{-3}(T(^{\circ}C) - 114)\phi_p\right] \\ c_p &= 1.2\phi_p \end{aligned} \quad (2.100)$$

where c_p – polymer concentration, g/cm^3 ; ϕ_m, ϕ_s, ϕ_p – volumetric fraction of monomer, solvent and polymer; f – fractional free volume.

The density was calculated using the following correlation:

$$\rho = \frac{1}{\frac{w_M}{\rho_M} + \frac{w_S}{\rho_S} + \frac{w_P}{\rho_P}} \quad (2.101)$$

where w_M, w_S, w_P – mass fraction of the monomer, solvent and polymer, respectively.

The densities for each component of the reaction mixture were calculated by [13, 16, 17]:

$$\rho_M = 966.5 - 1.1 \cdot T, \text{ kg/m}^3; \rho_S = 883 - 0.9 \cdot T, \text{ kg/m}^3, T \text{ in } ^{\circ}C \quad (2.102)$$

The polymer density was considered constant, $\rho_p = 1200 \text{ kg} / \text{m}^3$.

The specific heat for monomer and solvent were also considered constant:

$$c_{p_M} = 0.4 \frac{\text{cal}}{\text{g} \cdot \text{K}}; \quad c_{p_S} = 0.535 \frac{\text{cal}}{\text{g} \cdot \text{K}} \quad (2.103)$$

The thermal conductivity of the mixture was expressed as the weighted sum of the conductivities of MMA, toluene and PMMA. A similar procedure is used by Husain and Hamielec [30]. MMA and toluene thermal conductivities, k_M and k_S , were functions of temperature whereas the thermal conductivity of PMMA (k_P) is constant as given by Brandrup and Immergut [52]. The constitutive equations for thermal conductivity are presented in Table 2.7.

In order to select the number of intervals on the radial coordinate, a comparison of different discretization grids was performed.

Table 2.7. Thermal conductivity constitutive equations [31]

$$k = k_M w_M + k_S w_S + k_P w_P$$

$$k_M = \frac{47.61}{T(K)} \left(\frac{0.9665 - 0.00117 T(^{\circ}\text{C})}{100.2} \right)^{4/3} \frac{\text{cal}}{\text{cm} \cdot \text{s} \cdot \text{K}}$$

$$k_S = \frac{66.70}{T(K)} \left(\frac{0.8838 - 0.000877 T(^{\circ}\text{C})}{92.14} \right)^{4/3} \frac{\text{cal}}{\text{cm} \cdot \text{s} \cdot \text{K}}$$

$$k_P = 3.96 \cdot 10^{-4} \frac{\text{cal}}{\text{cm} \cdot \text{s} \cdot \text{K}}$$

w_M, w_S, w_P – weight fractions of monomer, solvent and polymer

Practically identical results were obtained when the number of grid points was over 50. Therefore, a number of 50 radial points was chosen, as a compromise between accuracy and calculation effort.

Figures 2.2 and 2.3 present simulation results for the reactor with characteristics given in Table 2.6. The radial conversion profiles are relatively abrupt, with a fast transition from small values to almost complete conversion (Figure 2.2). As seen from Figure 2.2, two flowing zones are developed inside the tubular reactor: a central zone where the fluid velocity is relatively high and a peripheral (plugged) one, where the fluid velocity is relatively low, approaching zero in the proximity of the wall. Consequently, the maximum residence time occurs in the neighborhood of the wall, and minimum one in the center of tube. The differences in residence times give monomer conversions that drastically vary in radial direction, with values smaller than 10 % in the central zone and nearly 100% in the peripheral one.

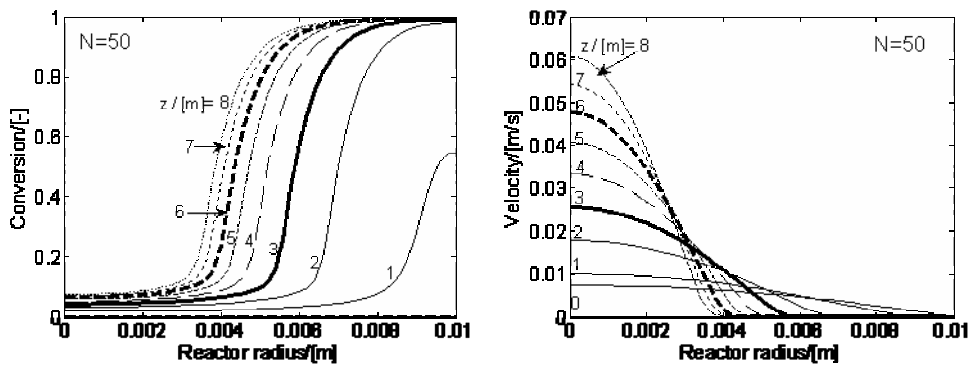


Figure 2.2. Profiles for monomer conversion (left) and axial velocity (right), at different positions (z) along the reactor

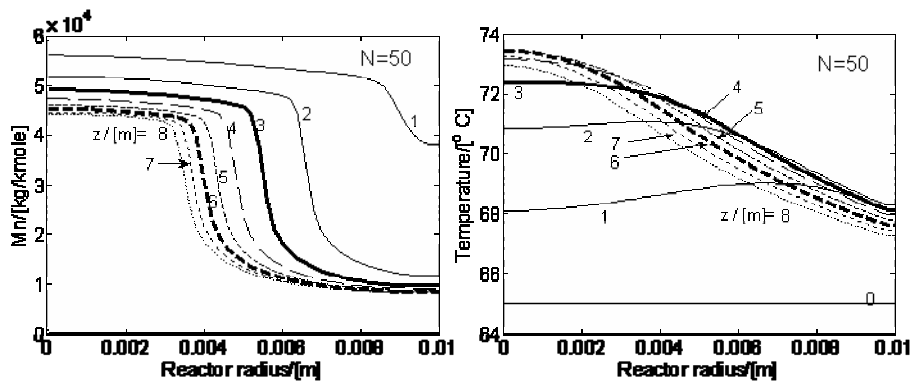


Figure 2.3. Number-average molecular weights (left) and temperature (right) profiles, at different positions (z) along the reactor

Figure 2.3 presents radial profiles of the number average molecular weights and temperature. In the plugged region close to the wall the polymer number-average molecular weight drastically decreases. This could be explained by the small ratio of propagation to the termination rate, unfavorable to the formation of long chains, in the last two thirds of reactor length. Due to low amounts of monomer, the polymer radicals initiated in this region present a slow growth. Moreover, the high concentration of solvent promotes termination by chain transfer to solvent, finishing prematurely the newly produced chains.

Due to the high ratio of heat transfer area to reaction volume, only a moderate rise of the reaction temperature along the reactor is observed (Figure 2.3). The radial temperature profile presents a maximum, which moves from the neighborhood of the wall towards the center, as the axial position increases. This is explained by the heat generation rate (monomer polymerization rate), higher in the peripheral zone, on the first meters of reactor length and displacing toward the center of tube with the increase of axial position.

Influence of tube diameter

The reactor diameter and length were varied keeping constant the mean residence time (the ratio between the reactor volume and feed volume flow) of the reaction mixture in the polymerization reactor. The dimensions of the reactors used in these simulations are presented in Table 2.8, the other process parameters being specified in Table 2.6. In this section, only the results for extremes configurations are presented (Reactor 2 and Reactor 3), the other being already presented above.

Table 2.8. Reactor configurations

Reactor configuration	Length, [m]	Diameter, [m]
Reactor 1	8	2×10^{-2}
Reactor 2	2	4×10^{-2}
Reactor 3	32	1×10^{-2}

The results illustrated in Figures 2.4 to 2.6 show that the reactor with small diameter (high ratio of heat transfer area to reactor volume) produces more homogenous final products and assures a more even thermal regime. The homogeneity is characterized by the values of polydispersion index, a maximum value of 5 being obtained for Reactor 2 comparatively with a maximum value of 3 for Reactor 3. As seen from Figure 2.6, the temperature profiles in Reactor 3 are more uniform due to a higher heat transfer area that is allowing a more efficient evacuation of the reaction heat.

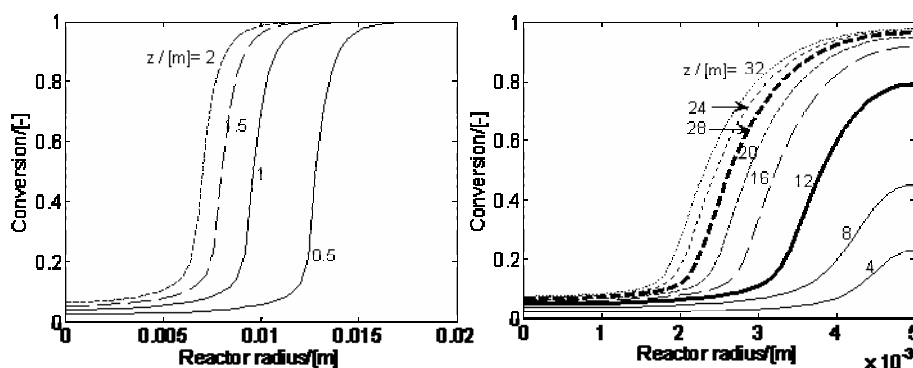


Figure 2.4. Radial profiles of monomer conversion, at different positions along the reactor. Left: Reactor 2; Right: Reactor 3

Comparatively, the temperature profiles in the Reactor 2 case presents an evident maximum, shifted to the centerline only with advancement of the polymerization mixture along the axial coordinate of the reactor. A rise in temperature of almost 3 °C for Reactor 3 produces higher molecular weight polymer close to the reactor wall, due to the smaller influence of chain transfer to solvent reaction in this region.

The results in this paragraph shows some benefits of the decrease of the tubular reactor diameter. However, the decrease of diameter presents the important drawback of higher pressure drop and consequently higher operational costs of the reactor.

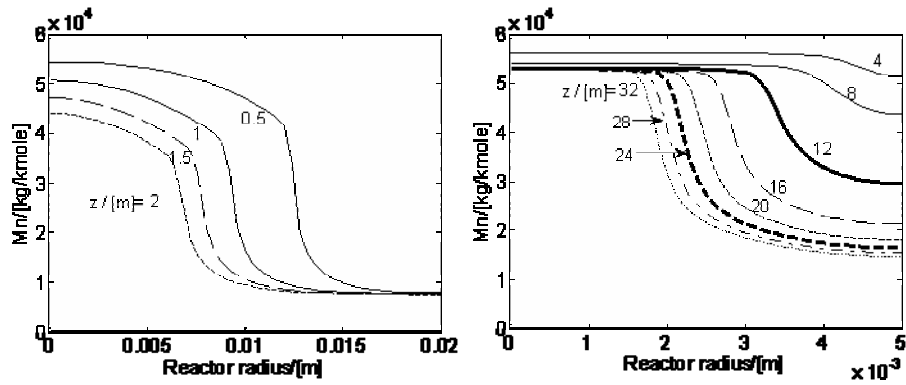


Figure 2.5. Radial profiles for number-average molecular weights, at different positions (z) along the reactor. Left: Reactor 2; Right: Reactor 3

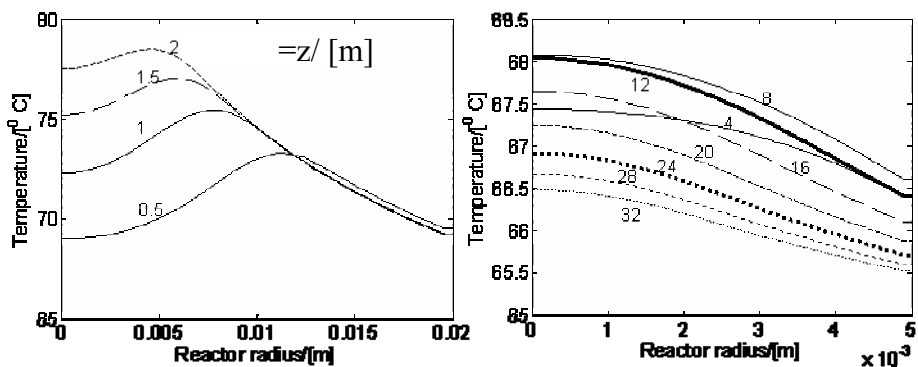


Figure 2.6. Radial profiles for temperature, at different positions (z) along the reactor. Left: Reactor 2; Right: Reactor 3

Influence of initiator concentration

The initiator concentration has an important influence on polymerization process, higher initiator concentrations producing polymers with lower molecular weights. Three values for the feed initiator concentrations (0.025, 0.05 and 0.1 mole/L) were tested for the Reactor 1 configuration (Table 2.8).

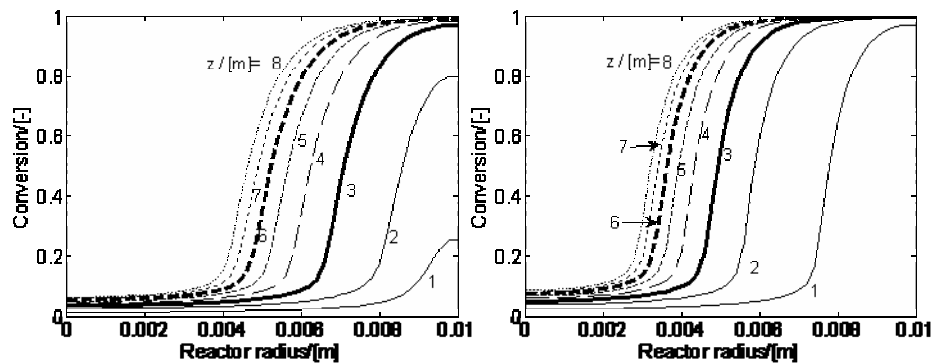


Figure 2.7. Monomer conversion profiles for feed initiator concentration of 0.025 mole/L (left) and 0.1 mole/L

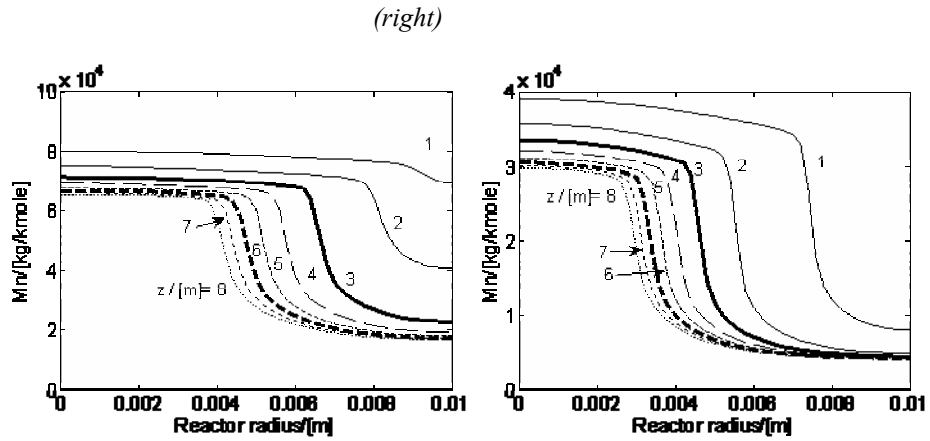


Figure 2.8. Number average molecular weight profiles for feed initiator concentration of 0.025 mole/L (left) and 0.1 mole/L (right)

Small initiator concentrations lead to a low initiation rate, and consequently to a small number of live polymer chains. This has two effects: firstly, a decrease of propagation rate having as result a low monomer conversion on the first 2 m of the reactor (Figure 2.7); secondly, an important increase of final polymer molecular weight (Figure 2.8). Also, a small propagation rate decreases the amount of heat generated (low temperature levels) with an increasing effect on the polymer molecular weight. Consequently, the feed initiator concentration proves to be an important parameter to control the final molecular weights of the polymer.

Influence of monomer concentration

It is known that a higher solvent fraction in a polymerization process improves the heat transport inside the reactor, but also induces higher solvent separation costs. Three solvent mass fractions were tested for Reactor 1 configuration (Table 2.8).

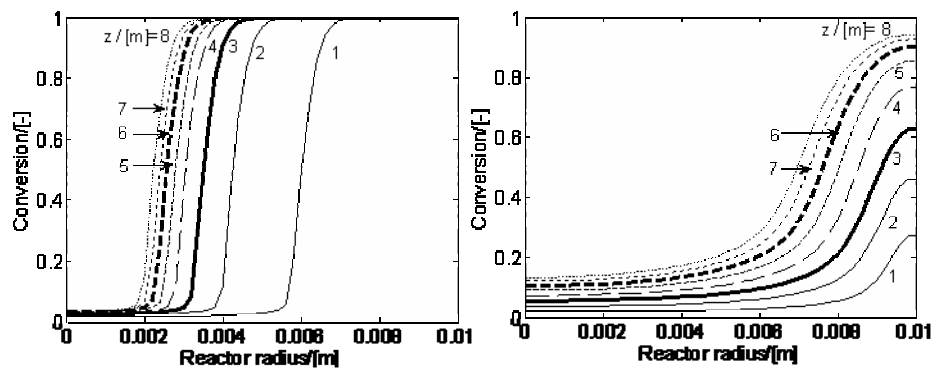


Figure 2.9. Monomer conversion profiles for smallest ($w_s = 0.3$, left) and highest ($w_s = 0.7$, right) feed weight solvent fractions

By increasing the fraction of solvent, a lower reaction temperature is developed along the

reactor. This is explained by two mechanisms: a) less heat is generated due to lower amount of monomer; b) heat transfer through the wall is improved due to a lower thermal resistance. Because the propagation step has a higher activation energy compared to the termination reactions, the conversion is lower (Figure 2.9) and shorter chains are obtained (Figure 2.10), as result of higher thermal sensitivity of propagation step. Additionally, a smaller monomer concentration contributes to a lower propagation rate, with the same overall effect.

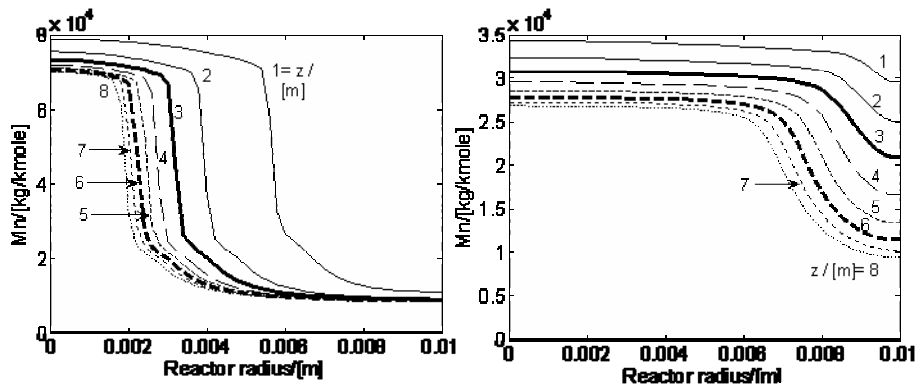


Figure 2.10. Number-average molecular weight for smallest ($w_s = 0.3$, left) and highest ($w_s = 0.7$, right) feed solvent fraction

It can be also remarked that increasing the solvent concentration leads to a polymer product with a more homogeneous molecular weight distribution (the calculated polydispersity index is 7.65 and 2.27, for solvent fraction of 0.3 and 0.7, respectively).

The simulation results presented above are showing that the non-uniform velocity profile of the laminar flow leads to a polymer of lower quality and to a less efficiently use of the reactor volume, comparing with the plug flow regime. This drawback can be limited by technical solutions that are flattening the radial velocity profile of the reaction mixture. One of these is the use of static mixers, which could change the velocity profile in order to approach rather closely the ideal plug-flow. This will be analyzed in the following section.

2.2.3. Comparison of laminar flow and plug flow reactor simulation results

For the laminar flow polymerization reactor, the values of monomer conversion and number-average molecular weight presented here are averages over the reactor cross-section, calculated by the relation:

$$\bar{Y} = \frac{2}{r^2} \int_0^r r \cdot Y \cdot dr \quad (2.104)$$

Where Y is the variable to be averaged (e.g. monomer conversion, number-average molecular weight, polydispersity index, reaction temperature). A comparison between the

simulation results obtained in the plug flow and laminar flow assumptions is presented in Figure 2.11. The two models predict similar values for the monomer conversion.

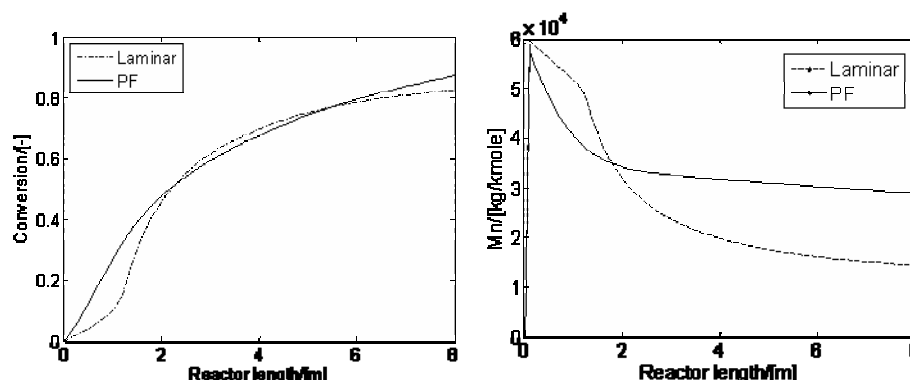


Figure 2.11. Plug flow and laminar flow reactor simulated monomer conversion and number-average molecular weights axial profiles (Reactor 1)

However, the plug-flow reactor produces a polymer with a higher molecular weight and a narrower distribution (the polydispersity index of the final product is 2.13, compared to 3.21 for the laminar flow reactor). This is an argument for the practical effectiveness of static mixers in tubular reactors, in order to promote velocity profiles that approach the plug-flow.

2.3. Optimization of MMA tubular polymerization reactor

2.3.1. A comparison of variational and genetic algorithms performances in the optimization of plug flow MMA polymerization reactor [55]

In the following paragraph, an optimization problem for MMA polymerization process is formulated and solved using two widely used methods, one based on Minimum Principle (MP) and the other on a Genetic Algorithm (GA). The main goal is to compare the performances of the two optimization algorithms in terms of convergence rate, initialization procedure and computation time.

The polymerization process is characterized by reaction temperature profile as independent (control) variable and four dependent (state) variables: initiator concentration (C_I), monomer concentration (C_M), and the 0th and 2nd order moments of polymer concentration distribution, μ_0 and μ_2 respectively. The state variables, C_M , μ_0 and μ_2 , are describing the monomer conversion and molecular weight distribution of the polymer. As it was specified above, the 1st order moment, involved in the calculation of the average molecular weights, is directly calculated from the monomer concentration (or conversion). As control variable was considered the reaction temperature profile

T(z). The objective of the problem is to calculate the temperature profile along the reactor that leads to desired values of polymer properties and monomer conversion at reactor exit, for a given reaction volume and flow rate (or equivalently, given reaction time). This is accomplished by the minimization of the performance index (2.73), where w_1 , w_2 and w_3 , are weighting factors so chosen, to insure close magnitude orders for all terms of the summation.

The problem so defined could be considered as one of average complexity for a polymerization process (a single control variable, no heat balance equation necessary in the mathematical model, plug flow of reaction mixture). More complex problems could be formulated by using more realistic mathematical models of chemical process and/or considering more control variables (the temperature of thermal agent along the reactor, the flow rate of thermal agent, the feed flow rate of reaction mixture and its composition and temperature).

Optimization by Minimum Principle method

The mathematical model of the plug-flow reactor and the optimal conditions were written in dimensionless variables:

$$\frac{dx_1}{dz} = -\frac{z_s}{u_z I_s} k_d x_1 I_s = f_1 \quad (2.105)$$

$$\frac{dx_2}{dz} = -\frac{z_s}{u_z M_s} (k_1 x_2 M_s x_1^{1/2} I_s^{1/2}) = f_2 \quad (2.106)$$

$$\frac{dx_3}{dz} = \frac{z_s}{u_z \mu_{0s}} (k_2 x_2 M_s x_1^{1/2} I_s^{1/2} + k_3 S x_1^{1/2} I_s^{1/2} + (k_{td} + 0.5k_{tc}) \lambda_0^2) = f_3 \quad (2.107)$$

$$\frac{dx_4}{dz} = \frac{z_s}{u_z \mu_{2s}} ((k_m x_2 M_s + k_s S) \lambda_2 + k_{tc} \lambda_1^2 + k_t \lambda_0 \lambda_2) = f_4 \quad (2.108)$$

$$x_1 = \frac{I}{I_s}; \quad x_2 = \frac{M}{M_s}; \quad x_3 = \frac{\mu_0}{\mu_{0s}}; \quad x_4 = \frac{\mu_2}{\mu_{2s}} \quad (2.109)$$

The index s is denoting the reference values used in the definitions of dimensionless variables.

The live polymer distribution moments are:

$$\lambda_0 = \left(\frac{2fk_d x_1 I_s}{k_t} \right)^{1/2}; \quad \lambda_1 = \frac{2fk_d x_1 I_s + A\lambda_0}{B}; \quad \lambda_2 = \lambda_1 + \frac{2k_p x_2 M_s \lambda_1}{B} \quad (2.110)$$

$$A = k_p x_2 M_s + k_s S + k_m M_s x_2; \quad B = k_t \lambda_0 + k_s S + k_m x_2 M_s$$

The performance index in dimensionless variables is:

$$J = w_1 M_s^2 (x_{2f} - \alpha)^2 + w_2 \mu_{0,d}^2 (x_{3f} - 1)^2 + w_3 IP_d^2 (\beta - 1)^2$$

$$\alpha = \frac{M_d}{M_s}; \beta = \frac{x_{3f} x_{4f} (1 - \alpha)^2}{(1 - x_{2f})^2} \quad (2.111)$$

The optimality conditions (2.76) - (2.78) can be easily particularized for the present optimization problem. The co-state (adjoint) equations (2.83) are particularized as:

$$\frac{dp_1}{dz} = -\frac{\partial H}{\partial x_1} = -\left(p_1 \frac{\partial f_1}{\partial x_1} + p_2 \frac{\partial f_2}{\partial x_1} + p_3 \frac{\partial f_3}{\partial x_1} + p_4 \frac{\partial f_4}{\partial x_1} \right) \quad (2.112)$$

$$\frac{dp_2}{dz} = -\frac{\partial H}{\partial x_2} = -\left(p_1 \frac{\partial f_1}{\partial x_2} + p_2 \frac{\partial f_2}{\partial x_2} + p_3 \frac{\partial f_3}{\partial x_2} + p_4 \frac{\partial f_4}{\partial x_2} \right) \quad (2.113)$$

$$\frac{dp_3}{dz} = -\frac{\partial H}{\partial x_3} = -\left(p_1 \frac{\partial f_1}{\partial x_3} + p_2 \frac{\partial f_2}{\partial x_3} + p_3 \frac{\partial f_3}{\partial x_3} + p_4 \frac{\partial f_4}{\partial x_3} \right) \quad (2.114)$$

$$\frac{dp_4}{dz} = -\frac{\partial H}{\partial x_4} = -\left(p_1 \frac{\partial f_1}{\partial x_4} + p_2 \frac{\partial f_2}{\partial x_4} + p_3 \frac{\partial f_3}{\partial x_4} + p_4 \frac{\partial f_4}{\partial x_4} \right) \quad (2.115)$$

With the boundary conditions at the reactor exit described by:

$$p_1(z_f) = \frac{\partial J}{\partial x_1} \Big|_{z=z_f} = 0 \quad (2.116)$$

$$p_2(z_f) = \frac{\partial J}{\partial x_2} \Big|_{z=z_f} = 2\omega_1 M_s^2 (x_{2f} - \alpha) + 2\omega_3 IP_d^2 (\beta - 1) \frac{\partial \beta}{\partial x_2} \quad (2.117)$$

$$p_3(z_f) = \frac{\partial J}{\partial x_3} \Big|_{z=z_f} = 2\omega_2 \mu_{0,d}^2 (x_{3f} - 1) + 2\omega_3 IP_d^2 (\beta - 1) \frac{\partial \beta}{\partial x_3} \quad (2.118)$$

$$p_4(z_f) = \frac{\partial J}{\partial x_4} \Big|_{z=z_f} = 2\omega_3 IP_d^2 (\beta - 1) \frac{\beta}{x_{4f}} \quad (2.119)$$

The Hamiltonian derivative in respect with the control variable (in this case the temperature) necessary in relation (2.85) is:

$$\frac{\partial H}{\partial T} = p_1 \frac{\partial f_1}{\partial T} + p_2 \frac{\partial f_2}{\partial T} + p_3 \frac{\partial f_3}{\partial T} + p_4 \frac{\partial f_4}{\partial T} \quad (2.120)$$

The derivatives of the functions f_i , $i = 1..4$ in respect with the temperature are:

$$\frac{\partial f_1}{\partial T} = -\frac{z_s}{u_z I_s} x_1 I_s \frac{dk_d}{dT} \quad (2.121)$$

$$\frac{\partial f_2}{\partial T} = -\frac{z_s}{u_z M_s} (x_2 M_s x_1^{1/2} I_s^{1/2}) \frac{dk_1}{dT} \quad (2.122)$$

$$\frac{\partial f_3}{\partial T} = \frac{z_s}{u_z \mu_{0,s}} \left(\frac{dk_2}{dT} x_2 M_s x_1^{1/2} I_s^{1/2} + \frac{dk_3}{dT} S x_1^{1/2} I_s^{1/2} + \left(\frac{dk_{td}}{dT} + 0.5 \frac{dk_{tc}}{dT} \right) \lambda_0^2 + 2(k_{td} + 0.5k_{tc}) \lambda_0 \frac{\partial \lambda_0}{\partial T} \right) \quad (2.123)$$

$$\frac{\partial f_4}{\partial T} = \frac{z_s}{u_z \mu_{2s}} \left(\left(\frac{dk_m}{dT} x_2 M_s + \frac{dk_s}{dT} S \right) \lambda_2 + (k_m x_2 M_s + k_s S) \frac{\partial \lambda_2}{\partial T} + \frac{dk_{tc}}{dT} \lambda_1^2 + 2k_{tc} \frac{\partial \lambda_1}{\partial T} \lambda_1 \right) + \frac{dk_t}{dT} \lambda_0 \lambda_2 + k_t \frac{\partial \lambda_0}{\partial T} \lambda_2 + k_t \lambda_0 \frac{\partial \lambda_2}{\partial T} \quad (2.124)$$

The numerical algorithm based on a gradient method used to solve this optimization problem is presented in paragraph 2.1.6.

The values of the different parameters and the working conditions used in the computation are given in Tables 2.9 and 2.10. For the problem such defined, finding the initial profile leading to the global minimum proved to be a rather difficult task. The calculation procedures failed to attain the global minimum of performance index for constant initial profiles, increasing temperature profiles and even certain decreasing profiles.

Several initialization temperature profiles and the corresponding solutions are presented in Figure 2.12 and Table 2.11. The global minimum was obtained only by initializing the algorithm with a slowly decreasing profile in the interval 329 – 323 K (profile 5 in Table 2.11 and Figure 2.12). Additionally, it is worth to stress that, besides the starting profile, the minimum value of the performance index is also dependent on the convergence limit, ε .

Table 2.9. Working conditions for reactor optimization

Process parameter	Numerical value
Feed monomer concentration, c_{M0} , mole/L	3.61
Feed initiator concentration, c_{I0} , mole/L	0.05
Solvent concentration, c_{S0} , mole/L	5.42
Reaction temperature value, T , °C	70
Reactor diameter, Dt , cm	15
L/Dt	~ 55

Table 2.10. Specified values in the performance index expression

Desired final monomer concentration	$C_{Md} = C_{M0} / 2;$ $(X_{Md} = 0.5)$
Desired zero order moment (corresponding to a given number-average molecular weight, $M_{n,d}$)	$\mu_{0d} = 3.008 \cdot 10^{-3}$ $(M_{n,d} = 60000)$
Desired polydispersion index	$IP_d = 2$
Weighting factors in the expression (2.73)	$w_1 = w_3 = 1;$ $w_2 = 10^8$
The convergence criterion in Minimum Principle method	$\varepsilon = 10^{-9}$

The best result reported in Table 2.11 was found with an extremely low value of this parameter, introduced in order to approach the same order of magnitude for performance index, as was achieved by the GA. The corresponding evolution of performance index in respect with the iteration number is presented in Figure 2.13 (semi-logarithmic scale). Initializing the iterative calcu-

lation by this profile, a number of 24 iterations are necessary in order to achieve the global minimum.

As a conclusion, it is to be noted that the convergence of the MP gradient method toward the global minimum was achieved only by starting with profiles close enough to the optimal solution and difficult to guess, demanding a rather important computational effort. Once an appropriate initialization profile is identified, the convergence is realized in a reasonable number of iterations.

Table 2.11. Minimization results by the MP algorithm for different initialization profiles

Number	Initialization temperature profile	Number of iterations	Minimum value of J	Computing time, (s)
1	Constant, 303 K	26	4.0262×10^{-3}	26
2	Constant, 323 K	24	4.2328×10^{-3}	25
3	Constant, 343 K	16	1.0513×10^{-2}	17
4	Linear decreasing	26	6.7468×10^{-4}	28
5	Nonlinear decreasing	24	1.7839×10^{-7}	34

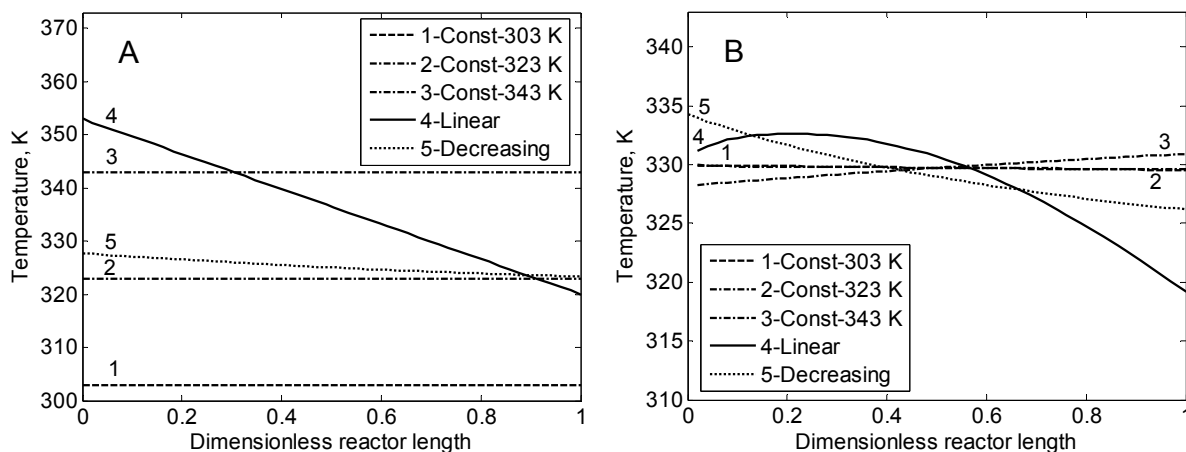


Figure 2.12. Starting temperature profiles (A) and the corresponding minimum profiles (B)

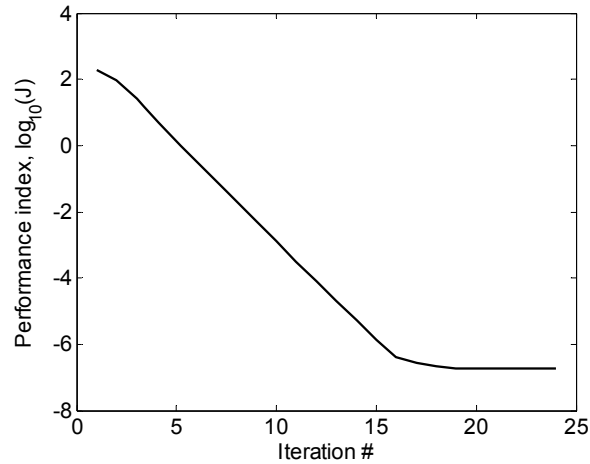


Figure 2.13. Performance index vs. iteration number

The relative errors between the calculated and imposed values for monomer conversion, number-average molecular weight and polydispersion index are calculated by the relations:

$$\varepsilon_x = \left| \frac{X_f - X_d}{X_d} \right| \cdot 100; \quad \varepsilon_{M_n} = \left| \frac{M_{n_f} - M_{n_d}}{M_{n_d}} \right| \cdot 100; \quad \varepsilon_{IP} = \left| \frac{IP_f - IP_d}{IP_d} \right| \cdot 100 \quad (2.125)$$

The numerical values are $\varepsilon_x = 0.26 \%$ for monomer conversion, $\varepsilon_{M_n} = 0.56 \%$ for number-average molecular weight and $\varepsilon_{IP} = 0.019 \%$ for polydispersion index.

Genetic Algorithm

The structure and principles of the genetic algorithm used to solve the optimization problem are presented in paragraph 2.1.6. The selection of parameters S and N is important both in the accuracy of optimal trajectory approach and the necessary computing time. In their selection one has to consider a dependence of the minimum iterations number on the value of S, due to the necessity to perform a minimum number of combinations inside the set of profiles, in order to reach at optimum. On the other side, the number of values considered for the independent variable in a profile, N, will influence the accuracy of the reactor model solution. To determine the most appropriate values of these parameters, preliminary runs are always necessary. Several excerpts of the performance index values along the iteration progress, for the MMA polymerization process described above, are presented in Tables 2.12 and 2.13, in order to illustrate the evolution of the calculation.

Table 2.12. Performance index values after 200 iterations

N	S=10	S=20	S=40	S=60	S=80	S=100	S=120	S=140
10	2.4110e-2	1.0248e-3	8.2596e-3	1.1766e-5	4.3193e-4	8.6686e-5	6.9200e-6	1.2479e-3
20	1.0613e-1	1.5852e-2	3.3376e-4	8.7496e-4	1.1287e-3	5.2343e-4	6.0216e-6	8.9473e-5
30	4.3252e-2	5.9702e-3	1.5676e-3	7.1252e-6	3.6407e-4	9.8289e-4	1.5857e-3	1.1550e-5
50	1.2340e-2	1.3946e-3	1.8636e-3	1.5336e-3	3.2863e-5	4.0689e-3	5.0178e-3	4.3661e-4
70	4.2900e-2	2.5833e-3	9.9842e-3	5.3730e-4	1.6242e-2	3.1264e-4	3.060e-4	1.9398e-3

As seen from Tables 2.12 and 2.13, the selection of temperature profile that minimizes the performance index is achieved practically by using $S = 60$ profiles, each one of $N = 30$ temperature values. Beyond 500 iterations no significant improvements in the performance index value were observed.

The optimal temperature profile obtained by GA, presented in Figure 2.14, corresponds to a minimum value of the performance index, $J_{\min} = \sim 2.8 \cdot 10^{-7}$, and is achieved in 60 seconds of running time.

As observed in Figure 2.15, the reactor exit values of the monomer conversion, number-average molecular weight and polydispersion index are practically equal to the imposed ones. The relative errors calculated using relations (2.125) are $\varepsilon_x = 0.3 \%$ for monomer conversion, $\varepsilon_{Mn} = 0.53 \%$ for number-average molecular weight and $\varepsilon_{IP} = 0.02 \%$ for polydispersion index.

Table 2.13. Performance index values after 500 iterations

N	S=10	S=20	S=40	S=60	S=80	S=100	S=120	S=140
10	1.3994e-3	8.2885e-4	2.6354e-4	1.1766e-5	9.6070e-3	3.3182e-6	1.2892e-6	4.5150e-7
20	7.2473e-2	9.2717e-6	9.9677e-7	5.6818e-6	9.2943e-7	2.5684e-6	8.0064e-7	3.5357e-6
30	4.2422e-2	5.2558e-4	4.1957e-7	2.7685e-7	1.0246e-4	1.6930e-5	1.2791e-4	3.6215e-7
50	4.1732e-3	9.2541e-5	4.9137e-5	1.7942e-5	1.6807e-6	9.8348e-4	2.5745e-6	3.8142e-7
70	4.2338e-3	3.8142e-4	1.4002e-3	1.2751e-5	9.6070e-3	4.7596e-6	2.1875e-4	2.4457e-4

Results and discussions

The main point that has to be revealed, when comparing MP and GA type optimization algorithms, is the difference in their working principles. The first one is developed on sound conditions of optimality based on mathematical reasons. The second one is essentially an empirical search procedure, able to find a numerical solution considering an extended set of values for the independent (control) variables on a given domain and following a set of combination/selection rules.

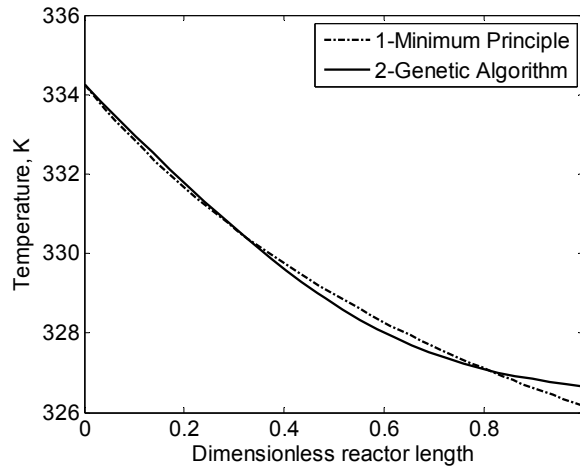


Figure 2.14. Temperature profiles calculated by Minimum Principle and Genetic Algorithm

The MP algorithm provides optimum conditions defined by a system of equations having a complexity dependent on the mathematical model of the process. For simpler processes, the optimal solution is easily obtainable either analytically or by numerical methods. However, for higher non-linear and multivariable systems, as is the case of polymerization processes, the equations expressing the optimum conditions feature high complexity and are difficult to solve. For these systems, the optimal solution can be obtained only iteratively by a trial and error procedure, testing different starting conditions until the sought extremum of the performance index is achieved. In the case study presented above, a rather high number of trials were necessary in order to find an appropriate starting temperature profile, this supposing a rather time consuming activity. However, once the starting profile was guessed, the MP algorithm was faster.

As seen above, 24 iterations were performed in 34 seconds by MP, imposing an extremely small convergence criterion, while the GA needs to calculate the solution on the same machine (Intel Core 2 Duo 1.8 GHz, 2 Gb RAM) 60 seconds for 500 iterations. However, when comparing the computing time of the two algorithms, there is to consider also the time necessary to guess a convenient starting solution for MP gradient method and the parameters values of GA algorithm respectively. This preparation time can be significant, especially for the first approaches of new optimization problems, when no information concerning the optimum is available.

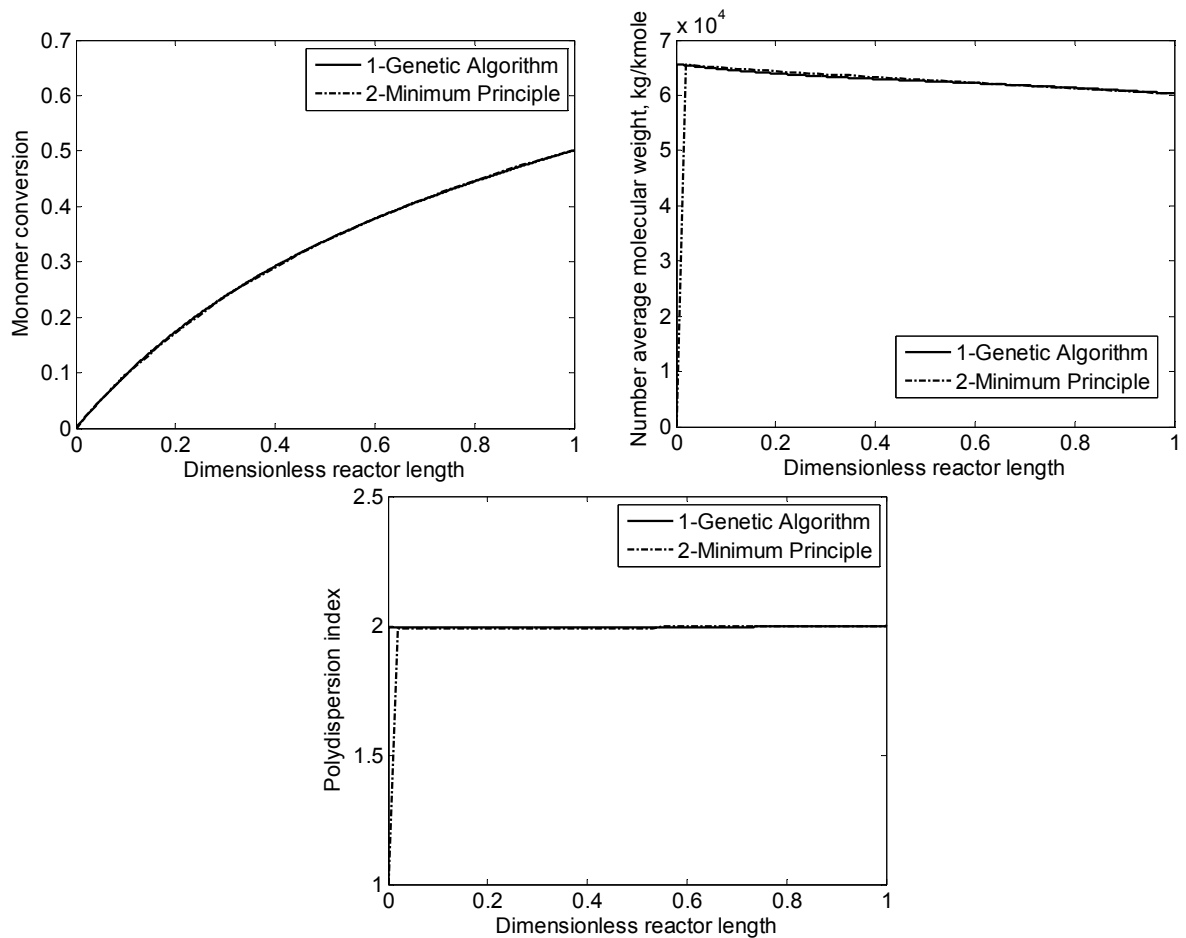


Figure 2.15. Optimal state variables profiles

The GA type algorithms are more robust in the localization of optimum, due to their working principle. There is no convergence radius and, provided that the working domain and the discretization of independent variables are appropriate, there is a small risk to converge towards a local optimum. Also, these algorithms do not induce initialization difficulties, due to their internal initiation mode with a family of independent variables profiles. Another important advantage of the GA is that they are not demanding any effort in the preparation and programming of the equations giving the conditions of optimum, as in the case of MP. These features are making GA convenient optimization tools, especially in the case of new complex nonlinear problems. Their only disadvantage is a rather high computing time necessary to find the optimum. However, in the conditions of the present progresses in the digital computing, this inconvenient is becoming less and less important.

In the case of optimization problem defined above for MMA polymerization process, MP and GA methods are giving reasonably close solutions. The minimum values of the performance index found by the two algorithms are practically equal, with a non-significant smaller value in the case of the MP ($\sim 1.78 \cdot 10^{-7}$ comparing with $\sim 2.77 \cdot 10^{-7}$). The corresponding optimal temperature

profiles comparatively presented in Figure 2.14, are practically overlapping. Also the optimal profiles for monomer conversion, number average molecular weight and polydispersity are graphically presented in Figure 2.15. The final monomer conversion, number-average molecular weight and polydispersion index calculated in optimal conditions, are practically identical with the corresponding imposed values, given in Table 2.10.

To summarize, it can be asserted that the differences between the two algorithms lie in the basic principles, complexity of the implementation and the computing times. For the case study we considered, the two algorithms gave practically the same result, but with a significant superior effort necessary to find an adequate starting temperature profile in the case of the gradient method based on the MP. Once this initial profile was identified, the convergence to the optimum was attained in a reasonable number of iterations. In the case of GA, the working principle is demanding a smaller preparation time, but implies a much higher number of iterations in calculation and consequently, a significant higher computing time. Supplementary runs are also necessary to optimize the values of the algorithm parameters (number of profiles, S , number of the discretization points in a profile, N , and the minimum number of iterations).

It is also worth to recall that the case study we considered represents an average complexity optimization problem for a polymerization process (a single control variable, no heat balance equation necessary in the mathematical model, plug flow of reaction mixture). For more complex optimization problems it could be expected supplementary difficulties in the application of MP algorithms and more evident advantages in using the GA.

2.3.2. Laminar flow and plug-flow tubular reactors optimization by a Genetic Algorithm

Optimization problem 1

Due to the strong exothermicity of the polymerization process, an appropriate control of reaction temperature along a polymerization tubular reactor usually involves a minimum number of cooling jackets [56]. The tubular reactors in laminar flow have pronounced temperature and composition variations across the flow direction that change the viscosity and alter the velocity profile from the simple parabolic one. Molecular diffusion acts in the direction of diminishing the radial gradients but will not completely eliminate them, particularly in liquid phase systems, where the diffusivities are of the order of magnitude 10^{-9} to 10^{-10} $\text{m}^2 \text{s}^{-1}$ for small molecules and much lower for the polymers [35].

The comparison of the simulation results for a MMA polymerization reactor in plug-flow and laminar flow assumptions performed in paragraph 2.2 showed significant differences in calculated reaction temperature profiles in the two cases.

In this paragraph an optimization study of the laminar flow and jacketed plug-flow reactor will be presented, based on the models described in paragraph 2.1.5. The performance index defined by relation (2.73) and the weighting factors presented in Table 2.10 were also considered in this problem. The Genetic Algorithm presented in paragraph 2.1.6 was adapted to solve the optimization problem so formulated. The control variables have to obey the following restrictions:

- Temperatures: $298\text{ K} < T < 373\text{ K}$;
- Mass flow rate, [kg/h]: $8 \times 10^{-4} < D_{M,0} < 1 \times 10^0$
- Initiator concentrations, [mole/L]: $5 \times 10^{-4} < c_{I,0} < 5 \times 10^{-2}$
- Solvent mass fraction in the mixture: $0.1 < w_s < 0.9$.

The reactor characteristics are given in Table 2.9. The imposed values for monomer conversion, number-average molecular weight and polydispersion index are given in Table 2.10.

The representative outlet values of temperature, monomer conversion and polymer characteristics are calculated as averages of their radial profiles by using the relation (2.104).

The objective of all studies was to determine the control policies that assure at the reactor outlet an imposed monomer conversion and specified polymer characteristics (mean molecular weight and polydispersion index). The optimization problems consider a tubular reactor with a jacket divided in 8 sections, each one kept at a constant temperature.

As mentioned, the selected control variables are the feed initiator concentration, the mass flow rate, the jacket temperature profile, the feed temperature of the reaction mixture and the feed solvent weight fraction. From practical reasons (to preclude uneconomical temperature policies involving cooling of the fed reactant mixture) the feed temperature was considered equal to the temperature on the first jacket section. The results of the optimization study in monomer conversion, number-average molecular weights and polydispersion index are presented in Table 2.14 (recall that the objective is to obtain at the reactor outlet a monomer conversion, $X_{M,d}=0.5$, a mean polymer molecular weight, $M_{n,d}= 60000$ kg/kmol and a polydispersion index, $I_{p,d}= 2$).

Optimization results for a laminar flow tubular reactor

The optimization problem was solved for two values of monomer conversion (0.5 and 0.8) and same specified values for polymer properties (number average molecular weight, $M_n=60000$

and polydispersity index, IP=2). The results of calculations are given in Figures 2.16 – 2.22 and

Table 2.14. As seen from this table, the calculated operation policies provide values for the monomer conversion and number-average molecular weight close to the imposed ones. A slightly weaker performance is obtained in achieving the specified value of polydispersion index. This result is explained firstly by the imposed value (IP=2), a relatively difficult goal and secondly by the strong variations of reaction rates across the flowing section, particular for the laminar flow.

Table 2.14. Optimization results for polymerization reactor in laminar flow

N ^o	Solvent mass fraction, ws, [-]	Mass flow rate D _{M,0} , [kg/s]	Feed initiator concentration, C _{I,0} , [mole/L]	Optimized process performances					
				X, [-]		Mn, [kg/kmole]		IP, [-]	
				Calculated	Imposed	Calculated	Imposed	Calculated	Imposed
1	0.810	7.391×10^{-3}	7.990×10^{-4}	0.502	0.5	60322	60000	2.04	2
2	0.346	2.870×10^{-2}	2.260×10^{-2}	0.808	0.8	59931		2.55	

The results presented in Table 2.14 and Figures 2.16 and 2.17 show that the optimal operation in the case of smaller monomer conversion is demanding smaller flow rates, lower initiator concentration, higher solvent amount in the feed and relatively higher temperatures. In this case it is required a higher reaction temperature in order to compensate the effect of lower monomer concentration on polymerization rate. By this combination of operating variables values, besides the monomer conversion and molecular weight, it is also provided a very good control for the molecular weight distribution (smallest polydispersion index).

Corresponding to a higher amount of solvent, Figure 2.17-A shows a more flat reaction temperature profiles, due to a more uniform radial velocity profile. Consequently, smaller radial variations occur for monomer conversion, number-average molecular weight and polydispersion index. Also, a more uniform initiator and monomer consumption in radial direction is observed (Figure 2.18 -A) and, consequently, a more uniform propagation rate. This has as effect a more homogeneous polymer (narrower molecular weight distribution, Figure 2.20 - A).

When a higher monomer conversion ($X_d=0.8$) is desired, the optimization algorithm is demanding an operation policy with higher flow rate, higher monomer and initiator concentrations in the feed and a lower temperature level. More pronounced radial variations of the initiator and

monomer concentrations can be observed in this case, due to a stronger variation of the fluid velocity. Consequently, stronger radial variations occur in polymerization rate and a larger distribution of polymer molecular weight is produced. Significant variations of initiator concentration are observed beyond 3 m of reactor length, mainly due to the temperature rise (Figure 2.21-B), with an important effect on the propagation step and consequently on the monomer conversion profile (Figure 2.20-B). As emphasized in preceding paragraphs, at high monomer concentrations the monomer consumption occurs in an annular zone that is moving from the wall toward the center of the tube, with the increase of axial position. Consequently, large radial variations are obtained for the molecular weight values (Figure 2.19-B) and polymer polydispersion index (Figure 2.20-B). In this way, the polydispersion index is less controllable at high monomer concentrations.

Of course, these results are strongly depending on the values of the weighting factors appearing in the performance index expression (2.126). The values corresponding to the results presented above are given in Table 2.15.

Table 2.15. Weighting coefficients in performance index (2.126)

w_1	w_2	w_3
1	$2.77 \cdot 10^{-12}$	$0.25 \cdot 10^{-4}$

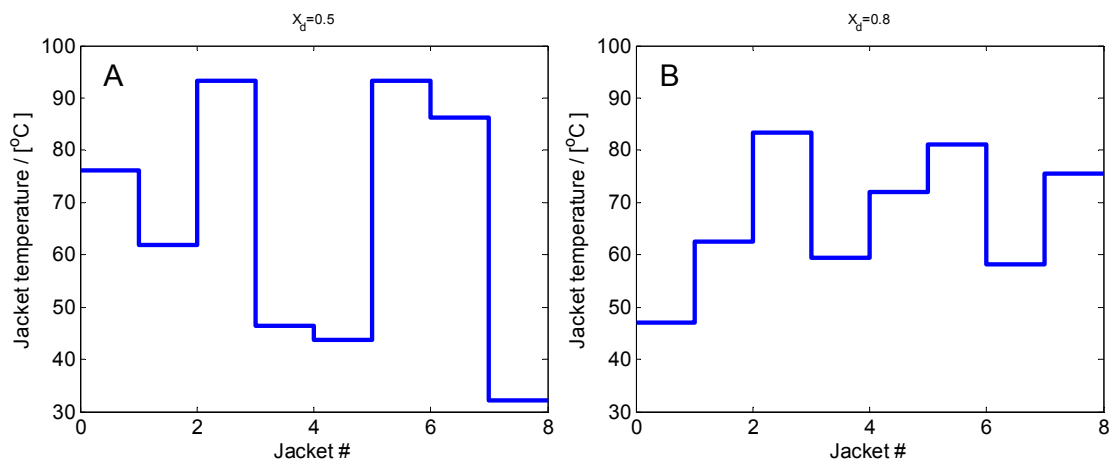


Figure 2.16 Optimal jacket temperature values ($NJ=8$); left: $X_d = 0.5$, right: $X_d = 0.8$

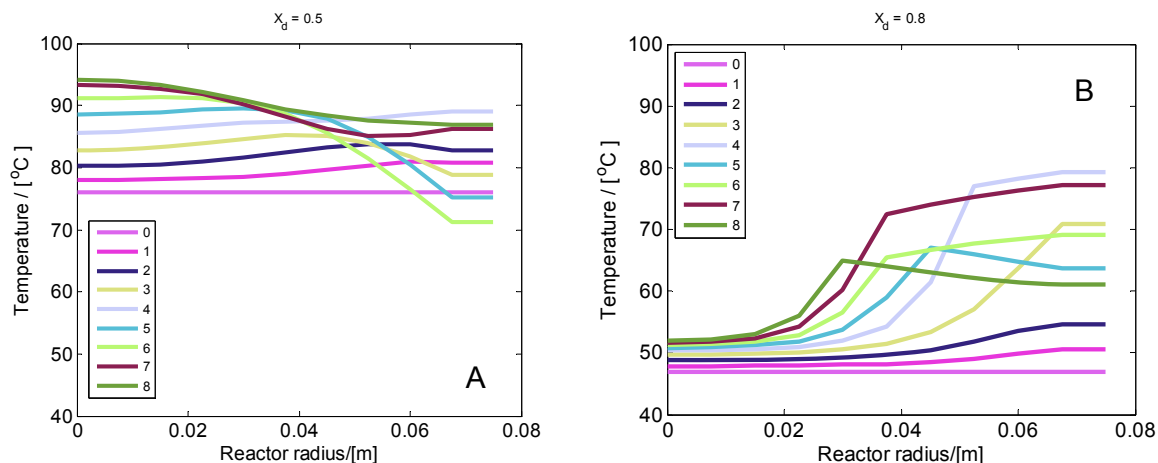


Figure 2.17. Reaction temperature profiles on radial direction calculated with the optimal control policy ($NJ=8$, A: $X_d = 0.5$, B: $X_d = 0.8$)

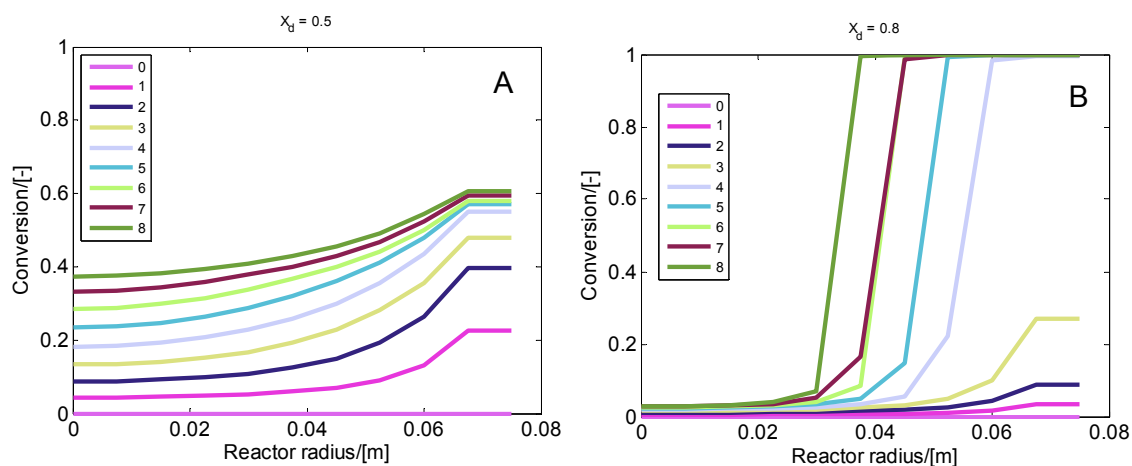


Figure 2.18. Monomer conversion profiles on radial direction calculated with the optimal control policy ($NJ=8$); left: $X_d = 0.5$; right: $X_d = 0.8$

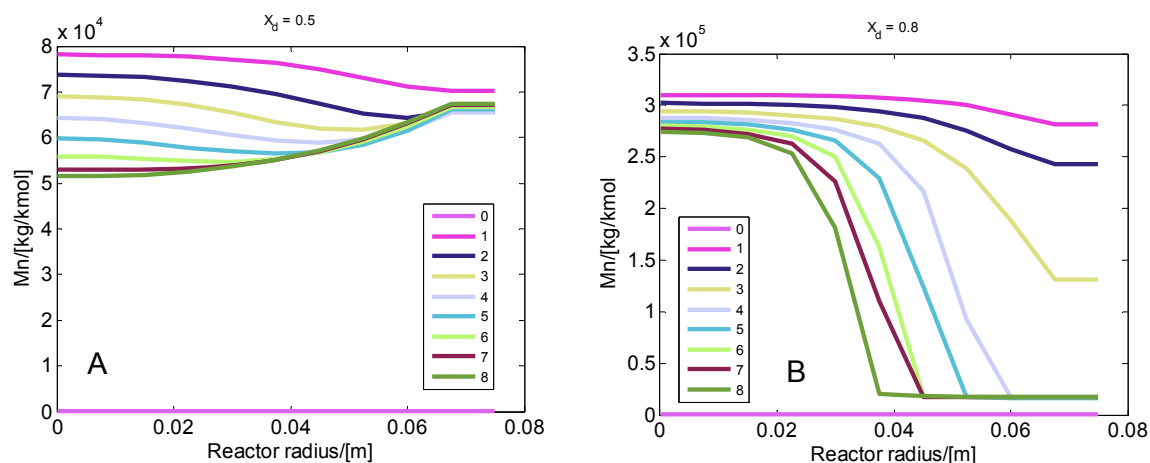


Figure 2.19. Number-average molecular weight profiles on radial direction calculated with the optimal control policy ($NJ=8$); left: $X_d = 0.5$, right: $X_d = 0.8$

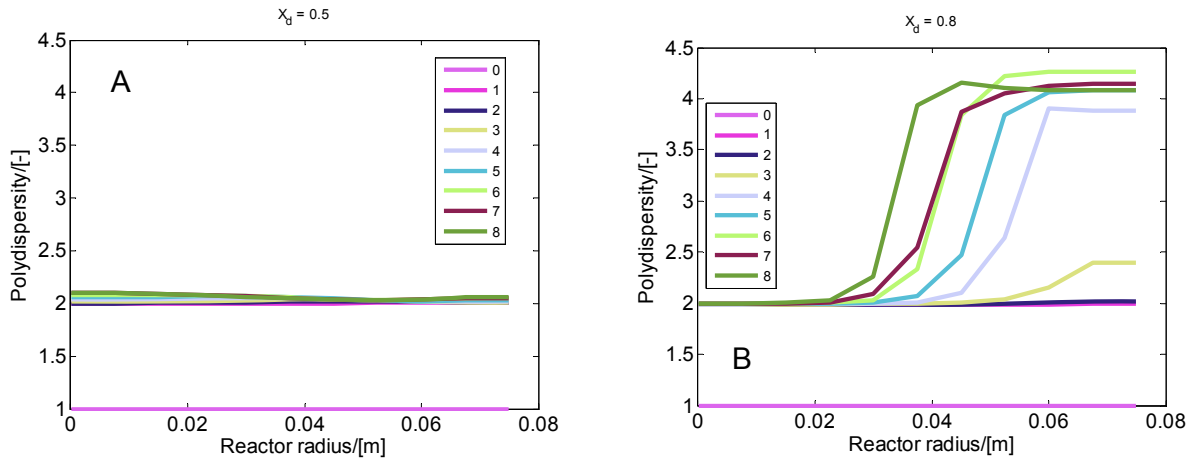


Figure 2.20. Polydispersity index profiles on radial direction calculated with the optimal control policy ($NJ=8$, A: $X_d = 0.5$, B: $X_d = 0.8$)

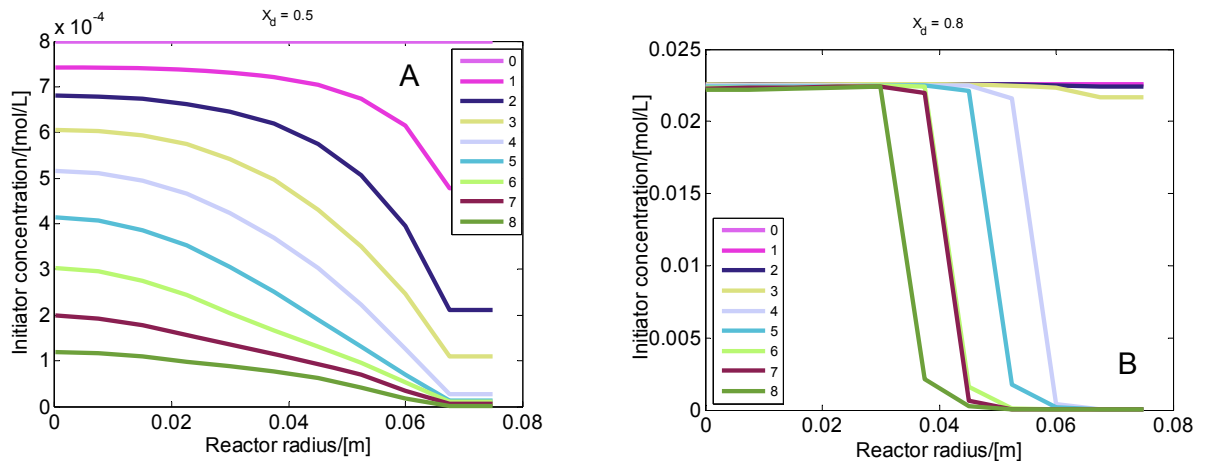


Figure 2.21. Initiator concentration profiles on radial direction calculated with the optimal control policy ($NJ=8$); left: $X_d = 0.5$, right: $X_d = 0.8$

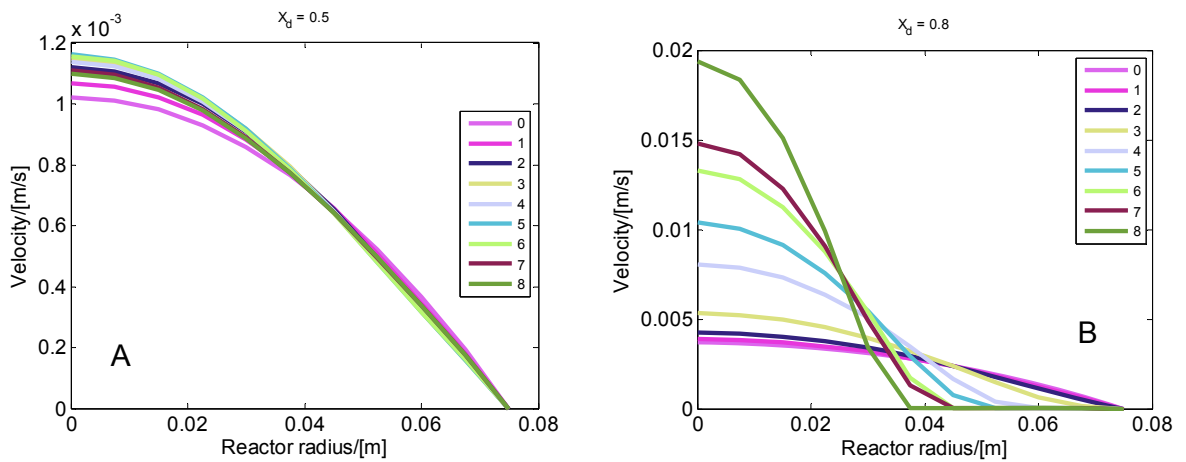


Figure 2.22 Velocity profiles on radial direction calculated with the optimal control policy ($NJ=8$); left: $X_d = 0.5$, right: $X_d = 0.8$

Optimization results for a jacketed plug-flow reactor

An optimization problem similar with the previous one was solved for a plug-flow tubular reactor having the same characteristics (see Table 2.9) and imposing the same monomer conversions (0.5 and 0.8) as in preceding problem. The same Genetic Algorithm described in paragraph 2.1.6 was adapted to solve the optimization problem so formulated. The optimization results, presented in Table 2.16, show a good agreement between the optimized and desired values for monomer conversion, number-average molecular weight and polydispersion index.

Table 2.16. Optimization results for a plug-flow polymerization reactor

N ^o	Solvent mass fraction, ws, [-]	Mass flow rate D _{M,0} , [kg/s]	Feed initiator concentration, C _{I,0} , [mole/L]	Optimized process performances					
				X, [-]		Mn, [kg/kmole]		IP, [-]	
				Calculated	Imposed	Calculated	Imposed	Calculated	Imposed
1	0.74	1.656×10^{-2}	1.32×10^{-3}	0.50	0.5	60000	60000	2.03	2
2	0.85	2.261×10^{-3}	1.97×10^{-3}	0.80	0.8	59912		2.12	

Comparing the plug flow reactor and laminar-flow reactor optimization results it is observed that a higher mass fraction of solvent (lower feed monomer concentration) is required for the plug-flow reactor to achieve the imposed objectives. Also, a more homogenous polymer is obtained for both conversions, comparatively with the laminar flow reactor. It is also confirmed that the polydispersion index is more difficult controllable when high monomer conversion are required.

When a monomer conversion of 0.5 is imposed, an almost complete depletion of the initiator (Figure 2.27-A) can be observed on the last 3 m of the reactor. As seen from Figures 2.24-A and 2.25-A, the polymerization process is practically finished on this zone (insignificant increase of monomer conversion and practically constant average molecular weight of the polymer). The absence of chemical reaction and consequently the lack of heat generation is leading to a temperature decrease on this zone (Fig. 2.24-A).

Referring to the thermal agent temperature profile, it can be seen that when a moderate monomer conversion is required ($X_d=0.5$), a relatively high temperature is required on the first half of the reactor, to assure a fast start-up for the polymerization process, followed by low temperature cooling agent on the final zone, in order to slow down the polymerization process. Several oscillations of cooling agent temperature insure a moderate increase of reaction temperature on the first half of the reactor (Figure 2.23-A).

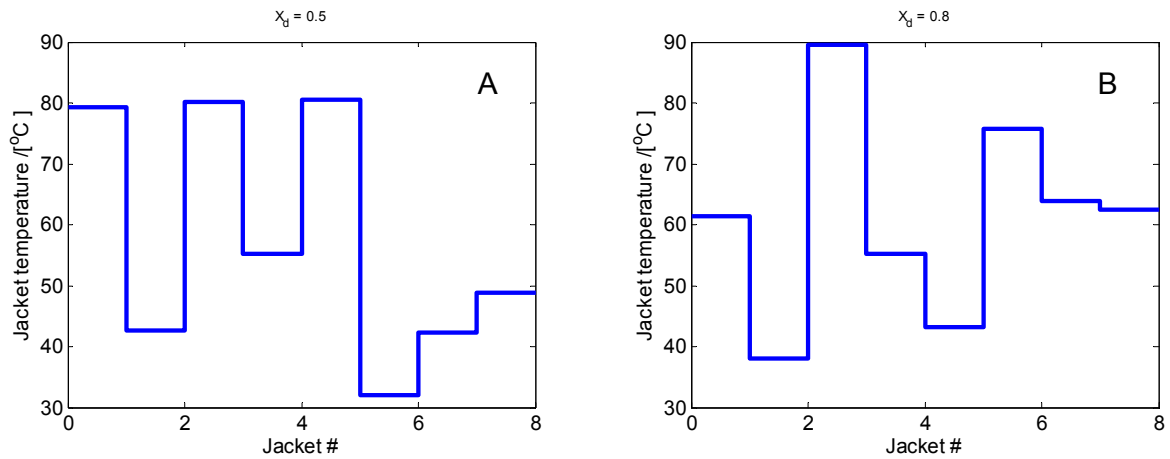


Figure 2.23. Optimal thermal agent profile for the plug-flow reactor (A: $X_d = 0.5$, B: $X_d = 0.8$)

The monomer conversion and polymer molecular weight reach values close to the desired ones in this region. The second half of the reactor is used only to finely tune the dependent process variables to the imposed objectives, fact confirmed by the decrease in the reaction temperature (Figure 2.26-A).

When a higher monomer conversion is imposed ($X_d=0.8$), a smaller flow rate, smaller feed monomer concentration and higher feed initiator concentration are required. The reaction is started with a more moderate cooling agent temperature than in the previous case and is finished with temperatures roughly at the same level. In this case, the desired monomer conversion is realized essentially by a longer residence time and not by a higher reaction temperature (Figure 2.26-B). This is probably explained by the necessity to control simultaneously the polydispersion index of polymer product.

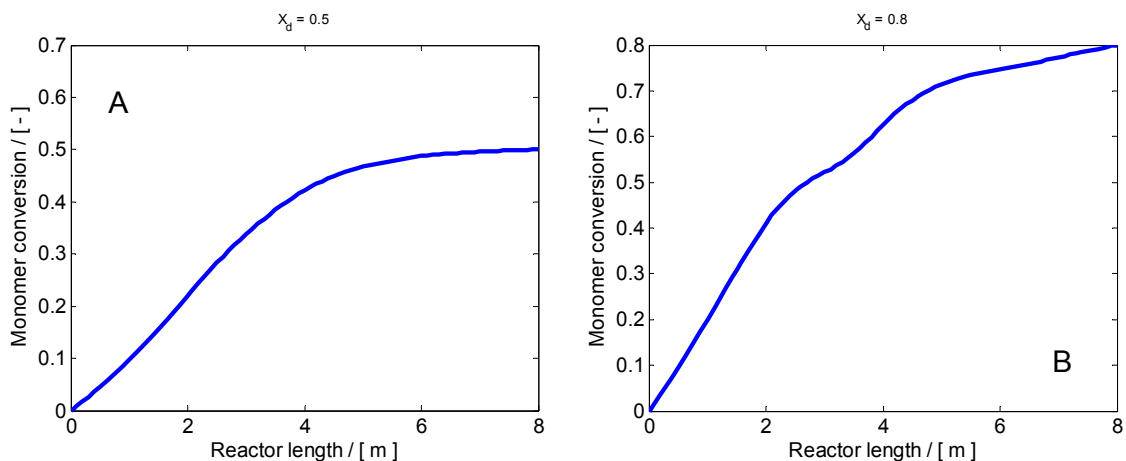


Figure 2.24. Monomer conversion profiles (optimization problem1, plug-flow reactor, A: $X_d = 0.5$, B: $X_d = 0.8$)

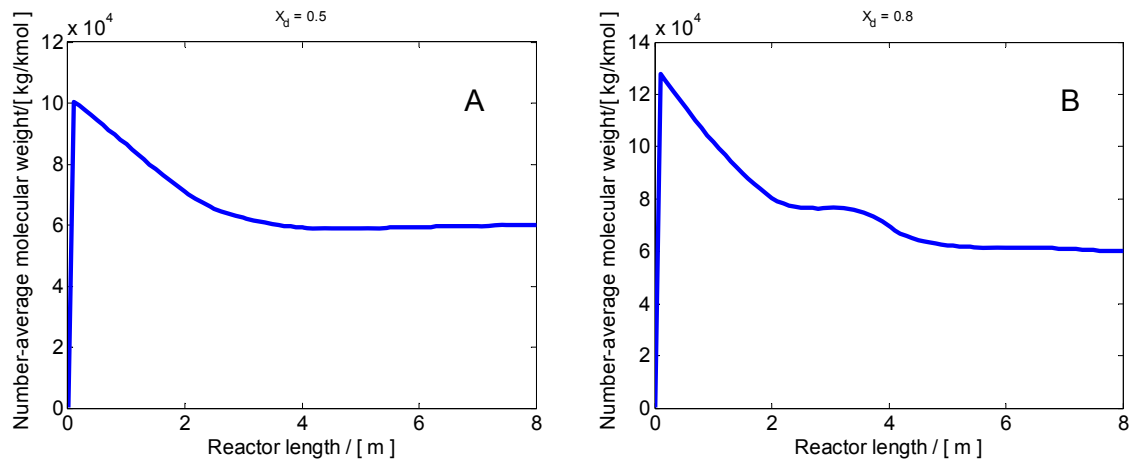


Figure 2.25. Polymer molecular weights profiles (optimization problem1, plug-flow reactor, A: $X_d=0.5$, B: $X_d=0.8$)

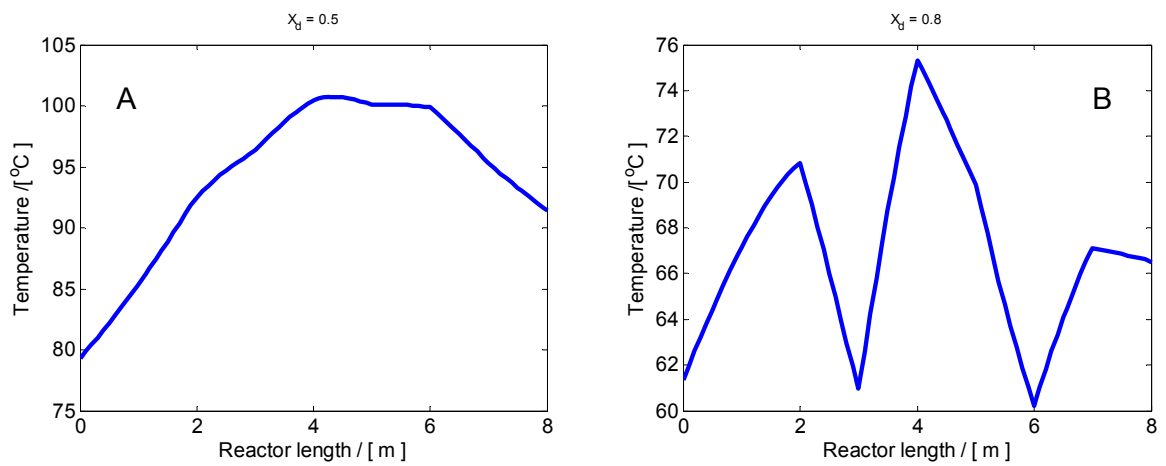


Figure 2.26. Reaction temperature profiles (optimization problem1, plug-flow reactor, A: $X_d=0.5$, B: $X_d=0.8$)

A curious particularity of the calculated optimal regime in this case is a somewhat curious evolution of the reaction temperature which is presenting several oscillations along the reactor (Figure 2.26-B). This is suggesting a tendency to keep the reaction temperature in close limits along the reactor, in order to better control the polymer properties.

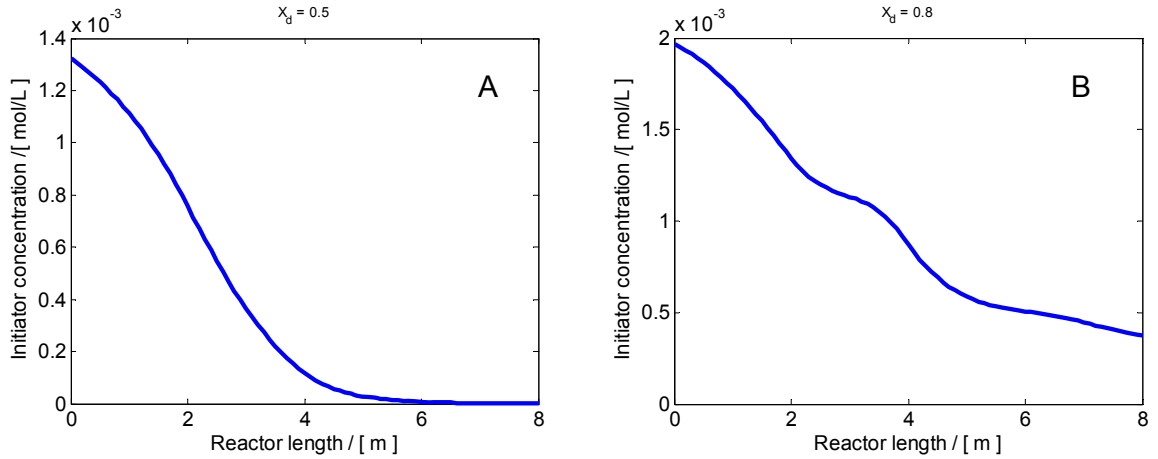


Figure 2.27. Initiator concentration profiles (optimization problem 1, plug-flow reactor, A: $X_d = 0.5$, B: $X_d = 0.8$)

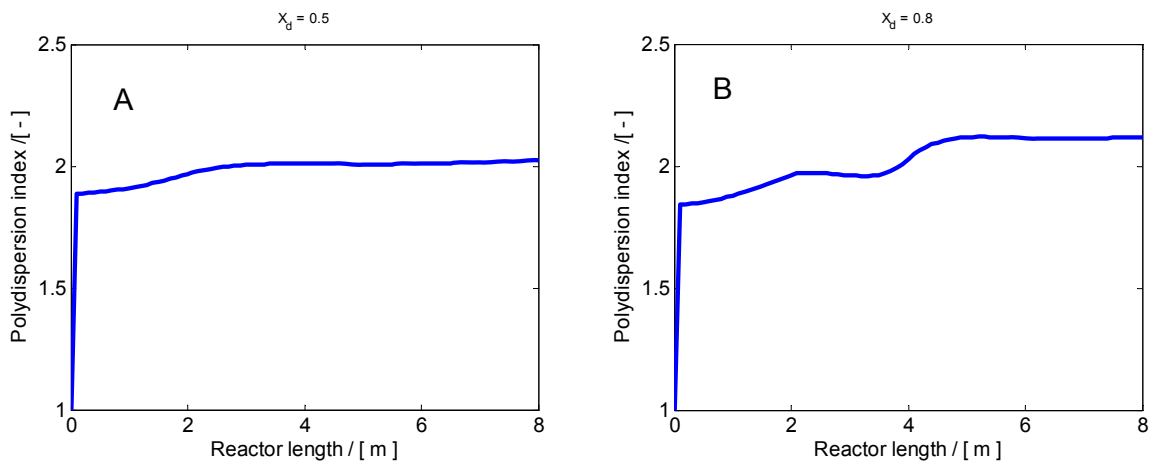


Figure 2.28. Polydispersity index profile (optimization problem 1, plug-flow reactor)

Optimization Problem 2: Maximization of the polymer production

The results of previous optimization problem showed that the imposed characteristics of the polymer (molecular weights and molecular weights distribution) at a specified value of monomer conversion are sometimes achieved with relatively low flow rates (low polymer production). In order to achieve a reasonable polymer throughput at the reactor exit, a term related to the polymer production was added to the performance index. The new objective is to produce a maximum polymer throughput with specified molecular weight and molecular weight distribution for a given monomer conversion. The performance index expression is re-written in the form:

$$J = w_1 (X_M(z_f) - X_{M,d})^2 + w_2 (M_n(z_f) - M_{n,d})^2 + w_3 (IP(z_f) - IP_d)^2 + w_4 \frac{1}{D_{m,M} X_M} \quad (2.126)$$

The term corresponding to the polymer throughput is given by the expression $D_{m,M} X_M$, re-

lated to the monomer conversion and the monomer mass flow rate. The new optimization problem was solved for the same tubular reactor, having the characteristics given in Table 2.9, for both laminar flow and plug-flow hypothesis.

The values of the weighting coefficients in the performance index (2.126) given in Table 2.17 were chosen by numerical experimentation to assure the same magnitude order for each of the terms in the considered performance index.

Table 2.17. Weighting coefficients in performance index (2.126)

Weighting coefficients			
w_1	w_2	w_3	w_4
1	$1.4 \cdot 10^{-11}$	$2.5 \cdot 10^{-5}$	$3.0 \cdot 10^{-6}$

Optimization of a laminar flow tubular reactor

The calculated optimal values of the solvent mass fraction, initiator concentration and mass flow rate are presented in Table 2.18. Close values for the calculated and imposed values for monomer conversion, polymer molecular weight and molecular weight distribution were obtained. As expected, these values are obtained with higher mass flow rates and initiator concentration, requiring relatively higher thermal agent temperatures along the reactor jacket (as compared with previous optimization problem). The optimal operation policy corresponds to the cooling temperature profile presented in Figure 2.29 and reaction temperature profiles presented in Figure 2.31 – A. This leads to the development of polymerization process, predominantly on the second half of reactor.

Table 2.18. Results of the laminar flow tubular reactor optimization problem

N ^o	Solvent mass fraction, w_s , [-]	Mass flow rate $D_{M,0}$, [kg/s]	Feed initiator concentration, $C_{I,0}$, [mole/L]	Optimized process performances					
				X, [-]		Mn, [kg/kmole]		IP, [-]	
				Calculated	Imposed	Calculated	Imposed	Calculated	Imposed
1	0.235	2.58×10^{-1}	4.40×10^{-2}	0.493	0.5	60600	60000	2.19	2

On the first half of the tubular reactor only a small amount of initiator is decomposed (Figure 2.31-B), corresponding to a low monomer conversion, due to the low level of temperature. The small amount of primary radicals produce high molecular weights polymers (Figure 2.30 - B) with a narrow molecular weight distribution (Figure 2.32 - A).

Due to the high monomer concentration in the feed, important radial variations of process variables occur on the second zone of reactor length where takes place the polymerization

reaction. As explained above, these are induced mainly by flow velocity radial profile and have as consequence the apparition of an annular reaction zone extending from the wall toward the center of the tube. These features of the process, illustrated in Figures 2.30 to 2.32, are already explained in the previous paragraphs.

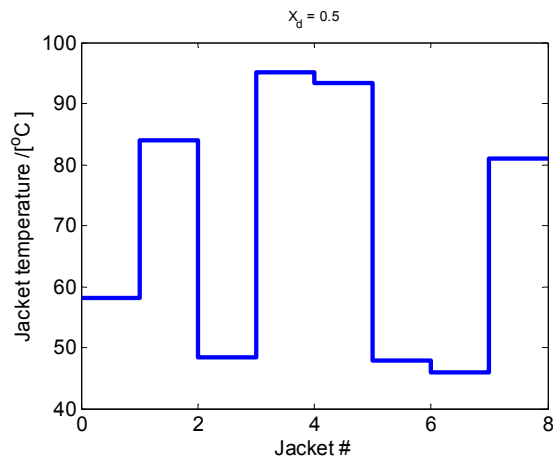


Figure 2.29. Optimal jacket temperature profile (laminar flow reactor, optimization problem 2)

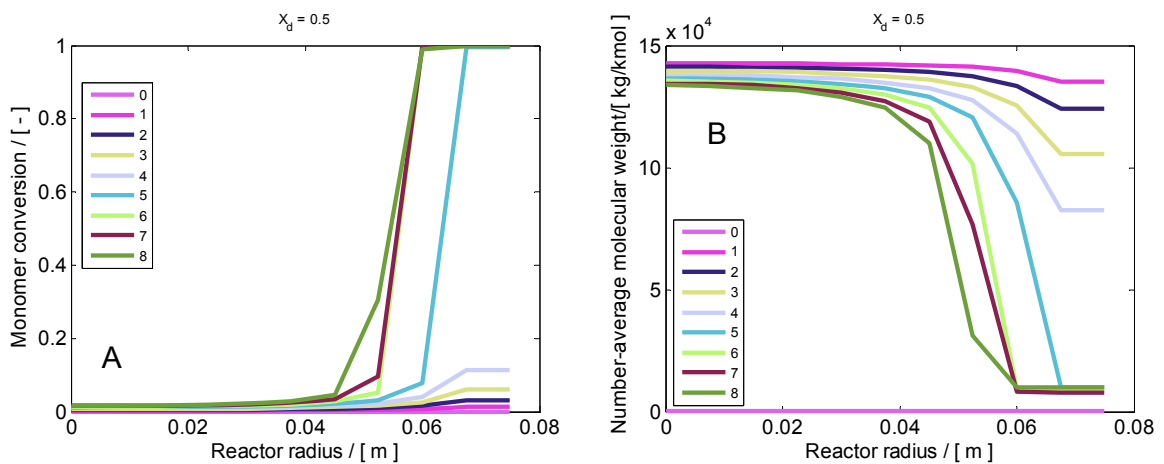


Figure 2.30. Monomer conversion (left) and number-average weight (right) profiles (laminar flow reactor, optimization problem 2)

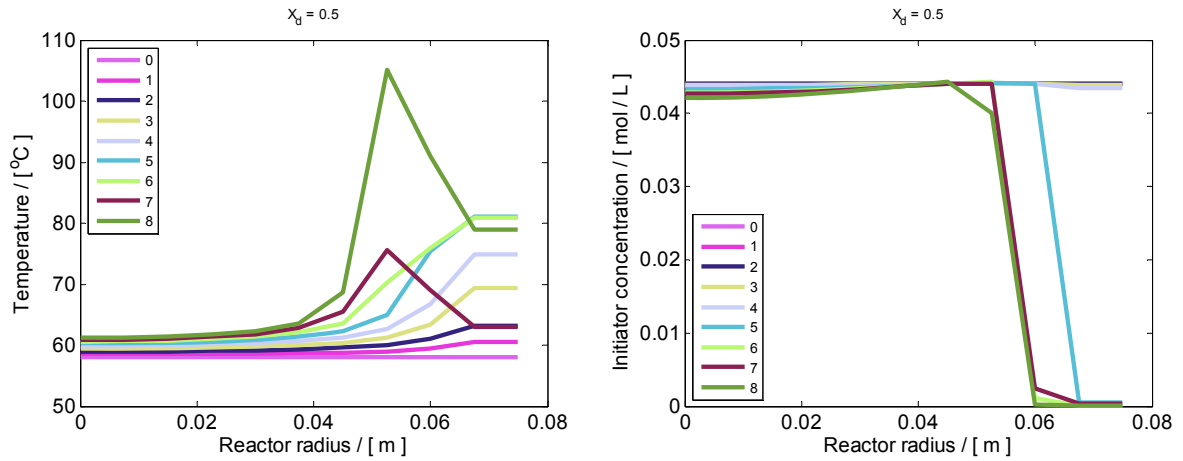


Figure 2.31. Reaction temperature (left) and initiator concentration (right) profiles (laminar flow reactor, optimization problem 2)

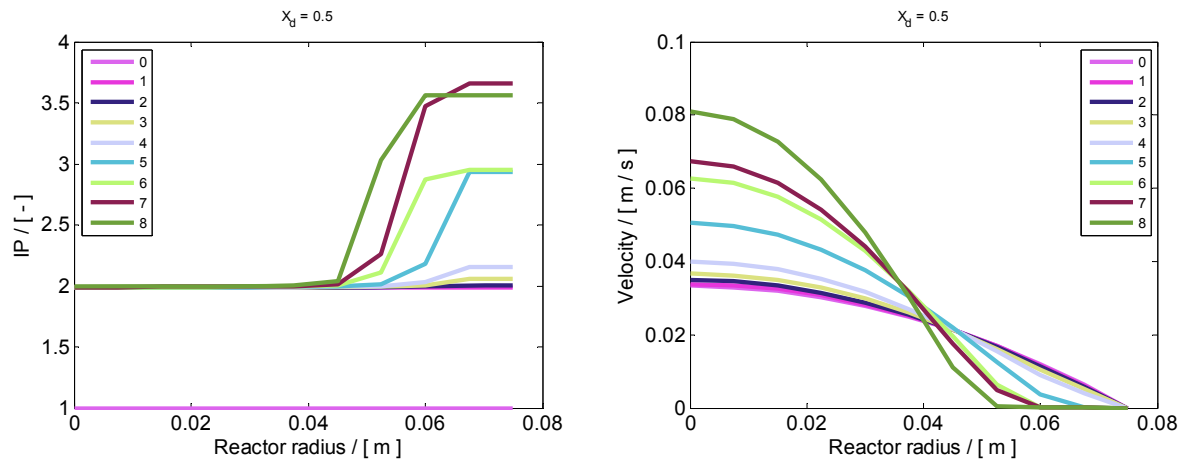


Figure 2.32. Polydispersity index (left) and flow velocity (right) profiles (laminar flow reactor, optimization problem 2)

Optimization of the plug-flow polymerization reactor

The calculated optimal values of the solvent mass fraction, initiator concentration and mass flow rate are presented in Table 2.19 and the optimal jacket temperature profile is presented in Figure 2.33. It can be observed that, comparing with the previous problem, the optimal solution is demanding a higher flow rate and higher monomer concentration in the feed; this is leading to a relatively higher temperature on the first cooling section, necessary to start the polymerization process with a reasonable rate. Then, an important amount of heat is generated in the polymerization process and the reactor has to be cooled to remove the reaction heat. Consequently, the cooling fluid temperature on the following segments of the jacket is kept at relatively low values. A rise of cooling temperature on the last two segments is finally demanded in order to increase the monomer conversion (as seen in Figure 2.34 - A, these increases by 20 % on the last two zones). This final

temperature evolution is perturbing the polydispersity index, which is displacing away from the desired value, on the last two reactor zones (Figure 2.36).

A value for polydispersity index closer to the desired one could be achieved by increasing the weighting factor w_3 , but with sacrifices in the approaching of desired values in number-average molecular weight and monomer conversion.

Table 2.19. Results of the plug-flow reactor optimization problem 2

No	Solvent mass fraction, w_s , [-]	Mass flow rate $D_{M,0}$, [kg/s]	Feed initiator concentration, $C_{I,0}$, [mole/L]	Optimized process performances					
				X, [-]		Mn, [kg/kmole]		IP, [-]	
				Calculated	Imposed	Calculated	Imposed	Calculated	Imposed
1	0.57	4.24×10^{-2}	2.31×10^{-3}	0.499	0.5	60007	60000	2.29	2

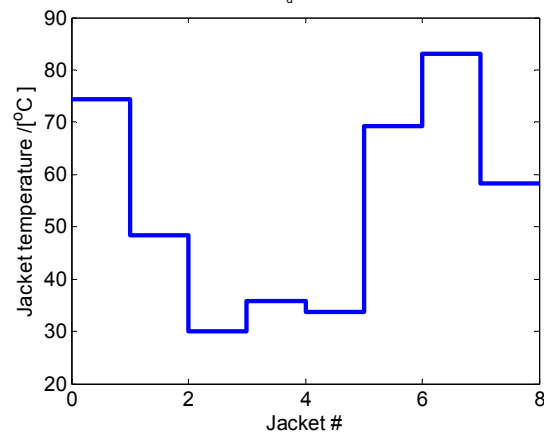


Figure 2.33. Optimal jacket temperature profile (plug-flow reactor, optimization problem 2)

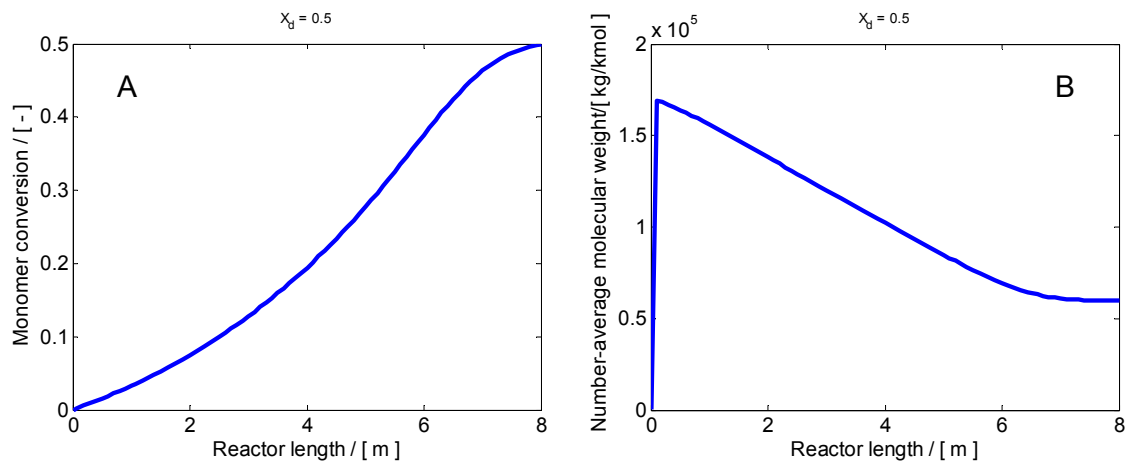


Figure 2.34. Monomer conversion (left) and number-average weight (right) profiles (plug-flow reactor, optimization problem 2)

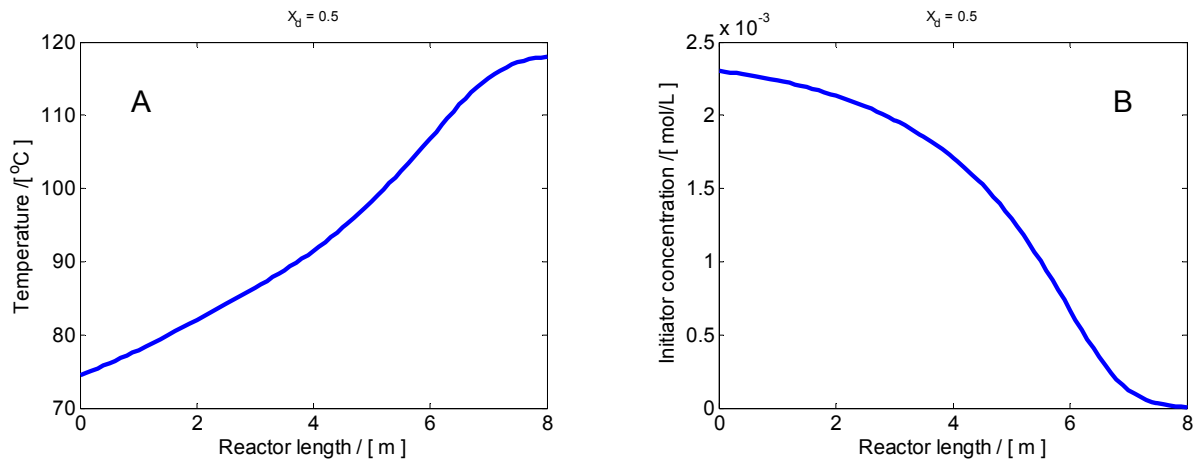


Figure 2.35. Reaction temperature (left) and initiator concentration (right) profiles (plug-flow reactor, optimization problem 2)

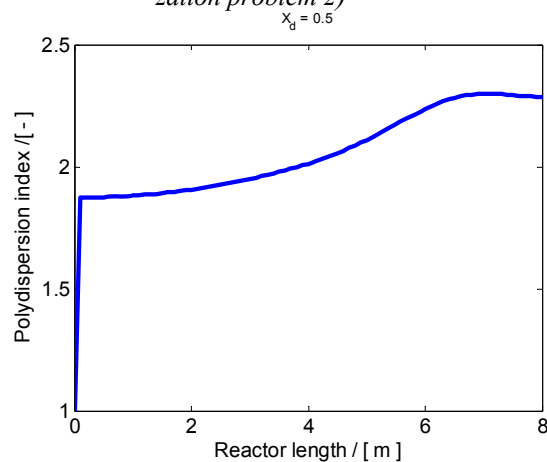


Figure 2.36. Polydispersity index profile (plug-flow reactor, optimization problem 2)

2.4. Conclusions

The objectives of this chapter was to investigate the particularities of modeling and optimization problems for tubular polymerization reactors and to compare the performance of two optimization methods, one based on Minimum Principle of Pontryagin and the other on a Genetic Algorithm. As a case study it was chosen the MMA solution polymerization process due to the availability of the kinetic data. Two types of tubular reactor models were developed, one in plug-flow assumptions and the other a bi-dimensional laminar flow, taking into account the radial variation of the flow velocity. The most representative among the published kinetic models was chosen by reactor simulations, comparing the agreement of the results in terms of simulated monomer conversion and number-average molecular weight. The model of Baillagou and Soong (1985) appeared from these stand point as the most representative.

Calculation procedures for the plug-flow and laminar flow regimes were developed and used in the polymerization reactor simulation. A comparison of reactor performances for the two flow

regimes of the reaction mixture, the laminar flow and the plug-flow was performed. The results show the limitations of the laminar flow reactor, due to the strong decreases of velocity near the reactor wall, limitations that are more pronounced at high feed monomer concentrations. The laminar flow provides a non-uniform utilization of the reaction volume and large variations of polymer characteristics across the flowing section, particularly at high monomer to solvent ratios. Due to lower velocities and higher reaction times near the wall, higher monomer conversions and polymer concentrations emerge in this region than in the core of tube. Another consequence is a less efficient radial heat transfer due to the lower thermal conductivity of polymer.

In order to compare the Minimum Principle and the GA methods, it was formulated an optimization problem for a plug-flow polymerization reactor. The objective of this problem was to determine the reactor temperature profile leading to a polymer product with desired number-average molecular weight and polydispersion index at a pre-specified monomer conversion. Considering the mathematical formulation, this optimization problem has an average level of difficulty.

To solve the optimization problem so formulated, there were developed numerical procedures based on Minimum Principle and a Genetic Algorithm. The optimization results are showing that both algorithms are able to localize the optimal solution, but with different efforts. Even if the MP algorithm is considered a more deterministic and rigorous from mathematical point of view, finding the solution of its characteristic optimum equations is a rather challenging task when applied to such complex nonlinear processes. In these cases the convergence of the existent numerical methods toward the optimum (global extreme of the performance index) is poor and is demanding important efforts to guess appropriate initialization values. This inconvenient can be surrounded by using GA method, that is guaranteeing more reliable results in the calculation of the global extreme of performance index. They are convenient optimization tools especially in the case of new complex nonlinear problems. Their main disadvantage, that of a higher computing time necessary to find the optimum, is becoming less and less important in the conditions of the actual progress of digital computers.

Several optimization problems for the laminar-flow and plug-flow polymerization tubular reactor were also formulated and solved by Genetic Algorithm. The results revealed a good capability of this algorithm in solving this class of optimization problems. From the technical point of view, the calculation results showed that reasonable homogeneous polymerization products can be obtained only at limited feed monomer concentrations and flow regimes close to the plug flow model. At high feed monomer concentration and high monomer conversion, the laminar reactor is producing a less homogeneous polymer, hardly controllable due to the strong radial variations of monomer conversion, generated by the important flow velocity radial gradients.

**3. Modeling and optimization of the PLA synthesis process
by reactive extrusion**

3.1. Literature survey

The world-wide production of consumer plastics continues to be dominated by petroleum-based polymers. The biodegradable polymers have been made economically attractive by two factors: the first, the environmental concern associated with waste disposal and the second, the future depletion of the most accessible petroleum reserves and consequently rising of the production costs.

Poly lactide (PLA) belongs to the family of synthetic aliphatic polyesters and is considered as biodegradable and compostable. It is a thermoplastic, high strength, high modulus polymer that can be obtained from annually renewable resources [57]. The degradability, versatility and anticipated price/performance of the new generation of polymers, PLA, will enable it to displace a significant volume of fossil fuel-based polymers.

Historical survey and PLA practical applications

Many investigations were performed along the last century on the lactic acid polymers. In 1985, Pelouze condensed lactic acid by distillation of water to form low molecular weight PLA, and the lactide (cyclic dimer of lactic acid) [58]. The polymer was produced for the first time in 1932 by Carothers (DuPont), heating lactic acid under vacuum to produce a low molecular weight product [59]. Although the polymer was known since the specified period, it was not of practical usefulness until recently. In 1988, Cargill Incorporated began the investigation of lactide and PLA and concluded that PLA is an interesting material. After years of research, Cargill managed to manufacture PLA in 1994, with 4000 t/year capacity. It was produced in a fully commercial manufacture by Cargill Dow in November 2001 [58]. In 2002, the PLA manufacture in the US federal state Nebraska had an production of 140 000 t/year PLA [60].

Nowadays, several companies in USA, Japan and Germany are currently creating modern technologies for production of lactic acid, polylactides and polymeric materials based on these raw materials. The basic manufacturers of these materials are: Cargill Dow Polymers (polymer and fibres NatureWorks™), Kanebo Goshen Ltd. (polymer and fibres Lactron™), Shimadzu Corp (Lactyl®), Ems Inventa Fischer GmbH & Co [61].

Subsequent work by DuPont and Ethicon has focused on the manufacture of PLA for medical-grade sutures, implants and controlled drug release applications. Shimadzu and Mitsui Tuatsu companies in Japan produce also limited quantities of PLA for “commodity” plastics applications. The advances in the fermentation of dextrose obtained from corn has dramatically reduced the cost

to manufacture the lactic acid monomer necessary to make PLA polymers [59].

Poly lactide is used mainly for medical applications, but recently it is accepted also to play a major role as a packaging material. Numerous studies indicate that the poly lactides are sufficiently biocompatible, with a minority suggesting otherwise [62-64]. The precise molecular structure determines their rate of degradation and since the degradation products are natural and metabolizable the process is generally well accepted [4]. It is stated in the published literature that the degradation time of L-PLA is much slower than that of DL-PLA requiring more than 2 years to be completely absorbed. A solution was to prepare copolymers of L-lactide with glycolide or DL-lactide in order to disrupt L-lactide crystallinity accelerating the degradation process [62].

PLA materials can be produced with a large range of properties, due to the nature of lactic acid, a chiral molecule with two asymmetric centers existing in four different forms. The molecular weights of PLA can vary from few thousands to over a million. Also, it can be easily converted into film, fiber, spun bond and melt blown products on existing processing equipment [59].

The rheological characteristics of PLA make it well suited for sheet extrusion, film blowing, and fiber spinning, but only marginally acceptable for some other types of fabrication [65]. The properties and temperature characteristics of poly lactide are comparatively close to polypropylene and polycapromide. The fiber and filament fabrication processes and equipment used are also similar. The usual production process includes spinning, thermal drawing, heat treatment (thermal relaxation), and final textile operations which are a function of the commercial forms and assortment of fibers and/or filaments. This is an almost no-waste process, since all wastes formed are recycled [61].

Monomers and polymerization processes

The basic constitutional unit of PLA, the lactic acid was first isolated in 1780 from sour milk by the Swedish chemist Scheele and produced commercially in 1881 [66]. It can be manufactured by carbohydrates fermentation or chemical synthesis [64, 67]. It is the simplest hydroxyl acid with an asymmetric carbon atom and it exist in two optically active configurations, the L(-) and D(+) isomers [68]. L-lactic acid is present in mammals while both stereoisomers are found in bacteria [57]. Nowadays, the majority of the fermentation processes use a genus of Lactobacilli which yields a high rate of lactic acid. Moreover, a recent study developed a process to produce mainly L-lactic acid including incubating acid-tolerant homolactic bacteria in nutrient medium [67]. It was found that hetero-fermentative lacto-bacteria produce a racemic mixture of D and L-lactic acid [60].

The conversion of lactic acid into PLA can be carried out following two routes. The first route involves the direct polycondensation reaction and removal of water product under high vac-

uum and high temperature [1, 10, 14], while vacuum and temperature are progressively increased [59]. The polycondensation could be seen as the easiest route, but it is difficult to reach high molecular weights through a solvent-free process [57]. Addition of acidic catalysts, such as boric or sulfuric acid accelerates the esterification and transesterification processes, but also catalyzes side reactions. Also the low molecular weights condensates could be of practical interest in preparation of biodegradable glues and lacquers because the -OH and -COOH end groups allow cross-linking with suitable inorganic or organic multivalent additives [59]. The properties of lactic acid oligomers, which can be further used to synthesize polyurethanes, can be controlled using different operating conditions and the type of catalyst and functional agents [69]. This approach was used by Carothers and it is still used by Mitsui Toatsu Chemicals Inc. to produce a low molecular weight polymer [59].

An alternative of PLA producing from lactic acid is the ring-opening polymerization of lactic acid dimer, di-lactide. Water is removed under mild conditions, without a solvent, to produce the cyclic dimer from lactic acid. A process in which lactide is purified by an improved distillation system with the substantially purified lactide removed as an intermediate boiling side-draw stream was proposed in the published literature [70]. Other efficient processes were proposed to transform lactic acid into its cyclic dimer [16-18]. The process was industrially applied by Cargill Dow [70-74]. Function of lactide purity can be obtained a large range of molecular weight polymers [59].

L-lactide ring-opening polymerization. Polymerization initiators and mechanisms

Considerable experimental work was done by various investigators to study the reaction kinetics of ring-opening polymerization. In experimental studies, various catalyst systems, solvents and reaction temperature have been used to obtain polymers of molecular weights ranging from a few thousands to over a million.

The lactide polymerization initiators could be divided into three categories:

- Lewis acids, $\text{Sn}(\text{Ph})_4$, SnBr_4 , stannous octoate - SnOct_2 , zinc acetate - ZnAc_2 , Sb_2O_5 , zinc lactate - ZnLac_2 . They promote the polymerization by compounds containing hydroxyl groups following the coordination-insertion mechanism. There are commercially available, easy to handle, soluble in common organic solvents. Some of them are potentially non-toxic.
- Metal-alkoxides: $\text{Al}(\text{OR})_3$, $\text{R}_3\text{SnOR}'$, $\text{Ti}(\text{OR})_4$, which are supposed to be the true initiators of ring-opening polymerization of L-lactide. However they have increased toxicity, for example aluminium tri-isopropoxyde, $\text{Al}(\text{O-iPr})_3$ is suspected of supporting Alzheimer's disease [75];

- Other initiators as N-carbenes, racemic catalyst, calcium and magnesium complexes, enzymes having the advantage of biocompatibility and low-toxicity. The main disadvantage of this third category of initiators is the impossibility to know exactly the kinetic mechanism.

Recent studies include dimeric aluminum chloride complexes of N-alkoxyalkyl- β -ketoimines (activation with propylene oxide), alkoxy-amino-bis (phenolate) Group 3 metal complexes [76], aluminum complexes bearing tetradentate bis(aminophenoxide) ligands, hetero-bimetallic iron(II) alkoxide/aryloxides, stannous octoate and diethanolamine, β -diiminate ligated magnesium and zinc complexes [77], zinc alkoxide complex, magnesium and zinc alkoxides [78], titanium alkoxide, iron alkoxide [79, 80], 2,6-dimethyl aryloxide, calcium coordination complexes [81], complexes of Cu, Zn, Co and Ni Schiff base derived from salicylidene and L-aspartic acid, dizinc-monoalkoxide complex supported by a dinucleating ligand, stannous octoate with adducts containing oligomers L-lactide and rac-lactide [82], tertiary amines, phosphines and N-heterocyclic carbenes, alkyl aluminum, aluminum – achiral ligands complexes and lithium chloride [83, 84]. Polymerization studies involving fully biocompatible initiators (creatinine) for L-lactide ring-opening polymerization were published but only low molecular weight polymers were produced [85].

The published works in the field of L-lactide polymerization were reviewed by Stridsberg et al [86], Drumright et al [65], Wu et al [87] and Dechy-Cabaret et al [75].

The published studies showed an increased effect in development of an efficient and simple kinetic mechanism for L-lactide polymerization. It was demonstrated that lactones polymerization using aluminium and tin alkoxides proceeds via an insertion mechanism [88]. Dubois et al hypothesized that the L-lactide ring-opening polymerization initiated by aluminium alkoxide proceeds through a “coordination-insertion” mechanism and selective rupture of the acyl-oxygen bond of the monomer [89-91].

The most used initiator for the L-lactide polymerization process is SnOct_2 , its advantages being the high catalytic activity, racemization-free polymerization of L-lactide, formation of high-molecular weight polymers with high yields and its acceptance by the US Food and Drug Administration, etc [92, 93]. Usually a primary alcohol is used as co-initiator, which fulfills three purposes: it accelerates the polymerization process, allows a control for molecular weights and does form ester end-groups which can be used for further preparative or analytical purposes (^1H NMR determination of the degree of polymerization) [94].

One of the first studies concerning L-lactide polymerization using stannous octoate as initiator was published in 1987 by Eenink [95]. The study reports data concerning the influence of proc-

ess parameters on the polymer characteristics. Other work reporting the influence of monomer purity on the polymer molecular weights for L-lactide/stannous octoate polymerization system was published by Lian-Xi et al [96].

Nijenhuis et al studied the kinetics and mechanism of L-lactide bulk polymerization using stannous octoate and zinc bis (2,2 – dimethyl –3,5 – heptanedionate – O, O'). The monomer conversions up to 80 % conversion were obtained and the rate of polymerization using tin compound was higher than that with zinc-containing initiator, while at conversions beyond 80%, the latter initiator gave the higher rate of polymerization. The differences in the rate of polymerization at high conversions for the two catalysts are suggested to be caused by a difference in crystallinity of the newly formed polymer. It is suggested that contaminants in the catalyst and the monomer are the true initiators. Initiation as well as polymerization is supposed to proceed through Lewis acid catalyzed transesterification between an activated lactone and a hydroxyl group [97].

Methyltriflat [98] and stannous(II) trifluormethane sulphonate [99] were mentioned as cationic initiators for L-lactide polymerization in the published literature. Few studies have speculated about a cationic mechanism [100, 101] for stannous octoate initiated L-lactide polymerization. Schwach et al [101] studied the ring opening polymerization of PLA in the presence of SnOct₂ under conditions allowing for the end – group characterization of growing chains by high-resolution ¹H-NMR.

For low values of monomer to initiator ratios, the D, L-Lactide ring was opened to yield lactyl octoate-terminated short chains. A cationic type mechanism (Figure 3.1) involving coordination by octanoic acid was proposed to account for experimental findings.

Kricheldorf et al performed the anionic L-lactide polymerization in solution was performed using potassium benzoate, potassium phenoxide, potassium tert-butoxide and butyllithium as initiators. Absence of initiator fragments in the isolated PLA chains suggested that initiator mainly involve deprotonation of L-lactide. It was also proved that the alkoxide chain end cause partial racemization [102].

The effect of Lewis bases co-initiators in the polymerization of L-lactide using SnOct₂ as initiator is studied by Degée et al [92]. The monomer was dried under reduced pressure before use and the initiator was purified by two vacuum distillations. The authors didn't discover any direct relationship between molecular weight and the maximum conversion. The polymerization rate decreases as the monomer/initiator ratio (M/I) is increased.

Degée et al revealed that M/I values lower than 1000, the number-average molecular weight values are higher than those expected on the basis of the initial monomer to catalyst initial ratio (assuming quantitative initiation) and they supposed that stannous octoate is not the actual initiator.

The monomer conversion levels off at 98 % in the 110 – 150 °C range, but decreases down to 95 % at 180°C. The PLA is opaque and appears to be heterogeneous when the polymerization temperature is below 150°C whereas it is transparent and homogeneous above this.

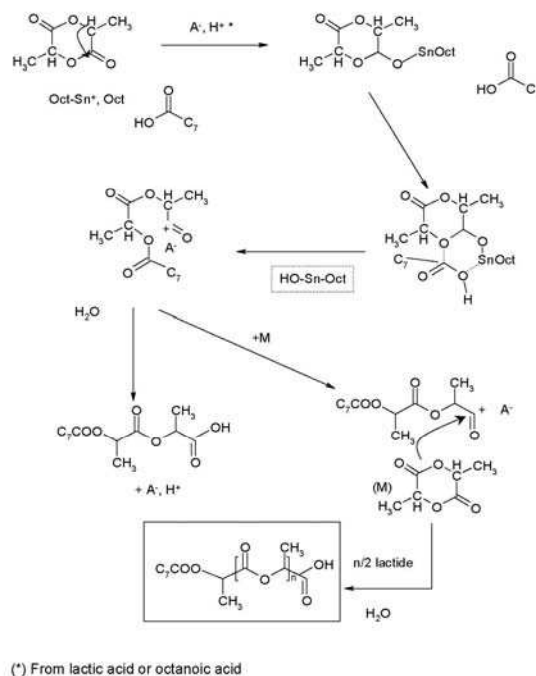


Figure 3.1. Cationic mechanism of lactide polymerization [101]

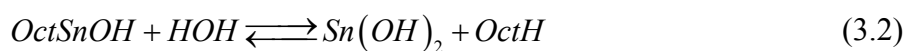
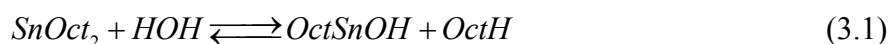
This observation explains the tendency of PLA chains to crystallize in the presence of the unreacted monomer. Three Lewis bases (4-picoline, thiophene and triphenylphosphine) had been added to SnOct₂ with the purpose of increasing the rate of lactide polymerization in preference to the transesterifications reactions. The addition of 4-picoline decreased the polymerization reaction compared with SnOct₂ alone. Thiophene does not significantly affect the kinetics whereas triphenylphosphine acts as an accelerator. The general effect of triphenylphosphine used as co-catalyst was a faster polymerization, which is better controlled leading to higher molecular weight and narrower molecular weight distribution, at least within the time required for reaching maximum monomer conversion.

The effect of hydroxylic and carboxylic acid compounds on the L-lactide polymerization initiated by stannous octoate was studied by Zhang et al [103, 104]. Stannous alkoxide, a product of reaction between stannous octoate and an alcohol (under formation of a Sn – O – R) was proposed as the substance initiating the polymerization through coordinative insertion of lactide. An alcohol can also affect the polymerization through reaction of initiator formation, chain transfer and trans-

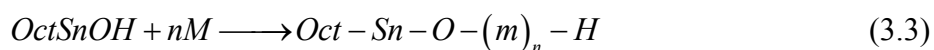
esterification. Zhang et al showed that the alcohol increases the PLA production rate while carboxylic acids decrease it. Both alcohol and carboxylic acids was found to reduce the PLA final molecular weights.

Kricheldorf [94, 105] studied model reactions between pure SnOct₂ and primary alcohols. Both L-lactide and stannous octoate were purified before using. The authors reveal the fact that a rapid equilibrium between SnOct₂ and benzylalcohol occurs even at 20°C and the formation of a SnOct₂ – alcohol complex was formulated. An increasing downfield shift of the OH – proton was observed with higher SnOct₂/alcohol ratios. The continuation of this study using ¹³C NMR spectroscopy has revealed that the CO – signal of SnOct₂ shifts upfield in direction of the value typical for the free octanoic acid when an alcohol is added. The NMR spectroscopy results revealed a rapid equilibrium between the octoate groups of Sn(Oct)₂ and the added alcohol leading to octanoic acid molecules.

Kowalski et al [106-108] revealed that the actual active centers can be formed with adventitious water, hydroxyl acids and some others unknown co-initiators present as impurities in the polymerization mixture. With water as impurity, the following interchange reactions take place:

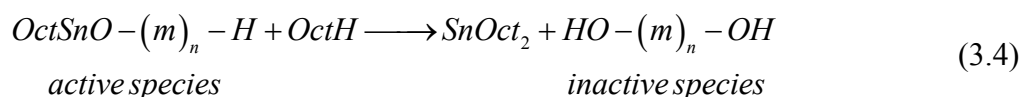


with subsequent propagation by monomer insertion into the –Sn-OH bonds:



where Oct denotes the 2-ethyl hexanoate group and m the polyester repeating unit derived from M.

Addition of 2-ethylhexanoic acid to the system was found to decrease the rate of polymerization and practically does not influence the number-average molecular weights. The rates decrease because growing chains are converted into the dormant ones by displacing the alkoxide active chain from tin atom. The higher the concentration of the added acid the lower the instantaneous concentration of growing chains::



To speed up the polymerization reaction, the acids present in the polymerization mixture should be removed. Storey and Taylor [109] reported NMR data showing that SnOct₂ reacts directly with hydroxyl groups giving eventually the respective 2-ethylhexanoate ester.

Esterification may also proceed with the already formed hydroxy-PLA, e.g.:

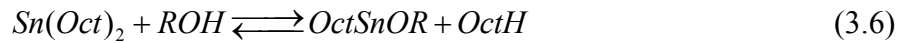


The presence of Sn atoms in macromolecules is the argument for polymerization proceeding with Sn – alkoxides as an active species.

Kowalski et al [4] published a comparison between polymerization of L-lactide initiated by SnOct₂ with and without adding a co-initiator. In the case of polymerization reaction using as initiator SnOct₂ alone, the dependence of relative polymerization rate in respect with initial concentration of stannous octoate was studied. At lower initiator concentrations the rate increases almost linearly with starting initiator concentration until a critical value is reached; then further increase of polymerization rate is less steep, and after reaching a maximum, it eventually decreases with further increasing initiator concentration. The result means that the adventitious co-initiator does exist in both solvent/monomer mixture and in SnOct₂ itself. Thus, above a certain initiator concentration any further increase in rate is only due to the co-initiator present in SnOct₂. A slight retarding effect is probably caused either by the octanoic acid introduced as an impurity with SnOct₂. The system used for polymerization contained approximately 10⁻³ mol/L of adventitious hydroxyl compounds as co-initiator.

When using as initiating system a mixture of stannous octoate and butanol (BuOH) at a constant concentration of SnOct₂, at lower starting concentrations of butanol, the polymerization rate increases proportionally to butanol initial concentration (BuOH₀). When a certain ratio BuOH/SnOct₂ is reached, the rate becomes independent of BuOH₀. Moreover, with increasing BuOH₀, molar weights decrease. In this case, it was revealed that the alcohol plays a double role, of co-initiator and of transfer agent. The same role could be played by any hydroxyl compound present in the polymerization mixture, as follows:

- formation of an initiator



- reversible chain transfer



The reaction (3.7) decreases the total concentration of macromolecules able to grow (active or dormant) by forming the dead molecules ($Oct-(m)_n - R$). Some new initiating species may be formed in the reaction of the esterification byproduct, H₂O, following the reactions (3.1) and (3.2) respectively. These reactions increase the number of the growing species, increasing polymerization rate this way. In parallel reactions, carboxylic acid is formed and inhibits polymerization.

Esterification and formation of octanoic ester end groups are much less important in L-

lactide polymerization than in the polymerization of caprolactone. Concentration of the esterified macromolecules at the final equilibrium would presumably be close to double the initial stannous octoate concentration.

Polymerization with an initial concentration of stannous octoate of 0.05 mol/L with no alcohol added was proved to be very slow by Kowalski et al because it is certainly initiated by compounds containing hydroxyl groups, adventitiously present in the system as impurities. The authors assumed that one molecule of co-initiator give rise to one macromolecule, the concentration of the co-initiator calculated from $M_n = 1.5 \times 10^5 \text{ mol} \cdot \text{L}^{-1}$ of the resulting polymer, was equal to $\approx 10^{-3} \text{ mol} \cdot \text{L}^{-1}$. Polymerization initiated with stannous butoxide in concentration of 0.05 mol/L was $2.4 \cdot 10^2$ times faster than with only SnOct₂ alone.

The rate of polymerization in the system with octanoic acid added to stannous butoxide was approximately 2 times lower. That support the hypothesis that approximately 90 % mol of stannous alkoxide became temporarily deactivated.

Kricheldorf et al [94, 105] has shown that both anionic and cationic polymerization of L-lactide involve strong racemization above 50°C, whereas SnOct₂ yields optically pure PLA even at 180 °C, when the reaction time is short. The SnOct₂ used in experiments was dried firstly by twice distillation with xylene under reduced pressure and finally subjected to a fractionated distillation in vacuum. The L-lactide from Boehringer KG (Ingelheim, Germany) was recrystallized from ethyl acetate.

The authors polymerized the L-lactide at 180°C with neat SnOct₂ under variation of M/I ratio. The molecular weight were dependent on the M/I ratio and all the samples contained significant amounts of octoate end groups. The values of degree of polymerization indicated that, on the average, only one octoate group per initiator was transformed into an end group. The highest monomer conversion was obtained at 180°C, using a M/I ratio of 200 and a reaction time of one hour.

Hyun et al. [110] recrystallized the monomer from ethyl acetate and the stannous octoate was purified by distilling three times under reduced pressure. The highest molecular weight was obtained at a catalyst concentration around 0.05 % wt. The authors suppose that the molecular weight is closely related to the trace amounts of water present in the polymerization system. The polymerization of L-lactide was carried out over a temperature range 120° C to 220°C. Both the monomer conversion and the molecular weights increase with time in the initial stage of polymerization, followed by a gradual decrease in conversion as well as in the molecular weights of polymer. This tendency became more pronounced at higher temperatures.

Duda et al. [111] published a comparison between two initiating system (stannous oc-

toate/butanol and stannous butoxide) for polymerization of L-lactide.

The commercially available SnOct₂ contained about 4.5 % wt of octanoic acid and up to 0.5 wt % of water. After two consecutive high vacuum distillations the concentration of the acidic protons in SnOct₂ was reduced about 20 times. The content of the impurities was then reduced (based on several distillation of THF (20 v/v) in and out of the sample under vacuum) down to 0.9 mol % (about 40 times).

Using a reaction temperature of 80°C, an initial concentration of SnOct₂, Duda et al obtained at the full monomer conversion the number-average molecular weight of $1.3 \cdot 10^5$ for polymerization of L-lactide. These values corresponded to the concentration (in mol·L⁻¹) of the macromolecules of $1.1 \cdot 10^3$ and it is supposed to be equal to the concentration of the hydroxyl groups containing impurities, adventitiously present in the polymerizing mixture and playing role of coinitiators and/or transfer agents. The authors used also the standard high vacuum technique and obtained molecular weights up to 10^6 . They proved that the molecular weight of the polyester could hardly be controlled and strongly depends of the purity of the components of the reacting mixture.

Other initiation systems for L-lactide polymerization were tested. Kowalski et al [112] compared the polymerization initiated by stannous octoate in presence of hydroxyl compounds (alcohols, water, carboxylic acids) with those initiated by stannous octoate/ primary amines systems. No significant mechanistically differences between the two initiations systems were shown.

More recent studies of Kowalski et al [113] provided supplementary proofs of the general alkoxide mechanism, for L-lactide polymerization initiated with zinc octoate and aluminium acetylacetonate. Similar behavior as in the case of stannous octoate was found.

The influence of the alcohols with different hydroxyl groups on the L-lactide polymerization initiated by stannous octoate was studied by Korhonen et al [114]. The NMR analysis of low molecular weight polymers showed that the number of hydroxyl groups initiating polymerization was near theoretical for 1,4-butanediol (2 OH groups) and pentaerythritol (4 OH groups). The numbers for polyglycerines were somewhat lower than theoretical (8 or 12 OH groups), but they clearly suggested the star-shaped structure, with more arms than in polymers initiated with pentaerythritol. The preparation of high molecular weight polymers showed that the polymerization rate increases with the number of hydroxyl groups in the co-initiator. Along with the faster polymerization, higher molecular weight polymers were obtained. High hydroxyl group content in the polymer did not cause a drop in the conversion level or enhanced backbiting during extended polymerization. Furthermore, the co-initiator did not affect the thermal properties of the polymers except that slightly lower melting temperatures were measured for star-shaped than linear polylactides.

The reversible kinetics of L-lactide initiated by stannous octoate was studied by

Witzke et al [115]. The propagation reaction was supposed to be reversible and the activation energy value for this reaction was calculated. The assumption that the total number of reaction centers is equivalent to the initial number of initiator molecules was made. The equilibrium monomer concentrations were calculated for different operating conditions.

The first conclusion is that the hydroxyl compounds present in the polymerization mixture have an important role in the initiation of the polymeric chains. The acidic and hydroxyl compounds produce the deactivation of the active polymer by chain transfer resulting inactive polymer species. A simple reaction mechanism that doesn't take into account the reversibility of the initiator formation could contain elementary steps of initiation, propagation, chain transfer to monomer and solvent.

PLA thermal and rheological properties

Like in the case of other polymers, the thermal properties of PLA are related to the structure of the polymeric chains. Polylactides are very sensitive to heat, for temperature larger than 190 °C. Most of degradative reactions were supposed to involve the highly concentrated ester bond on the main chain. Low molecular weight compounds (water, monomer, oligomers, polymerization catalyst) associated with the polymer seemed to play an important role in lowering molecular weights at high temperatures [116]. The PLA chain could be considered stable for monomer amounts lower than 2% in the final product [70, 72-74].

Even if stannous octoate can promote sufficiently fast lactide polymerization, it is also known to have adverse effect on the PLA molecular weight and properties, as a result of backbiting and intermolecular transesterification reactions, not only during the lactide polymerization but also during any further melt processing [117].

Degradation studies were performed by McNeil et al [118] for a temperature range of 230 - 440 °C. The authors proposed a degradation mechanism and activation energy of 28.5 kcal/mol was determined. The influence of an inhibitor (1,4 - diaminoantraquinone) in amount of 1 % wt on the degradation reaction of PLA was reported. A beneficial effect of the inhibitor was observed, indicating that a free radical chain process is involved in PLA degradation. A commercially available product (ULTRANOX 626), based on Bis (2,4-di-*t*-butylphenyl) Pentaerythritol Diphosphite was successfully tested by Jacobsen et al [63, 119] to stabilize a L-lactide reactive extrusion process.

The glass transition temperature (T_g) is one of the most important characteristics of a polymer since it defines the operating temperature for polymer manufacturing. Variations in T_g for a particular polymer system may reflect different molecular weights, the presence of adventitious

plasticizers, physical aging, polymer architecture and the degree of crystallinity. The T_g of high molecular PLA was found in the range 35 – 60 °C [120].

The rheological properties of different molecular weights PLA were studied by Cooper-White et al [121]. PLA polymers are noted to require substantially larger molecular weights in order to display similar melt viscoelastic behavior at a given temperature, as that for conventional non-biodegradable polymers such as polystyrene.

PLA reactive extrusion

To make economically viable the L-lactide polymerization process, Jacobsen et al [63, 119] developed a continuous process using reactive extrusion technology. Small polymerization times (5 – 7 min) were found to be suitable for this process (predetermined by the residence time in extruder). An equimolar amount of a Lewis base (triphenyl phosphine) was found to have a beneficial effect on the L-lactide polymerization process [122]. Extruder flow rate in the range of 0.75 – 1.25 kg/h and screw speeds of 50 – 200 rpm were tested and their influence on the monomer conversion and polymer molecular weights were discussed.

3.2. Experimental study of the L-lactide polymerization kinetics

3.2.1. Experimental set-up, materials and polymerization method

Experimental apparatus

The polymerization reactions have been carried out in a Haake Rheocord internal mixer with a R600 chamber. The set-up allows the monitoring of the torque and the control with a good accuracy of the reaction temperature. The schema of the experimental setup is presented in Figure 3.2.

The setup is electrically heated, the resistances being incorporated in three steel plates, allowing the complete closing of the reaction chamber and the temperature control. The cooling is performed with a flow of air at room temperature. The maximum temperature allowed by the apparatus is 400 °C. The device is provided with two compatible Roller Rotors, having an external diameter of 19.05 mm. The free volume of the reaction chamber is 69 cm³ and the maximum speed of the rotors is 250 min⁻¹.

A second apparatus used in the kinetic study was a DSM Micro 15 TS Compounder device presented in Figure 3.3.

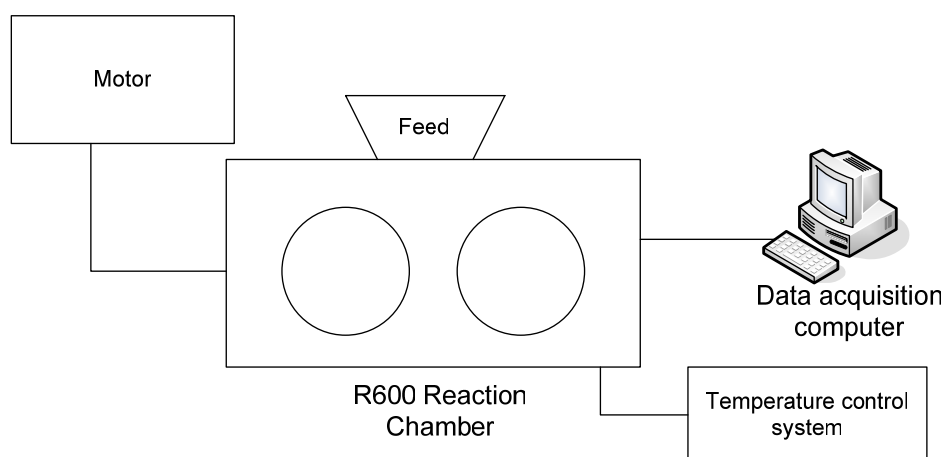


Figure 3.2. HAAKE Rheocord Mixer simplified schema



Figure 3.3. DSM Micro 15 TS Compounder

A detailed view of the screw chamber is presented in Figure 3.4. The apparatus can work in continuous or discontinuous (with recirculation of the material between the two screws) operating modes. It is electrically heated and cooled by a flow of air at room temperature, or a flow of cold water.

The core of this laboratory compounder is a mixing compartment containing two detachable, conical mixing screws. Both the screws and the housing are specially treated to minimize wear and to make them resistant against chemicals. The batch volume is 15 ml and the maximum allowed

temperature is 350 °C. The temperature control is possible on 6 zones, and the screw speed can be varied between 0 to 250 rpm.

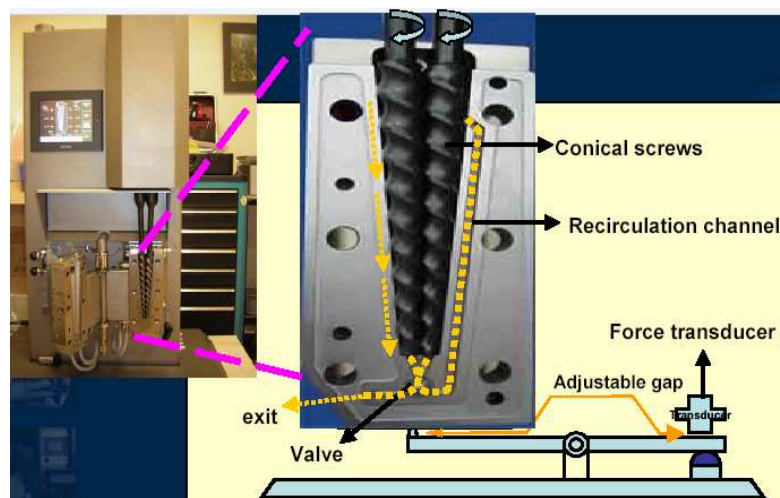


Figure 3.4. Detailed view of the reaction chamber

Materials

The L-Lactide dimer was purchased from Boehringer Ingelheim and the stannous octoate (Sn bis-ethyl-2-hexanoate) initiator and triphenyl phosphine co-initiator from Sigma Chemicals. One of the aims of the study was to investigate the process characteristics by using the commercial purity L-lactide and initiator. According to the specifications of the producer, the purity of L-lactide was minimum 99 % (wt), the heavy metals content of maximum 10 ppm, a maximum water content of 0.02 %, free acid content 0.027% and residual solvent (toluene) maximum 0.2 %. Also a maximum percent of 0.2 % mesolactide could be found.

The purity of stannous octoate was 95%, the main impurities according to Kowalski et al and Duda et al [111, 113, 123] being water (0.5 wt-%) and octanoic acid (4.5 wt-%). L-lactide dimer, stannous octoate and triphenyl phosphine initiator were used as received, without any purifying treatment. In the case of polymerization reactions co-initiated by triphenyl phosphine, the compound was added in equimolecular ratio with stannous octoate.

Method

In the experiments performed on the HAAKE Mixer, a quantity of approximately 50 g monomer was fed into the reaction chamber. In order to insure a better control of the initiator quantity it has been first dissolved in anhydrous toluene. As an example, in the experiments with the minimum concentration of initiator ($M/I = 4500$) a volume of 0.025 ml stannous octoate has to be mixed

with 50 g L-lactide. In this aim, a solution of 1 ml stannous octoate in 40 ml anhydrous toluene was prepared and then, 1 ml of the solution so obtained was mixed with the specified L-lactide quantity in a flask. The resulted mixture was fed into the reaction chamber, previously heated at reaction temperature. In order to extract composition samples from the molten reaction mixture, the device screws were stopped for about 5 seconds for each sample.

For the second category of experiments, on the Micro 15 Compounder, a total mass of 10 g monomer was fed into the reaction chamber. In order to insure a good initiator dosage, the same procedure was adopted, based on the use of a toluene solution of initiator. To extract composition samples, the exit valve was used (see Figure 3.4), without stopping the device screws rotation.

In both cases, the extracted composition samples were immediately cooled in a stream of cold air and then hermetically closed into plastic bags and stored at the refrigerator to stop the reaction. The polymerization times up to 60 min were used [124].

Experiments were performed for L-lactide polymerization initiated either by stannous octoate (at monomer/initiator molar ratios of 225, 2250 and 4500), or by stannous octoate-tryphenyl phosphine (at monomer/initiator molar ratios 2250 and 4500). In the last case, the mixture octoate-tryphenyl phosphine used as initiator was always equimolecular.

The screw speed was fixed at 50 rpm, irrespective the device used to perform the batch ring-opening L-lactide polymerization process.

3.2.2. Polymer characterization

Nuclear magnetic resonance

The composition of a polymeric mixture could be determined by conventional spectroscopic techniques such as nuclear magnetic resonance (NMR). Among the physical analysis methods, the NMR is the method that offers the largest quantity of structural information. Both spectra, ^1H and ^{13}C offers information that could be strictly related to the structure of the analyzed compound [125]. The ^1H -NMR analyses were performed in deuterated chloroform at 25°C, using a Bruker 250 instrument. A number of 128 scans were performed for each sample, until the complete separation for the characteristic frequencies for polymer and monomer. The measurement of monomer concentration was performed by ^1H -NMR spectroscopy analysis of reaction mixture, from integration between methine quartets of monomer ($\delta\text{CH}_{\text{L-LA}}=5.01$ ppm position “a” in Figure 3.5) and those of the polymer ($\delta\text{CH}_{\text{PL-LA}}=5.14$ ppm – positions “b” and “c” in Figure 3.5) [126-128].

To calculate the monomer conversion (X_M), from the $^1\text{H-NMR}$ spectra, the following relation is used:

$$X_M = \frac{A_p}{A_m + A_p} \cdot 100 \quad (3.8)$$

where A_p is the characteristic area of the polymer peak ($\delta\text{CH}_{\text{PL-LA}}=5.14$ ppm, position “b” and “c” in Figure 3.6) and A_m is the corresponding area of the monomer peak ($\delta\text{CH}_{\text{L-LA}}=5.01$ ppm, position “a” in Figure 3.6).

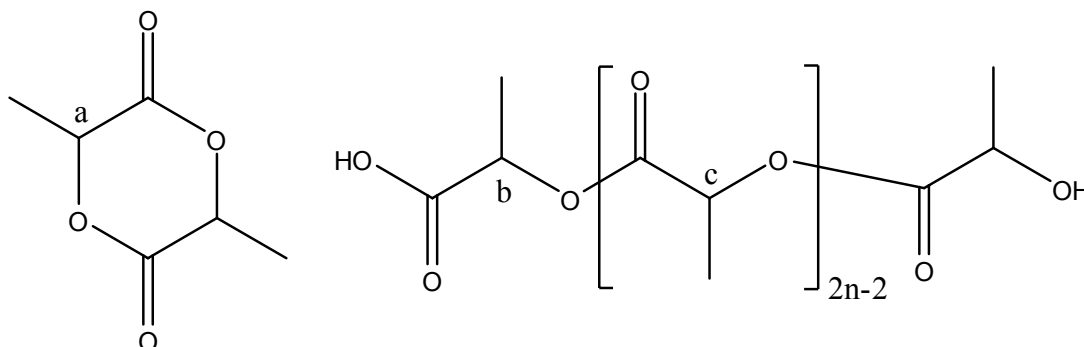


Figure 3.5. Characteristic proton positions for L-LA and PLA

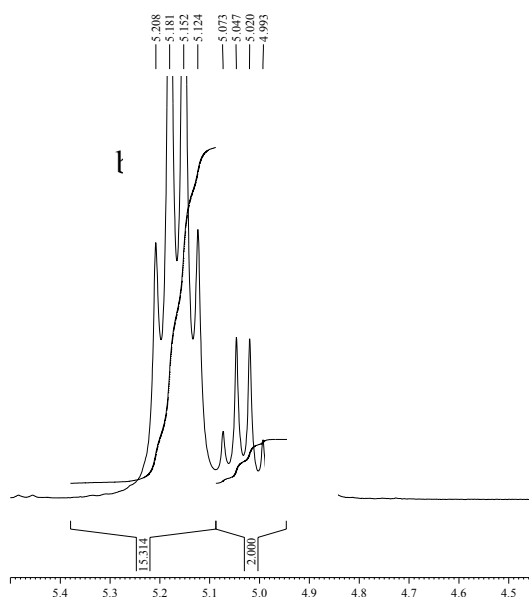


Figure 3.6. Example of $^1\text{H-NMR}$ spectra of PLA

Size-exclusion chromatography (SEC)

The SEC method is based on the fact that, when a porous particle is immersed in a polymeric solution, smaller molecules penetrate the pores more deeply than larger ones. The polymer solution is injected into a continuous stream of solvent flowing through a chromatographic column

filled with a porous material. Since the dimension of a macromolecule reflects its molar mass, polymer molecules which possess low masses are eluted by the flowing solvent at later times. The SEC measurements have been performed at 30°C using chloroform as solvent and a solution of 5 mg/ml of L-lactide, on a Waters 510 apparatus using a Polymer Laboratory PLGel 5 μm Mixed-C column. The detector was a Waters 410 differential refractometer, and the scaling has been made using polystyrene standards provided by PolymerLab. A flow rate of 1 mL/min (total time of 12 minutes) was used for each analysis. The method was used to determine the molecular weight distribution and the mean-molecular weights of the polymers.

It is known from the published literature that, for a given temperature and solvent, at any given retention volume, it is fulfilled the relation [129]:

$$\eta_{\text{PLA}}M_{\text{PLA}} = \eta_{\text{PS}}M_{\text{PS}} \quad (3.9)$$

Where PS denotes the polystyrene standard, PLA denotes the working polymer (polylactide), η – the intrinsic viscosity of the polymer solution and M is the molecular weight of the polymer. The viscosity is generally represented by a Mark-Houwink equation:

$$\eta = K \cdot M^\alpha \quad (3.10)$$

Published values of Mark-Houwink parameters in common SEC solvents are available for many polymers. If Mark-Houwink constants (K and α) for the analyzed polymer and for the standard are known, from equations (3.10) and (3.9) one obtains:

$$M_{\text{PLA}} = \left(\frac{K_{\text{PS}}M_{\text{PS}}^{\alpha_{\text{PS}}+1}}{K_{\text{PLA}}} \right)^{1/(\alpha_{\text{PLA}}+1)} \quad (3.11)$$

In our determinations, the Mark-Houwink constants were: for polystyrene: $K_{\text{PS}} = 1.64 \cdot 10^{-4}$, $\alpha_{\text{PS}} = 0.692$ and for polylactide, $K_{\text{PLA}} = 1.05 \cdot 10^{-3}$, $\alpha_{\text{PLA}} = 0.563$ [119].

The accuracy of the molecular weights determination by SEC is in the range $\pm 5\%$ as reported in the published literature [130]. An example of PLA chromatogram is presented in Figure 3.7. The high peak on the right is characteristic to un-reacted monomer (small molecular weight species) and the other is characteristic for the polymeric (high molecular weight species) products in the reaction mixture [131].

This method, usually used for determination of molecular weights and molecular weights distributions, also permits the determination of the monomer conversion in this case, by using the peak areas for polymers (A_p) and the corresponding area for monomer (A_m). The relation used to calculate the monomer conversion (X_M) is [131]:

$$X_M = \frac{A_p}{A_m + A_p} \cdot 100 \quad (3.12)$$

In Table 3.1 are presented comparatively the values for monomer conversion obtained by $^1\text{H-NMR}$ and SEC for all the reaction samples in two experiments at 2250 and 4500 molecular M/I ratios.

Comparative tests for the conversion values calculated by SEC and $^1\text{H-NMR}$ were randomly made for other samples and the results proved to be similar with those presented in Table 3.1 In this way it is proven that the SEC can be a reliable technique to determine the conversion for the L-lactide ring-opening polymerization process comparatively with the most precise $^1\text{H-NMR}$ [131].

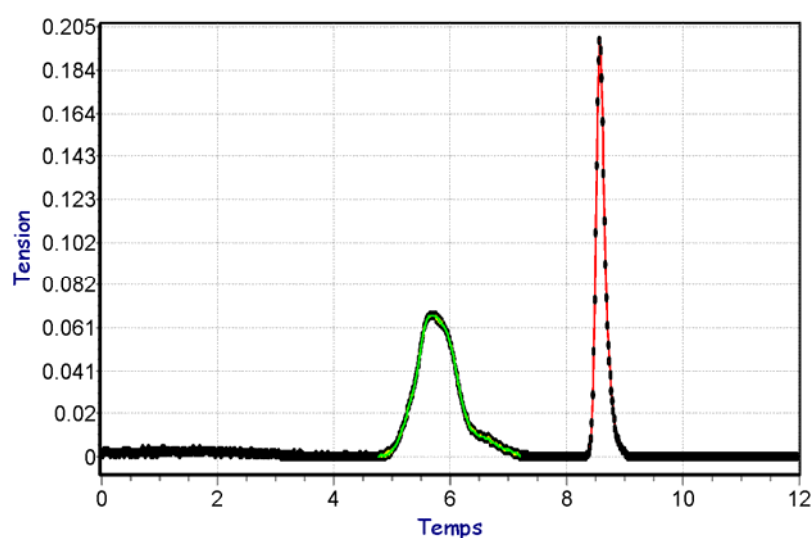


Figure 3.7. SEC chromatogram for a PLA/L-LA mixture

Table 3.1. Conversion values estimated by $^1\text{H-NMR}$ and GPC for two kinetic experiments (initiator SnOct_2)

Sample name	Monomer to initiator molar ratio M/I	Time [min]	Conversion (%) $^1\text{H-NMR}$	Conversion (%) SEC
KD11	4500	2	22	23
KD12	4500	6	38	32
KD13	4500	12	50	48
KD14	4500	22	71	70
KD15	4500	36	83	82
KD51	2250	2	33	33
KD52	2250	6	54	62
KD53	2250	12	84	80
KD54	2250	22	89	87
KD55	2250	36	94	92

Infrared spectroscopy (FT-IR)

A part of the polymer samples were characterized in solid state by FT-IR spectroscopy, using a Bruker VERTEX 70 instrument, equipped with a Harrick MVP2 diamond ATR device. For the other part, the measurements in transmittance/absorbance were realized on a Perkin Elmer spectrometer. The spectra were registered between 400 cm^{-1} and 4000 cm^{-1} with a resolution of 4 cm^{-1} . For rising the signal to background and in the same time to have a reasonable time for the acquisition (3 – 4 minutes for each sample) 16 scans were performed. The reference spectrum was recorded using the pure KBr pastille. For the solid samples the measurements were performed on KBr pastille containing 1 wt-% polymer. The main objective of this analysis was to qualitatively observe the advancement of the polymerization process. The obtained FT-IR spectra corresponding to the first and last samples in Table 3.1 for both considered M/I ratios, are presented in Figure 3.8 and Figure 3.9, comparatively with the L-lactide monomer spectra.

It can be observed that the diminution of the ring specific vibration (650 and 935 cm^{-1}) is proportionate with the L-lactide polymerization time, until the complete disappearance. These bands were selected according to [132], but the the 935 cm^{-1} monomer specific band is reported also by other literature studies [63, 119, 122].

This behavior shows the starting of the ring-opening polymerization in the first 2 minutes and almost total consumption of the monomer after 36 minutes.

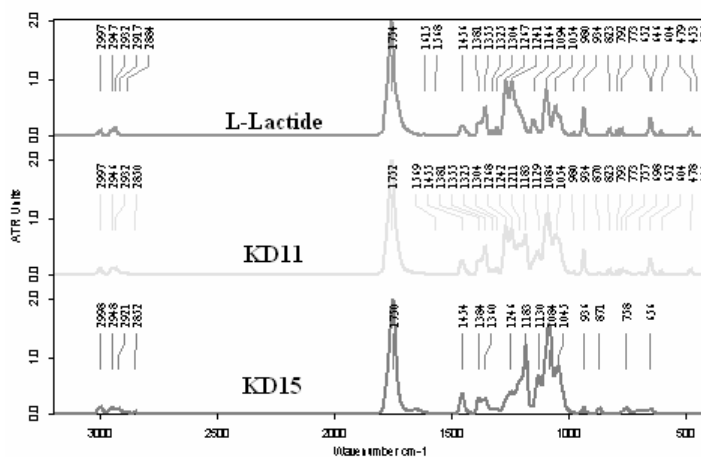


Figure 3.8. FT-IR spectra for M/I= 4500 series

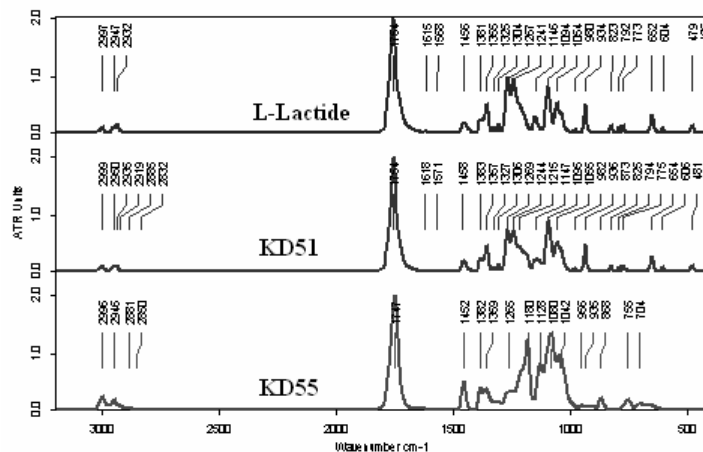


Figure 3.9. FT-IR spectra for $M/I = 2250$ series

3.2.3. Experimental results

A. L-lactide polymerization initiated by stannous octoate

The kinetics of L-lactide polymerization initiated by stannous octoate is studied at temperatures between 185– 200 °C, and M/I ratios of 225, 2250 and 4500. The times for samples pre-levation as well as the polymer characteristics for $M/I = 2250$ and $M/I = 4500$ are presented in Tables 3.2 – 3.7 The monomer conversions were determined by $^1\text{H-NMR}$ and the molecular weights by GPC, using the methods described in the paragraph 3.2.2. The experiments were compared on the base of working temperature, monomer to initiator ratio and reaction time. The molecular weight values were rounded corresponding to the SEC analysis method accuracy.

Table 3.2. Polymer characteristics for 170 °C and $M/I = 2250$ (initiator SnOct_2)

Sample	Time, [min]	Monomer conversion, [-]	Number-average molecular weight, [kg/kmole]	Polydispersity index, [-]
	0	0	144	1
K6P1	3	0.23	1200	1.4
K6P2	6	0.41	5500	1.5
K6P3	10	0.58	8600	1.5
K6P4	15	0.68	11000	1.6
K6P5	25	0.85	11500	1.6
K6P6	35	0.89	12200	1.6

Table 3.3. Polymer characteristics for 185 °C and $M/I = 2250$ (initiator SnOct_2)

Sample	Time, [min]	Monomer conversion, [-]	Number-average molecular weight, [kg/kmole]	Polydispersity index, [-]
	0	0.00	144	1.0
K5P1	4	0.47	8500	1.1
K5P2	10	0.89	13000	1.3
K5P3	18	0.89	15000	1.7
K5P4	30	0.95	16100	1.8

K5P5	50	0.96	16500	2.0
------	----	------	-------	-----

Table 3.4. Polymer characteristics for 195 °C and M/I = 2250(initiator SnOct₂)

Sample	Time, [min]	Monomer conversion, [-]	Number-average molecular weight, [kg/kmole]	Polydispersity index, [-]
-	0	0.00	144	1.0
K3P1	2	0.31	8300	1.2
K3P2	5	0.72	10000	1.4
K3P3	8	0.84	12000	1.8
K3P4	12	0.88	14000	1.8
K3P5	17	0.93	16000	2.3
K3P6	22	0.95	17500	2.2
K3P7	30	0.96	18000	2.1

Table 3.5. Polymer characteristics for 185 °C and M/I = 4450(initiator SnOct₂)

Sample	Time, [min]	Monomer conversion, [-]	Number-average molecular weight, [kg/kmole]	Polydispersity index, [-]
-	0	0.00	144	1.0
K7P1	7	0.31	8600	1.1
K7P2	10	0.38	11000	1.6
K7P3	15	0.60	13000	1.6
K7P4	25	0.77	15500	1.7
K7P5	45	0.89	16300	2.2
K7P6	55	0.90	17000	2.5

Table 3.6. Polymer characteristics for 195 °C and M/I = 4500(initiator SnOct₂)

Sample	Time, [min]	Monomer conversion, [-]	Number-average molecular weight, [kg/kmole]	Polydispersity index, [-]
-	0	0.00	144	1.0
K4P1	4	0.55	10000	1.7
K4P2	11	0.84	14500	1.8
K4P3	20	0.94	18000	2.3
K4P4	35	0.94	18500	2.3

Table 3.7. Polymer characteristics for 200 °C and M/I = 225. First experiment (initiator SnOct₂)

Sample	Time, [min]	Monomer conversion, [-]	Number-average molecular weight, [kg/kmole]	Polydispersity index, [-]
-	0	0.000	144	1.0
K8P1	2	0.962	31000	2.6
K8P2	4	0.962	29500	2.7
K8P3	6	0.955	26500	2.6
K8P4	10	0.949	17500	2.7
K8P5	20	0.954	16000	2.3
K8P6	30	0.965	11500	2.5

Table 3.8. Polymer characteristics for 200 °C and M/I = 225. Second experiment (initiator SnOct₂)

Sample	Time, [min]	Monomer conversion, [-]	Number-average molecular weight, [kg/kmole]	Polydispersity index, [-]
-	0	0.000	144	1.0
K9P1	2	0.950	31500	2.6
K9P2	4	0.965	29000	2.7
K9P3	6	0.952	26000	2.6
K9P4	10	0.951	17000	2.8
K9P5	20	0.957	16500	2.4

To check the reproducibility of L-lactide polymerization data, several experiments were repeated in identical working conditions. The results showed a good reproducibility of data all over the working domain. An excerpt of these is given in Tables 3.7 and 3.8. As seen from Table 3.7, working at high temperature and high initiator concentration, almost complete monomer conversion values are obtained after only 2 minutes of polymerization time. The high initiator concentration promotes the formation of numerous polymeric chains, and the propagation rate rise proportionally to their concentration, providing the high monomer conversions. An explanation for the decrease in polymer molecular weights after 2 minutes could be a significant termination rate corroborated with a depolymerization process, due to the high temperature in the polymerization reactor.

In spite of the relatively large scatter of experimental points, the data presented in Tables 3.2 – 3.6 permit to draw several conclusions regarding the L-lactide polymerization process. An important conclusion is that the bulk polymerization process cannot be conducted at reactions times of the same order of magnitude as the residence times of the melts in twin-screw extruders. However, the use of industrial TSE with longer residence times can be envisaged. Also, the values of molecular weights of the polymers are particularly low, insufficient to produce a polymer of practical interest.

As already mentioned, several previous studies showed a weak reversibility of L-lactide polymerization [110, 115]. This particularity could explain the fact that the conversion curves tend to plateau out on the last time interval and the time dependence of Mn at high temperatures present an evolution with a weak maximum.

Temperature influence

It is well known that the temperature has an enhancing effect on the propagation rates, but also augments the side reactions, as de-polymerization and inter and intra-molecular transesterification. The temperature dependence of monomer conversion and number average molecular weight, for two monomer/initiator molecular ratios, is presented in Figures 3.10 and 3.11.

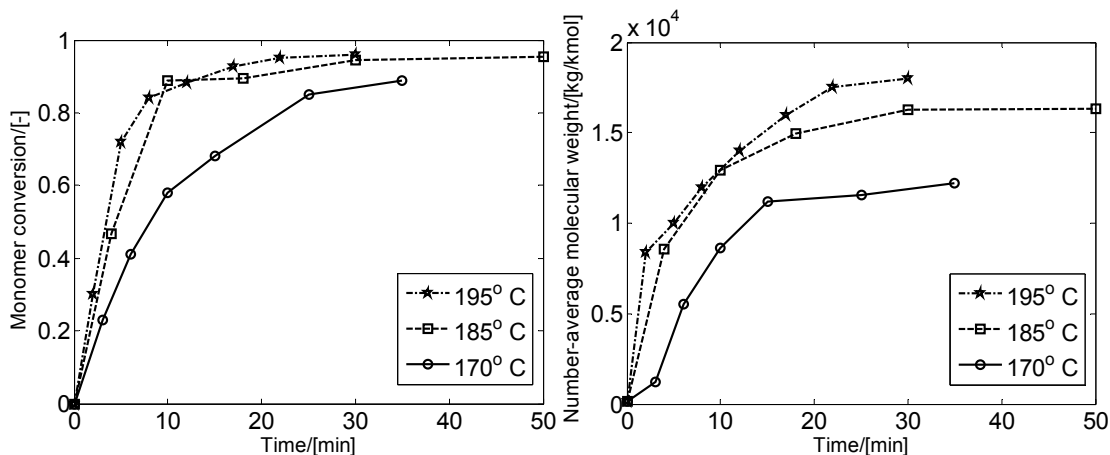


Figure 3.10. Monomer conversion and number-average molecular weight profiles (M/I of 2250, initiator SnOct₂)

It is observed an important effect of the temperature onto the propagation rate at smaller polymerization times (for a reaction time of 5 minutes, the obtained monomer conversion is 72 % at 195 °C, as compared with approximately 50 % at 185 °C). Also, higher temperatures provide higher polymer molecular weights, due to a more important effect of temperature on the propagation rate than on the termination ones.

The experimental results obtained at the temperatures of 185°C and 195°C show close values of monomer conversion at M/I of 2250 (Figure 3.10), and rather different monomer conversions at M/I of 4500 (Figure 3.11). The conclusion that could be drawn is that the reaction temperature has a stronger influence on the monomer conversion at lower initiator concentration. Also, the experimental results are showing that increasing the reaction temperature determines the increase of polymer molecular weights, irrespective of the monomer to initiator ratio.

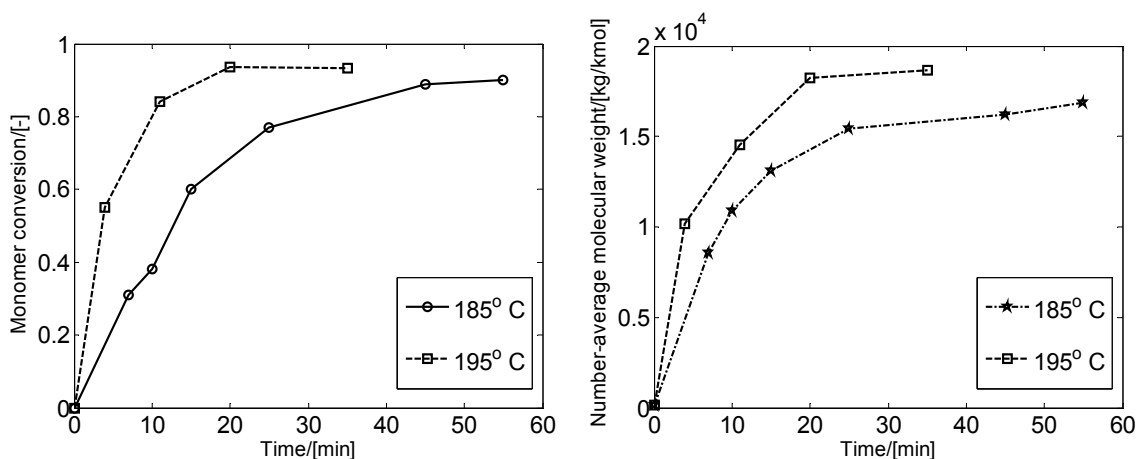


Figure 3.11. Monomer conversion and number-average molecular weight profiles (M/I of 4500, initiator SnOct₂)

Initiator concentration influence

The experimental results presented in Tables 3.2 – 3.3 show no significant differences in monomer conversion on the domain of higher temperatures and variable M/I. For polymerization times smaller than 10 minutes, higher monomer conversions are observed for smaller M/I ratios (higher initiator concentration). Practically close values are obtained for monomer conversion at polymerization times higher than 10 minutes probably due to close values of propagation rates (0.88 after 12 min for M/I = 2250 comparatively with 0.84 after 11 min and M/I = 4500; 0.95 after 22 min for M/I = 2250 comparatively with 0.93 after 20 min for M/I = 4500). Slightly higher monomer conversions are measured in the case of higher initiator concentrations, especially for polymerization times smaller than 10 minutes (Figure 3.12).

The molecular weights are slightly different, a higher initiator concentration leading to a lower molecular weight, as result of higher number of initiated radicals, and consequently shorter polymeric chains.

It can be concluded that higher initiator concentrations provide higher monomer conversions and smaller molecular weights due to the increased number of growing live polymers.

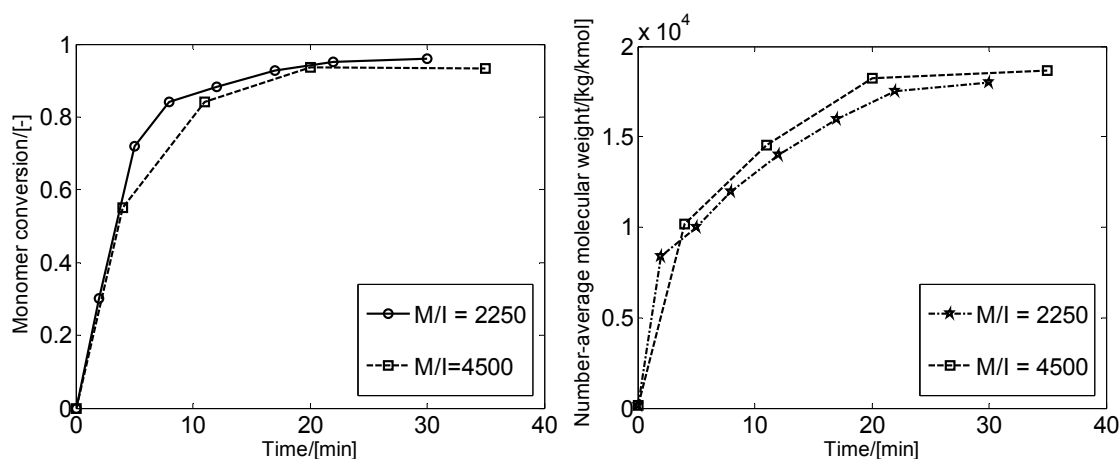


Figure 3.12. Monomer conversion and number-average molecular weight profiles for a temperature of 195 °C (initiator SnOct₂)

No important variations of monomer conversion with initiator concentration are observed at a temperature of 195 °C, proving that the influence of initiator on the propagation rate is insignificant.

B. L-lactide polymerization initiated by stannous octoate and co-initiated by triphenyl phos-

phine

Several studies published in the literature [63, 119, 122] showed that triphenyl phosphine can be used as an efficient coinitiator for L-lactide bulk polymerization. The main effects of this co-initiator is a faster polymerization reaction, which is better controlled, leading to higher molecular weights and narrower molecular weight distributions [122]. In order to obtain a higher molecular weight polymer comparing with that obtained in the presence of solely stannous octoate, L-lactide polymerization experiments initiated by stannous octoate and co – initiated by tryphenil phosphine were carried out in similar operating conditions (temperature range of 185 – 205 °C and monomer to initiator molecular ratios of 2250 and 4500 respectively). An equimolecular mixture of stannous octoate and triphenyl phosphine was used to initiate L-lactide polymerization. The monomer conversions as well as the molecular weights were determined by SEC method, as described above. The experimentally determined characteristics of final reaction mixture are presented in Tables 3.9 to 3.13.

Table 3.9. Time evolution of polymer characteristics for 185 °C and M/I = 4500 (initiator SnOct₂/TPP)

Sample	Time, [min]	Monomer conversion, [-]	Number-average molecular weight, [kg/kmole]	Polydispersity index, [-]
-	0	0	144	1
I3P1	5	0.282	68000	1.4
I3P2	10	0.454	86000	1.5
I3P3	15	0.536	88000	1.7
I3P4	20	0.576	85000	1.8
I3P5	25	0.607	86000	1.8
I3P6	30	0.639	84500	1.9

Table 3.10. Time evolution of polymer characteristics for 195 °C and M/I = 4500 (initiator SnOct₂/TPP)

Sample	Time, [min]	Monomer conversion, [-]	Number-average molecular weight, [kg/kmole]	Polydispersity index, [-]
-	0	0	144	1
I4P1	5	0.534	76000	1.8
I4P2	10	0.744	92000	2.1
I4P3	15	0.840	94000	2.3
I4P4	20	0.908	87000	2.4
I4P5	25	0.913	85000	2.5
I4P6	30	0.916	84000	2.6

Table 3.11. Time evolution of polymer characteristics for 205 °C and M/I = 4500 (initiator SnOct₂/TPP)

Sample	Time, [min]	Monomer conversion, [-]	Number-average molecular weight, [kg/kmole]	Polydispersity index, [-]
-	0	0	144	1
I5P1	5	0.517	96000	1.3
I5P2	10	0.823	98000	1.5
I5P3	15	0.899	100000	1.6
I5P4	20	0.921	97000	2.1

It is well known that the residence times of flowing materials in twin screw extruders are generally smaller than 10 min. Consequently, the experimental data obtained on the initiating system SnOct₂/TPP showed the possibility to perform L-lactide polymerization by the method of reactive extrusion. The beneficial effect of the TPP is proved by higher propagation rates corroborated with smaller termination rates that conduct to longer polymer chains. The higher values of molecular weights could be explained by smaller termination corroborated with higher initiation rates. The values show an important acceleration effect of the TPP co-initiator onto the polymerization steps, as stated in the literature [63, 119, 122, 133].

The experiments used to determine the polymerization kinetics have to be performed in drastically operating conditions (inert atmosphere, high purity of the raw materials, uniform homogeneity of the mixing etc.). In our kinetic study the L-lactide and initiator were used as purchased, without supplementary purification, so that the nature of the impurities and their influence on the polymerization mechanism is not known.

Table 3.12. Time evolution of polymer characteristics for 185 °C and M/I = 2250 (initiator SnOct₂/TPP)

Sample	Time, [min]	Monomer conversion, [-]	Number-average molecular weight, [kg/kmole]	Polydispersity index, [-]
-	0	0	144	1
I6P1	5	0.497	68000	1.6
I6P2	10	0.754	70000	2.3
I6P3	15	0.866	73000	2.5
I6P4	20	0.879	67000	2.6
I6P5	25	0.919	66000	2.6
I6P6	30	0.967	56000	2.6

Table 3.13. Time evolution of polymer characteristics for 195 °C and M/I = 2250 (initiator SnOct₂/TPP)

Sample	Time, [min]	Monomer conversion, [-]	Number-average molecular weight, [kg/kmole]	Polydispersity index, [-]
-	0	0	144	1
I7P1	5	0.64	66000	2.1
I7P2	10	0.88	67500	2.6
I7P3	15	0.92	56500	2.6
I7P4	20	0.929	56000	2.7
I7P5	25	0.934	46000	2.7
I7P6	30	0.941	40000	2.9

Temperature influence

For a fixed monomer to initiator ratio, an increase in the working temperature can have a beneficial effect on the monomer conversion as well as on the polymer number - average molecular

weight. The experimental results for a M/I of 4500 at three different temperatures are presented in the Figure 3.13 (note that in this case I represents the stannous octoate).

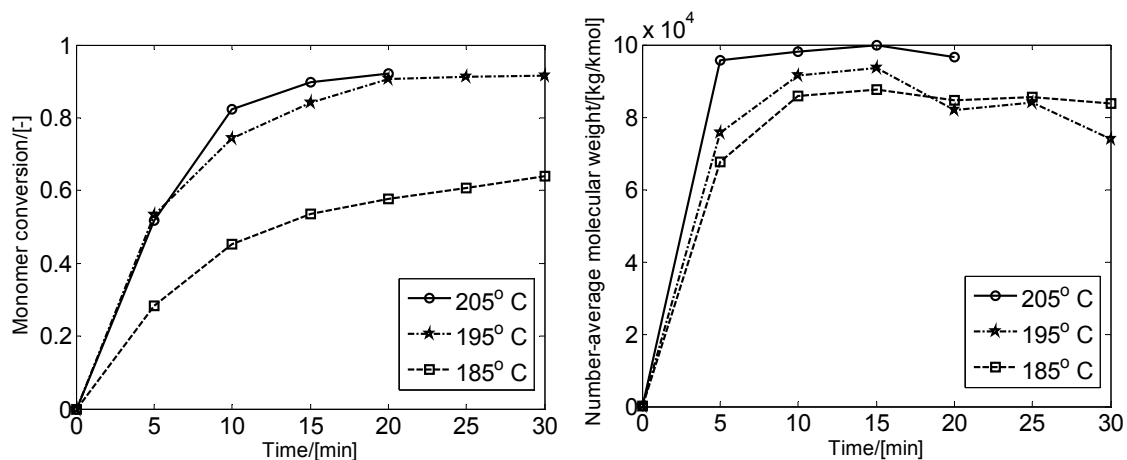


Figure 3.13. Monomer conversion and number-average molecular weights profiles for a M/I of 4500 (Initiator SnOct₂/TPP)

From these experimental results, it can be concluded that, in the case of L-lactide polymerization initiated by an equimolar mixture of stannous octoate and triphenyl phosphine (M/I = 4500), the reaction temperature favors both the monomer conversion and polymer molecular weight.

Nevertheless one can point out that the molecular weight distributions at 20 minutes are wider at higher temperatures (195 and 205 °C), presumably due to the promotion of secondary depolymerization or transesterification reactions.

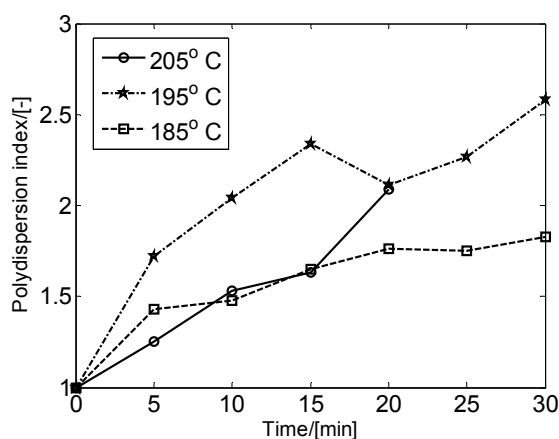


Figure 3.14. Polydispersion index for a M/I of 4500 (Initiator SnOct₂/TPP)

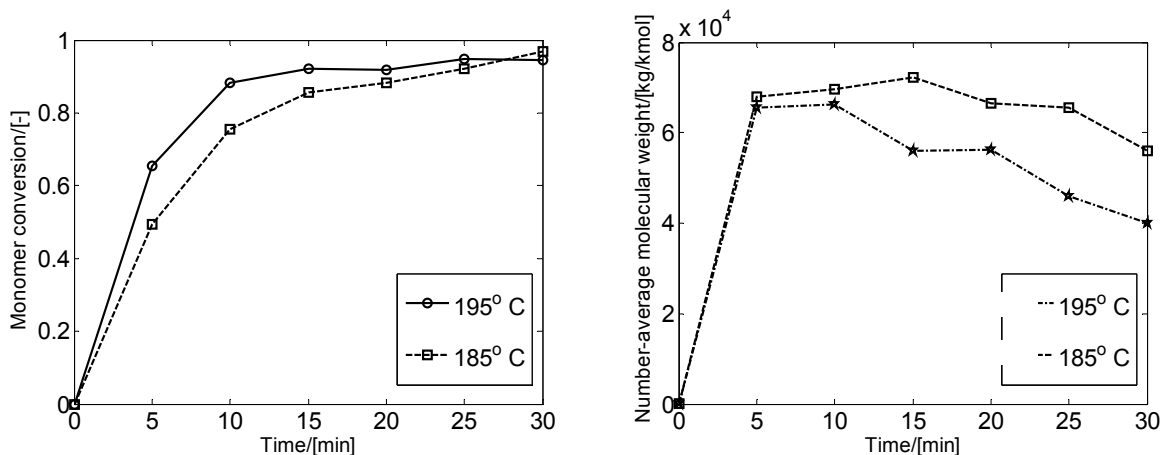


Figure 3.15. Monomer conversion and number-average molecular weights profiles for a M/I of 2250 (Initiator SnOct₂/TPP)

As observed from Fig. 3.15 and 3.16, like in preceding cases, increasing the temperature higher monomer conversion and molecular weights as well as wider molecular weight distributions are obtained. A comparison of the experience at 195°C and two experiences at 200°C at a M/I of 2250 is presented in Figure 3.17. A particularity of the results presented in Figure 3.17 is that the experience at 195°C is performed in a Haake Mixer and the two experiments at 200°C are performed in a DSM Minicompunder.

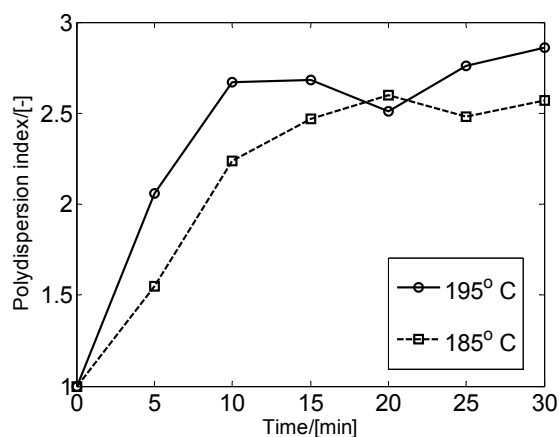


Figure 3.16. Polydispersity index for a M/I of 2250 (Initiator SnOct₂/TPP)

These diagrams reveal a stronger temperature influence on the polymer molecular weight than on monomer conversion. Practically, the same values for monomer conversion are obtained, at two temperatures, whereas the molecular weight is significantly lower, presumably due to the intensification on de-polymerization phenomenon.

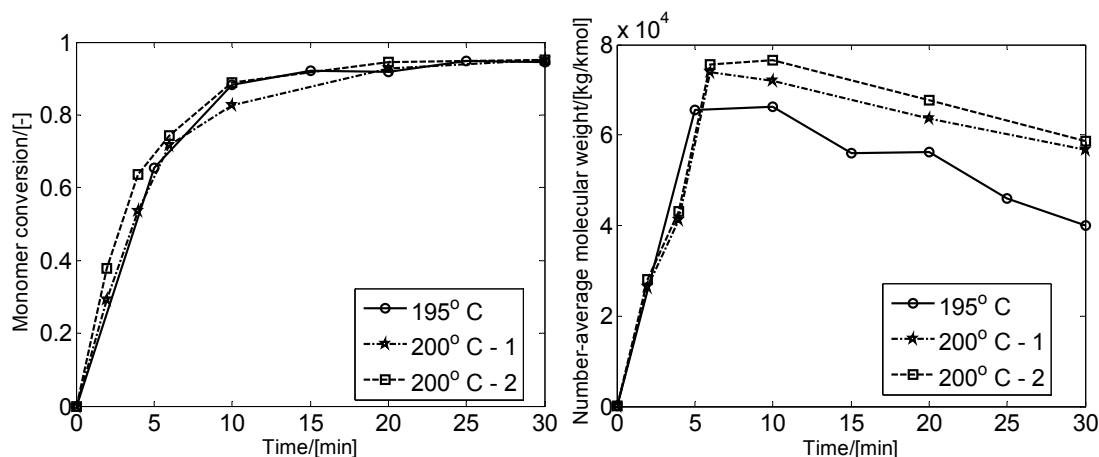


Figure 3.17. Comparison of monomer conversion and number-average molecular weights profiles for the kinetics and reproducibility tests (Initiator $\text{SnOct}_2/\text{TPP}$)

M/I influence

From Figure 3.18 can be seen that at a given temperature (195°C in this case) the molecular weight increases with the decrease of initiator concentration (increase of monomer to initiator ratio).

As seen, by halving the initiator concentration the polymer molecular weight is practically doubled. However, the influence on monomer conversion at this temperature is less important. Close final values for monomer conversion are obtained for both monomer to initiator ratios, with higher propagation rates for the first 15 min in the case of higher M/I ratio.

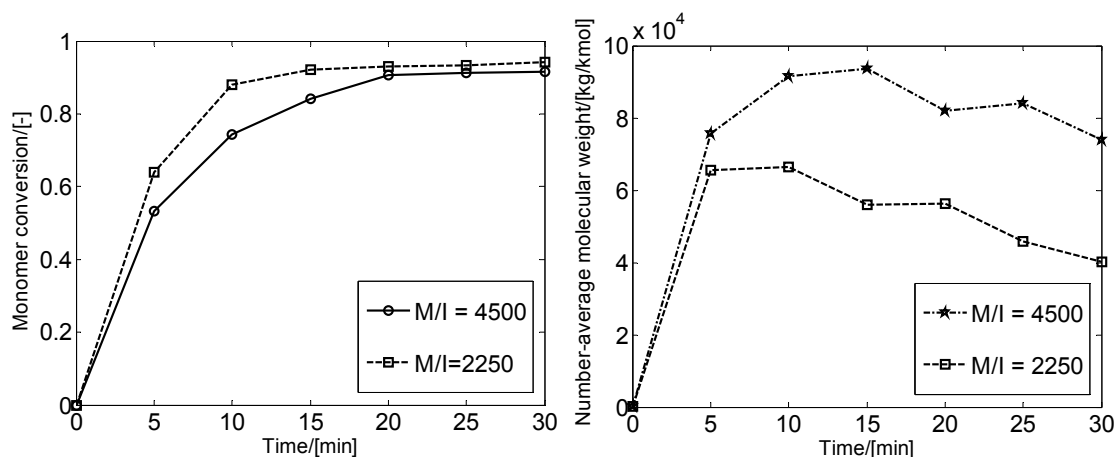


Figure 3.18. Monomer conversions and number-average molecular weights profiles at a temperature of 195°C (Initiator $\text{SnOct}_2/\text{TPP}$)

It is also worth to note that lower M/I ratios (higher initiator concentrations) produce a polymer with larger molecular distribution (Figure 3.19), probably due to a higher number of initiated chains at the beginning of the process.

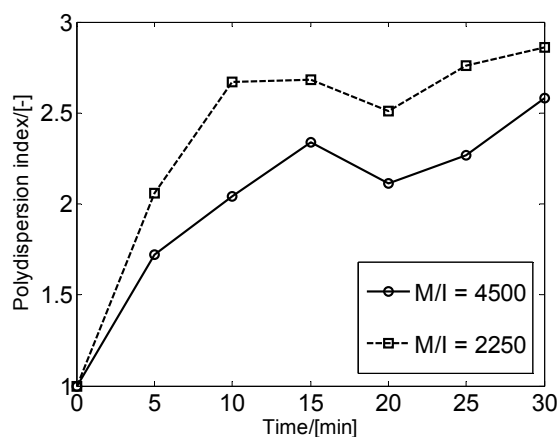


Figure 3.19. Number-average molecular weights at a temperature of 195 °C (Initiator SnOct₂/TPP)

3.2.4. Polymerization kinetics modeling

In order to develop a kinetic model for the polymerization process, we adopted the reaction mechanism proposed by Kowalski et al [106]. This mechanism is assuming that the polymerization of L-lactide /stannous octoate occurs by the simple monomer insertion described in Figure 3.20. In addition to Kowalski scheme, we considered that, besides the termination reactions occurring by chain transfers to monomer, termination reactions take also place with the impurities present in the reaction mixture.

It is stated in the published literature that the hydroxyl compounds could have a beneficial effect in the initiation reaction of L-lactide by stannous octoate. In the reaction system considered in this work, the only hydroxyl compound available could be the water, adventitious introduced in the system from the atmospheric humidity. The propagation reaction takes place on the tin center that opens the dimmer cycle. Both chain transfer reactions produce hydroxyl terminated PLA at both chain ends. The result of the termination reactions is the regeneration of the stannous initiating species.

In order to develop the kinetic model based on the mechanism presented above, four reactions were considered: initiation, propagation, chain transfer with monomer and chain transfer with the impurities present in the reaction mixture. In the following section, the impurities present in the reaction mixture will be formally called “solvent” and the corresponding kinetic constant named “chain transfer with solvent” constant. All the reactions are considered irreversible.

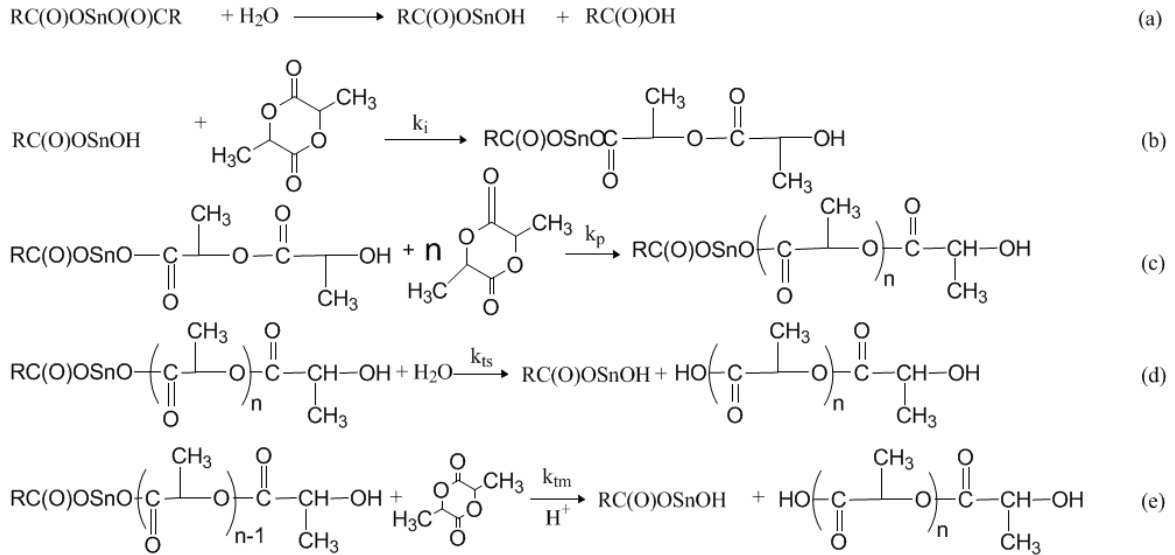


Figure 3.20. Mechanism of polymerization of dilactide in the presence of stannous octoate

In a simplified way, are written as following:



Where I – initiator, M – monomer, R_j – active polymer chain, P_j – dead polymer chain

In addition, the following hypotheses are considered:

- The density of the reaction mixture is considered constant in respect with time;
- Each initiator molecule initiates a polymer chain;
- Termination occurs by transfer to monomer and impurities (S) respectively and is irreversible;
- Concentrations of the reactants and intermediary radicals may depend upon time but are independent of spatial position within the reaction vessel (no gel effect appears in the reaction mixture);
- Rate constants are not dependent on the chain length.

In accord with the hypothesis presented above, the mathematical model for the ring-opening polymerization process in a batch reactor is represented by the equations (3.17) - (3.25). The structure of this model is based on a scheme published by Mehta et al [134], adapted by adding, as mentioned above, the termination reaction by chain transfer to impurities present in the reaction mix-

ture.

$$\frac{dI}{dt} = -k_i IM \quad (3.17)$$

$$\frac{dM}{dt} = -k_i IM - k_p M \lambda_0 - k_{tm} M \lambda_0 \quad (3.18)$$

$$\frac{d\lambda_0}{dt} = k_i IM \quad (3.19)$$

$$\frac{d\lambda_1}{dt} = k_i IM + k_p M \lambda_0 + k_{tm} M (\lambda_0 - \lambda_1) + k_{ts} S (\lambda_0 - \lambda_1) \quad (3.20)$$

$$\frac{d\lambda_2}{dt} = k_i IM + 2k_p M \lambda_1 + k_p M \lambda_0 + k_{tm} M (\lambda_0 - \lambda_2) + k_{ts} S (\lambda_0 - \lambda_2) \quad (3.21)$$

$$\frac{d\mu_0}{dt} = k_{tm} M \lambda_0 + k_{ts} S \lambda_0 \quad (3.22)$$

$$\frac{d\mu_1}{dt} = k_{tm} M \lambda_1 + k_{ts} S \lambda_1 \quad (3.23)$$

$$\frac{d\mu_2}{dt} = k_{tm} M \lambda_2 + k_{ts} S \lambda_2 \quad (3.24)$$

$$\frac{dS}{dt} = k_{ts} S \lambda_0 \quad (3.25)$$

$$t=0, I=I_0, M=M_0, S=S_0, \lambda_i = 0, \mu_i = 0, i=0..2$$

where: I – initiator concentration; M–monomer concentration; S - impurities concentration;

λ_i –moments of active polymers concentrations distribution ($i = 0..2$);

μ_i –moments of dead polymers concentrations distribution ($i = 0..2$);

k_i –initiation kinetic constant; k_p – the propagation kinetic constant;

k_{tm} –chain transfer to monomer rate constant;

k_{ts} –chain transfer to solvent rate constant.

To determine the impurities concentration, S_0 , we considered that, mainly, it consists in the water present in the monomer. Its concentration was measured by drying experiments and was evaluated to be about 0.07 % (wt).

The polymer and monomer mixture melt density was calculated using the relation published by Witzke et al [115]:

$$\rho = \frac{1.145}{1 + 0.0007391(T - 150)} \quad (3.26)$$

With T – process temperature, °C and ρ – density in g cm^{-3} ;

Based on the monomer conversion, number-average and weight-average molecular weight measurements in different working conditions, the unknown parameters appearing in the differential equations (3.17) to (3.25) were estimated by a multi-response least square method [135, 136]. The

temperature dependencies of reaction rate constants, k_i , k_p , k_{tm} , k_{ts} , were expressed through Arrhenius relationships:

$$k_j = A_j \times \exp\left(-\frac{E_j}{RT}\right) \quad (3.27)$$

It is well known that A_j and E_j in equation (3.27) are highly correlated, and hence it is recommended [135, 136] to re-parameterize the equation around the mean temperature of the experimental runs, T_0 , in order to reduce the degree of correlation:

$$k_j = \bar{k}_j \exp\left(-\frac{E_j}{R}\left(\frac{1}{T} - \frac{1}{\bar{T}}\right)\right); \quad \bar{k}_j = A_j \exp\left(-\frac{E_j}{R\bar{T}}\right) \quad (3.28)$$

\bar{T} was taken as arithmetic mean of the experimental temperatures used in the polymerization process. A nonlinear estimation procedure was developed and used to evaluate the kinetic parameters (\bar{k}_j and E_j for the initiation, propagation and the two chain transfer reactions). The model error expression considered in the estimation calculus has the form:

$$J = \sum_{j=1}^2 \sum_{i=1}^N e_{i,j}^T W_j e_{i,j}; \quad e_{i,j} = y_{\text{exp},i,j} - y_{c,i,j} \quad (3.29)$$

In relation (3.29), $y_{\text{exp},i,j}$ and $y_{c,i,j}$ represent the measured and calculated values of the monomer conversion ($j=1$) and number-average molecular weight ($j=2$) respectively; W_j are weighting factors (w_1 for the monomer conversion, w_2 for number-average molecular weight). The calculations were carried out by using the MATLAB “lsqcurvefit” procedure coupled with ode15s integrating function.

A. Estimation results for L-lactide polymerization initiated by stannous octoate

In order to insure comparables values of the terms appearing in the error function (3.29), the weighting factors were taken, $w_1 = 40$ (for the monomer conversion), $w_2 = 3 \cdot 10^{-3}$ (for number-average molecular weight). The numerical results of the estimation calculus are presented in Table 3.14.

The estimated value of activation energy for the propagation step, $E_p=86000$ J/mol, is reasonable close to those reported by other authors (80 kJ/mole reported by Eenink [95], 70.9 kJ/mole by Witzke et al [115] and 86.2 kJ/mole by Ryner et al [137]).

The calculated values of monomer conversion and polymer molecular weights are presented,

comparatively with experimental points, in Figure 3.21 to 3.23. As seen from these figures, a fairly good quality of the fit was obtained for monomer conversion and the number-average molecular weight.

Table 3.14. Calculated kinetic parameters values [124]

Parameter	$\bar{k}_i,$ $l \cdot mol^{-1} min^{-1}$	$\bar{k}_p,$ $l \cdot mol^{-1} min^{-1}$	$\bar{k}_{tm},$ $l \cdot mol^{-1} min^{-1}$	$\bar{k}_{ts},$ $l \cdot mol^{-1} min^{-1}$
Values	4.43×10^{-1}	6.172×10^3	1.53×10^0	1.236×10^3
Parameter	$E_i,$ $J \cdot mole^{-1}$	$E_p,$ $J \cdot mole^{-1}$	$E_{tm},$ $J \cdot mole^{-1}$	$E_{ts},$ $J \cdot mole^{-1}$
Values	3.00×10^4	8.6×10^4	4.14×10^4	3.00×10^4

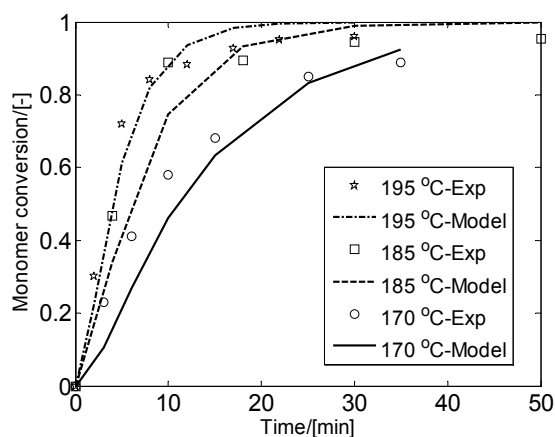


Figure 3.21. Time dependence of L-lactide conversion, $M/I=2250$ (initiator $SnOct_2$)

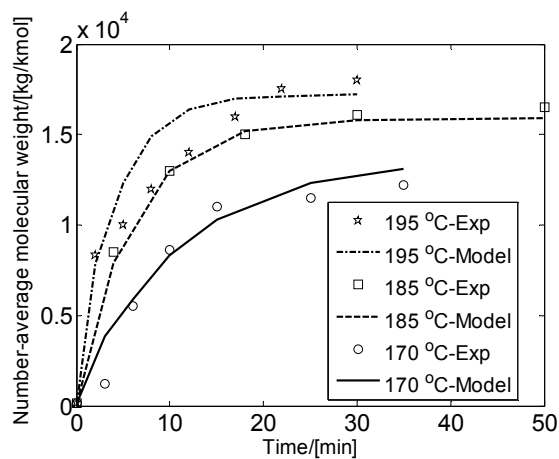


Figure 3.22. Time dependence of the number average molecular weight, $M/I=2250$ (initiator SnOct_2)

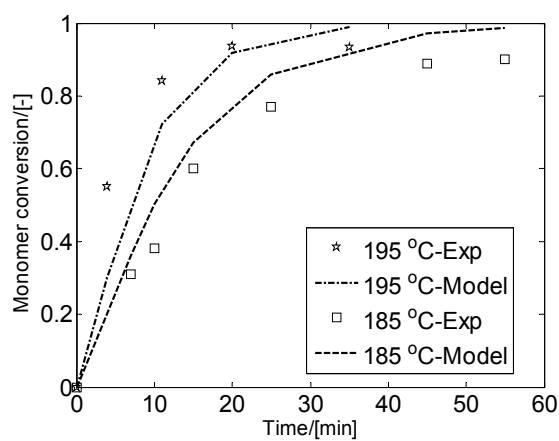


Figure 3.23. Time dependence of *L*-lactide conversion, $M/I=4500$ (initiator SnOct_2)

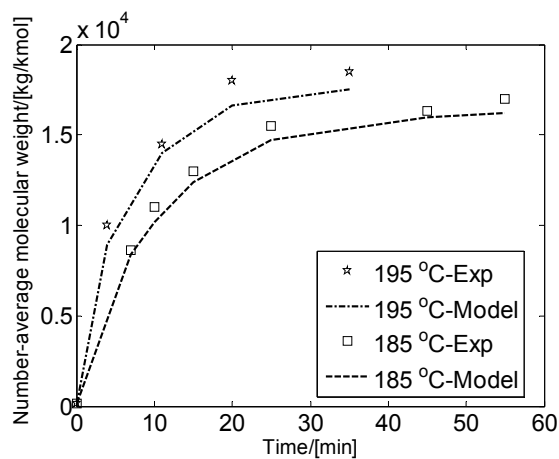


Figure 3.24. Time dependence of number average molecular weight, $M/I=4500$ (initiator SnOct_2)

Table 3.15. The calculated kinetic parameters for the L-lactide – SnOct₂ polymerization system

Temperature	k_i	k_p	k_{tm}	k_{ts}
170	6.27×10^{-2}	2.252×10^1	1.03×10^{-1}	1.78×10^{-2}
185	8.19×10^{-2}	4.843×10^1	1.49×10^{-1}	2.33×10^{-2}
195	9.69×10^{-2}	7.852×10^1	1.87×10^{-1}	3.76×10^{-2}

B. Estimation results for L-lactide polymerization initiated by stannous octoate and co-initiated by triphenylphosphine

To describe the polymerization kinetics, the same reaction scheme and rate expressions were considered as in the case of initiation with stannous octoate alone. The kinetic parameters were estimated by the procedure described above, based on experimental data previously presented. The weighting factors appearing in the error function (3.29) were $w_1 = 2$ for the monomer conversion and $w_2 = 2 \times 10^{-3}$ for number-average molecular weight. The estimation results are presented in the Table 3.16 and the kinetic constants values at different working temperatures are presented in Table 3.17.

A comparison of calculated with experimental values of monomer conversion and polymer molecular weight are presented in Figure 3.25 and Figure 3.26 for different temperatures and a M/I of 4500. Considering the limited accuracy of the experimental data the quality of model predictions depicted in these figures could be considered as acceptable.

Table 3.16. Estimated values for the kinetic parameters (initiator SnOct₂/TPP)

Parameter	$\overline{k_i}$, $l \cdot mol^{-1} min^{-1}$	$\overline{k_p}$, $l \cdot mol^{-1} min^{-1}$	$\overline{k_{tm}}$, $l \cdot mol^{-1} min^{-1}$	$\overline{k_{ts}}$, $l \cdot mol^{-1} min^{-1}$
Values	1.279×10^1	5.53×10^1	6.99×10^{-2}	2.05×10^1
Parameter	E_i , $J \cdot mole^{-1}$	E_p , $J \cdot mole^{-1}$	E_{tm} , $J \cdot mole^{-1}$	E_{ts} , $J \cdot mole^{-1}$
Values	5.46×10^4	9.11×10^4	7.65×10^4	1.06×10^5

Comparing the estimated kinetic parameters values for the two initiator systems investigated, one can conclude that the activation energy for propagation step, $E_p=91100$ J/mol, is slightly higher, but still close to the values published in the literature (80 kJ/mole reported by Eenink [95], 70.9 kJ/mole by Witzke et al [115] and 86.2 kJ/mole by Ryner et al [137]).

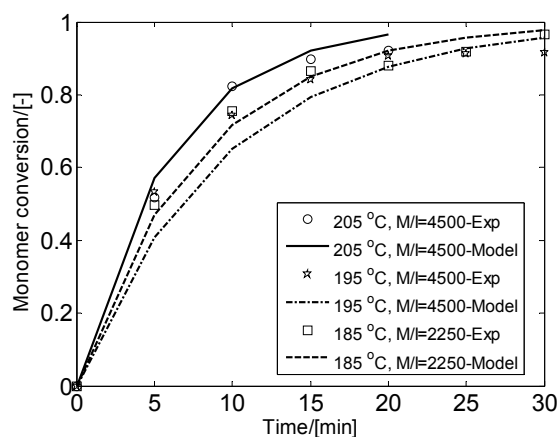


Figure 3.25. Experimental vs. calculated monomer conversion for kinetic experiments (initiator SnOct₂/TPP)

Table 3.17. The calculated kinetic parameters for the L-lactide – (initiator SnOct₂/TPP)

Temperature	k_i	k_p	k_{tm}	k_{ts}
185	1.00×10^1	3.67×10^1	4.95×10^{-2}	1.27×10^1
195	1.35×10^1	6.12×10^1	7.60×10^{-2}	2.31×10^1
205	1.82×10^1	9.99×10^2	1.15×10^{-1}	4.10×10^1

As compared with the polymerization in absence of TPP, higher activation energies were obtained for initiation step and for chain transfer reactions.

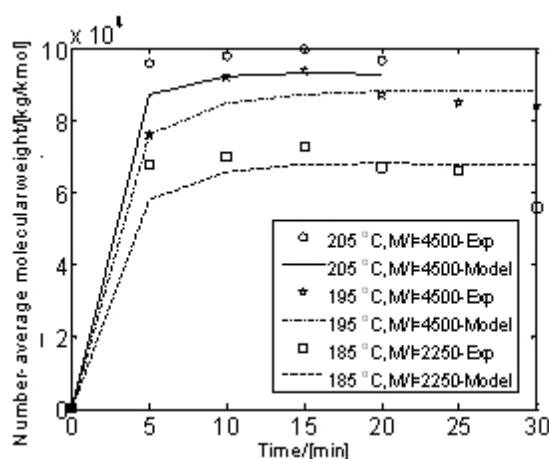


Figure 3.26. Experimental vs. calculated number average molecular weight for kinetic experiments (initiator SnOct₂/TPP)

Comparing the values of the kinetic parameters given in Table 3.15 (initiator stannous octoate alone) and Table 3.17 (initiator stannous octoate/TPP), higher propagation and initiation rate constants and smaller termination rate constants were obtained in the second case. The smaller termination rates, corroborated with higher initiation and propagation rates are higher values of the molecular weights obtained when initiating with SnOct₂/TPP. The results described in this para-

graph, prove that practical interesting monomer conversion and average polymer molecular weight can be obtained at reaction times and temperature levels realizable in twin-screw extruders. Thus, this lactide bulk polymerization process is suited to be conducted in twin-screw extruders as polymerization reactors, taking the benefits of the reactive extrusion advantages.

3.3. Experimental study of reactive extrusion process

3.3.1. Extruder characteristics

The apparatus used in the polymerization experiments was a Leistritz LSM 30-34 co-rotating twin-screw extruder, having the following characteristics: barrel length, $L = 1.2$ m, center-line distance, $CL = 30$ mm, screw external diameter, $D = 34$ mm (corresponding to a ratio, $L/D = 35$). The barrel is divided into ten equivalent sections, each one being equipped with an electrical resistance for heating and a water cooling system, these providing an independent control of the temperature on segments. The structure of the screw we used for the polymerization of L-lactide initiated by stannous octoate/ triphenylphosphine mixture is presented in Figure 3.27 (referred onward as Screw 1). It is including three kneading discs sections having the role to increase the mixing intensity of the reaction mixture. The barrel temperature was set at 200 °C on each barrel section, excepting the first two sections (counting from the feed) which were not heated.

For the reactive extrusion of L-lactide initiated only by SnOct_2 , the barrel temperature was fixed at 180 °C for each of the last 8 sections of the barrel (Figure 3.28– referred onward as Screw 2).

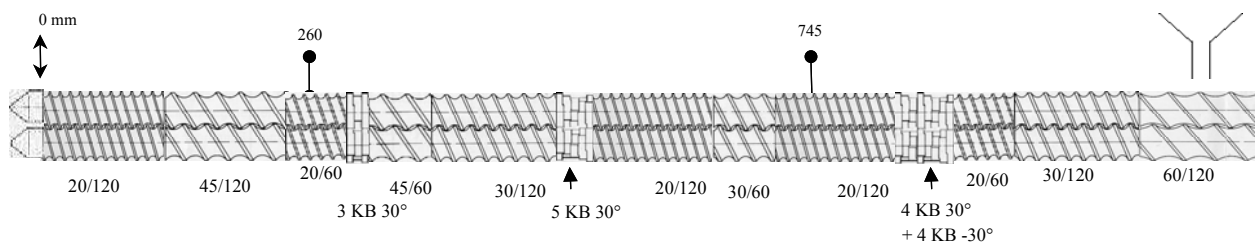


Figure 3.27. Screw profile for L-lactide polymerization initiated by $\text{SnOct}_2/\text{TPP}$ (Screw 1)

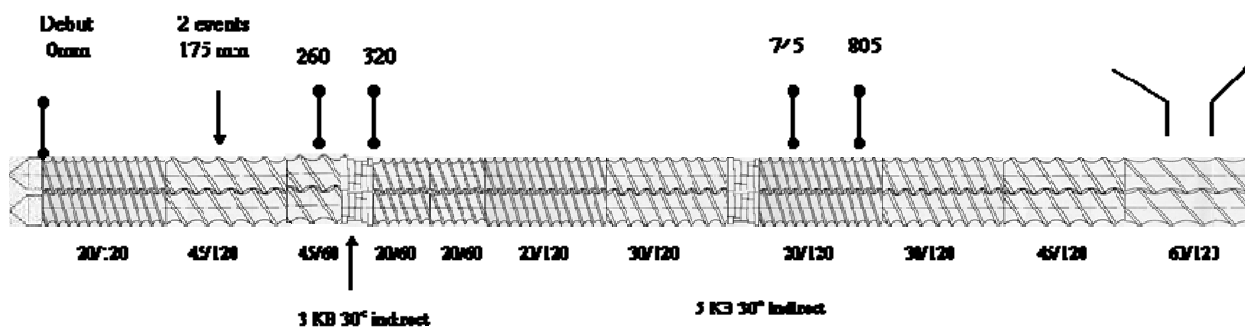


Figure 3.28. Screw profile for L-lactide polymerization initiated by SnOct2 (Screw 2)

3.3.2. Polymerization procedure

L-lactide initiated with stannous octoate

After opening the packing container, the L-lactide monomer was kept in hermetically closed plastic recipients having the capacity of 1 kg. Before each experiment, 1 kg of monomer was mixed with the corresponding quantity of initiator by manual homogenization in a plastic bag. Then the mixture was fed into a K-tron gravimetric feeder, providing the continuous measurement and control of the flow rate into the extruder. The experiments were carried out at flow rates of 0.75 – 1.5 kg/h, temperatures between 150 - 200 °C, screw speeds 50 - 300 rpm and monomer to initiator molecular ratios (M/I) of 225, 2250 and 4500.

L-lactide initiated with stannous octoate/triphenyl phosphine

In this case, the experiments were conducted at flow rates between 0.75 – 1.5 kg/h, temperature of 200 °C, screw speeds of 50 - 300 rpm and M/I of 2250 and 4500. To assure the M/I = 4500, 0.625 g of stannous octoate with an equimolecular ratio of TPP (0.393 g), were dissolved into 5 ml of anhydrous toluene and then manually mixed with 1 kg of monomer in a plastic bag. To assure M/I = 2250, a quantity of 1.251 g stannous octoate and the corresponding equimolecular ratio of TPP (0.786 g), were used in the same volume of toluene. Then the mixture was fed into the extruder K-tron gravimetric feeder and the extrusion process was started. After a stabilization time of approximately 10 min, the polymer samples were taken in small aluminum recipients, cooled in a current of cold air and then stored in a refrigerating space, to be sent for analysis.

3.3.3. Experimental results of reactive extrusion

Only few operating parameters (the extruder mass flow rate, the screw speed and the temperature profile) can be used to control a reactive extrusion process. A set of reactive extrusion experiments using the stannous octoate/triphenylphosphine as initiating system was performed on Screw 1 configuration at 200 °C, screw speeds of 50-300 rpm, mass flow rates of 0.75 – 1.5 kg/h and two M/I, 2250 and 4500 respectively. The results are presented in Tables 3.18 and 3.19.

From the experimental results could be drawn the following conclusions:

- A rise in screw speed at constant flow rate conduct to a decrease of monomer conversion and number-average molecular weight, as a results of the decrease in reaction time;

- The increase of the mass flow rate in the feed at constant screw speed has a similar effect on the monomer conversion and number-average molecular weights as the increase of the screw speed at constant flow rate.
- A rise in M/I ratio in the feed conduct to a slightly decrease in monomer conversion and a relatively high increase of number-average molecular weight. This fact could be explained by a smaller concentration of live polymers and, consequently of the rate of monomer consumption in the propagation step.

The experimental conditions and the polymer characteristics obtained by reactive extrusion of L-lactide initiated by stannous octoate alone, using Screw 2, are presented in the Table 3.20. As expected, the results show a higher monomer conversion and a higher number-average molecular weight at a higher temperature, due to the increase of propagation rate stronger than the termination rates.

Comparing experiments X1P6 and X1P7 (Table 3.20), we observe that the polymer molecular weights increase with the rise of the temperature, the explanation being a more important temperature influence on the propagation rate and, presumably, a better mixing (temperatures above the melting temperature of the PLA). No significant different molecular weights were obtained in the tested operating conditions. Comparing the experiments X1P7 and X2P2, both performed at 180 °C, one can observe that an increase of the screw speed gives slighter lower molecular weights of the polymer, probably due to the shorter residence time and stronger axial mixing. The same effect can be observed at smaller temperatures, with a stronger influence on monomer conversion and a smaller influence onto the molecular weights (experiences X2P4 and X2P5). The reproducibility of the reactive extrusion measurements is tested in experiences X1P4 and X1P6 for a temperature of 150 °C and in experiences X1P2 and X1P3 for a temperature of 180 °C. As observed, a rather good reproducibility of the results was obtained.

The experimental results presented in Table 3.20 correspond to relatively low conversions of monomer and polymer molecular weights and consequently are of limited practical interest. In order to increase the conversion, the operating variables that can be handled out are the reaction time, reaction temperature and initiator feed concentration. The main way to reduce the reaction time is by diminishing the feed rate of material. However, the feed rates used in the previous experiments represent the lowest interval on the range of technically possible values. Therefore, a second set of L-lactide reactive extrusion experiments were performed on the same feed rate interval, increasing the initiator concentration and temperature.

Table 3.18. Reactive extrusion results at 200 °C and M/I = 2250 on Screw 1 (initiator SnOct₂/TPP)

Experience identifier	Rotation speed, [rot/min]	Mass flow rate, [kg/h]	Monomer conversion, [-]	Mn, [kg/kmole]	IP
1	50	0.75	0.91	70000	2.4
2	200	0.75	0.82	63000	2.5
3	300	0.75	0.80	62000	2.7
4	50	1.25	0.87	65000	2.7
5	200	1.25	0.74	64000	2.4
6	300	1.25	0.68	60000	2.3
7	50	1.5	0.72	61000	1.9
8	200	1.5	0.65	59000	2.1
9	300	1.5	0.52	57000	2.3

Table 3.19. Reactive extrusion results at 200 °C and M/I = 4500 on Screw 1 (initiator SnOct₂/TPP)

Experience identifier	Rotation speed, [rot/min]	Mass flow rate, [kg/h]	Monomer conversion, [-]	Mn, [kg/kmole]	IP
1	50	0.75	0.80	95000	2.3
2	200	0.75	0.75	90000	2.3
3	300	0.75	0.70	72000	1.6
4	50	1.25	0.73	81000	1.9
5	200	1.25	0.65	73000	2.4
6	300	1.25	0.60	60000	1.6
7	50	1.5	0.70	75000	2.4
8	200	1.5	0.50	67000	1.9
9	300	1.5	0.47	55000	1.8

The operating conditions and process performances are given in Table 3.21. As observed, higher lactide conversion values are obtained and slightly superior molecular weights of polymer (mainly as consequence of temperature increase. In spite of some advantages regarding the monomer conversion and polymer molecular weights, the relatively high content of stannous compounds is an important drawback of the process conducted in these operating conditions.

For a low M/I ratio, practically the same monomer conversion is obtained for all operating conditions presented in Table 3.21. This fact could be explained by higher initiation and consequently higher propagation rates, due to the higher initiator concentration that produces very fast monomer consumption in short polymerization times. At constant flow rate, higher molecular

weights were obtained at slower screw speeds. Rather close values of molecular weights were obtained in this series of experiments, meaning that at high initiator concentrations the polymerization reaction is extremely fast and the initiation centers probably with the same density, producing polymers with not very scattered characteristics.

Table 3.20. Reactive extrusion of L-lactide initiated by stannous octoate (Screw 2, initiator SnOct₂)

Experience identifier	Temperature, [°C]	Screw speed, [rpm]	Mass flow rate, [kg/h]	Monomer conversion, [%]	Mn, [kg/kmole]	Mw, [kg/kmole]	IP
X1P2	180	100	1	96.1	23000	43600	1.9
X1P3	180	100	1	96.2	23200	44000	1.9
X1P4	150	100	1	86.8	21500	43000	2.0
X1P6	150	100	1	84.10	21000	37000	1.8
X1P7	180	100	1	98.10	22500	43600	1.9
X2P2	180	180	1	96.40	20500	34000	1.7
X2P3	180	180	1	95.00	20000	34500	1.7
X2P4	150	180	1	82.50	14200	21000	1.5
X2P5	150	100	1	88.40	14500	25000	1.7

Comparing the polymerization experiments of L-lactide initiated by SnOct₂/TPP and those of L-lactide initiated by SnOct₂ alone, it can be drawn the conclusion that SnOct₂/TPP system permits the formation of longer polymer chains (higher molecular weights), in similar operating characteristics of the extruder. Therefore this initiation system is more appropriate to carry on the polymerization by reactive extrusion technique.

Table 3.21. Reactive extrusion results at 200 °C and M/I = 225 on Screw 1 (initiator SnOct₂)

Experience identifier	Rotation speed, [rot/min]	Mass flow rate, [kg/h]	Monomer conversion, [-]	Mn, [kg/kmole]	IP
1	50	0.75	0.96	30000	2.3
2	200	0.75	0.96	26000	2.4
3	300	0.75	0.96	25000	2.5
4	50	1.25	0.96	30000	1.9
5	200	1.25	0.96	26000	2.4
6	300	1.25	0.96	21000	2.8
7	50	1.5	0.97	36500	2.0
8	200	1.5	0.96	30000	2.5
9	300	1.5	0.95	21000	3.0

The data given in Table 3.18, are also showing important decreases of monomer conversion and polymer molecular weight with the increase of screw speed. This is explained mainly by the increase of axial mixing intensity with the increase of rotation speed of the screw. The polydispersion index values are also higher than in the previous case (in the range 1.5 – 3), probably due to some secondary effects induced in the presence of this more efficient initiation system.

3.4. Modeling of the flow and mixing of the melting material in the extruder. Evaluation of the residence time distribution in the extruder by the simulator Ludovic®

The complexity of the flow in twin-screw extruders, as well as the large number of parameters and interrelated variables that affect the flow and mixing in these apparatus, make the reactive extrusion process difficult to understand, control, and optimize. As underlined by Vergnes et al [138], two different approaches can be distinguished in the modeling of flow in twin-screw extruders. The first one uses a local description of the flow velocities in the extruder channels, by momentum balance equations. This approach is, theoretically, the most accurate one, but rather complex, leading to difficulties regarding the accurate identification of the transport properties of the material, identification of the boundary conditions or difficulties in numerical calculations. The second approach is based on a global description of the entire flow process, from the feed to the exit section of the extruder, and, consequently, is a simpler one [139]. This second approach was often used in the published literature to describe the flow and mixing in twin screw extruders [140, 141] It is based on a global description of the flow characteristics along the screw channels by using the concept of flow models, classical in chemical engineering. The information needed in this aim is obtained from experimental residence distribution (RTD) measurements, performed by using appropriate tracer techniques. The main advantage of this global approach is to avoid the difficulties in modeling the flow in the extruder screw, a complex geometry apparatus. Nevertheless, the parameters of models haven't always physical signification, and the number of parameters could be a difficulty encountered in fitting the experimental data.

Our modeling study is based essentially on the simpler, global approach. However, the necessary RTD data were not directly measured due to the lack of an appropriate tracer permitting to work in the presence of melted polylactide mixture. This was replaced by a theoretical evaluation of the RTD of L-lactide polymerization mixture, performed by flow simulation with the software Ludovic®, a specialized package for the calculus of material flow in twin-screw extruders. In addition,

although the measurement of RTD for polylactide mixture was not possible, some experimental RTD measurements were performed on the extruder and screw structures used in the polymerization study, in order to obtain minimum information concerning the material flow in this apparatus. In this aim we used melted polypropylene as flowing material and a fluorescent tracer technique developed by Cassagnau et al [142]. The results of this experimental study were used to evaluate the ability of Ludovic[®] simulator to predict the RTD curves.

3.4.1. Experimental study of polymer flow in the twin-screw extruder

The RTD measurement is based on the use of hydroxymethyl anthracene tracer (as a dispersion in polypropylene) developed by Cassagnau et al, combined with an UV spectroscopic method to detect its concentration in the melted propylene at the extruder exit [142, 143]. A fused-silica fiber optic probe, which has a higher transmittance to UV than glass fibers, was made-up by Foretec Company. This probe was mounted in the die in the Dynisco hole standard. An optical fiber of 0.9 mm in diameter carries the excitation UV light and 12 others with diameters of 0.1 mm transmit the fluorescence emission to a photomultiplier (PM) tube. The probe has a diameter of 1.5 mm. Furthermore, a monochromatic filter with a wavelength near 380 nm is placed at the exit of a mercury lamp and an optical filter, absorbing the light of wavelengths lower than 405 nm, is placed on the fluorescence fiber. The most important precaution that should be taken is to ensure that the volume, in the die surrounding the window probe, is protected against daylight. Finally, the intensity of the fluorescence signal is transformed in an analog fluorescence signal by an electronic magnification device, with a full scale between 0 and 5 V [142, 143].

The DDS experiments were effectuated on the ‘Screw 1’ profile at flow rates of 0.75 – 1.5 kg/h, 200 ° C and 50 – 300 rpm. Experimentally measured residence time distributions at constant screw speed and increasing flow rate are presented in Figures 3.29 and 3.30.

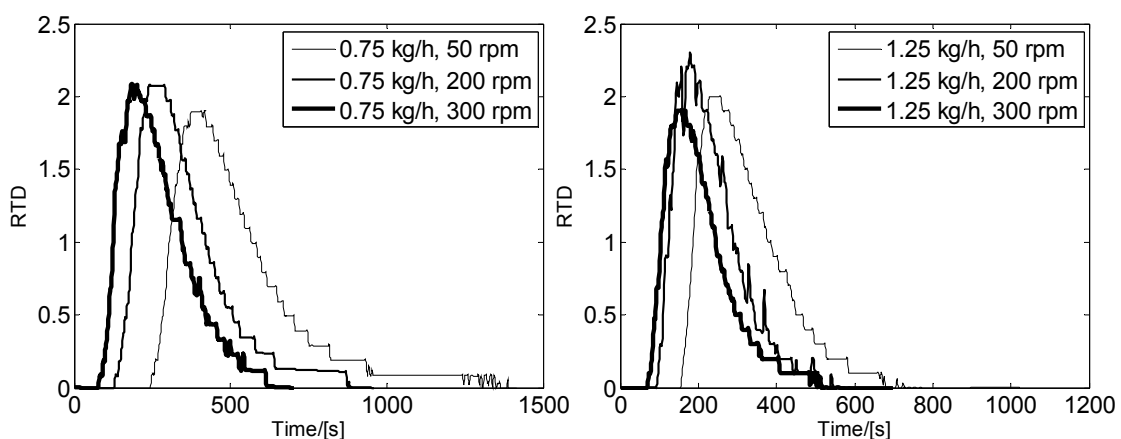


Figure 3.29. RTD curves at constant flow rate and variable screw speed (left: 0.75 kg/h, right: 1.25 kg/h)

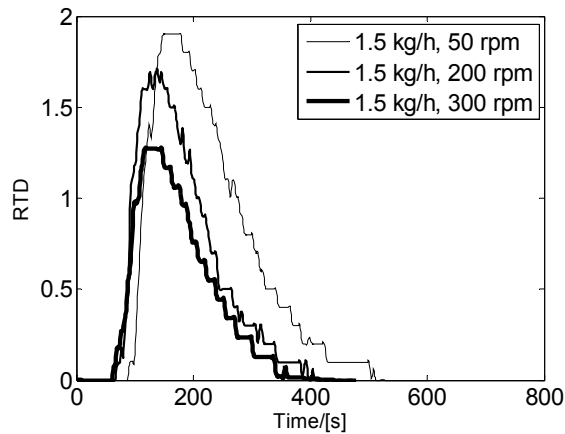


Figure 3.30. RTD curves at 1.5 kg/h and variable screw speed

Several conclusions concerning the influence of the operating parameters onto the polymer flow can be drawn from these diagrams. Higher throughput and screw speed assure shorter residence times into the twin screw extruder. At constant screw speed, the residence time is in inverse ratio with the flow rate. The increase of the screw speed at constant flow rate gives smaller residence times and larger dispersion of residence times distribution, due to a higher shear rate and an augmented degree of mixing. The overall conclusion of the flow study is that the highest influence on the mean residence time has the flow rate, then the screw speed. The dispersion of the RTD curves is an indicator of the degree of mixing in the twin-screw extruder. As we can see from Table 3.23, a high degree of mixing is produced by high flow rates and screw speed, corroborated with high values of the RTD dispersion values.

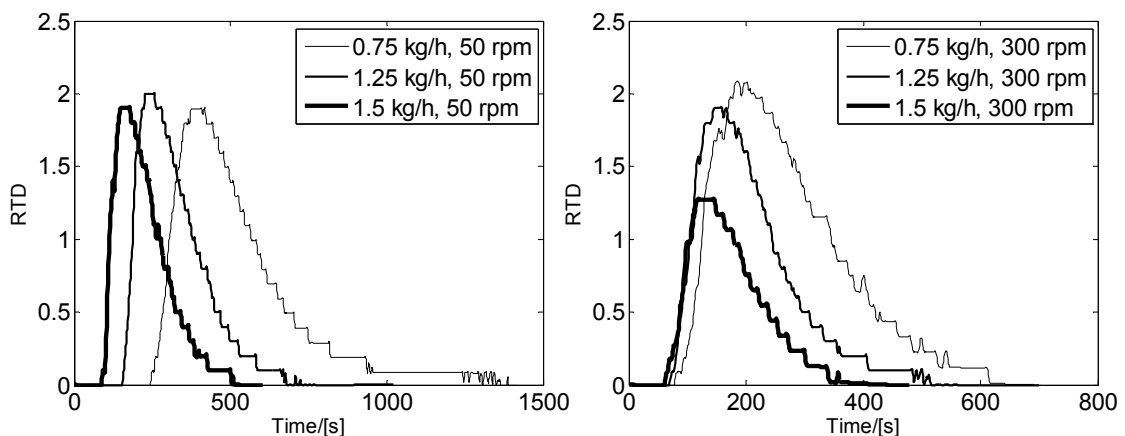


Figure 3.31 RTD curves at constant screw speed and variable flow rate (left: 50 rpm, right: 300 rpm)

3.4.2. RTD evaluation for melted polypropylene flow by Ludovic® simulator

Ludovic® is a software package designed to simulate the flow and mixing in twin-screw extruders [144]. The global model of the TSE include equations for the flow in right and left screw elements as well as for the direct and indirect kneading disc regions [138]. In our study, this software was used to calculate the degree of filing for the screws channels, the local and global residence times for each screw element and the pressure variation along the extruder. To estimate the accuracy of the RTD prediction by Ludovic® software, a test was carried out using the experimental RTD data described in the previous section, on polypropylene (PP) as flowing material.

The simulations were performed in similar working conditions as for PLA synthesis, using a barrel temperature of 200 °C and Screw 1 configuration. The rheological properties of the material were experimentally evaluated for a sample of polypropylene and fitted on a Carreau-Yasuda viscosity model:

$$\eta = \eta_0 \left(1 + (\lambda \dot{\gamma})^a \right)^{\frac{m-1}{a}} \quad (3.30)$$

The calculations were performed by approximating a constant averaged viscosity along the TSE. Figure 3.32 shows an excellent adequacy of the Carreau-Yasuda viscosity model in fitting the experimental rheological values for PP. The parameters of the model are presented in Table 3.22.

Table 3.22. Carreau-Yasuda parameters for PP model

Model	η_0	λ	a	m
1	2.549×10^3	3.301×10^{-1}	5.938×10^{-1}	5.100×10^{-1}

The RTD curves calculated by Ludovic® software for a flow rate of 0.75 kg/h and different screw speeds are presented in the Figures 3.33, 3.34 and 3.35.

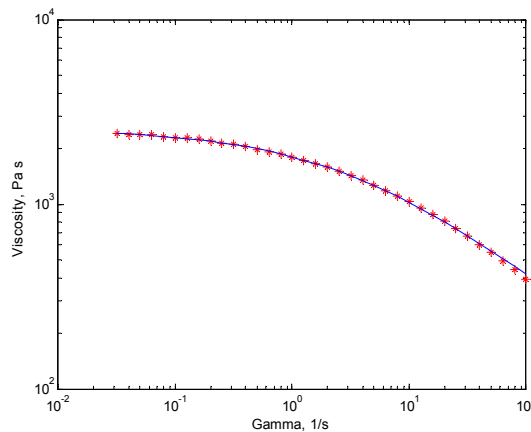


Figure 3.32. Experimental (points) and calculated (line) values of polypropylene viscosity

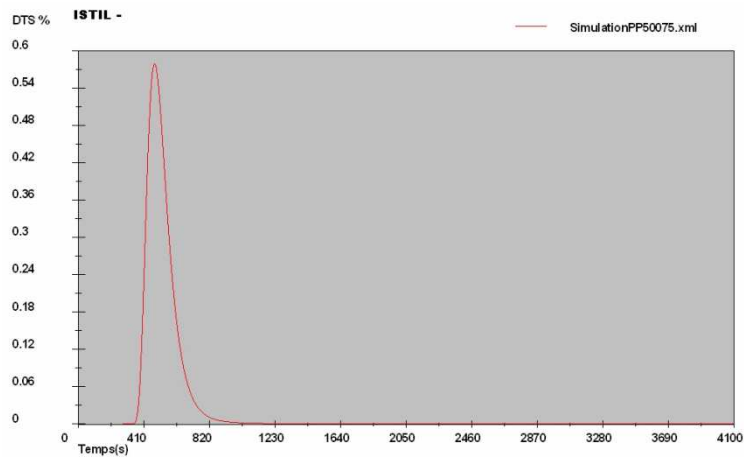


Figure 3.33. Simulated RTD curve: 0.75 kg/h, 50 rpm

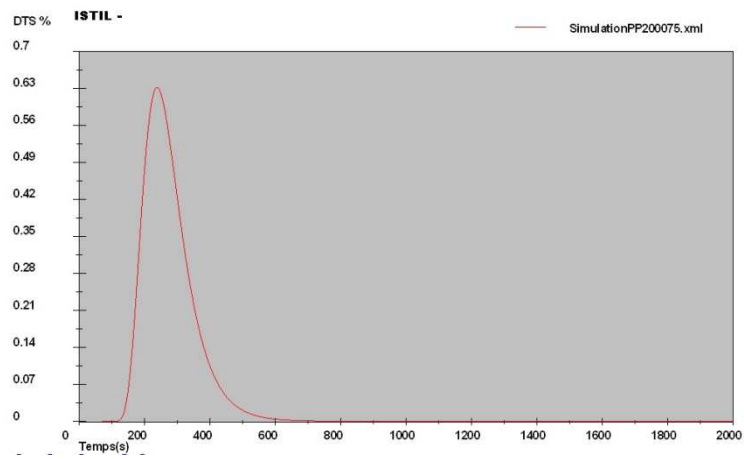


Figure 3.34. Simulated RTD curve: 0.75 kg/h, 200 rpm

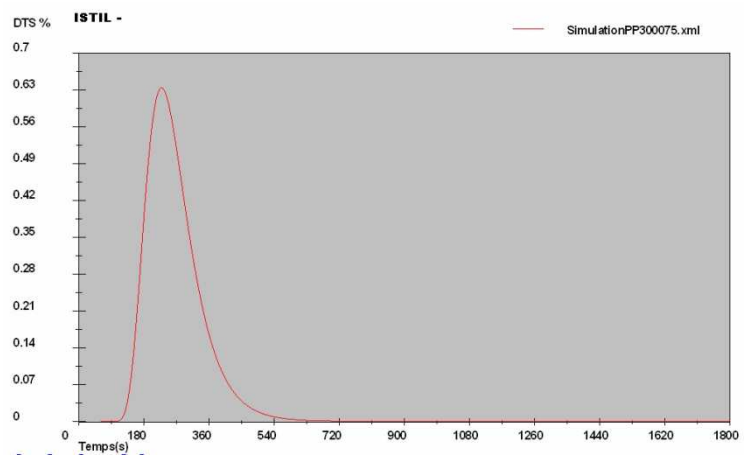


Figure 3.35. Simulated RTD curve: 0.75 kg/h, 300 rpm

From the results presented in these figures it can be observed a displacement of the RTD curves toward smaller residence times and an increase of the RTD dispersion, by the increase of the

screw rotation speed, an observation in agreement with the experimental results described above and other published data. Other working parameter influences on the RTD characteristics, obtained by simulation (decrease of mean residence time by the increase of the flow rate etc) are also in agreement with the experimental results.

The simulation results for the polypropylene flow on the ‘Screw 1’ configuration of the extruder are presented comparatively with the measured ones in Table 3.23. From the data given in this table, a fairly good agreement between experimental and simulated mean residence time values and a weaker concordance for the RTD dispersions could be observed. The quality of the mean residence time predictions is improving with the increase of the screw speed.

Table 3.23. Experimental and simulated residence times at 200 °C

Experience	Mass flow rate, [kg/h]	Screw speed, [rpm]	\bar{t} /[min], Experimental	\bar{t} /[min], Ludovic	σ_t^2 Experimental	σ_t^2 Ludovic
1	0.75	50	7.44	8.26	0.1136	0.1142
2	0.75	200	4.94	4.20	0.1697	0.2174
3	0.75	300	3.75	4.03	0.2247	0.2257
4	1.25	200	3.32	2.78	0.2599	0.3270
5	1.25	300	2.61	2.58	0.2918	0.3518
6	1.50	200	2.55	2.44	0.3350	0.3751
7	1.50	300	2.49	2.22	0.3486	0.4093

\bar{t} - mean residence time, σ_t^2 – variance of the RTD

The results presented above prove a relatively good capability of Ludovic® simulator to predict both \bar{t} and σ_t^2 of the polymer flow in the twin screw extruder used in PLA synthesis. It is well known from the published literature [8] that σ_t^2 is a measure of the spread of residence time distribution. This can be an argument for using the Ludovic® simulated RTD curves in the modeling of L-lactide polymerization process by reactive extrusion.

3.5. Mathematical modeling of the PLA reactive extrusion

The simulation results obtained by Ludovic® package describing the PLA flow in extruder, are further used in the development of a mathematical model for the L-lactide polymerization process by reactive extrusion. In this aim two flow models were used, the axial dispersion model and a compartment type model which is approximating the flow volume of screw elements by a series of ideal flow zones (plug flow and perfectly mixed zones). The parameters of these models (Pe number for the axial dispersion model and the nature of ideal zones and their mean residence times in the second model) were determined from Ludovic® simulation results.

3.5.1. Modeling of polymer flow by axial dispersion model. Evaluation of the Pe values

The mass balance of a chemically inert tracer corresponding to axial dispersion model is expressed by the equation [8, 145]:

$$\frac{\partial C}{\partial \theta} + \frac{\partial C}{\partial X} = \frac{1}{Pe} \cdot \frac{\partial^2 C}{\partial X^2} \quad (3.31)$$

$$X = \frac{z}{L}; \quad \theta = \frac{t}{t_0}; \quad Pe = \frac{u \cdot L}{D_L}; \quad t_0 = L / u \quad (3.32)$$

D_L – axial dispersion coefficient; z-axial coordinate of the reactor; u – flow velocity; C- tracer concentration.

The used boundary conditions are of the type “open system”. To obtain the density function of residence time distribution, $E(t)$, the mass flow equation (3.31) is integrated for a Dirac (δ) pulse signal, resulting:

$$E(\theta) = \frac{1}{2} \cdot \sqrt{\frac{Pe}{\pi \cdot \theta}} \cdot \exp \left[-\frac{(1-\theta)^2}{4 \cdot \theta} \cdot Pe \right] \quad (3.33)$$

The axial dispersion model describes the mixing onto the whole length of the extruder by its single parameter, the Péclet dimensionless number (Pe). The space time t_0 cannot be considered as a parameter, being calculated directly from the experimental RTD data and independently of the flow model .

Based on the Ludovic simulated RTD curves (for PP flow in the TSE) the parameter Pe of the axial dispersion model was estimated by the MATLAB function „fminunc”.

Table 3.24. Estimated parameters of the axial dispersion model

Extruder mass flow rate , [kg/h]	Screw speed, [rpm]	Pe values	Mean residence time, [min]
0.75	50	103.4	8.26
0.75	200	31.5	4.21
0.75	300	28.7	4.04
1.25	200	36.1	2.78
1.25	300	32.4	2.58
1.5	200	38.5	2.44
1.5	300	33.8	2.23

Several comparisons between the AD model predictions and Ludovic simulated RTD curves for PP flow in the TSE are graphically presented in Figures 3.36 and 3.37 for a flow rate of 1.25 kg/h.

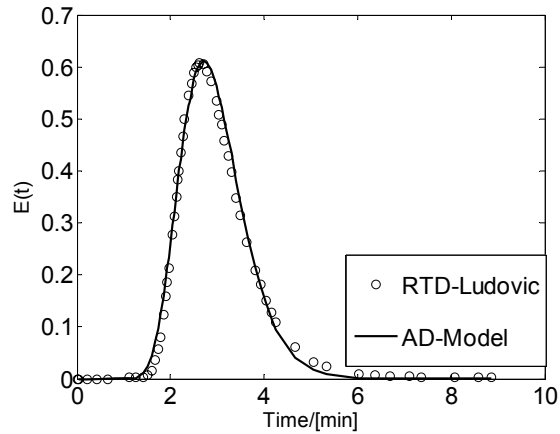


Figure 3.36. Comparison of RTD curves for a flow rate of 1.25 kg/h and screw speed of 200 rpm

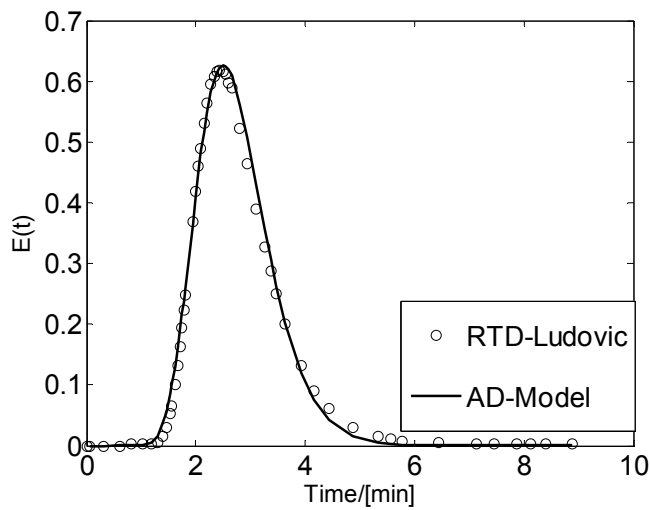


Figure 3.37. Comparison of RTD curves for a flow rate of 1.25 kg/h and screw speed of 300 rpm

A good agreement can be observed between the calculated and Ludovic simulated RTD curves, this proving that the AD model is suitable for the flow modeling in twin screw extruder. As seen, at constant flow rate, a higher screw speed gives a higher degree of mixing for the reaction mixture (smaller values for Pe).

3.5.2. Flow simulation by Ludovic® software for PLA reactive extrusion

The viscosity data for PLA were taken from the published literature [121] and fitted on a Carreau-Yasuda viscosity model. The calculations were performed approximating a constant averaged viscosity along the TSE. The weight-average molecular weights for the polymers are generally higher than 50000 kg/kmole. Two viscosity models for 40000 and 130000 kg/kmole weight-average molecular weights were implemented.

The parameters η_0 , λ , m and a of the Carreau-Yasuda equation (3.30) were estimated by

using the viscosity data published by Cooper-White and Mackay [121] . The calculated parameters are given in Table 3.25 and a comparison between the predicted and published values of polymer viscosity is presented in Figure 3.38.

Table 3.25. Estimated values for the parameters of the Carreau-Yasuda viscosity model

Model	η_0	λ	a	m	M_w
1	1.029×10^2	7.658×10^{-3}	2.018×10^0	7.711×10^{-1}	40000
2	7.118×10^3	1.133×10^{-1}	9.033×10^{-1}	5.100×10^{-1}	130000
3	9.525×10^5	1.081×10^1	3.843×10^{-1}	3.582×10^{-1}	360000

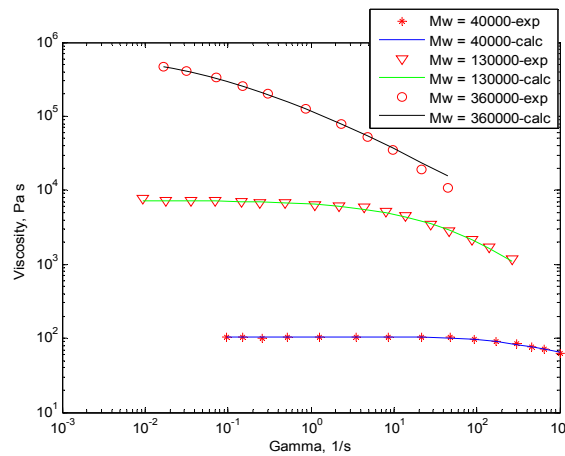


Figure 3.38. Published [121] and calculated viscosity values at 200 °C

Several local and global residence times predicted by Ludovic® are presented in the following figures for the screw profile in Figure 3.27 (Screw 1). A constant temperature of 200 °C was considered along the extruder barrel, accordingly with the experimental operating conditions.

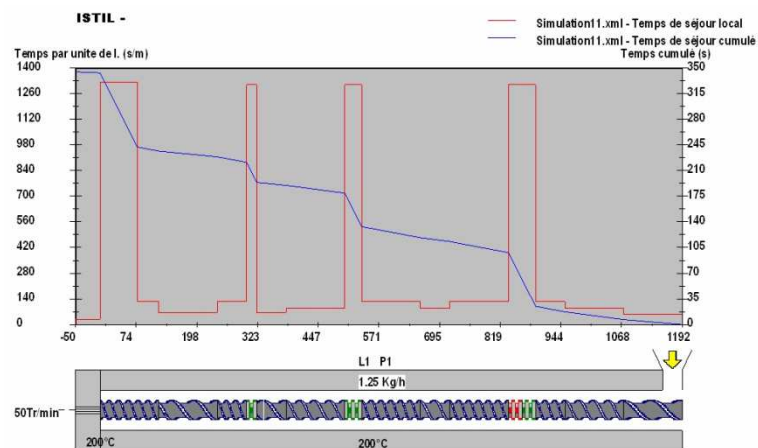


Figure 3.39. Residence time for the viscosity model 1

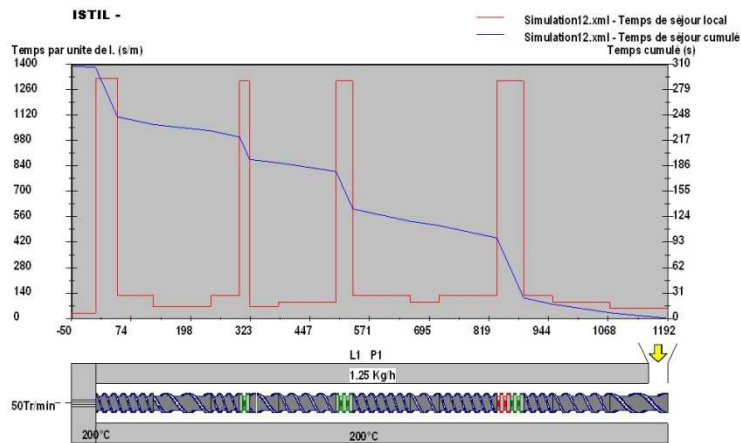


Figure 3.40. Residence time for the viscosity model 2

As seen from the two figures above, small differences in global residence times are attained by the two viscosity models. The Ludovic[®] simulations result was an argument for the insensitivity of the residence time with the weight average molecular weight of the PLA and consequently with the viscosity model implemented in the calculations.

The filling ratio is relatively high only on the first section of kneading discs and before the die (Figure 3.41 and 3.42). Further, the reactive extrusion modeling will be performed using the viscosity model 1. Ludovic simulations for PLA reactive extrusion were performed for the representative values of the flow rate and screw speeds. As underlined above, the simulation performed by Ludovic offers two approaches for modeling the flow in twin screw extruder, one with the axial dispersion model based on the RTD curves and the other considering the apparatus as a succession of ideal flow zones (perfectly mixed and plug flow).

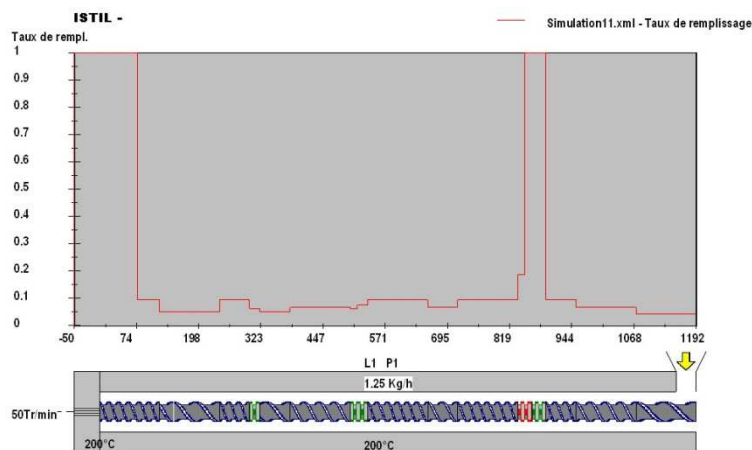


Figure 3.41. Filling ratio for the viscosity model 1

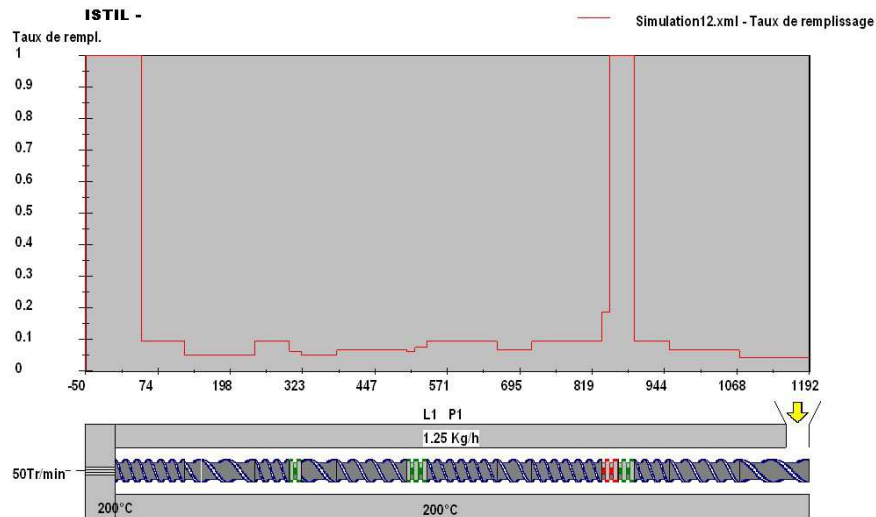


Figure 3.42. Filling ratio for the viscosity model 2

3.5.3. Mathematical modeling of reactive extrusion process

The modeling of the reactive extrusion process will be performed using two approaches, the first based on an axial dispersion model and the second a compartment model (a succession of perfectly mixed and plug-flow regions). The characteristics of the two models are determined from the Ludovic™ simulations of L-lactide/polylactide mixture flow in the TSE. The simulation results used to calculate the models characteristics are given in Appendix 1.

Polymerization modeling by axial dispersion model approach (Ludovic simulation)

Based on Ludovic calculated RTD curves presented in Appendix 1, an axial dispersion model can be used to describe the flow and mixing in the twin screw extruder, and then to predict the polymer characteristics at the extruder exit. The parameters of the AD model will be determined using the same procedure as in paragraph 3.5.1.

Table 3.26. AD model parameters for Ludovic simulated RTD

Extruder mass flow rate , [kg/h]	Screw speed, [rpm]	Pe values	Mean residence time, [min]
0.75	50	44.2	7.54
0.75	200	30.0	5.84
0.75	300	28.2	5.67
1.25	50	57.6	5.38
1.25	200	32.3	5.00
1.25	300	30.4	3.61
1.50	50	68.2	4.82
1.50	200	35.0	3.25

The mass balance equation for a chemical species, particular for the axial dispersion model, has the form:

$$\frac{1}{P_e} \frac{\partial^2 C}{\partial X^2} + \frac{\partial C}{\partial X} - t_0 v_{R,C} = 0 \quad (3.34)$$

With the boundary conditions:

$$X = 0, \quad C_0 - C = -\frac{1}{P_e} \frac{\partial C}{\partial X} \quad (3.35)$$

$$X = 1, \quad \frac{\partial C}{\partial X} = 0 \quad (3.36)$$

Where C stands for C_M -monomer concentration, C_I – initiator concentration, C_S – impurities concentration, 0th, 1st and 2nd order moment for radical (λ_i , $i=0..2$) and polymers distribution concentrations (μ_i , $i= 0..2$); C_0 – the value of C in the feed.

For the distribution moments, the boundary condition (3.35) becomes:

$$X = 0, \quad C = \frac{1}{P_e} \frac{\partial C}{\partial X} \quad (3.37)$$

The reaction rates for the chemical species in the mixture are:

$$v_{R,I} = k_i IM \quad (3.38)$$

$$v_{R,M} = k_i IM + k_p M \lambda_0 + k_{tm} M \lambda_0 \quad (3.39)$$

$$v_{R,\lambda_0} = -k_i IM \quad (3.40)$$

$$v_{R,\lambda_1} = -(k_i IM + k_p M \lambda_0 + k_{tm} M (\lambda_0 - \lambda_1) + k_{ts} S (\lambda_0 - \lambda_1)) \quad (3.41)$$

$$v_{R,\lambda_2} = -(k_i IM + 2k_p M \lambda_1 + k_p M \lambda_0 + k_{tm} M (\lambda_0 - \lambda_2) + k_{ts} S (\lambda_0 - \lambda_2)) \quad (3.42)$$

$$v_{R,\mu_0} = -(k_{tm} M \lambda_0 + k_{ts} S \lambda_0) \quad (3.43)$$

$$v_{R,\mu_1} = -(k_{tm} M \lambda_1 + k_{ts} S \lambda_1) \quad (3.44)$$

$$v_{R,\mu_2} = -(k_{tm} M \lambda_2 + k_{ts} S \lambda_2) \quad (3.45)$$

$$v_{R,C_S} = -k_{ts} S \lambda_0 \quad (3.46)$$

The mathematical model was solved using a procedure based on the estimation function „bvp4c” (MATLAB). This function solves the two-point boundary value conditions problems, as in this case.

TSE extruder as a compartment model

The objective of this paragraph is to simulate the behavior of the twin screw extruder approximated as a compartment model (series of perfectly mixed and plug-flow zones) for all operat-

ing conditions used in practical experiences. The regions with higher filling ratios (degree of mixing) and residence time (kneading discs sections) are treated as perfectly mixed regions whereas the transport sections, with lower intensity of mixing (smallest filling ratio) and lower residence time, as plug-flow regions. The plug-flow regions are supposed to be the extruder transport elements. The main elements for this simulation approach are presented in the following table for a flow rate of 0.75 kg/h and a screw speed of 50 rpm. The flow study was carried out by Ludovic[®] software and the corresponding data for all operating conditions are presented in Appendix 1.

The data presented in Table 3.27 are extracted by reading the local and global residence time profiles given by Ludovic[®] simulations.

Table 3.27. The parameters for 1.25 kg/h, 50 rpm, screw 1 (Figure 3.27) and viscosity model 1 (Table 3.25)

Zone #	Type	Residence time,[s]	Zone length, [mm]
Zone 1	Plug-flow	27	300
Zone 2	Perfectly mixed	73	-
Zone 3	Plug-flow	35	300
Zone 4	Perfectly mixed	46	-
Zone 5	Plug-flow	14	177
Zone 6	Perfectly mixed	28	-
Zone 7	Plug-flow	20	223
Zone 8	Perfectly mixed	100	-
Zone 9	Plug-flow	2	50

The mass balance of the monomer for the i^{th} perfectly mixed zone assuming equal inlet and outlet volume flow-rates,

$$x^{i-1} = x^i - t_s^i v_{R,i} \quad (3.47)$$

Where x_i represents the concentration of the species x in the i^{th} region.

The expressions of the reaction rates involved in equation (3.47) are given by relations (3.38) - (3.46), presented in the previous section. From equations (3.47) one can calculate successively the concentrations at the exit of the perfectly mixed region, knowing the feed concentrations and the mean residence times t_s^i . This is performed by solving the nonlinear algebraic system of mass balance equations (3.47) particularized for a series of perfectly mixed zones, by the Newton-Raphson method.

The mass balance for the i^{th} plug flow (PF) region is given by:

$$\frac{dx_i}{dt} = -v_{R,i}, \quad t = \frac{z}{u_{z,i}} \quad (3.48)$$

Where: x_i - the concentration of the species x in the i^{th} zone;

$u_{z,i}$ - the flow speed in the i^{th} zone;

$v_{R,i}$ - the consumption rate of the x_i species;

The integration of the PF model was performed with a procedure based on a Runge-Kutta fifth order algorithm implemented in MATLAB[®] programming package. An example of simulation will be made for a mass flow-rate of 1.25 kg/h, a screw speed of 50 rpm, using the results obtained for first viscosity model. Using the flow parameters specified in Table 3.27 the kinetic constants presented in paragraph 3.2.4, the behavior of the reactive extrusion process was simulated. The results in terms of monomer conversion and number-average molecular weights profiles are presented in Figure 3.43.

A monomer conversion of 0.81 and a number-average molecular weight of 71000 kg/kmole are obtained at the extruder exit.

The characteristics of the compartment model for all operating conditions are presented in Appendix 1. The comparison of the two modeling approaches in terms of monomer conversion and number-average molecular weights profiles along the extruder will be presented in Figures 3.45 – 3.51. A comparison with the experimental results is shown in Tables 3.28 and 3.29.

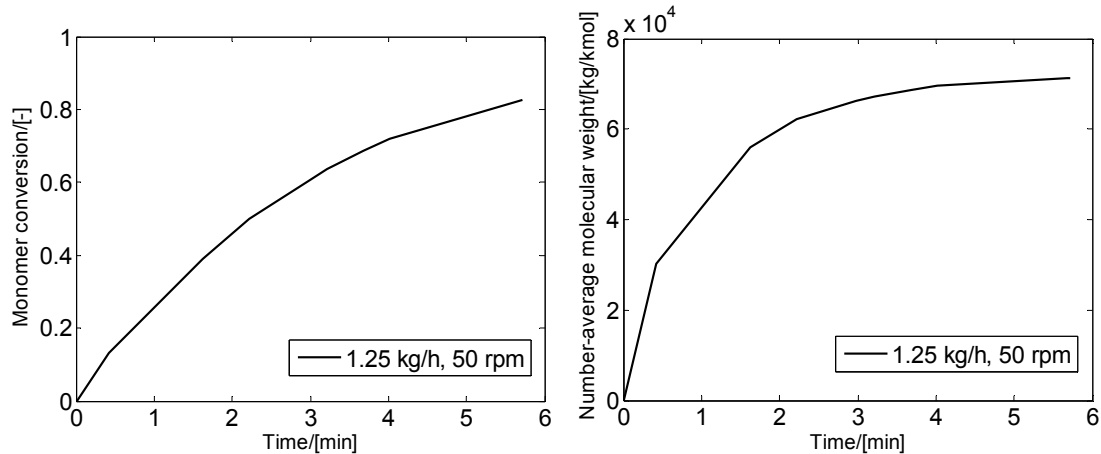


Figure 3.43. Simulated chemical transformation for a M/I of 2250 (initiator $\text{SnOct}_2/\text{TFF}$, flow rate 1.25 kg/h, screw speed 50 rpm)

Comparison of simulation results predicted by the two modeling approaches

A global comparison of monomer conversions and number-average molecular weights profiles predicted by both approaches is performed in this paragraph. A flow rate of 0.75 kg/h and a screw speed of 50 rpm are used to simulate the twin-screw extruder, for both M/I ratios, and the results are graphically presented in Figure 3.44. From the diagrams presented in this figure it can be

observed that the two models predict practically the same values at the extruder exit for both monomer conversion and number-average molecular weights.

The difference between the approaches consists only in mathematical implementation. The compartment model is simpler to implement, due to a simpler form of the mass balance equations, usually not involving convergence problems in calculating the solution.

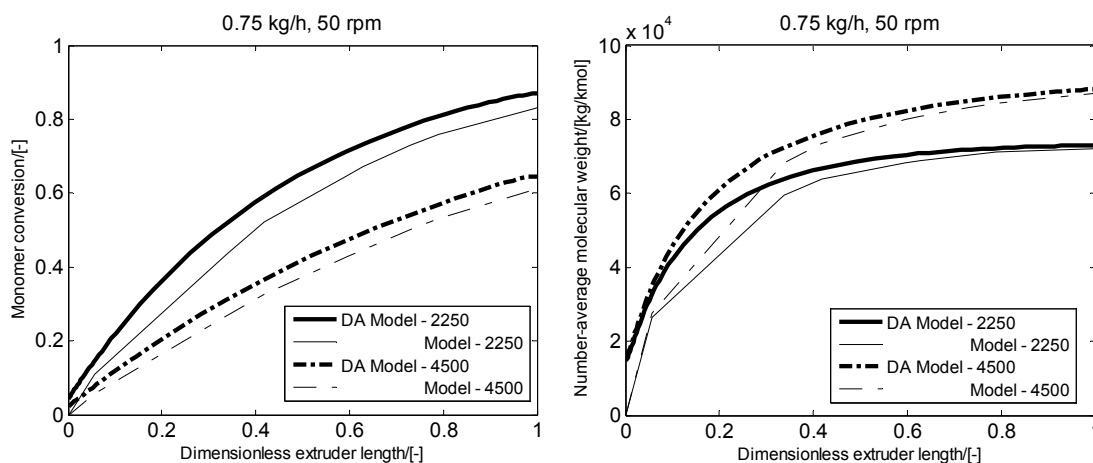


Figure 3.44. Twin screw extruder simulation by the two modeling approaches (DA Model – axial dispersion model, Compart Model – Compartment model)

By comparison, the AD model stands for solving a two point boundary values problem, which could sometimes have convergence problems. Also higher calculation time is required to the simulations by AD model. The conclusion that can be draw is that, in the modeling of the reactive extrusion process can be further used the mathematical model for which we have all parameters. Nevertheless, the structure of the compartment model formulated in these calculations is less rigorously formulated as compared with the DA model.

In what follows, a simulation of the PLA polymerization process will be performed using the AD model, based on the Ludovic[®] simulated RTD data, with its parameters given in Table 3.24 and the kinetic model developed in the paragraph 3.2. An example of the simulated monomer conversion and number-average molecular weight profiles for a flow rate of 0.75 kg/h and screw speeds of 200 and 300 rpm are graphically presented in Figures 3.45 and 3.46. A comparison of the simulated results with the experimental data for all operating conditions is presented in Tables 3.28 and 3.29.

The comparison of polymer characteristics calculated by the AD Model with the experimental data is given in Tables 3.28 – 3.29 and the parity diagrams in Figure 3.53. As seen, the concordance is not very satisfactory for all of the operating conditions. The average modeling errors are 14.7 % for monomer conversion and 11.3 % for number-average molecular weight. As seen from

the parity diagrams these errors are systematic in nature, indicating a modeling source.

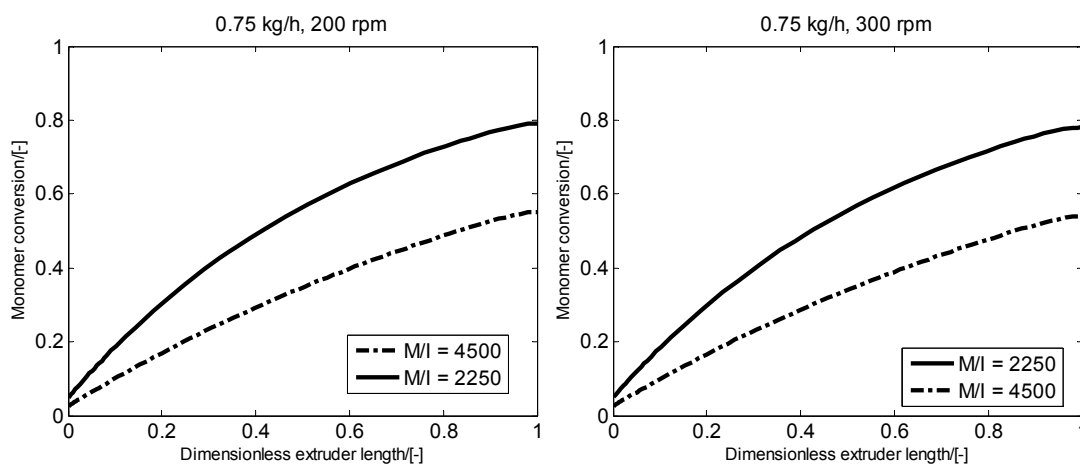


Figure 3.45. Monomer conversion profiles for both M/I ratios at a flow rate 0.75 kg/h; left: 200 rpm, right: 300 rpm

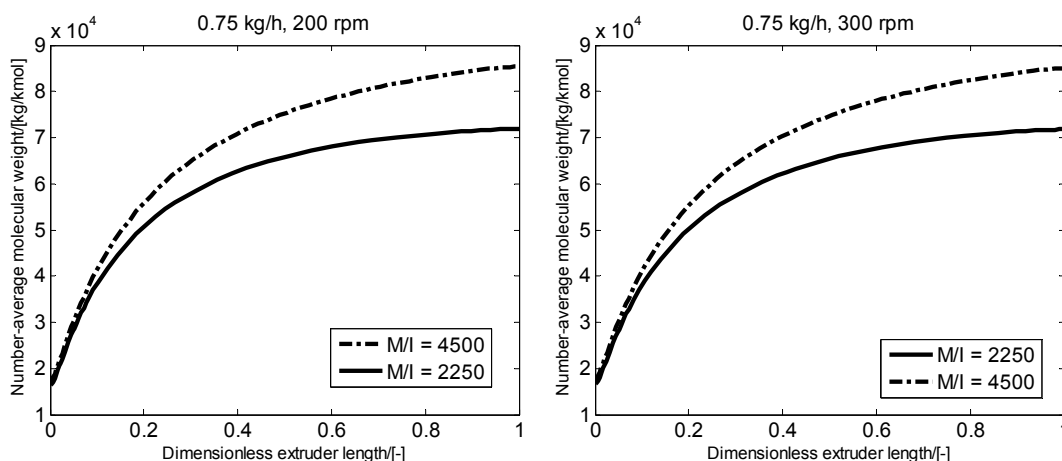


Figure 3.46. Number-average molecular weights profiles for both M/I ratios at a flow rate 0.75 kg/h; left: 200 rpm, right: 300 rpm

This could originate in all the main steps involved in the study: the development of polymerization kinetic model, the experimental study of reactive extrusion process and modeling of melt flow in extruder.

However, considering the dimension of the modeling study, the number of parameters involved, the accuracy of extruder operating parameters measurement and control as well as the approximations used in the extruder flow model, the results are acceptable.

Further improvements of the extruder model can be done firstly by including the reversibility of polymerization process in the kinetic model and a more precise description of material flow along the extruder (based on RTD measurements on PLA melt and a more accurate viscosity model).

Table 3.28. Experimental and predicted polymer characteristics for $M/I = 2250$ (initiator $\text{SnOct}_2/\text{TPP}$)

Mass flow rate, [kg/h]	Screw speed, rpm	Monomer conversion, [-] (experimental)	Monomer conversion, [-] (model)	Number-average molecular weight, [kg/kmol] (experimental)	Number-average molecular weight, [kg/kmol] (model)
0.75	50	0.91	0.87	70000	73000
0.75	200	0.82	0.80	63000	72000
0.75	300	0.80	0.79	62000	71000
1.25	50	0.87	0.78	65000	71500
1.25	200	0.74	0.75	64000	71000
1.25	300	0.68	0.63	60000	68000
1.5	50	0.72	0.74	61000	71000
1.5	200	0.65	0.60	59000	67000

Table 3.29. Experimental and predicted polymer characteristics for $M/I = 4500$ (initiator $\text{SnOct}_2/\text{TPP}$)

Mass flow rate, [kg/h]	Screw speed, rpm	Monomer conversion, [-] (experimental)	Monomer conversion, [-] (model)	Number-average molecular weight, [kg/kmol] (experimental)	Number-average molecular weight, [kg/kmol] (model)
0.75	50	0.80	0.65	95000	90000
0.75	200	0.75	0.56	90000	86000
0.75	300	0.70	0.55	72000	85000
1.25	50	0.73	0.53	81000	85000
1.25	200	0.65	0.49	73000	83000
1.25	300	0.60	0.40	60000	79000
1.5	50	0.70	0.49	75000	84000
1.5	200	0.50	0.37	67000	76000

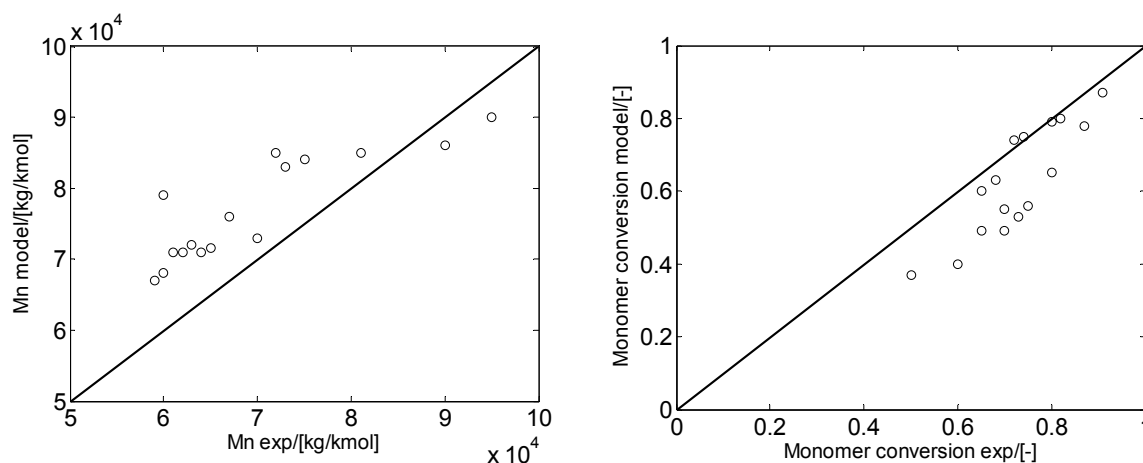


Figure 3.53. Comparison of experimental and predicted monomer conversion (left) and number-average molecular weight (right)

3.6. Reactive extrusion optimization study

The reactive extrusion processes are very sensitive to the operating parameters and it is necessary a tight control to produce a final polylactide with maximum productivity and with specified characteristics. Usually, to assure a certain polymer characteristics, it is necessary to maintain the

reaction temperature very close to a specified optimal trajectory. Due to the fact that the polymer flow in the TSE is strongly related to the device geometry, the optimization problem will be formulated in this paragraph for a feed flow rate of 0.75 kg/h and a screw speed of 50 rpm. The mathematical model of the twin screw extruder use the kinetic model proposed in paragraph 3.2.4 and the AD model for the polymer flow. The parameters of the AD model are given in Table 3.24.

The objective of this problem will be to achieve at the extruder exit a maximum monomer conversion and an imposed value for the number-average molecular weight of the PLA. Mathematically, the objective function is written:

$$J = w_1 (X - X_d)^2 + w_2 (M_n - M_{n,d})^2 \quad (3.49)$$

The weighting coefficients are chosen to assure the same magnitude order of the two corresponding terms, in this case their values being $w_1 = 10^{-1}$ and $w_2 = 10^{-8}$. The construction of the TSE used to perform the experimental reactive process has 10 regions with individual heating/cooling system. The control variables are in this case the temperature values for each of the barrel sections and, moreover, the initiator concentration in the feed.

It was shown in Chapter 2 that the Genetic Algorithms have superior performances in solving the complex optimization problems. The same genetic algorithm will be implemented to solve the present optimization problem. The variable limits will be imposed as follows: $2500 < M/I < 4500$ and $185 < T_k < 215$ °C, where k is related to the number of jacket sections in the TSE.

The number of variables in a solution that must be tested will be represented by 10 values of temperature and 1 value of initiator concentration, all normalized in the range [0, 1]. A number S of 20 solutions are tested each iteration. To achieve the convergence, it was imposed a maximum number of 1000 iterations. The results of the optimization study are presented in Table 3.30. Close values for monomer conversion and number-average molecular weight are obtained. The results reveal that higher temperatures corroborated with higher initiator concentrations must be used to achieve the maximum monomer conversion and the imposed value of number-average molecular weight.

Table 3.30. Reactive extrusion optimization results

Nº	Feed flow rate, D_m , [kg/h]	Screw speed, [rpm]	Optimal M/I, [-]	Reaction mixture characteristics			
				Monomer conversion, X, [-]		Number-average molecular weight, M_n , [kg/kmole]	
				Objective	Result	Objective	Result
1	0.75	50	2534	1	0.96	80000	79600

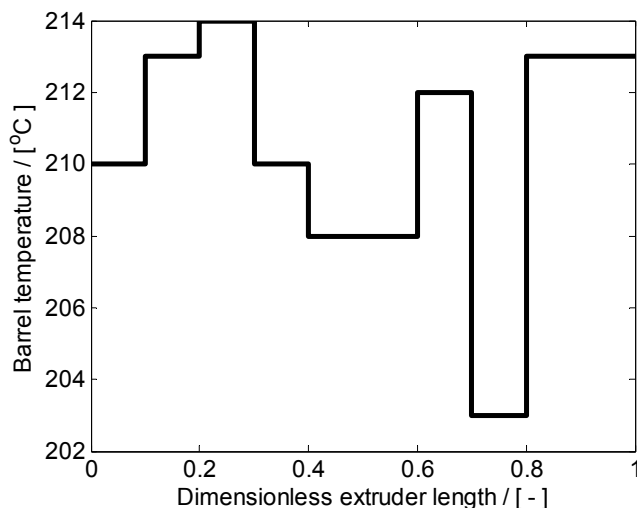


Figure 3.47. Optimal temperature profile for the reactive extrusion optimization problem

Figure 3.48 shows a rapid start of the polymerization process in the TSE due to the high temperatures required on the first two extruder barrel sections. Consequently, the monomer conversion profile has a faster increase in the first half of screw and a slower one on the final zone.

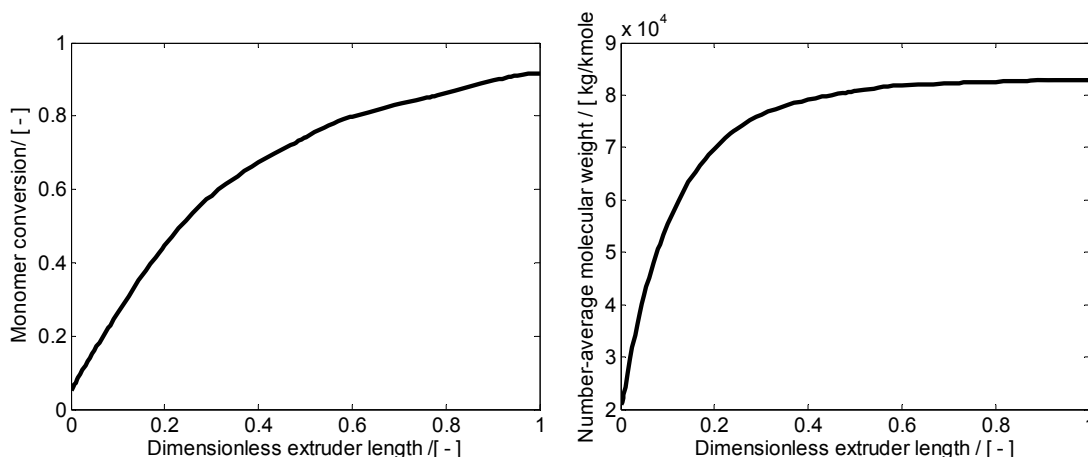


Figure 3.48. Monomer conversion and number-average molecular weight profiles calculated with the optimal policy

3.7. Conclusions

The objectives of this chapter were to realize a comprehensive modeling study for L-lactide reactive extrusion polymerization process based on experimental investigations. The first step of the study was to develop a kinetic model of L-lactide polymerization, necessary to build the mathematical model of the reactive extrusion polymerization process. The primary approach in developing the kinetic model has involved the L-lactide polymerization process initiated by only stannous octoate. Experimental studies using commercial purity of monomer and initiator were carried out at

different temperatures and monomer to initiator ratios. A polymerization mechanism was adopted, involving four elementary steps (initiation, propagation, chain transfer to monomer and solvent) and the kinetic parameters of the corresponding rate expressions were estimated based on obtained experimental data. The results of this primary investigation showed that the polymerization process initiated by stannous octoate at reasonable monomer/initiator ratios cannot be conducted on the available extruder, due to the longer reaction time necessary to realize monomer conversions and polymer molecular weights of practical interest. The process could be conducted at longer residence times in industrial twin-screw extruders. Therefore, a second experimental study was carried on based on a more active initiating system described in literature, consisting in an equimolecular mixture of stannous octoate and triphenyl phosphine.

The experimental studies confirmed the superior activity of this initiation system, higher monomer conversions and polymer molecular weights being obtained in shorter reaction times, realizable in the twin-screw extruder. In order to describe the process kinetics, the same polymerization mechanism was adopted as in previous case and its parameters were estimated. Taking into account the degree of uncertainties involved in the experimental study, the proposed kinetic model predicted with a reasonable accuracy the monomer conversion and number-average molecular weights.

The second goal of the study developed in this section was to develop a mathematical model for the PLA reactive extrusion process. Due to the lack of technical means necessary to measure the RTD in extruder on PLA melts, the flow and mixing of the PLA reaction mixture were described by using the simulation package Ludovic™. The capability of this software to describe the flow of melts in a twin screw extruder was evaluated by an experimental test, using polypropylene as flowing material. An acceptable concordance was obtained between the measured RTD characteristics and the calculated ones by Ludovic package, for a screw structure used in L-lactide polymerization experiments.

Based on the RTD features predicted by Ludovic package for the lactide polymerization mixture, the flow in the TSE was described by two flow models: (i) axial dispersion model and (ii) a compartment model. Comparing the calculation results obtained by the two mathematical models, only negligible differences in polymer characteristics were observed. Further, the reactive extrusion process was simulated for a set of experimental operating conditions using the axial dispersion model. A moderately concordance between the calculated and experimental polymer characteristics was shown. The quality of the formulated model for the PLA reactive extrusion process could be improved, mainly by a more elaborated polymerization mechanism and a better description of the material flow along the extruder.

An optimization problem for a set of operating conditions was formulated and solved using a genetic algorithm. As expected, the results revealed that relatively high temperatures and initiator concentrations are required to achieve high monomer conversions.

4. General Conclusions

This work presented a theoretical and experimental study treating the subjects of modeling and optimization of tubular polymerization reactors. The research studies had the following main objectives:

- Comparison of the performances of two widely used numerical algorithms in the optimization of polymerization tubular reactors, Pontryagin's Minimum Principle (MP) and a Genetic Algorithm (GA), based on polymerization process with a well known kinetics.
- Development of a mathematical modeling study and an optimization application for the L-lactide polymerization process in a co-rotating twin screw extruder.

Original results

The theoretical studies associated to the first objective consisted of the following main steps and led to the following conclusions:

- As case study for the comparison of MP and GA, it was selected the MMA solution polymerization process, a chemical system well described in literature. The main published kinetic models for this process were reviewed and compared in terms of monomer conversion and number-average molecular weights, by plug-flow reactor simulation in identical operating conditions. Among the published kinetic models tested, the results showed as the most representative, the kinetic model published by Baillagou et Soong (1985).
- Based on the kinetic model published by Baillagou et Soong (1985), mathematical models and numerical simulation procedures for the MMA tubular polymerization reactor were developed considering plug-flow and laminar flow regimes. The simulation results are highlighting significant limitations of the laminar flow reactor, due to the strong decrease of fluid velocity near the reactor wall. As consequence, the reaction times in the center of the reactor tube are much lower than at the periphery and the contribution of the central zone to the chemical transformation becomes less important, resulting in a non-uniform utilization of the reaction volume. Due to lower velocities and higher reaction times near the wall, higher monomer conversions and polymer concentrations emerge in this region than in the core of tube. These limitations are growing with the monomer concentration in the feed, becoming hardly acceptable, particularly at high monomer to solvent ratios.
- It was formulated an optimization problem for the tubular MMA polymerization reactor, based on plug-flow hypothesis, having as objective to identify the reaction temperature profile corresponding to a polymer product with given properties at a given monomer conversion. This is an average difficulty optimization problem for a polymerization tubular reactor.

There were developed calculation procedures using Matlab® scientific package, for solving this problem by MP method (associated to an iterative gradient numerical algorithm) and GA respectively. The results are showing that both algorithms are able to localize the optimal solution, but with different calculation and programming efforts. Even if the MP algorithm is more deterministic and rigorous from mathematical point of view, finding the solution of its optimum equations proved a rather challenging task. The convergence toward the optimum (global extreme of the performance index) was poor and demanding important efforts to guess appropriate initialization values. This inconvenient is not characterizing the GA method that is guaranteeing in this way a more reliable result in the localization of the performance index global minimum. The main conclusion of this comparison is that in solving optimization problems of this complexity or more complex ones (more complicated reactor models, more complex expressions of performance index and more control variables) the GA method is more recommended.

- Further, more complex optimization problems are formulated and solved, using a GA solving procedure. In these problems the optimization objective was the same, but an increased number of control variables were considered (cooling fluid temperature profile, flow rate, feed composition and temperature). Both plug-flow and bi-dimensional laminar flow models were considered in the process mathematical model. The results showed that high monomer concentrations produce a less homogeneous polymer, due to the strong variations of flow velocities generated by the important density and viscosity radial differences along the tubular reactor.

The second objective of the thesis was to develop a comprehensive experimental and theoretical study of L-lactide reactive extrusion process. The main achievements of this study are the following:

- There were carried out experimental investigations in two batch (bulk) polymerization systems, using commercial purities of monomer and initiator, at different temperatures and monomer to initiator ratios. In order to develop a polymerization kinetic model, it was adopted a mechanism involving four elementary steps (initiation, propagation, chain transfer to monomer and solvent) and the kinetic parameters of the corresponding rate expressions were estimated based on measured experimental data. The proposed kinetic model is predicting with a reasonable accuracy the monomer conversion and polymer number-average molecular weights. The results are also proving that the initiation system based on stannous octoate/tryphenyl phosphyne is more appropriate for the reaction times achievable in the twin screw extruders.

- The flow of the L-lactide/polylactide mixture was investigated by experimental and modeling studies. Due to the lack of technical means necessary to measure the RTD in extruder on PLA melts, the flow and mixing of the PLA reaction mixture were described by using the simulation package Ludovic™. The capability of this software to predict the flow of polymer melts in a twin screw extruder is proved by an experimental test, using polypropylene as flowing material. An acceptable concordance was obtained between the measured RTD characteristics and the calculated ones by Ludovic package, for a screw structure used in L-lactide polymerization experiments.
- Based on the RTD features predicted by Ludovic package for the lactide polymerization mixture, the flow of L-lactide/PLA melt in the TSE is described by two flow models: (i) the axial dispersion model and (ii) a compartment type model. Comparing the calculation results based on the two flow models, only negligible differences in polymer characteristics were observed. Further, the reactive extrusion process was simulated for a set of experimental operating conditions using the axial dispersion model. A moderately good concordance between the calculated and experimental polymer characteristics is revealed. The quality of the formulated model for the PLA reactive extrusion process could be improved, mainly by a more elaborated polymerization mechanism and a better description of the material flow along the extruder.
- An optimization problem was further developed and solved, concerning the optimization of the thermal regime for the L-lactide reactive extrusion process. The results showed that rather high temperatures and initiator concentrations are required, in order to achieve total monomer conversion.

Suggestions for future work

The present study has inherent limitations generated by the conditions and working domains of experimental investigations, their accuracy and the simplification hypotheses introduced in the theoretical developments. Consequently, future developments could improve the quality of results, particularly regarding the modeling of the L-lactide polymerization process by reactive extrusion.

A first direction for further development is regarding the experimental and theoretical study of the process kinetics. Also, a more accurate investigation could be performed, in conditions of higher purity of materials and larger domains of working conditions. The quality of the kinetic model could be improved by taking into account the de-polymerization reactions, as well as inter and intra-molecular transesterification reactions. A design of experiments procedure can be implemented to discriminate among the degree of influence of different process parameters on the polymerization.

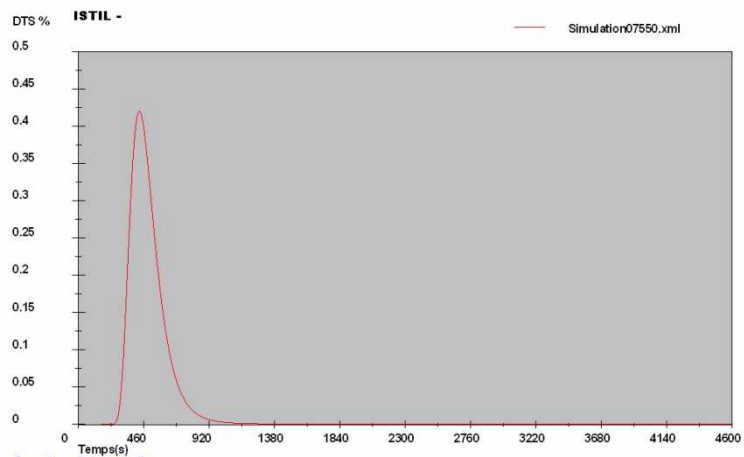
The second direction of possible improvements concerns the flow modeling of the reactive extrusion process. An experimental study of RTD of polylactide synthesis mixture in the extruder using an appropriate tracer could provide further information concerning the melt material flow and mixing in the TSE. The flow and mixing modeling can also be improved by a more complete rheological study of L-lactide/polylactide mixture, giving a better description of viscosity dependence on the temperature and composition.

Finally an optimization dynamic study for the start-up and shut-down steps, the study of the parameter sensitivity and of the reactor operating stationary points can provide extensive data for the considered polymerization process.

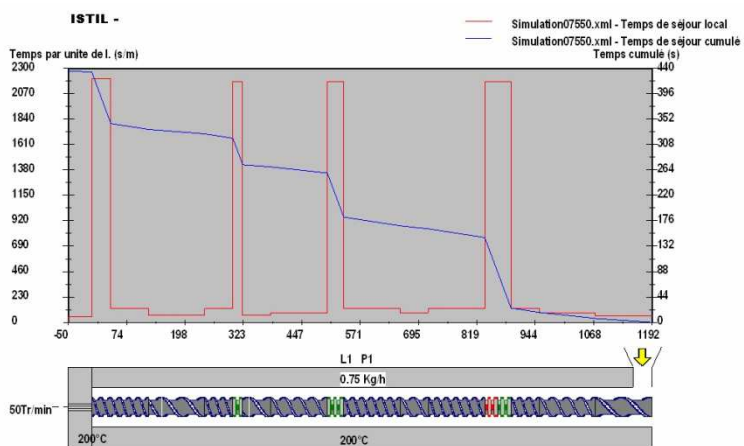
**5. Appendix 1: PLA reactive extrusion simulation by Ludovic.
RTD curves and compartment model data**

In this paragraph are presented the simulation results for PLA flow in the twin-screw extruder (by Ludovic® software). The local and global RTD profiles, as well as the residence times associated to screw zones will be graphically presented.

Flow rate: 0.75 kg/h, Screw speed: 50 rpm



Figure_Apx 1. Ludovic simulated RTD curve (0.75 kg/h, 50 rpm)

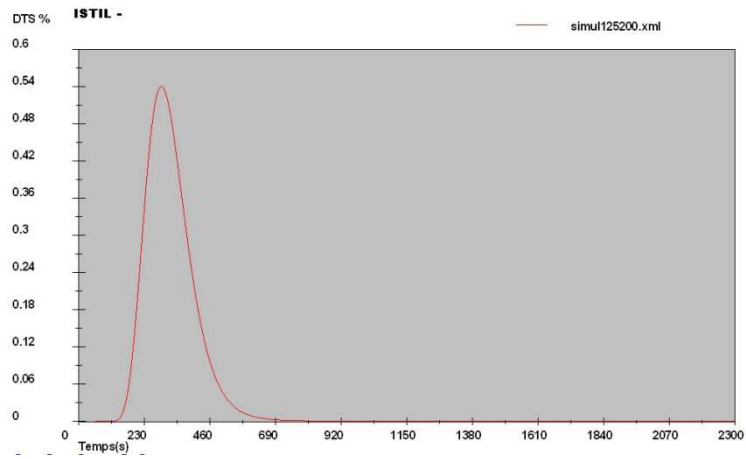


Figure_Apx 2. Local and global residence time profiles (0.75 kg/h, 50 rpm)

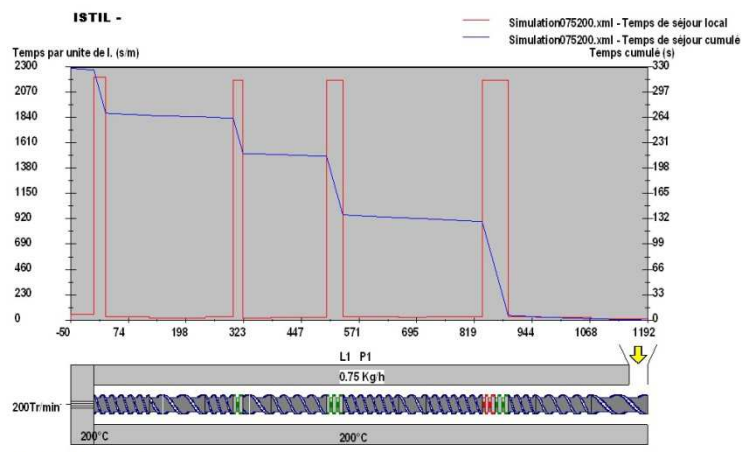
Table_Apx 1. Compartment model parameters (0.75 kg/h, 50 rpm)

Zone #	Type	Residence time,[s]
Zone 1	Plug-flow	25
Zone 2	Perfectly mixed	123
Zone 3	Plug-flow	35
Zone 4	Perfectly mixed	77
Zone 5	Plug-flow	14
Zone 6	Perfectly mixed	45
Zone 7	Plug-flow	26
Zone 8	Perfectly mixed	89
Zone 9	Plug-flow	3

Flow rate: 0.75 kg/h, Screw speed: 200 rpm



Figure_Apx 3. Ludovic simulated RTD curve (0.75 kg/h, 200 rpm)

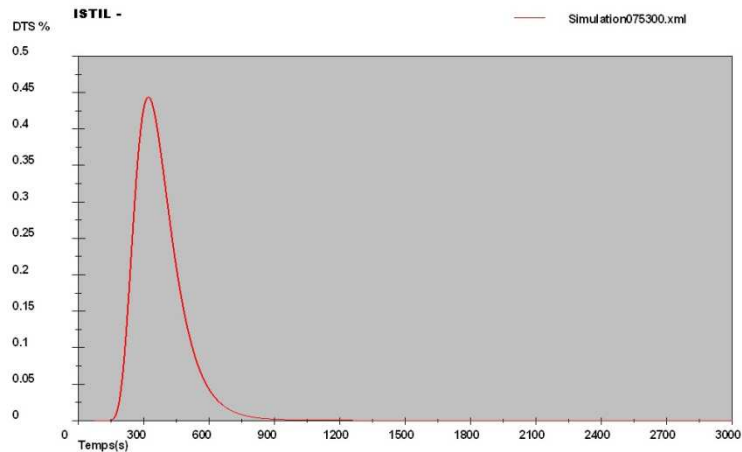


Figure_Apx 4. Local and global residence time profiles (0.75 kg/h, 200 rpm)

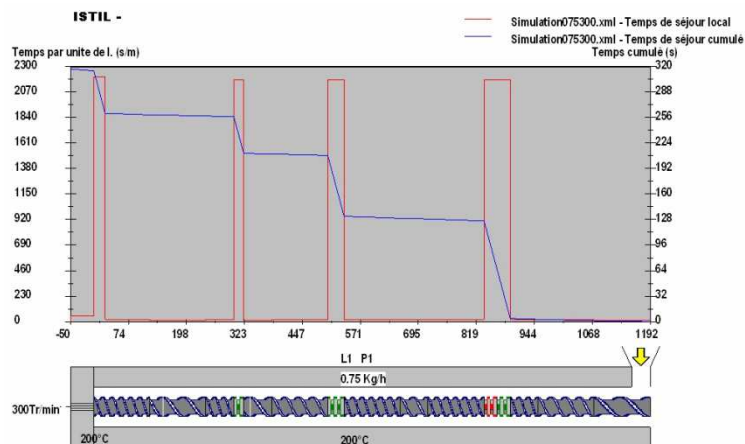
Table_Apx 2. Compartment model parameters (0.75 kg/h, 200 rpm)

Zone #	Type	Residence time,[s]
Zone 1	Plug-flow	7
Zone 2	Perfectly mixed	122
Zone 3	Plug-flow	10
Zone 4	Perfectly mixed	75
Zone 5	Plug-flow	4
Zone 6	Perfectly mixed	45
Zone 7	Plug-flow	7
Zone 8	Perfectly mixed	56
Zone 9	Plug-flow	2

Flow rate: 0.75 kg/h, Screw speed: 300 rpm



Figure_Apx 5. Ludovic simulated RTD curve (0.75 kg/h, 300 rpm)

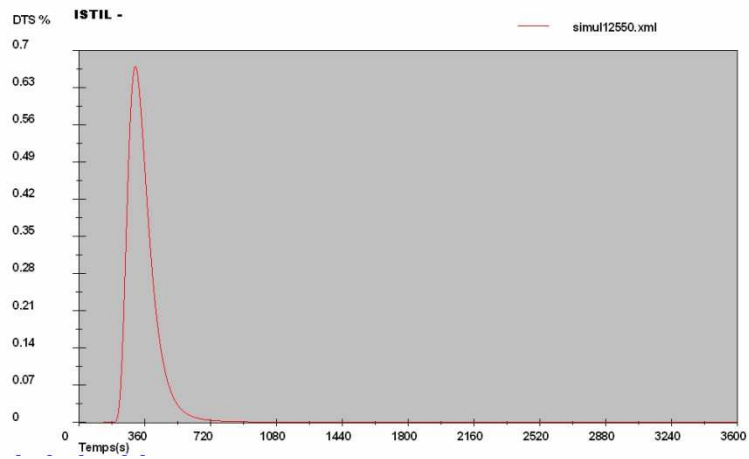


Figure_Apx 6. Local and global residence time profiles (0.75 kg/h, 300 rpm)

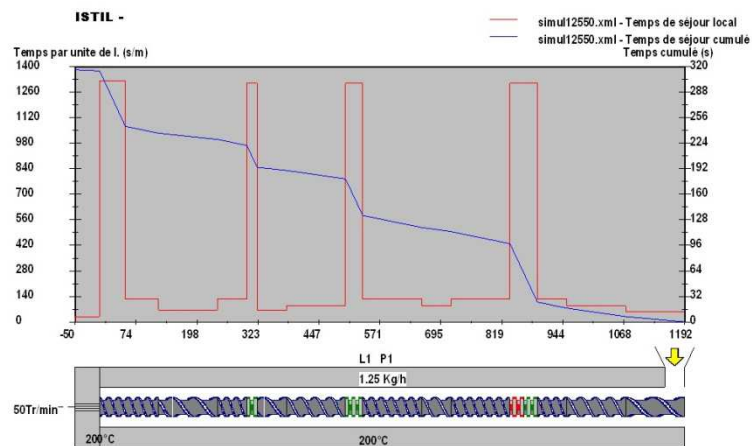
Table_Apx 3. Compartment model parameters (0.75 kg/h, 300 rpm)

Zone #	Type	Residence time,[s]
Zone 1	Plug-flow	5
Zone 2	Perfectly mixed	122
Zone 3	Plug-flow	7
Zone 4	Perfectly mixed	75
Zone 5	Plug-flow	3
Zone 6	Perfectly mixed	46
Zone 7	Plug-flow	4
Zone 8	Perfectly mixed	53
Zone 9	Plug-flow	2

Flow rate: 1.25 kg/h, Screw speed: 50 rpm



Figure_Apx 7. Ludovic simulated RTD curve (1.25 kg/h, 50 rpm)

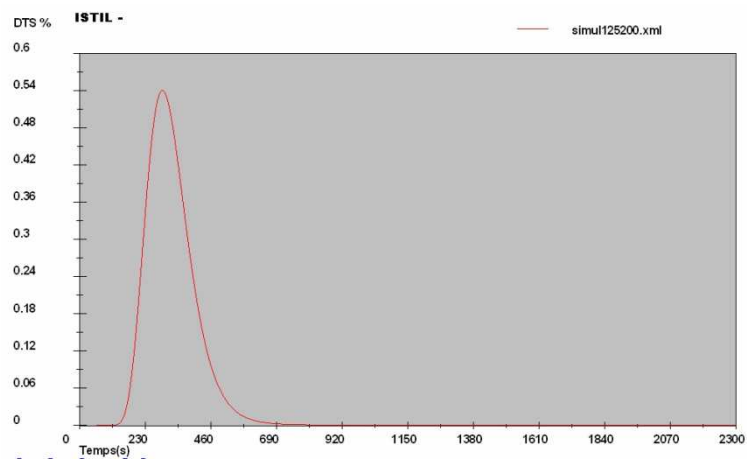


Figure_Apx 8. Local and global residence time profiles (1.25 kg/h, 50 rpm)

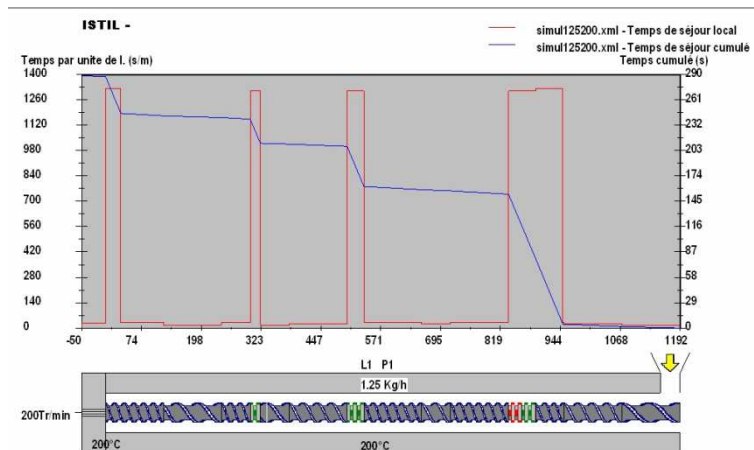
Table_Apx 4. Compartment model parameters (1.25 kg/h, 50 rpm)

Zone #	Type	Residence time,[s]
Zone 1	Plug-flow	25
Zone 2	Perfectly mixed	73
Zone 3	Plug-flow	36
Zone 4	Perfectly mixed	45
Zone 5	Plug-flow	14
Zone 6	Perfectly mixed	28
Zone 7	Plug-flow </td <td>23</td>	23
Zone 8	Perfectly mixed	69
Zone 9	Plug-flow	2

Flow rate: 1.25 kg/h, Screw speed: 200 rpm



Figure_Apx 9. Ludovic simulated RTD curve (1.25 kg/h, 200 rpm)

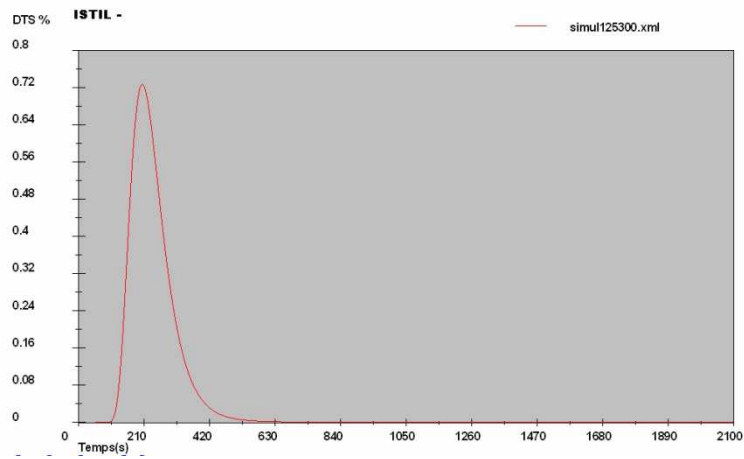


Figure_Apx 10. Local and global residence time profiles (1.25 kg/h, 200 rpm)

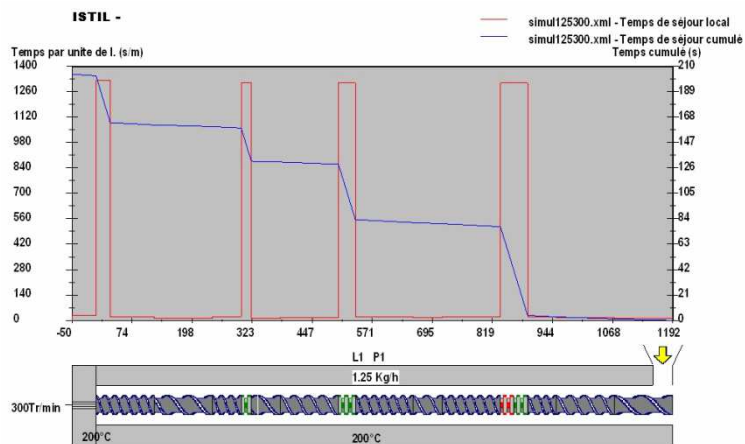
Table_Apx 5. Compartment model parameters (1.25 kg/h, 200 rpm)

Zone #	Type	Residence time,[s]
Zone 1	Plug-flow	5
Zone 2	Perfectly mixed	148
Zone 3	Plug-flow	9
Zone 4	Perfectly mixed	45
Zone 5	Plug-flow	5
Zone 6	Perfectly mixed	26
Zone 7	Plug-flow	7
Zone 8	Perfectly mixed	42
Zone 9	Plug-flow	1

Flow rate: 1.25 kg/h, Screw speed: 300 rpm



Figure_Apx 11. Ludovic simulated RTD curve (1.25 kg/h, 300 rpm)

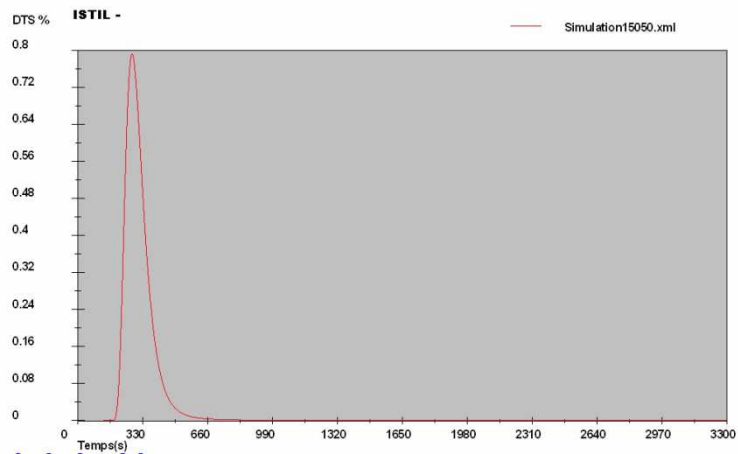


Figure_Apx 12. Local and global residence time profiles (1.25 kg/h, 300 rpm)

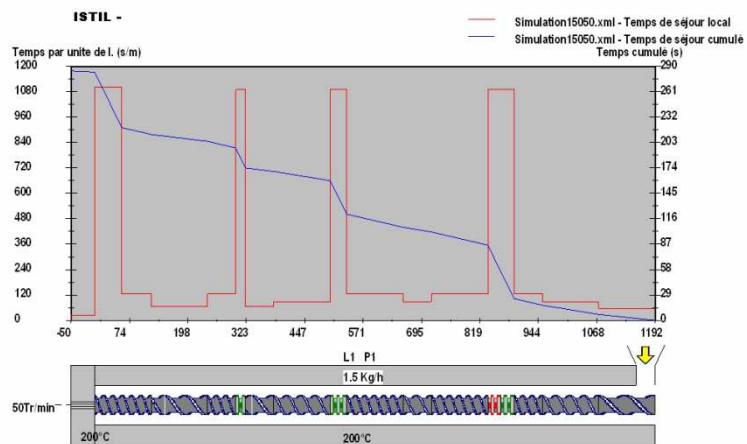
Table_Apx 6. Compartment model parameters (1.25 kg/h, 300 rpm)

Zone #	Type	Residence time,[s]
Zone 1	Plug-flow	4
Zone 2	Perfectly mixed	73
Zone 3	Plug-flow	6
Zone 4	Perfectly mixed	46
Zone 5	Plug-flow	2
Zone 6	Perfectly mixed	27
Zone 7	Plug-flow	4
Zone 8	Perfectly mixed	39
Zone 9	Plug-flow	2

Flow rate: 1.5 kg/h, Screw speed: 50 rpm



Figure_Apx 13. Ludovic simulated RTD curve (1.5 kg/h, 50 rpm)

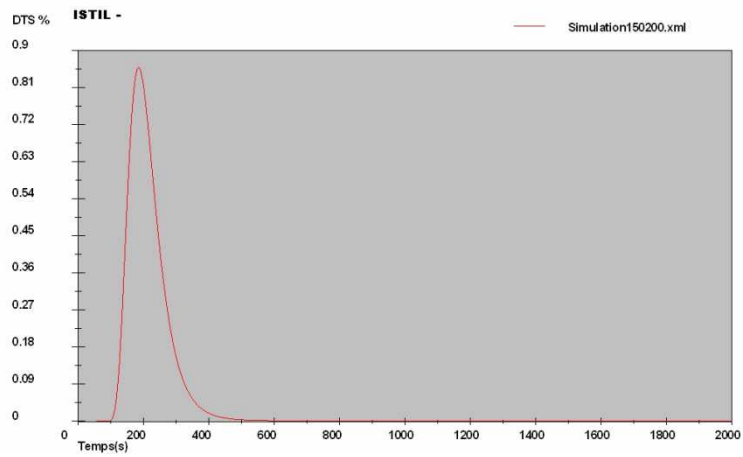


Figure_Apx 14. Local and global residence time profiles (1.5 kg/h, 50 rpm)

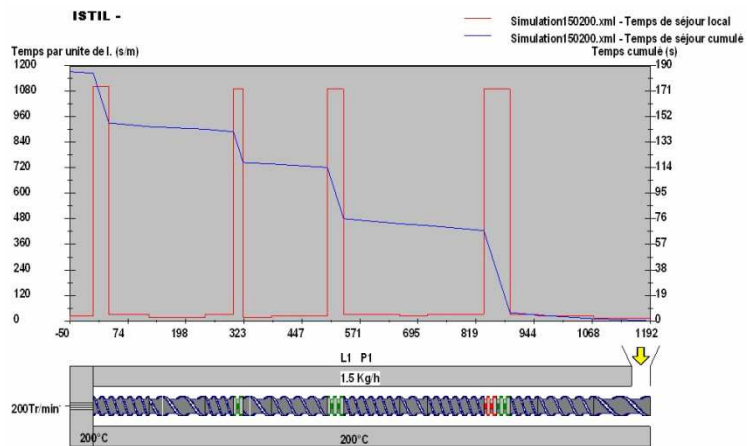
Table_Apx 7. Compartment model parameters (1.5 kg/h, 50 rpm)

Zone #	Type	Residence time,[s]
Zone 1	Plug-flow	25
Zone 2	Perfectly mixed	61
Zone 3	Plug-flow	36
Zone 4	Perfectly mixed	38
Zone 5	Plug-flow	15
Zone 6	Perfectly mixed	23
Zone 7	Plug-flow	23
Zone 8	Perfectly mixed	63
Zone 9	Plug-flow	2

Flow rate: 1.5 kg/h, Screw speed: 200 rpm



Figure_Apx 15. Ludovic simulated RTD curve (1.5 kg/h, 200 rpm)



Figure_Apx 16. Local and global residence time profiles (1.5 kg/h, 200 rpm)

Table_Apx 8. Compartment model parameters (1.5 kg/h, 200 rpm)

Zone #	Type	Residence time,[s]
Zone 1	Plug-flow	6
Zone 2	Perfectly mixed	61
Zone 3	Plug-flow	9
Zone 4	Perfectly mixed	37
Zone 5	Plug-flow	4
Zone 6	Perfectly mixed	23
Zone 7	Plug-flow	7
Zone 8	Perfectly mixed	37
Zone 9	Plug-flow	1

6. List of publications

A. Journal papers

- J. P. Puaux, I. Banu, I. Nagy, G. Bozga, *A study of L-lactide ring-opening polymerization kinetics*, Macromolecular Symposia, 259 (1), **2007**, 318 – 326.
- Banu I., G. Bozga, I. Nagy, J. P. Puaux, *A Comparison of Variational and Genetic Algorithm Performances in the Optimization of a Polymerization Process*, Chemical Engineering and Technology, 31(10), **2008**, 1516-1525.
- Banu I., S. Bildea, G. Bozga, J. P. Puaux, *Simulation of a laminar flow tubular reactor*, Studia Universitatis Babeş-Bolyai Chemia, 1, **2009**, 227-242.
- Banu I., N. D. Stanciu, J. P. Puaux, G. Bozga, *A study of L-lactide ring-opening polymerization in molten state*, U.P.B. Sci. Bull., Series B, 71(2), **2009**.
- Banu I., J. P. Puaux, G. Bozga, I. Nagy, *Modeling of L-lactide polymerization by reactive extrusion*, Macromolecular Symposia, **2009**, accepted for publication.

B. Papers published in the proceedings of national and international conferences

- Banu I., G. Bozga, J. P. Puaux, *Optimization of a molecular weight distribution in a batch free radical polymerization process*, Proceedings of Romanian International Conference of Chemistry and Chemical Engineering (RICCCE 14), 22 – 24 September **2005**, vol. 3, 174 – 181.
- Banu I., G. Bozga, I. Nagy, J. P. Puaux, *A comparison of the Minimum Principle and Genetic Algorithms in the optimization of the thermal regime for methyl methacrylate polymerization in solution*, 18th International Congress of Chemical and Process Engineering, 24-28 august **2008**, Prague, Czech Republic (published on CD).

C. National and international conferences communications

- Banu I., G. Bozga, *Optimization of a batch polymerization reactor*, CAPE Forum, 25-26 February **2005**, Cluj-Napoca, Romania.
- J. P. Puaux, I. Banu, I. Nagy, G. Bozga, *Optimization of a tubular reactor for MMA polymerization in solution*, Vingtiemes Entretiens du Centre Jacques Cartier, 3 – 4 December **2007**, Lyon, France
- Banu I., G. Bozga, I. Nagy, J. P. Puaux, *Optimization of a tubular polymerization reactor*, Polymer Reaction Engineering 7, May 3-9, **2009**, Niagara Falls, Ontario, Canada.
- Banu I., J. P. Puaux, G. Bozga, I. Nagy, *Modeling of L-lactide polymerization by reactive ex-*

7. References

1. Vega, M.P., E.L. Lima, and J.C. Pinto, *Control of a loop polymerization reactor using neural networks*. Brazilian Journal of Chemical Engineering, 2000. **17**: p. 471-482.
2. Embirucu, M., E.L. Lima, and J.C. Pinto, *A survey of advanced control of polymerization reactors*. Polymer Engineering and Science, 1996. **36**(4): p. 433 - 447.
3. Asua, J.M., ed. *Polymer reaction engineering*. 2007, Blackwell Publishing Ltd.: Oxford.
4. *Ullmann's Encyclopedia of Industrial Chemistry*. 1997.
5. *Kirk-Othmer Encyclopedia of Chemical Technology*. 2008, John Wiley & Sons.
6. Odian, G., *Principles of Polymerization*. 2004, John Wiley & Sons, Inc.: New Jersey.
7. Schork, F.J., P.B. Deshpande, and K.W. Leffew, *Control of polymerization reactors*. 1993, New York: M. Dekker.
8. Bozga, G. and I. Nagy, *Reacteurs Chimiques. Theorie et applications*. 2001, Bucuresti: Ed. Bren.
9. Kricheldorf, H.R., O. Nuyken, and G. Swift, eds. *Handbook of Polymer Synthesis*. 2nd ed. 2005, Marcel Dekker: New York.
10. Bauer, W., *Processes for producing acrylic acid esters*, R.a.H.A.-. Gesellschaft, Editor. 1928: United States. p. 1.
11. Maschio, G., T. Bello, and C. Scali, *Optimal operation strategies to control the molecular weight distribution of polymer products*. Chemical Engineering Science, 1994. **49**(24B): p. 5071-5086.
12. Schmidt, A.D. and W.H. Ray, *The dynamic behavior of continuous polymerization reactors - I. Isothermal solution polymerization in a CSTR*. Chemical Engineering Science, 1981. **36**: p. 1401 - 1410.
13. Chiu, W.Y., G.M. Carrat, and D.S. Soong, *A computer model for the gel effect in free-radical polymerization*. Macromolecules, 1983. **16**: p. 348-357.
14. Carter, J., *Modeling the polymerization of methylmethacrylate in wood under nonisothermal conditions*, in *Graduate Academic Unit of Chemical Engineering*. 2000, University of New Brunswick.
15. Tulig, T. and M. Tirrell, *Toward a Molecular Theory of the Trommsdorff Effect*. Macromolecules, 1981. **14**(5): p. 1501-1511.
16. Baillagou, P.E. and D.S. Soong, *Majors factors contributing to the nonlinear kinetics on free-radical polymerization*. Chemical Engineering Science, 1985. **40**(1): p. 75 - 86.
17. Baillagou, P.E. and D.S. Soong, *Molecular weight distribution of products of free radical nonisothermal polymerization with gel effect. Simulation for polymerization of poly(methyl methacrylate)*. Chemical Engineering Science 1985. **40**(1): p. 87-104.
18. Nising, P., *High temperature radical polymerization of methylmethacrylate in a continous pilot scale process*. 2006, Ecole Polytechnique Federale de Lausanne: Lausanne.
19. F. Fenouillot, J.T., T. Rimlinger,, *Polymerization of methyl methacrylate at high temperature with 1-butanethiol as chain transfer agent*. Journal of Applied Polymer Science, 1999. **72**(12): p. 1589-1599.
20. Ahn, S.-M., S.-P. Chang, and H.-K. Rhee, *Application of optimal temperature trajectory to batch PMMA polymerization reactor*. Journal of Applied Polymer Science 1998. **69**: p. 59 - 68.
21. Chang, J.-S. and J.-L. Lai, *Computation of optimal temperature policy for molecular weight control in a batch polymerization reactor*. Ind. Eng. Chem. Res., 1992. **31**: p. 861 - 868.
22. Chang, J.-S. and P.-S. Liao, *Molecular weight control of a batch polymerization reactor: experimental study*. Ind. Eng. Chem. Res., 1999. **38**: p. 144 - 153.

23. Ponnuswamy, S.R., S.L. Shah, and C.A. Kiparissides, *Computer optimal control of batch polymerization reactors*. Ind. Eng. Chem. Res., 1987. **26**(11): p. 2229 - 2236.
24. Crowley, T. and K.Y. Choi, *Calculation of molecular weight distribution from molecular weights moments in free radical polymerization*. Ind. Eng. Chem. Res, 1997. **36**: p. 1419 - 1423.
25. Crowley, T.J. and K.Y. Choi, *Discrete optimal control of molecular weight distribution in a batch free radical polymerization process*. Ind. Eng. Chem. Res., 1997. **36**: p. 3676-3684.
26. Kiparissides, C., P. Seferlis, G. Mourikas, and A.J. Morris, *Online Optimizing Control of Molecular Weight Properties in Batch Free-Radical Polymerization Reactors*. Ind. Eng. Chem. Res., 2002. **41**(24): p. 6120-6131.
27. Scali, C., R. Ciari, T. Belo, and G. Maschio, *Optimal temperature for the control of the product quality in batch polymerization: simulation and experimental results*. Journal of Applied Polymer Science, 1995. **55**: p. 945 - 959.
28. Mihail, R., *Modele cinetice de polireactii*. 1986, Bucuresti: Editura Stiintifica si Enciclopedica.
29. Ponnuswamy, S.R., *On-line measurements and control of a batch polymerization reactor*. 1984, University of Alberta: Edmonton. p. 252.
30. Husain, A. and A.E. Hamielec, *Bulk thermal polymerization of styrene in a tubular reactor - a computer study*. AiChE Symposium Series, 1976.
31. Baillagou, P.E. and D.S. Soong, *Free radical polymerization of methyl methacrylate in tubular reactors*. Polymer Engineering & Science, 1985. **25**(4): p. 212 - 231.
32. Lynn, S. and J.E. Huff, *Polymerization in a tubular reactor*. AIChE Journal, 1971. **17**(2): p. 475 - 481.
33. Wyman, C.E. and L.F. Carter, *A numerical model for tubular polymerization reactors*. AiChE Symposium Series, 1976.
34. Ghosh, M. and D.W. Foster, *A model of a tubular reactor for the continuous polymerization of styrene: experiments at low molecular weight*. AiChE Symposium Series, 1976.
35. Nauman, B.E., ed. *Chemical Reactor Design, Optimization, and Scaleup*. 2002, McGraw-Hill
36. Hicks, J., A. Mohan, and W.H. Ray, *The optimal control of polymerization reactors*. Canadian Journal of Chemical Engineering, 1969. **47**: p. 590 - 597.
37. Sacks, M.E., S.I. Lee, and J.A. Biesenberger, *Optimal policies for batch, chain addition polymerizations*. Chemical Engineering Science, 1972. **27**(12).
38. Louie, B.M. and D.S. Soong, *Optimization of batch polymerization processes - Narrowing the MWD. I. Model simulation*. Journal of Applied Polymer Science, 1985. **30**: p. 3707 - 3749.
39. Takamatsu, T., S. Shioya, and Y. Okada, *Molecular weight distribution control in a batch polymerization reactor*. Ind. Eng. Chem. Res., 1988. **27**(1): p. 93 - 99.
40. Schmidt, A.D. and A.H. Ray, *The dynamic behavior of continuous polymerization reactors-I. isothermal solution polymerization in a CSTR*. Chemical Engineering Science, 1981. **36**: p. 1401 - 1410.
41. Kirk, D.E., *Optimal Control Theory: An Introduction*. Networks Series, ed. R.W. Newcomb. 1970, Englewood Cliffs, New Jersey: Prentice-Hall.
42. Crisan, M.V. and S.P. Agachi, *Elemente de teoria sistemelor*. 2002, Cluj-Napoca: E. RISO-PRINT.
43. Lucaci, A.I. and P.S. Agachi, *Optimizarea proceselor din industria chimica*. 2002, Bucuresti: Ed. Tehnica.
44. Bryson, A.E. and Y.-C. Ho, *Applied Optimal Control*. 1969, Waltham, Massachusetts: Blaisdell Publishing Company.
45. Chakravarti, S., W. Harmon-Ray, and S.X. Zhang, *Kinetic study of olefin polymerization with a supported metallocene catalyst. IV. Comparison of bridged and unbridged catalyst in*

- gas phase*. Journal of Applied Polymer Science, 2001. **81**(6): p. 1451-1459.
46. Lee, M.H., C. Han, and K.S. Chang, *Hierarchical time-optimal control of a continuous copolymerization reactor during start-up or grade change operation using genetic algorithms*. Computers Chem. Engng., 1997. **21**, **Suppl.**: p. S1037-S1042.
 47. Chakravarthy, S.S.S., D.N. Saraf, and S.K. Gupta, *Use of genetic algorithms in the optimization of free radical polymerizations exhibiting the trommsdorff effect*. Journal of Applied Polymer Science, 1997. **63**(4): p. 529-548.
 48. Haupt, R.L. and S.E. Haupt, *Practical Genetic Algorithms (2nd ed.)* Journal of the American Statistical Association. Vol. 100. 2005: American Statistical Association. 1099-1099.
 49. Kennedy, J. and W.M. Spears. *Matching Algorithms to Problems: An Experimental Test of the Particle Swarm and Some Genetic Algorithms on the Multimodal Problem Generator*. in *Evolutionary Computation Proceedings, 1998. IEEE World Congress on Computational Intelligence., The 1998 IEEE International Conference 4-9 May 1998*.
 50. Marco, N., et al., *A genetic algorithm compared with a gradient-based method for the solution of an active-control model problem*. 1996, Institut National De Recherche En Informatique Et En Automatique.
 51. Perry, R.H., D.W. Green, and J.O. Maloney, *Perry's Chemical Engineer's Handbook*. 1997, McGraw Hill: New York.
 52. Brandrup, J., E.H. Immergut, and E.A. Grulke, eds. *Polymer Handbook*. 1999, John Wiley and Sons, Inc. : New York.
 53. Banu, I., S. Bildea, G. Bozga, and J.-P. Puaux, *Simulation of a laminar flow tubular reactor*. Studia Universitatis Babeş-Bolyai Chemia, 2009(1): p. 227-242.
 54. The MathWorks, I., *MATLAB Documentation*. 1984-2008.
 55. I. Banu, G. Bozga, I. Nagy, and J.-P. Puaux, *A Comparison of Variational and Genetic Algorithm Performances in the Optimization of a Polymerization Process*. Chemical Engineering and Technology, 2008. **31**(10): p. 1516-1525.
 56. Logist, F., I.Y. Smets, and J.F. VanImpe, *Derivation of generic optimal reference temperature profiles for steady-state exothermic jacketed tubular reactors*. Journal of Process Control, 2008. **18**: p. 92-104.
 57. *Polylactides*, in *Kirk-Othmer Encyclopedia of Chemical Technology, 5th edition*. 2004, John Wiley & Sons, Inc.: New Jersey. p. 297-318.
 58. Gruber, P. and M. O'Brien, *Polylactides "Natureworks PLA" () Biopolymers, Polyesters III - Applications and Commercial Products*, ed. Y. Doi and A. Steinbüchel. Vol. 4. 2002, New York: John Wiley and Sons.
 59. Mehta, R., *Modeling and Simulation of Poly(Lactic Acid) Polymerization*, in *Department of Chemical Engineering*. 2007, Deemed University, Thapar Institute of Engineering and Technology: Patiala.
 60. Bechthold, I., *Technologisch Relevante Aspekte Der Ringöffnungspolymerisation Von L,L-Dilactid* 2003, Fakultät III - Prozesswissenschaften - der Technischen Universität Berlin Berlin.
 61. Perepelkin, K.E., *Polylactide fibers: fabrication, properties, use, prospects. A review*. Fibre Chemistry, 2002. **34**(2): p. 85-100.
 62. Middleton, C.J. and J.A. Tipton, *Synthetic biodegradable polymers as orthopedic devices*. Biomaterials, 2000. **21**: p. 2335 - 2346.
 63. Jacobsen, S., et al., *Single-step reactive extrusion of PLLA in a corotating twin-screw extruder promoted by 2-ethylhexanoic acid tin(II) salt and triphenylphosphine*. Polymer 2000. **41**: p. 3395-3403.
 64. Auras, R., B. Harte, and S. Selke, *An Overview of Polylactides as Packaging Materials*. Macromolecular Bioscience, 2004. **4**: p. 835-864.
 65. Drumright, R.E., P.R. Gruber, and D.E. Henton, *Polylactic Acid Technology*. Advanced Materials, 2000. **12**(23): p. 1841-1846.

66. Kurcok, P., et al., *Substituent Effect in Anionic-Polymerization of Beta-Lactones Initiated by Alkali-Metal Alkoxides*. *Macromolecular Rapid Communications*, 1995. **16**(7): p. 513-519.
67. Carlson, T.L. and E.M. Peters-Jr., *Low PH lactic acid fermentation*. 1997, Cargill, Inc.: United States.
68. Garlotta, D., *A Literature Review of Poly (Lactic Acid)*. *Journal of Polymers and the Environment*, 2001. **9**(2): p. 63-84.
69. Seppala, J., J.-F. Selin, and T. Su, *Method for producing lactic acid based polyurethane*. 1995, Neste OY: United States.
70. Gruber, P.R., et al., *Continuous process for manufacture of a purified lactide*. 1993, Cargill, Incorporated: United States.
71. Gruber, P.R., *Poly(lactide) copolymer and process for manufacture thereof*. 1994, Cargill, Incorporated: United States.
72. Gruber, P.R., et al., *Continuous process for manufacture of lactide polymers with controlled optical purity*. 1999, Cargill, Incorporated: United States.
73. Gruber, P.R., et al., *Continuous process for manufacture of lactide and lactide polymers*. 2001, Cargill, Inc.: United States.
74. Gruber, P.R., et al., *Continuous process for manufacture of lactide polymers with controlled optical purity*. 2001, Cargill, Inc.: United States.
75. Dechy-Cabaret, O., B. Martin-Vaca, and D. Bourissou, *Controlled Ring-Opening Polymerization of Lactide and Glycolide*. *Chemical Reviews*, 2004. **104**(12): p. 6147-6176.
76. Amgoune, A., C.M. Thomas, T. Roisnel, and J.F. Carpentier, *Ring-opening polymerization of lactide with group 3 metal complexes supported by dianionic alkoxy-amino-bisphenolate ligands: Combining high activity, productivity, and selectivity*. *Chemistry - A European Journal*, 2006. **12**(1): p. 169-179.
77. Chamberlain, B.M., et al., *Polymerization of lactide with zinc and magnesium beta-diiminate complexes: Stereocontrol and mechanism*. *Journal of the American Chemical Society*, 2001. **123**(14): p. 3229-3238.
78. Wu, J.C., et al., *Ring-opening polymerization of lactide initiated by magnesium and zinc alkoxides*. *Polymer*, 2005. **46**(23): p. 9784-9792.
79. Stolt, M. and A. Sodergard, *Use of Monocarboxylic Iron Derivatives in the Ring-Opening Polymerization of L-Lactide*. *Macromolecules*, 1999. **32**: p. 6412-6417.
80. O'Keefe, B.J., S.M. Monnier, M.A. Hillmyer, and W.B. Tolman, *Rapid and controlled polymerization of lactide by structurally characterized ferric alkoxides*. *Journal of the American Chemical Society*, 2001. **123**(2): p. 339-340.
81. Chrisholm, M.H., J.C. Gallucci, and C. Krempner, *Ring-opening polymerization of L-lactide by organotin(IV)alkoxides, R₂Sn(OPrⁱ)₂: Estimation of the activation parameters*. *Polyhedron* 2007. **26**: p. 4436-4444.
82. Storey, R.F., et al., *Soluble Tin(II) Macroinitiator Adducts for the Controlled Ring-Opening Polymerization of Lactones and Cyclic Carbonates*. *Journal of Polymer Science. Part A: Polymer Chemistry*, 2002. **40**: p. 3434-3442.
83. Mehta, R., V. Kumar, H. Bhunia, and S.N. Upadhyay, *Synthesis of Poly (Lactic Acid): A Review*. *Journal of Macromolecular Science Part C: Polymer Reviews*, 2005. **45**: p. 325-349.
84. Mehta, R., V. Kumar, and S.N. Upadhyay, *Mathematical Modeling of the Poly(lactic acid) Ring-Opening Polymerization Kinetics*. *Polymer-Plastics Technology and Engineering*, 2007. **46**(3): p. 257 — 264.
85. Wang, C., H. Li, and X. Zhao, *Ring opening polymerization of L – lactide initiated by creatinine*. *Biomaterials*, 2004. **25**: p. 5797 – 5801.
86. Stridsberg, K.M., M. Ryner, and A.-C. Albertsson, *Controlled Ring-Opening Polymerization: Polymers with designed Macromolecular Architecture*, in *Degradable Aliphatic Polyesters*. 2001. p. 41-65.
87. Wu, J., T.-L. Yu, C.-T. Chen, and C.-C. Lin, *Recent developments in main group metal*

- complexes catalyzed/initiated polymerization of lactides and related cyclic esters*. Coordination Chemistry Reviews, 2006. **250**(5-6): p. 602-626.
88. Kricheldorf, H.R., M. Berl, and N. Scharnagl, *Poly(lactones). 9. Polymerization Mechanism of Metal Alkoxide Initiated Polymerizations of Lactide and Various Lactones* Macromolecules, 1988. **21**: p. 286-293
 89. Degee, P., P. Dubois, and R. Jerome, *Bulk polymerization of lactides initiated by aluminium isopropoxide*. Macromol. Chem. Phys., 1997. **198**: p. 1985-1995.
 90. Degee, P., P. Dubois, and R. Jerome, *Bulk polymerization of lactides initiated by aluminium isopropoxide, 3^a) Thermal stability and viscoelastic properties* Macromol. Chem. Phys., 1997. **198**: p. 1985-1995.
 91. Degee, P., P. Dubois, and R. Jerome, *Bulk polymerization of lactides initiated by aluminium isopropoxide, 2^a) Beneficial effect of Lewis bases and transfer agents* Macromol. Chem. Phys., 1997. **198**: p. 1973-1984.
 92. Degee, P., et al., *Beneficial effect of triphenylphosphine on the bulk polymerization of L, L – lactide promoted by 2 – ethyl hexanoic acid tin(II)salt*. Journal of Polymer Science, Part A: Polymer Chemistry, 1999. **37**: p. 2413 – 2420.
 93. Jacobsen, S., et al., *Single-step reactive extrusion of PLLA in a corotating twin-screw extruder promoted by 2-ethylhexanoic acid tin(II) salt and triphenylphosphine*. Polymer, 2000. **41**(9): p. 3395-3403.
 94. Kricheldorf, H.R., *Tin-initiated polymerizations of lactones: mechanistic and preparative aspects*. Macromol. Symp., 2000. **153**: p. 55-65.
 95. Eenink, M.J.D., *Synthesis of biodegradable polymers and development of biodegradable hollow fibres for the controlled release of drugs*. 1987, Twente University.
 96. Lian-xi, C., W. Jun, F. Jie, and L. Jia-heng, *The syntheses and properties of poly(L - lactide)*. Wuhan University Journal of Natural Sciences, 2002. **7**(4): p. 473-476.
 97. Nijenhuis, A.J., D.W. Grijpma, and A.J. Pennings, *Lewis acid catalyzed polymerization of L-lactide. Kinetic and mechanism of the bulk polymerization*. Macromolecules, 1992. **25**: p. 6419 – 6424.
 98. Khanna, A., Y. Sudha, S. Pillai, and S. Rath, *Molecular modeling studies of poly lactic acid initiation mechanisms*. Journal of Molecular Modeling, 2008. **14**(5): p. 367-374.
 99. Moller, M., et al., *Stannous (II) trifluoromethane sulphonate: A versatile catalyst for the controlled ring-opening polymerization of lactides: formation of stereoregular surfaces from polylactides “brushes”*. Journal of Polymer Science: Part A: Polymer Chemistry, 2001. **39**: p. 3529 – 3538.
 100. Schwach, G., J. Coudane, R. Engel, and M. Vert, *Ring Opening Polymerization of D,L-Lactide in the Presence of Zinc Metal and Zinc Lactate*. Polymer International, 1998. **46**: p. 177-182.
 101. Schwach, G., J. Coudane, R. Engel, and M. Vert, *More about the polymerization of lactides in the presence of stannous octoate*. Journal of Polymer Science. Part A: Polymer Chemistry, 1997. **35**: p. 3431 – 3440.
 102. Kricheldorf, H.R. and I. Kreiser-Saunders, *Poly(lactones), 19^a) Anionic polymerization of L-lactide in solution*. Makromol. Chem., 1990. **191**: p. 1057-1066
 103. Zhang, H., U.P. Wyss, D. Pichora, and M. Goosen, *An investigation of the synthesis and thermal stability of poly(D,L-lactide)*. Polymer Bulletin, 1992: p. 623 - 629.
 104. Zhang, X., D.A. Macdonald, M. Goosen, and K. McAuley, *Mechanism of lactide polymerization in the presence of stannous octoate: The effect of hydroxy and carboxylic acid substances*. Journal of Polymer Science: Part A: Polymer Chemistry, 1994. **32**: p. 2965 - 2970.
 105. Kricheldorf, H.R., I. Kreiser – Saunders, and A. Stricker, *Poly(lactones) 48. SnOct₂ - initiated polymerizations of lactide: A mechanistic study*. Macromolecules, 2000. **23**: p. 702 – 709.
 106. Kowalski, A., A. Duda, and S. Penczek, *Kinetics and mechanism of cyclic esters polymerization initiated with tin(II) octoate: 3. Polymerization of L, L – Dilactide*. Macromolecules,

2000. **33**: p. 7359 – 7270.
107. Kowalski, A., A. Duda, and S. Penczek, *Kinetics and mechanism of cyclic esters polymerization initiated with tin(II) octoate, 1. Polymerization of ϵ -caprolactone*. *Macromol. Rapid Commun.*, 1998. **19**: p. 567–572.
 108. Kowalski, A., A. Duda, and S. Penczek, *Mechanism of Cyclic Ester Polymerization Initiated with Tin (II) Octoate. 2. Macromolecules Fitted with Tin (II) Alkoxide Species Observed Directly in MALDI-TOF Spectra*. *Macromolecules*, 2000. **33**: p. 689-695.
 109. Storey, R.F. and A.E. Taylor, *End-group analysis of poly(ϵ -caprolactone) initiated with water, ethylene glycol, and 1,4-butanediol*. *Journal of Macromolecular Science-Pure and Applied Chemistry*, 1996. **A33**(1): p. 77-89.
 110. Hyon, S.-H., K. Jamshidi, and Y. Ikada, *Synthesis of polylactides with different molecular weights*. *Biomaterials*, 1997. **18**: p. 1503-1508.
 111. Duda, A., S. Penczek, A. Kowalski, and J. Libiszowski, *Polymerizations of ϵ -caprolactone and L, L – dilactide initiated with stannous octoate and stannous butoxide – a comparison*. *Macromol. Symp.*, 2000. **153**: p. 41 – 53.
 112. Kowalski, A., et al., *Kinetics and Mechanism of Cyclic Esters Polymerization Initiated with Tin(II) Octoate. Polymerization of ϵ -Caprolactone and L,L-Lactide Co-initiated with Primary Amines*. *Macromolecules*, 2005. **38**: p. 8170-8176.
 113. Adam Kowalski, et al., *Kinetics and mechanism of ϵ -caprolactone and l,l-lactide polymerization coinited with zinc octoate or aluminum acetylacetonate: The next proofs for the general alkoxide mechanism and synthetic applications*. *Polymer*, 2007. **48**(14): p. 3952-3960.
 114. Korhonen, H., A. Helminen, and J.V. Seppala, *Synthesis of polylactides in the presence of co-initiators with different numbers of hydroxyl groups*. *Polymer*, August 2001. **42**(9): p. 7541-7549.
 115. Witzke, D.R., R. Narayan, and J.J. Kolstad, *Reversible kinetics and thermodynamics of the homopolymerization of L-lactide with 2-ethylhexanoic acid tin(II) salt*. *Macromolecules*, 1997. **30**: p. 7075 – 7085.
 116. Jamshidi, K., S.-H. Hyon, and Y. Ikada, *Thermal characterization of polylactides* *Polymer*, 1988. **29**: p. 2229-2234.
 117. Gogolewski, S., et al., *The effect of melt-processing on the degradation of selected polyhydroxyacids: polylactides, polyhydroxybutyrate, and polyhydroxybutyrate-co-valerates**. *Polymer Degradation and Stability*, 1993. **40**: p. 313-322.
 118. McNeill, I.C. and H.A. Leiper, *Degradation Studies of Some Polyesters and Polycarbonates-2. Polylactide: Degradation Under Isothermal Conditions, Thermal Degradation Mechanism and Photolysis of the Polymer* *Polymer Degradation and Stability*, 1985. **11**: p. 309-326
 119. Jacobsen, S., et al., *Continuous reactive extrusion polymerisation of L-lactide - an engineering view*. *Macromol. Symp.*, 2000. **153**: p. 261-273.
 120. Baker, G.L., E.B. Vogel, and M.R. Smith, *Glass Transitions in Polylactides*. *Polymer Reviews*, 2008. **48**(1): p. 64 - 84.
 121. Cooper-White, J.J. and M.E. Mackay, *Rheological properties of poly(lactides). Effect of molecular weight and temperature on the viscoelasticity of poly(L-lactic acid)*. *Journal of Polymer Science Part B: Polymer Physics*, 1999. **37**(15): p. 1803-1814.
 122. Degee, P., et al., *Beneficial effect of triphenylphosphine on the bulk polymerization of L, L – lactide promoted by 2 – ethyl hexanoic acid tin(II)salt*. *Journal of Polymer Science, Part A: Polymer Chemistry*, 1999. **37**: p. 2413 – 2420.
 123. Kaihara, S., S. Matsumura, A.G. Mikos, and J.P. Fisher, *Synthesis of poly L-lactide and polyglycolide by ring-opening polymerization*. *Nature protocols*, 2007. **2**(11): p. 2767 - 2771.
 124. J. P. Puaux, I. Banu, I. Nagy, and G. Bozga, *A study of L-lactide ring-opening polymerization kinetics*. *Macromolecular Symposia*, 2007. **259**(1): p. 318-326.

125. Balaban, A.T., M. Banciu, and I.I. Pogany, *Aplicatii ale metodelor fizice in chimia organica*. 1983, Bucuresti: Editura Stiintifica si Enciclopedica.
126. Jalabert, M., C. Fraschini, and R.E. Prud'homme, *Jour. Polym Sci: Part A: Polymer Chemistry*, 2007. **45**: p. 1944.
127. Kricheldorf, H.R., Kreiser-Saunders, I., Boettcher, C., *Polylactones: 31. Sn(II) octoate-initiated polymerization of L-lactide: a mechanistic study*. *Polymer*, 1995. **36**(6): p. 1253-1259.
128. Takizawa, K., et al., *Molecularly defined (L)-lactic acid oligomers and polymers: Synthesis and characterization*. *Journal of Polymer Science Part A: Polymer Chemistry*, 2008. **46**(18): p. 5977-5990.
129. Barth, H.G. and J.W. Mays, *Modern methods of polymer characterization*. Chemical analysis, 1991, New York: Wiley. x, 561 p.
130. Lustig, S.R., *Peak-referenced integral method for size exclusion chromatography and its application to aromatic polyesters*. *Journal of Chromatography A*, 1999. **839**(1-2): p. 1-14.
131. Banu, I., N.D. Stanciu, J.-P. Puaux, and G. Bozga, *A study of L-lactide ring-opening polymerization in molten state*. *U.P.B. Sci. Bull., Series B*, 2009. **71**(2).
132. Zhang, Y.M., P. Wang, N. Han, and H.F. Lei, *Microwave Irradiation: A Novel Method for Rapid Synthesis of D,L-Lactide*. *Macromolecular Rapid Communications*, 2007. **28**(4): p. 417 - 421.
133. Degee, P., et al., *New catalyst fost fast bulk ring-opening polymerization of lactide monomers*. *Macromolecular Symposia*, 1999. **144**: p. 289 - 302.
134. Mehta, R., V. Kumar, H. Bhunia, and S.N. Upadhyay, *Synthesis of Poly(Lactic Acid): A Review*. *Journal of Macromolecular Science, Part C: Polymer Reviews*, 2005. **45**: p. 325-349.
135. Ponnuswamy, S.R. and A. Penlidis, *Batch solution polymerization of MMA: parameter estimation*. *The Chemical Engineering Journal*, 1988. **39**: p. 175 - 183.
136. Englezos, P. and N. Kalogerakis, *Applied Parameter Estimation for Chemical Engineers*. 2001, New York: Marcel Dekker.
137. Ryner, M., et al., *Mechanism of Ring Opening Polymerization of 1,5 Dioxepan 2 One and L Lactide with Stannous 2 Ethylhexanoate A Theoretical Study*. *Macromolecules*, 2001. **34**: p. 3877-3881.
138. Vergnes, B., G.D. Valle, and L. Delamare, *A Global Computer Software for Polymer Flows in Corotating Twin Screw Extruders*. *Polymer Engineering and Science*, 1998. **38**(11): p. 1781 - 1792.
139. Zagal, A., E. Vivaldo-Lima, and O. Manero, *A Mathematical Model for the Reactive Extrusion of Methyl Methacrylate in a Co-rotating Twin-Screw Extruder*. *Ind. Eng. Chem. Res.*, 2005. **44**(26): p. 9805-9817.
140. Poulesquen, A. and B. Vergnes, *A Study of Residence Time Distribution in Co-Rotating Twin-Screw Extruders. Part I: Theoretical Modeling*. *Polymer Engineering and Science*, 2003. **43**(12): p. 1841 - 1848.
141. Poulesquen, A., et al., *A Study of Residence Time Distribution in Co-Rotating Twin-Screw Extruders. Part II: Experimental Validation*. *Polymer Engineering and Science*, 2003. **43**(12): p. 1849 - 1862.
142. Cassagnau, P., C. Mijangos, and A. Michel, *An ultraviolet method for the determination of the residence time distribution ina twin screw extruder*. *Polymer Engineering and Science*, 1991. **31**(11): p. 772 - 778.
143. Cassagnau, P., M. Courmont, F.Melis, and J.P.Puaux, *Study of Mixing ofLiquid/Polymer in Twin Screw Extruder by Residence Time Distribution*. *Polymer Engineering & Science*, 2005: p. 926 - 934.
144. Vergnes, B., ed. *LUDOVIC® User's Guide, Version 3.1*.
145. Bozga, G. and O. Muntean, *Reactoare chimice*. 2000, Bucuresti: Ed. Tehnica.

Modélisation et optimisation des réacteurs tubulaires de polymérisation

Le but de cette thèse est l'investigation des particularités des problèmes d'optimisation et modélisation des réacteurs tubulaires de polymérisation. La partie originale du travail est divisé en deux sections, la première traitant de l'étude théorique de la modélisation et de l'optimisation des réacteurs tubulaires de polymérisation du méthacrylate de méthyle en solution, et la deuxième, une étude expérimentale et théorique de l'extrusion réactive de L-lactide.

Dans la première partie, afin de sélectionner un modèle cinétique représentatif, parmi les modèles publiés pour le processus de polymérisation de MMA, des simulations ont été effectuées en conditions identiques de fonctionnement. Deux algorithmes numériques, l'un basé sur le Principe du Minimum de Pontriaguine et l'autre de type Génétique, ont été comparés pour un problème d'optimisation de complexité moyenne. Les résultats ont montré une robustesse supérieure de l'Algorithme Génétique pour cette catégorie de problèmes.

La deuxième partie de la thèse est consacrée à la modélisation et à l'optimisation de l'extrusion réactive du L-lactide. Nous avons proposé un modèle cinétique et ses paramètres ont été estimés en utilisant des procédures numériques basées sur les données cinétiques expérimentales. Les expériences d'extrusion réactives ont été exécutées dans les conditions de fonctionnement représentatives. L'écoulement de L-lactide/poly lactide dans l'extrudeuse a été caractérisé par la simulation en utilisant un logiciel commercial, LUDOVIC[®]. Les caractéristiques de la distribution des temps de séjour simulées sont utilisées pour modéliser le processus d'extrusion réactive en utilisant deux approches, un modèle à dispersion axiale et un modèle à base de compartiments, dont les caractéristiques sont déduites des simulations effectuées avec LUDOVIC[®]. Les résultats de la modélisation du processus sont en bon accord avec des données mesurées en mêmes conditions opératoires.

Modeling and optimization of tubular polymerization reactors

The aim of this thesis is the investigation of modeling and optimization particularities of tubular polymerization reactors. The original work is divided in two sections, the first treating a modeling and optimization study of tubular reactors for methyl methacrylate polymerization in solution, and the second, an experimental and theoretical study of L-lactide reactive extrusion.

In the first section, reactor simulations in similar operating conditions were performed in order to select a representative kinetic model among the published kinetic models for MMA solution polymerization. Two widely used numerical algorithms, one based on Pontryagin's Minimum Principle and the other a Genetic Algorithm, were compared for an average-complexity optimization problem. The results showed a superior robustness of the Genetic Algorithm for this category of problems.

The second part of the thesis deals with the modeling and optimization of L-lactide reactive extrusion. A kinetic model is proposed and its parameters estimated using nonlinear estimation numerical procedures based on experimentally measured data. Reactive extrusion experiments were performed in representative operating conditions. The L-lactide/poly lactide flow in the extruder was characterized by simulation using the commercial software LUDOVIC[®]. The simulated residence time distributions characteristics are used to model the reactive extrusion process of two approaches, an axial dispersion model and a compartment model, based on compartments whose characteristics are deduced from the simulations using LUDOVIC[®]. The modeling results are in good agreement with the measured data in the same operating conditions.